

**Evolutionary Methods for Topology
Optimisation of Continuum Structures:
Static and Dynamic Problems**

by

Ms Xiaoying Yang, B.E., M.E.



**Thesis submitted in fulfilment of the requirement of
the degree of Doctor of Philosophy
to Victoria University of Technology**

School of the Built Environment
Victoria University of Technology
Melbourne, Australia
February, 2002

FTS THESIS

624.17713 YAN

30001007614284

Yang, Xiaoying

Evolutionary methods for
topology optimisation of
continuum structures :

To my Sister, Xiaoyu

-With Gratitude and Love

ACKNOWLEDGEMENTS

I wish to express my sincere gratitude to my supervisor, Prof. Mike Xie. Mike has been offering unfailing support over the past years. He is always encouraging, patient and responsive. Every student has been benefited from his prompt feedback when seeking advice on a subject, a report or a paper. Mike always thinks of the welfare and career development of his students and shares their concerns. He has provided me with great career prospects and opportunities. His advice and support have been invaluable in my securing a position with an engineering consultancy company. His understanding and consideration are highly appreciated, especially when I have been occupied with the thesis writing and a full-time job towards the end of the PhD study. I feel I am fortunate to be one of his many postgraduate students, to have him as a mentor and friend, guiding me through this important part of my life.

It is in the excellent School of Built Environment, Victoria University of Technology that my postgraduate research has been carried out. The School has provided research resources and facilities and a stimulating and positive study environment. My PhD study has been sponsored by the Victoria University Postgraduate Research Scholarship, which is gratefully acknowledged.

This thesis has benefited greatly from the Engineering Design Centre (EDC), of University of Cambridge. Chapter 7 was the results of a six-month joint program in the Centre under the supervision of Drs. P.J. Clarkson and G.T. Parks, who have led the Design Optimisation Group (DOG). Dr. J.S. Liu, a group member and a major collaborating researcher, has made invaluable effort and work on the joint program. The Centre has sponsored me a conference in Swansea; And the group, especially Dr. G.T. Parks, have helped me tremendously in preparing one journal paper. From the group and its members, I have experienced the unique research culture and spirit of Cambridge. Their kindness and assistance have made the stay fruitful and enjoyable.

I am grateful to Prof. G.P. Steven of University of Durham, U.K., the former Head of Dept. of Aeronautical Engineering of University of Sydney, Australia. Thanks for his encouragement to me as a young researcher. I also wish to thank Dr. O.M. Querin, of

University of Leeds, U.K., for his initial work on Bi-directional ESO (BESO), and his advice and assistance. I have been inspired and encouraged by the researchers in Melbourne and Sydney, especially by Dr. D. Manickarajah, Dr. Q. Li and Ms. W. Li. Thanks also go to Prof. J.H. Rong who was a visiting research fellow on a ESO project. His outstanding work and personal assistance are invaluable in the early stage of my PhD study.

At the School of Built Environment, I wish to thank all the staff for their kindness and encouragement, especially to Assoc. Prof. C. Perera, Dr. D. Tran, Assoc. Prof. Ö. Turan, Ms. G. Geyer, Assoc. Profs. C. Bhuta, T. Graham and M. Sek. Special thanks are due to Mr. T. Do who has helped greatly in the computer lab. Gratitude is extended to my fellow students who have shared and experienced all the frustrations and achievements of being a research student. Thanks to David, Li, Anne and Quang, for their friendship. Quang's computer excellence has been very helpful.

I wish to thank my fiancé Qiang, who has always been by my side and put up with my preoccupation with this thesis. Thanks for his understanding, caring love and companionship.

Finally, it is a pleasure to acknowledge my family in China: my parents, my sister, my brother-in-law and my little nephew. They are a source of constant love, understanding and encouragement. I am deeply indebted to my sister, who has, in my absence, been taking the family responsibility and making great sacrifice, and to whom, this thesis is dedicated.

CERTIFICATE OF RESEARCH

This is to certify that except where specific reference to other investigation is made, the work described in this thesis is the result of the candidate's own investigations.

Candidate



Xiaoying Yang

Supervisor



Yi-Min Xie

DECLARATION

This is to certify that neither this thesis, nor any part of it, has been presented or is being concurrently submitted in candidature for any other degree at any other university.

Candidate



Xiaoying Yang

SUMMARY

This thesis studies the topology optimisation of continuum structures. Two methods have been investigated, namely, Evolutionary Structural Optimisation (ESO) and Bi-directional ESO (BESO). The basic concept of ESO is that by systematically removing inefficient materials from the structure, the residual shape evolves toward an optimum. BESO is an extension of ESO by allowing for adding efficient materials.

The ESO and BESO methods are applied to static (stiffness) and dynamic (natural frequency) problems. The design objectives are the mean compliance and natural frequency, respectively. The element sensitivity number α_e is obtained by performing sensitivity analysis on the objective function. This number is a measure of element efficiency. The modification is conducted by removing elements of the smallest sensitivity number and adding elements around those of the largest sensitivity number. The structural analysis and modification proceed iteratively until an optimum is reached.

The stiffness optimisation is extended to accommodate design dependent loads. The load dependency can be due to the transmissible loading, surface loading and gravity loading. In frequency optimisation, special issues are discussed and addressed, including the sensitivity of repeated and closely-spaced eigenvalues, and optimising the frequency of a particular mode shape. The latter involves a mode tracking technique known as MAC (mode assurance criteria).

Several parameters are used in the ESO and BESO algorithms, including the modification ratio, addition ratio, stage ratio and initial structure. Their effects on the optimal solution are investigated and recommendations on parameter selection are made. Apart from those parameters, the solution can be affected by the finite element mesh discretisation. This mesh dependency problem is addressed by using a perimeter control technique.

A number of 2D and 3D examples are presented. Solutions by ESO and BESO are similar and this demonstrated the feasibility of the evolutionary algorithms. BESO can provide a balance between the solution accuracy and computing efficiency. By introducing the perimeter control technique to BESO, the solution generally becomes convergent with respect to the finite element grid for 2D problems. And also, the configuration complexity can be controlled and the resulting topology is simpler and easier to manufacture. It is concluded that the ESO and BESO methods are effective in solving the stiffness and frequency optimisation problems and their variants. The procedure is simple in concept, and easy to implement and generalise.

PUBLICATION LIST

The following papers/reports have been produced during the candidate's PhD study:

1. Yang, X.Y., Xie, Y.M, Liu, J.S., Parks, G.T. and Clarkson, P.J (2001). Perimeter control of the bi-directional evolutionary optimisation method. *Struct. Multidisc. Optim.* (in press).
2. Rong, J.H., Xie, Y.M and Yang, X.Y (2001). An improved method of evolutionary structural optimisation against buckling. *Compt. & Struct.*, **79**, 253-263.
3. Rong, J.H., Xie, Y.M., Yang, X.Y. and Liang, Q.Q. (2001). Topology optimisation of structures under dynamic response constraints. *Sound & Vibration*, **23**(4), 177-189.
4. Xie, Y.M., Yang, X.Y., Liang, Q.Q., Steven, G.P. and Querin, O.M. (2001). Evolutionary structural optimisation. An invited chapter for *ASCE Optimal Structural Design Technical Committee's State of the Art Report*.
5. Yang, X.Y., Xie, Y.M., Steven, G.P. and Querin, O.M. (1999). Topology optimisation for frequencies using an evolutionary method. *Journal of Structural Engineering, ASCE*, **125** (12), 1432-1438.
6. Yang, X.Y., Liu, J.S., Parks, G.T., Clarkson, P.J. and Xie, Y.M (2000). An investigation of the effect of element size on optimal topology design of 2D continua. *Proceeding of the 2nd ASMO UK /ISSMO Conference on Engineering Design Optimisation*, Swansea, Wales, UK, 257-263.
7. Yang, X.Y., Xie, Y.M., Steven, G.P. and Querin, O.M. (1999). Evolutionary structural optimization method for static and dynamic problems. *Proceedings of the 4th Asian-Pacific Conference on Computational Mechanics for the Next Millennium*, Singapore, 1215-1220.

CONTENTS

ACKNOWLEDGEMENTS	i
CERTIFICATE OF RESEARCH	iii
DECLARATION	iv
SUMMARY	v
PUBLICATION LIST	vii
Chapter 1 Introduction	1
1.1 Structural Optimisation	1
1.2 Aims and Scope of Investigation	5
1.3 Statement of Significance	7
1.4 Layout of Thesis	9
Chapter 2 Overview of Structural Optimisation	12
2.1 Mathematical Formulation of Optimisation Problems	12
2.1.1 Mathematical Statement	12
2.1.2 Analytical Approaches	12
<i>Differential Calculus</i>	12
<i>Calculus of Variations</i>	16
2.2 Basic Numerical Algorithms	17
2.2.1 Mathematical Programming	17
2.2.2 Optimality Criteria	18
2.2.3 Genetic Algorithms	19
2.3 Current Methods for Shape and Topology Optimisation	20
2.3.1 Layout optimal design for discrete structures	20
2.3.2 Shape and topology optimisation for continuous structures	21
2.3.2.1 Boundary variation approach to shape optimisation	21
2.3.2.2 Ground structure approach to topology optimisation	22
<i>Homogenisation design methods</i>	24
<i>Simplified Isotropic Material with Penalization (SIMP)</i>	25
<i>Soft-kill methods</i>	24
<i>Hard-kill methods</i>	27

Chapter 3	ESO and BESO for Stiffness Optimisation	32
3.1	Mathematical Background	32
3.1.1	Problem Statement	32
3.1.2	Evolution Criteria	35
3.1.2.1	Sensitivity analysis	35
3.1.2.2	Optimal criteria	36
3.2	Implementation of ESO and BESO	37
3.2.1	Procedure of ESO	37
3.2.2	Procedure of BESO	38
3.2.3	Suppression of Checkerboard Pattern	42
3.2.4	Maintaining the Structural Symmetry	44
3.3	Examples	45
<i>Example 3.3.1.</i>	<i>A deep beam</i>	45
<i>Example 3.3.2</i>	<i>A cubic block subjected to inclined pull-out forces</i>	51
3.4	Conclusions	55
Chapter 4	On Topology Optimisation with Design Dependent Loading	56
4.1	Introduction	56
4.2	Topology Optimisation with Transmissible Loads	59
4.2.1	Problem Statement	59
4.2.2	Evolution Procedure	61
4.2.3	Examples	62
<i>Example 1</i>	<i>4.2.3.1 A hinged beam structure</i>	62
4.3	Topology Optimisation with Gravity Loading	65
4.3.1	Load Conversion	66
4.3.2	Sensitivity Analysis	67
4.3.3	Examples	70
<i>Example 4.3.3.1</i>	<i>A 3D arch bridge</i>	70
<i>Example 4.3.3.2</i>	<i>A box block</i>	73
<i>Example 4.3.3.3</i>	<i>A cable bridge</i>	75

4.4	Topology Optimisation with Surface Loading	78
4.4.1	Basic Concept	79
4.4.2	Sensitivity Analysis	79
4.4.3	Examples	83
	<i>Example 4.4.3.1 2D arch bridge</i>	83
	<i>Example 4.4.3.2 A block supporting pressure</i>	84
4.5	Conclusions	89
Chapter 5	ESO and BESO for Frequency Optimisation	90
5.1	Introduction	90
5.2	Basic Concepts	92
5.2.1	Problems Statement	92
5.2.2	Sensitivity Analysis	93
5.2.3	Evolutionary Procedures	94
5.3	Special Issues Related to Frequency Optimisation	95
5.3.1	Optimisation Involving Repeated Eigenvalues	95
5.3.2	Optimisation Involving Closely-Spaced Eigenvalues	97
5.3.3	Optimisation Considering Mode-Tracking	98
5.4	Examples	99
	<i>Example 5.4.1 A frame to be reinforced</i>	99
	<i>Example 5.4.2 A diagonal supported plate</i>	102
	<i>Example 5.4.3 A simply supported beam</i>	106
	<i>Example 5.4.4 A diagonal supported block</i>	109
	<i>Example 5.4.5 A cantilever beam: to track the torsion mode</i>	111
	<i>Example 5.4.6 A hinged beam: to track the bending mode</i>	117
5.5	Conclusions	122
Chapter 6	Various Aspects on Numerical Implementation and Image Processing	124
6.1	Introduction	124
6.2	Verification of Sensitivity Analysis	128
6.2.1	Measure of Accuracy	128
6.2.2	Numerical Implementation	129

6.2.3	Examples	132
6.2.3.1	Basic stiffness optimisation: external loading only	132
6.2.3.2	Stiffness optimisation with surface loading	133
6.2.3.3	Stiffness optimisation with gravity loading	134
6.2.3.4	Stiffness optimisation with combination of external loads and gravity	135
6.2.3.5	Frequency Optimisation	135
6.2.4	Discussions	136
6.3	Parameter Studies	137
6.3.1	Modification Ratio (<i>MR</i>)	138
6.3.1.1	Effect on ESO	138
6.3.1.2	Effect on BESO	142
6.3.1.3	Discussions	145
6.3.2	Stage Ratio (<i>SR</i>)	146
6.3.3	Initial Structure	149
6.3.4	Addition Ratio (<i>AR</i>)	152
6.4	Design Post-processing	153
6.5	Conclusions	156
Chapter 7	Perimeter Control for BESO	158
7.1	Introduction	158
7.2	Perimeter Measure	160
7.2.1	Definition	160
7.2.2	Characteristic Groups	161
7.3	Evolutionary Methodology with Perimeter Control	163
7.3.1	Problem Statement	163
7.3.2	Implementation	163
7.4	Examples	167
7.4.1	2D Continuous Structures	167
	<i>Example 7.4.1.1 A MBB beam</i>	167
	<i>Example 7.4.1.2 A Michell type structure</i>	172
	<i>Example 7.4.1.3 A Shear wall</i>	176
7.4.2	3D Continuous Structures	180

<i>Example 7.4.2.1 A 3D Michell type structure</i>	180
<i>Example 7.4.2.2 A 3D MBB beam</i>	188
7.4.3 Discussions	190
7.5 Conclusions	196
Chapter 8 Conclusions and Recommendations	199
8.1 Conclusions	199
8.2 Recommendation for Further Investigations	205
REFERENCES	207

Introduction

1.1 Structural Optimisation

Structural optimisation is closely related to structural analysis and design. A structure is designed to satisfy various requirements in mechanical, geometrical, manufacturing, functional and aesthetical aspects. At the same time, it is desired that the design be economical. These two aspects of considerations mostly conflict with each other. To find the ‘best’ possible design satisfying prescribed requirements with the minimum amount of material/cost is the main task of structural optimisation.

The traditional design process is a ‘trial-and-error’ one. An initial guess of the design is first given from the intuition and experience of the designer. Then the structural performance is evaluated and checked against the prescribed requirements. An improved design is obtained by attempting to make the response closer to the requirements, followed by re-analysis procedure. This ‘design–analysis–redesign’ routine is repeated until a design satisfying the requirements is achieved. There are a few disadvantages in this routine. First, as the solution is not unique for most design tasks, how good or bad the final design is heavily depends on the designer’s knowledge and experience. Second, although the design and analysis modules can be completed with the computer implementation, there may be not an automatic interface between them and the designer’s interactions play a significant role. This interactive process can be trivial and time-consuming.

Structural optimisation is developed to overcome the above drawbacks. It integrates the analysis and design and the iterative process can be conducted automatically. Several factors have contributed to make this possible. First, the formulation of various methods for computational mechanics, typically, the finite element method (FEM). This has facilitated the numerical simulation and analysis of structure with considerable accuracy and generality. Second, the enhancement of computer power which significantly reduces the computing cost of structural analysis.

Structural optimisation is a broad field and there are different ways to classify it. The conventional classification is the size optimisation, shape optimisation and topology optimisation. Size optimisation is to find the optimal design by modifying the size variables, such as the section properties of a beam and the plate thickness. This is the basic kind of optimisation and most initial research efforts were focused on this sub-field. Shape optimisation is mainly performed on continua where the external boundaries are modified to reach an optimum. Topology optimisation for discrete structures such as trusses and frames is to find the spatial order and connectivity of structural members. For continuum structures, it is to determine both the external and internal boundaries. As the topology of a particular design is unknown *a priori* and may go beyond the designer's experience, size and shape optimisation performed on a fixed topology may be insufficient. At this point, it is necessary to conduct topology optimisation to find the best design.

The earliest interest in structural optimisation may be dated back to 1700s based on the Newton classical mathematics. Systematic studies on this topic started in 1950s and various analytical and numerical methods have been developed. While analytical methods remained to be significant in the theoretical background, various numerical algorithms in the context of powerful and inexpensive computers proved to be efficient and robust, and pointed to the development trend. There are a few features during the course of development. First, optimisation algorithms for computer implementation are well established, among which mathematical programming (MP) and

optimality criteria (OC) are the most widely used ones. Based on the linear programming, non-linear programming algorithms are developed, such as feasible direction (Zoutendijk 1960), gradient projection (Rosen 1961) and generalised geometric programming (CGP) (Avriel and William 1970). As for optimality criteria algorithms, fully stressed design (FSD) (Gellatly and Berke 1971) and optimal layout theory (Prager and Rozvany 1977; Rozvany 1989) are two typical examples. Furthermore, the work on structural optimisation tends to be engineering oriented, e.g. the very early attempt was due to the optimal design of airplane wings. Understandably, the optimisation tool is particularly important for aerospace industries for mechanical and safety considerations. Additionally, many software packages performing structural optimisation were developed and used in practice, such as TSO (Lynch *et al.* 1977) developed by Air Force Wright Aeronautical Laboratories and STARS (Wellen and Bartholomew 1990) by Royal Aerospace Establishment.

It is noted during this development that while the research on size and shape optimisation has reached a mature level, investigations into topology optimisation are more recent due to its inherent difficulties. In topology optimisation, the traditional concept of design variables is not as straightforward as in size or shape optimisation. For skeleton structures, the node co-ordinate is usually chosen as the design variable. The fact that the co-ordinate can be discontinuous precludes the direct use of MP or OC algorithm. For 2D and 3D continua, the co-ordinates of key points of the boundary shape can be the design variable, which is also adopted in the boundary variation approach to shape optimisation. However, the boundary variation approach is inconvenient for topology optimisation as holes/boundaries can be created or eliminated and their dimensions and shapes can be significantly changed. The requirement of mesh re-generation further complicates the topology optimisation. To overcome those difficulties has proposed a ground structure approach. The ground structure is a design domain consisting of a large number of potential elements and nodes. Those potential entities can be present or absent and a sub-domain of optimal element distribution constitutes a solution. In such a setting, topology optimisation poses a typical discrete problem of binary (0 or 1) design variables.

Based on the ground structural approach, there have appeared various methods. Factors considered in classifying those methods can be: First, the treatment of discrete design variable as opposed to the conventional continuous ones, and second, the search direction, whether it being exhaustive search, gradient search or simply based on heuristics. It is noted here that exhaustive search methods like genetic algorithms (GA), despite a few successive applications (Chapman *et al.* 1994), may not be efficient for topology optimisation due to the prohibitively high number of ‘coding strings’. Given the above considerations, methods for topology optimisation can be classed into three groups (Bulman and Hinton 1999), namely, homogenisation based (h-based), evolution based (e-based) and hybrid methods. In the **h-based** method, the discrete problem is transferred to a continuous one, by either introducing microscopically composite material, or employing interpolation functions. The former is represented by the homogenisation design method (Bensøe and Kikuchi 1988) and the latter by Simplified Isotropic Material with Penalization (SIMP) (Zhou and Rozvany 1991). Mathematical programming and optimality criteria algorithms are employed in those methods as solution routines. In contrast, most **e-based** methods directly tackle the discrete problems. Heuristics such as mimicking the biological adaptive growth to reach a fully-stressed design is associated in the initial development. Evolutionary Structural Optimisation (ESO) (Xie and Steven 1997) can be a representative of the e-based group. As this group can generate very sound engineering designs, ‘e’-based can also be understood as ‘engineering’ based, as recommended in the literature (Fuchs *et al.* 2001). **Hybrid** methods are so called because they can have gradients of both h-based and e-based methods. In Constrained Adaptive Topology Optimisation (CATO) (Bulman and Hinton 1999), for example, microstructures are assumed and stress ratio as featured in fully stressed design is used.

Let us further examine the ESO method as mentioned above. The principle of ESO is: in a finite element model of a structure, inefficient elements are removed from a ground structure in an iterative manner so that the residual shape gradually evolves towards an optimum. ESO can be called a hard-kill method, as opposed to the so-called soft-kill

methods, such as cellular automation generation (Inou *et al.* 1994) and Soft Kill Option (SKO) (Mattheck 1997). While the soft-kill criterion is usually based on the stress, ESO has been extended significantly to accommodate problems of a variety of objectives/constraints, such as stiffness/displacement, natural frequency or buckling. In comparison to using a stress ratio in the initial form of ESO, sensitivity analysis is involved in considering the above objectives/constraints. There have been a few variants and improvements of ESO from independent researches, including Reverse Adaptive (RA) (Reynolds *et al.* 1999) and Metamorphic Development (MD) (Liu *et al.* 1999). Based on the similar principle to ESO of stress and/or stiffness criteria, those methods have their own features such as using adaptive mesh and/or defining ‘groups’ of removed and added elements.

A technique called bi-directional ESO (BESO) (Querin 1997) was formulated, which allows elements to be added to the structure. BESO has a few advantages. First, in ESO, as the transition between two generations of designs should be gradual and smooth, the solution can be sensitive to the step size. BESO can alleviate this problem to some extent because it allows those previously deleted elements to be reinstated and new elements to be added. Second, it can be computationally more efficient because the finite element model in BESO can be much smaller than that in ESO.

BESO for stiffness/displacement constraints has been studied by the candidate in a Masters study, which was focused on 2D plane stress problems. It is necessary to extend to 3D continua. There have been limited investigations reported in the literature on 3D topology optimization. Apart from the static problems, the dynamic design is of great significance in many engineering fields such as vibration control and structural aseismic design. ESO and BESO can be extended to address optimisation problems with dynamic requirements.

1.2 Aims and Scope of Investigation

The general aim of the study is to develop ESO/BESO methods to solve the stiffness

(static) and natural frequency (dynamic) optimisation for 2D and 3D continuous structural system.

The specific aims are to:

- Explore the general mathematical representation of the ESO/BESO for continuous structures.
- Construct algorithms to be implemented on PC in conjunction with finite element analysis.
- Investigate general stiffness optimisation using the above mathematics model and computer algorithms.
- Consider specific stiffness optimisation accommodating design dependent loading conditions, which can be due to transmissible loads, surface load and self-gravity.
- Investigate general frequency optimisation considering different objective functions: maximising a single frequency, maximising multiple frequencies and reaching a set of prescribed frequencies.
- Address the repeated/close-spaced frequency problem by modifying the problem statements or sensitivity analysis.
- Solve the optimisation of a prescribed mode shape by using a mode track technique.
- Investigate the ESO/BESO algorithm reliability and stability, i.e. the accuracy of sensitivity analysis and the effect of algorithm parameters.
- Investigate the effect of finite element mesh and propose methods to suppress the mesh dependency.
- Conduct numerical tests and compare results to those obtained by alternative methods.

The scope of the study thus consists of three major parts:

Part 1. Stiffness Optimisation (3D)

Part 2. Natural frequency optimisation (2D, 3D).

Part 3. Numerical aspects of ESO/BESO.

1.3 Statement of Significance

The work in this thesis will improve the theoretical basis of ESO and BESO, further extend its application scope to cover more engineering design requirements, thus facilitate its development into a practical design tool addressing real-life problems in the computer-aided-design context.

As for the ESO/BESO theory, while the uniform stress design is the basic concept of the very early ESO investigation, the extension to the sensitivity analysis criterion can be a significant milestone. The sensitivity analysis for general static and dynamic problems has been a mature topic and well addressed. In the static case, the previous work is mainly focused on the sensitivity of mean compliance with variations in an individual design condition, being it the physical modifications, boundary conditions (e.g. support locations), or load conditions. There is less study on the sensitivity due to combined structural variations, e.g. changes in structural boundaries which subsequently lead to load variations. This will be studied in length as the basis of optimisation involving design-dependent loads. As for the sensitivity of dynamic characteristics, there have been extensive literatures dealing with eigenvalue, eigenvector and dynamic response. The contribution of this thesis lies in developing some simplified yet reliable methods for complicated problems such as repeated and close eigenvalues, or tracking a mode shape of interests.

Another theoretical aspect is that BESO is more than a simple extension of ESO. It is a very promising tool in that it provides the possibility that a structure grows from 'nothing'. It poses more problems, however, such as: 1) By which criterion the structure should 'grow' or 'shrink'; 2) How are its reliability and efficiency compared to ESO, so that a designer can choose a 'better' method for a particular problem. For stress-based problems, the stage of grow/shrink is based on a heuristic rule (Querin 1997; Young *et al.* 1998). For sensitivity based problems on 2D continua, there are some rigorous grow/shrink criteria, as investigated in the candidate's Master's study. For 3D structures, the problem can be more involved, which will be addressed in this thesis.

As for the ESO/BESO scope, the research has been very extensive in terms of structural systems and objective functions/constraints. For 2D and 3D trusses and plate type structures, the primary design requirements can be on the stress, stiffness, or stability, which have been covered in a number of studies (Xie and Steven 1997; Manickarajah 1998; Rong *et al.* 2000b). For 2D and 3D continuous structures, the research status is shown in Table 1.1, where the shaded areas are already covered, and the ticked items are contributions of this thesis.

Table 1.1. ESO/ BESO Research Status on Continuous Structures

Objective functions/constraints		2D Continua		3D Continua	
		ESO	BESO	ESO	BESO
Static	1. Stress based			√ ¹	
	2. Stiffness/Displacement				
	Fixed load condition	√ ¹		√	√
	Varying load condition	√	√	√	√
Dynamic	1. Single frequency		√	√	√
	2. Multiple frequencies	√	√	√	√
	3. Frequency target	√	√	√	√
	4. Frequency of a particular mode	-- ²	--	√	√

1. Based on the previous study, an example or two will be examined.
2. 2D structures have less basic mode shape types (axial, bending, etc) than 3D structures (axial, in-plane bending, out-of-plane bending torsion, etc.), thus only the 3D problem is studied in this category.

Another contribution of this thesis is including the manufacturing constraint. The structural optimisation result can be a design of great performance, but may be too complicated to manufacture. In industries, there is a need to balance the structural and manufacture costs, and the optimisation method developed in this thesis can be a very practical design tool.

Furthermore, a practical design package is to be user friendly. A user of basic structural analysis background should be aware of the impact of parameters input and be advised

of general guidelines. Such guidelines are results of a parameter study in this thesis.

While ESO/BESO is to date an academic code, the work in this thesis will complement the previous research outcome, and is significant in its future development into a commercial design package.

1.4 Layout of the Thesis

The thesis consists of eight chapters. The first two chapters are for introduction and literature review, respectively. The last chapter is for the overall summary. The main body from Chapters 3 to 7 deals with three topics: Chapters 3&4 for stiffness optimisation, Chapters 5 for dynamic problems and Chapters 7&8 for parameter studies and design post-processing. An outline is given as follows.

Chapter 1 discusses the general background of structural optimisation. The aims and significance of the thesis are stated.

Chapter 2 is a literature review on structural optimisation. Analytical methods for optimisation including the differentiation calculus and calculus of variations are briefly introduced. This is followed by a review on numerical methods including the mathematical programming, optimality criteria and genetic algorithms. Methods for shape and topology optimisation of discrete and continuum structures are reviewed in more details. The major part of this chapter is devoted to methods for topology optimisation of continuum structures, such as the homogenisation design method, Simplified Isotropic Materials with Penalization (SIMP), soft-kill methods and hard-kill methods.

Chapter 3 deals with topology optimisation with stiffness requirement for 3D continuous structures using the Evolutionary structural optimisation (ESO) and bi-directional ESO (BESO). The main body consists of sections devoted to the

mathematical basis of ESO (problem statement and sensitivity analysis), computer algorithms and implementations. A number of examples are given and results are compared with available benchmarks. Conclusions are drawn regarding effectiveness and efficiency of the ESO/BESO method.

Chapter 4 is on a special type of stiffness optimisation where a changing loading condition is considered. Three factors can cause such changes. The first is the transmissible loading where the exact load location is not known but only a loading action line is prescribed. The second is the surface loading where the location of loading depends on the outer shape of structures. The third is the inclusion of self-weight in structural analysis. ESO/BESO can be easily adapted to these problems with minor modifications on the problem statement and/or sensitivity calculation. Examples on 2D and 3D are presented.

Chapter 5 is for optimisation considering dynamic respects. The ESO/BESO method is used to address natural frequency optimisation with different objective functions, namely, to maximise a single frequency, to maximise multiple frequencies and to obtain a prescribed set of frequencies. They can be generalised in terms of sensitivity number. Also, three special topics are dealt with including the repeated eigenvalues, closely spaced eigenvalues and tracking a desired mode shape. A range of examples of 2D plane stress and 3D continua are presented to demonstrate the feasibility and effectiveness of the proposed method.

Chapter 6 investigates a number numerical aspects associated with ESO/BESO, including the reliability of sensitivity analysis and parameter studies. Another attempt is on design post-processing.

Chapter 7 deals with optimisation with non-structural constraints. One of many such constraints is the perimeter constraint on the optimal design. The investigation is motivated by reducing the mesh dependency of ESO and BESO algorithms as well as simplifying the design configuration. For 2D structures, the proposed perimeter control

technique can achieve the above objectives. Though mesh independency can be still observed in 3D structures, the perimeter control technique remains its strength of reducing structural configuration.

Chapter 8 draws the conclusions of the investigation of this thesis. Further investigations on this topic are recommended.

Overview of Structural Optimisation

This chapter reviews the development in the field of structural optimisation. Sect. 2.1 presents the basic mathematical formulation of the optimisation problem, on which analytical methods such as differential calculus and calculus of variations are formulated. Numerical methods are reviewed in Sect. 2.2, including the mathematical programming (MP), optimality criteria (OC) and genetic algorithms (GA). While those methods have been readily applied to size optimisation, shape and topology optimisations are more involved and are presented in detail in Sect. 2.3. This section consists of two sub-sections. Sect. 2.3.1 deals with shape and topology optimisation of discrete structures and Sect. 2.3.2 is on continuum structures. In Sect 2.3.2, shape optimisation on continua using boundary variation approach is briefly introduced. The remainder of this sub-section reviews the topology optimisation regarding topology description, design variables and problem statement. Various solution routines are grouped into three groups: those based on homogenisation, evolutionary methods and hybrid methods. Typical methods in those groups are introduced and their strengths and weaknesses are discussed. Towards the end, the application of structural optimisation as an engineering design tool is presented.

2.1 Mathematical Formulation of Optimisation Problems

2.1.1 Mathematic Statement

The optimisation problem can be mathematically interpreted as determining the extremum (usually, the minimum) of functions subject to certain constraints (Haftka and Gürdal 1992), i.e.

$$\text{Minimise } f(\mathbf{x}). \quad (2.1a)$$

$$\text{Such that } g_j(\mathbf{x}) = 0, \quad j = 1, \dots, n_e, \quad (2.1b)$$

$$h_j(\mathbf{x}) \geq 0, \quad j = n_e + 1, \dots, n_g, \quad (2.1c)$$

$$\underline{\mathbf{x}} \leq \mathbf{x} \leq \bar{\mathbf{x}}, \quad (2.1d)$$

where \mathbf{x} is the vector of *design variables* and $f(\mathbf{x})$ is the *objective function*. $g_j(\mathbf{x})$ and $h_j(\mathbf{x})$ are equality and inequality *constraints*, thus the problem is called constrained optimisation. Similarly, problems without constraints are called unconstrained optimisation. Equation (2.1d) is the side constraint where $\underline{\mathbf{x}}$ and $\bar{\mathbf{x}}$ are the lower and upper bounds of design variables.

In structural optimisation, the *objective function* $f(\mathbf{x})$ is usually chosen to be the criterion/criteria representing the structural volume, weight, cost, performance, serviceability or their combinations. *Constraints* $g_j(\mathbf{x})$ or $h_j(\mathbf{x})$ can be imposed on structural behaviour such as stress, displacement or mean compliance. They can also be limitations on the functionality and manufacturing tolerance, such as requirements on the number of structural components or cross-sectional dimensions. *Design variables* are independent quantities which define a structure system and can be modified to obtain an optimal solution.

Structural optimisation can be classed into three types:

Size optimisation: the design variable can be the thickness of plates or shells, cross sectional properties of bars, beams or columns, either being the section area or the moment of inertia, etc.

Shape optimisation: It mainly deals with modification of structural geometry. Geometrical variables can be the coordinates of member joints in discrete structures, the length and location of supports of beam structures and the height of shell structures. Shape optimisation for continuous structures is usually performed by varying existing boundaries.

Topology optimisation: for discrete skeletal structures such as trusses, frames or honeycombs, topology optimisation is also known as layout optimisation. It is used to determine the pattern of member connection as well as the number and spatial sequence of nodes and elements. Both size and geometrical variables can be involved. For continuous structures, the optimal topology design is to find the optimum profile of external and internal boundaries. Topology optimisation is usually accompanied by size and shape optimisations and is the most difficult and challenging task among the three, as will be further discussed in Sect. 2.3.

2.1.2 Analytical Approaches

Differential Calculus

In *differential calculus*, conditions for existence of extreme values are stated as that the first order of derivative of objective functions with respect to the design variable is equal to zero, i.e.

$$\nabla f_i(\mathbf{x}) = 0, \quad i = 1, 2, \dots, n. \quad (2.2)$$

The solution vector $\{x_1, x_2, \dots, x_n\}$ to the system of equations constitutes the extreme points.

The above situation can only be applied to very simple cases of *unconstrained* optimisation. For *equality constrained* optimisation, there are two techniques for deriving the necessary conditions. Firstly, if the constraint equation can be solved to obtain the relationship between dependent design variables, the constrained problems are transformed into unconstrained ones. Secondly, in cases where constraints are implicit functions of design variables, a general method called *Lagrangian multiplier* can be used, i.e. an auxiliary function using the Lagrangian multiplier λ_j is formulated as follows:

$$L(\mathbf{x}, \lambda) = f(\mathbf{x}) + \sum_{j=1}^{n_e} \lambda_j g_j \quad (2.3)$$

with the necessary conditions of an extremum expressed as

$$\begin{aligned} \frac{\partial L}{\partial x_i} &= 0, \quad i = 1, \dots, n, \\ \frac{\partial L}{\partial \lambda_j} &= 0, \quad j = 1, \dots, n_e. \end{aligned} \quad (2.4)$$

Optimisation is to solve the above system of equations with altogether $n + n_e$ unknowns.

The number of Lagrangian multipliers n_e is equal to that of constraints.

For a general class of problems with both equality and inequality constraints, the necessary condition for an extremum is summarised as the Kuhn-Tucker conditions, which can be expressed in a simple form as:

$$\nabla f_i(\mathbf{x}) + \sum_{j=1}^{n_e} \lambda_j \nabla g_j(\mathbf{x}) + \sum_{j=n_e+1}^{n_e} \lambda_j \nabla h_j(\mathbf{x}) = 0, \quad i = 1, 2, \dots, n, \quad (2.5)$$

The complementary slackness conditions are needed to consider in the above equation and the Lagrangian multipliers for inequality constraints λ_j ($j = n_e + 1, \dots, n_g$) are required to be greater than zero.

Calculus of Variations

It is a generalisation of the differentiation theory. It deals with optimisation problems having an objective function f expressed as a definite integral of a functional F defined by an unknown function y and some of its derivatives (Haftka and Gürdal 1992).

The objective function can be defined as

$$f = \int_a^b F(x, y, \frac{dy}{dx}, \dots, \frac{d^n y}{dx^n}) dx, \quad (2.6)$$

where y is directly related to the design variable x . Optimisation is to find the form of function $y = y(x)$ instead of individual extreme points.

Analogous to the case of differential calculus, the necessary condition for an extremum is the vanish of the first order of variation, i.e.

$$\delta f = \int_a^b \left(\frac{\partial F}{\partial y} + \frac{\partial F}{\partial y'} + \dots \right) dx = 0. \quad (2.7)$$

Applying boundary conditions, after arrangement, equation (2.7) can be finally expressed in form of *Euler-Lagrange Equation* as follows:

$$\frac{\partial F}{\partial y} - \frac{d}{dx} \left(\frac{\partial F}{\partial y'} \right) = 0, \quad (2.8a)$$

with the natural boundary conditions ($x=a$ and $x=b$):

$$\left[\frac{\partial F}{\partial y'} \right]_{x=a} = 0, \text{ and } \left[\frac{\partial F}{\partial y'} \right]_{x=b} = 0 \quad (2.8b)$$

The differential calculus and calculus of variations emphasize the analytical exploration of optimisation problems. Their earliest application to structural design might be due to Maxwell (1895) in designing the least weight layout of frameworks. The later research on the optimal topology of trusses by Michell (1904) was well known as Michell type structures. Except for those results, the application of classical analytical methods is very limited because of the mathematical complexity and impractical idealisations. Nonetheless, analytical methods are of fundamental importance in that they explore the mathematical nature of optimisation and provide the lower bound optimum against which the results by alternative methods can be checked.

2.2 Basic Numerical Algorithms

2.2.1 Mathematical Programming

Mathematical programming (MP), initially formulated in 1950s (Heyman 1951), can be the most popular optimum search technique. It starts from an initial design defined by a selected set of design variables. An improved design is searched in the direction of gradient of behaviour functions in the form of Lagrangian auxiliary functions. At each step, the value of behaviour function of a new structural design is evaluated. Design variables are modified gradually until the objective function achieves convergence.

At the earlier stage, the mathematical programming method is limited to linear problems where the objective functions and constraints are linear functions of design variables. In 1960s, *nonlinear programming* (NLP) was integrated with finite element analysis as first suggested by Schmit (1960). Since then, numerous algorithms of nonlinear programming techniques have appeared such as feasible direction (Zoutendijk 1960),

gradient projection (Rosen 1961), penalty function methods (Fiacco and McCormick 1968) and generalised geometric programming (CGP) (Avriel and William 1970). Each technique can suit a certain type of problems. For example, CGP combined with a monomial treatment can handle problems with a large number of mixed equality /inequality constraints (Burns 1987).

2.2.2 Optimality Criteria

Optimality criteria (OC) method was analytically formulated by Prager and co-workers (Prager and Shield 1968; Prager and Taylor 1968). It is then developed numerically and becomes a widely accepted structural optimisation method (Venkayya *et al.* 1968). It also adopts concepts of objective functions and constraints and defines *a priori* criterion. The optimum is achieved when the criterion is satisfied. Defining such a criterion may take advantage of special design conditions and engineering judgement.

In general, most of OC algorithms consist of four fundamental steps: structural analysis, stating criteria, scaling and resizing.

The Kuhn-Tucker condition constitutes the optimality criteria:

$$\sum_{j=1}^n e_{ij} \lambda_j = 1, \quad i = 1, 2, \dots, n, \quad (2.9)$$

Where $e_{ij} = \frac{\partial g_j}{\partial x_j} / \frac{\partial f}{\partial x_i}$, is the Lagrangian energy density, and λ_j is the Lagrangian multiplier. Equation (2.9) means that in an optimal design, the weighted sum of Lagrangian energy density is the same for all structural elements. The equation can be transferred to a recurrence formula to resize the design variable.

The mathematical programming and optimal criteria methods are the two best established and widely accepted optimisation techniques. Mathematical programming is

featured by its mathematical elegance and generality. It is less problem specific and is particularly suitable for problems of multiple constraints problem. However, the computational cost increases dramatically when a large number of constraints or design variables are considered. This somehow limits its application to large size structures. In contrast, optimality criteria method is less size dependent and offers a high convergence speed. Although the convergence may become unstable, especially in the case of inappropriately defined initial designs, the relatively low computational cost of OC makes it particularly appealing for large structural systems.

These two methods are reconciled, to a large extent, by formulating *dual MP* methods (Fleury 1979), which can be interpreted as *generalised OC* methods. In dual methods, the constrained primary minimisation problem is transformed into the maximisation of a quasi-unconstrained dual function which is only related to the Lagrangian multipliers. When the primal problem is convex, explicit and mathematically separable, use of dual methods is very effective by introducing some intermediate design variables. Based on the use of reciprocal design variable, the convex linearisation method (CONLIN) (Fleury and Braibant 1986) was well developed, and was later generalised as the method of moving asymptotes (MMA) (Svanberg 1987). As dual methods search the optimum direction in the space of Lagrangian multipliers instead of that of the primal design variables, it can save considerable computing efforts when the number of constraints is smaller than that of design variables.

2.2.3 Genetic Algorithms

Genetic algorithms (GA), as originally developed in 1970s (Holland 1975), has been extended to solve the structural optimisation problems (Goldberg 1989). Its principle uses Darwinian's theory of survival of the fittest and adaptation. The procedure consists of reproduction, crossover and mutation. In the beginning, an initial population of designs (individuals) is randomly created, with design variables represented by a code of bit strings. The fitness of each individual is evaluated according to a fitness function. Those fittest members are allowed to reproduce and cross among themselves, resulting

in a new generation with member having higher degree of most favourable characteristics than the parent generation. This process repeats until the best individual of the population reaches a near-optimum solution.

Genetic algorithms may not be as efficient as traditional MP or OC methods because they are quite computationally intensive. Nonetheless, they still serve as reliable and robust techniques for their merits. Compared to the gradient-based search methods, genetic algorithms search the solution more extensively in that it involves a set of candidate solutions (individuals). They work on the objective function itself rather than its derivatives and is more likely to converge to a global optimum. Furthermore, genetic algorithms transfer design variables into a code representation, typically, into a binary bit-string, which is integer in nature. Therefore, it is highly potential for problems involving a mix of continuous, discrete and integer design variables, such as optimisation of composite structures (Nagendra *et al.* 1993; Le Riche and Haftka 1994).

When using the above MP, OC and GA algorithms to perform *size optimisation*, i.e. changing the size variables, aspects as to design variable, objective and constraints poses no particular problems. Indeed, size optimisation has been well addressed and reached a mature level, both in research and industrial applications. Recently, there has been increasing interest in shape and topology optimisation and this is further discussed in the following sections.

2.3 Current Methods for Shape and Topology Optimisation

Compared to size optimisation, shape and topology optimisations are more complicated due to difficulties associated in parameterising the optimisation problems. The design variable for describing the geometry or topology is not straightforward. Also, the variable may not be explicit in expressing the objective function and constraint. In this section, methods are reviewed on optimisation of discrete structures and continuum structures.

2.3.1 Layout Optimal Design for Discrete Structures

Topology optimisation for discrete structure is referred to as optimal layout design. The topic has its origin in Michell's least weight design of truss structures (Michell 1904). His work has been further developed by Prager and Rozvany and the results are well known as the layout theory (Prager and Rozvany 1977; Rozvany 1989). A survey on this topic is give by Topping (1993).

In layout optimisation, there are size variables (the section property) and geometry variables (e.g. the coordinator of structural joints). In the *geometry approach* (Schmit 1960), the number of joints and connecting members is fixed unless some joint coalesce leads to change in the structural configuration. As the mixed design variables can be of magnitude of rather different orders, it may cause difficulties in overall convergence. This leads to the formulation of the *hybrid approach* (Vanderplaats and Moses 1972). The size and geometrical variables can be divided into two design spaces and accordingly, there are two steps in updating design variables.

The most recent approach might be the *ground structural approach*. A ground structure consists of a dense set of nodes and a large number of potential connections between those nodes. The number and position of nodes are fixed while the number and size of connecting elements are altered. Size variables are still continuous, but if the section area of some elements reduces to zero during optimisation, these elements are deleted from the structure and the structural topology changes accordingly.

2.3.2 Shape and Topology Optimisation for Continuous Structures

2.3.2.1 Boundary variation approach to shape optimisation

The structural shape boundary, either external or internal, can be represented by parameters, and the shape optimisation is described by moving the boundary. There are many literatures on shape optimisation regarding the mathematical model, description of

boundary shapes, generation of finite element mesh and solution strategies (Bennett and Botkin 1986; Haftka and Grandhi 1986).

The description of boundary shapes is essential to the boundary variation approach. There are several ways to represent the boundary, such as the boundary nodes, polynomials and splines. In the survey by Ding (1986), different ways are compared in respects of design variable selection, numerical accuracy and optimal shape. For the numerical implementation of the boundary variation approach, a capability of automated mesh refinement is indispensable. The refinement can be undertaken either globally by re-dividing the whole structure or locally by introducing additional elements or increasing the order of finite elements.

The above boundary variation method only modifies structural boundaries which are existing. It is not able to remove an existing boundary or create a new one, thus precludes changes in the connectivity of the structural geometry. The optimal design has the same topology as the initially given topology, which somehow restricts the optimal solution. In fact, any fine tuning of the structural boundary cannot offset an improperly defined topology.

In topology optimisation, the topology is not known *in prior*, but is allowed to change during the solution procedure. The final design may be significantly different from the initial guess. Topology optimisation can generally produce designs of improved performance and lower cost than the shape optimisation.

2.3.2.2 Ground structure approach to topology optimisation

Topology optimisation has been a topic of extensive research in the last two decades. While algorithms such as mathematical programming and optimal criteria are well developed, the complexity in topology optimisation firstly lies in the description of the topology and definition of design variable. Use of parameterised geometry as in the boundary variation approach is not adequate because there are boundaries or holes of

different shape, dimensions and numbers. For this limitation, methods for topology optimisation are largely based on the concept of a ground structure.

In a continuum setting, let Ω be the given candidate design domain consisting of the loading and displacement boundary conditions. The topology optimisation consists of finding the sub-domain Ω_s of Ω , with the prescribed volume V^* in which a given objective function f is extremised. In other words, the connectedness, the shape and number of holes are to be decided in the design domain. If one defines the material density as the design variable, the optimisation problem can be written as

$$\text{Minimise } f(\rho). \tag{2.10a}$$

$$\text{Subject to } g = \int_{\Omega} \rho \, dx \leq V^*, \tag{2.10b}$$

$$\rho(\mathbf{x}) = 0 \text{ or } 1, \mathbf{x} \in \Omega. \tag{2.10c}$$

In a finite element model of the continuum, the density at each node is taken as the design variable, and the problem is translated to:

$$\text{Minimise } f(\rho). \tag{2.11a}$$

$$\text{Subject to } g = W^* - \sum_{i=1}^n \rho_i x_i = 0, \tag{2.11b}$$

$$\rho_i \in \{0,1\}, \quad i = 1, \dots, n. \tag{2.11c}$$

The optimisation problem is thus intrinsically discrete. A natural way to solve it is to use the genetic algorithms (GA) as the binary design variable is analogous to the 0-1 coding. There are some successful examples, such as optimising of 2D continua (Chapman *et al.* 1994). However, in an exhaustive search method, the scale of the problem solved is limited by the high computing demands. In fact, methods based on a limited search direction (e.g. gradient direction) are more practical and popular.

Alternatively, the search can be based on heuristics, e.g. stress ratio as adopted in practical design routine. Those methods can be classified into three groups (Bulman and Hinton 1999):

- 1) Those based on the homogenisation theory, or h-based, typically represented by the homogenisation (Bendsøe and Kikuchi 1988) method and Simplified Isotropic Material with Penalization (SIMP) (Zhou and Rozvany 1991). In these methods, the discrete optimisation problem is transferred to a continuous one, by either introducing micro-structures or assuming continuous densities and interpolation function.
- 2) Those based on evolution, or e-based, which are initially developed from the heuristic concept of fully stressed design (FSD). A design of uniform stress can be evolved by gradually ‘killing’ elements of low stress in hard kill methods such as ESO (Xie and Steven 1993), and in soft-kill methods such as adaptive biologic growth (Mattheck 1997). While the soft-kill methods focus on stress-based optimisation, ESO has been significantly extended to accommodate other design objectives and constraints. Sensitivity analysis rather than stress ratio is used as the evolution criteria.
- 3) Hybrid methods, which shares characteristics of the above two methods, such as the Constrained Adaptive Topology Optimisation (CATO) (Bulman and Hinton 1999). The algorithm has the same feature of stress ratio as in the e-based methods, but may also involve microstructures as in the h-based methods.

The first two groups form the base of structural topology optimisation and the remainder of this section reviews typical methods in these groups.

Homogenisation Design Method

This method assumes that the continuum structure includes materials with periodic, perforated microstructures. There are many types of microstructures, such as a square cell with square hole, a rank-1 layered material and a rank-2 layered material. The homogenisation theory (Babuska 1976 and 1977) as used for composite material is applied to compute the material properties, e.g. elasticity tensor. The design variable used here is the microstructure orientation and density which are calculated from microstructure geometries.

Use of continuous density means that there are three phases of material in the structure: solid material (1), void (0) and intermediate material (0~1). It is necessary to exclude the intermediate material and force a manufacturable design of 0-1 density. Techniques for suppressing the chattering design can be either introducing *a priori* restriction on the microstructures (Suzuki and Kikuchi 1991) or imposing *postiori* penalty on the intermediate value of material density (Allaire and Korn 1993).

The homogenisation method has been used successfully since its numerical implementation first presented by Bendsøe and Kikuchi (1988). It has been extended to optimisation under multiple loads (Díaz and Bendsøe 1992) and design of compliant mechanism (Ananthasuresh *et al.* 1994; Saxena and Ananthasuresh 1998). In structural dynamic design, the method has addressed the eigenvalue problems (Tenek and Hagiwara 1993; Ma *et al.* 1995), structural harmonic response (Ma *et al.* 1993), transient response (Min *et al.* 1999), and unified static and dynamic designs (Min *et al.* 2000). Apart from 2D problems, 2D plate/shell microstructure and 3D microstructure have been examined (Kikuchi *et al.* 1991; Díaz and Lipton 1997; Olhoff *et al.* 1998). A full presentation and detailed bibliographies can be found in books on this topic (Bendsøe 1995; Hassani and Hinton 1999).

Simplified Isotropic Material with Penalization (SIMP)

This method transfers discrete variables to continuous ones by introducing interpolation functions (Bendsøe 1989; Zhou and Rozvany 1991). The continuous variables are often

interpreted as material densities ρ . Physical quantities, say, the elasticity tensor E can be expressed as:

$$E(\rho) = \rho^P E_0, \quad (2.12)$$

where E_0 is the elasticity tensor of the fixed material and P is some chosen power. Unlike in the homogenisation method where ρ corresponds to a certain microstructure, the density here is considered rather as a programming strategy than a realistic material type. For this reason, the SIMP method has been previously regarded as an ‘artificial’ material model. However, it has been proved recently that the approach can be physically permissible if the power satisfies simple conditions (Bendsøe and Sigmund 1999), e.g. $p \geq 3$ for Poisson’s ratio equal to $\frac{1}{3}$.

By using a power greater than one, the stiffness at an intermediate density is penalised in that a certain amount of material gives less than proportional stiffness (as $\rho \leq 1$). The power has significant effects on the solution. A reasonable range can be 1.2~4.0. By increasing the value, the penalty on the intermediate density becomes heavier which leads to a more distinct black-and-white topology. Also, the value of the penalty exponent can be varying during iterations and this technique is called the continuation approach (Jog 1993). Theoretically, a sufficiently high value of P steers solutions to discrete 0-1 values. In practice, alternative strategies are used in SIMP to obtain a black-and-white topology, such as the filter technique (Sigmund 1994) and perimeter control (Haber *et al.* 1996). A survey on SIMP is given by Sigmund and Petterson (1998).

Soft Kill Methods:

There are various heuristically based methods for topology optimisation using the concept of ‘soft kill’. The objective is normally a fully stressed, or uniform stress design. This design is obtained by strengthening the over-stressed part and decreasing the under-stressed part, which to some extent mimics the adaptive biological growth. In the soft kill option (SKO) (Mattheck 1997), the Young’s modulus E is adjusted at each

iteration by setting the value of the element stress. This means that the stronger part will sustain more loads, and the weaker part will become even weaker and eventually be 'killed'. Similarly, in the cellular automation generation method (Inou *et al.* 1994), elements of low elasticity modulus are gradually killed by applying some 'birth-and-death' rule.

Hard Kill Methods:

In the above methods, the discrete problem of topology optimisation is replaced with some continuous approach, by either heuristic rules or some more mathematically rigorous approaches. In contrast, hard kill methods direct deals with the 0-1 discrete variable.

● *Evolutionary Structural Optimisation (ESO)*

It is based on the concept that by systematically removing inefficient materials from the structure, the residual shape evolves toward an optimum (Xie and Steven 1993). There are two kinds of removing criteria, which can be based on a certain average stress or on the sensitivity number. The former was the original form of ESO and the latter is a significant extension.

When using the *stress* as design criteria, a cut-off element stress is defined as the reject ratio (RR) times the maximum stress. Elements with stress lower than the cut-off stress (i.e. $\sigma_e \leq RR_i \sigma_{\max}$, where i is the iteration step) are removed. This procedure repeats until there are no elements satisfying the inequality. This means that the cut-off stress should be increased, and the removal ratio is updated to $RR_{i+1} = RR_i + ER$ where ER is the evolution ratio. By this procedure, the stress distribution in the structure becomes more uniform.

There are a few variants in the stress-based approach, such as:

- *Nibbling ESO*: elements can only be nibbled away from the structural boundary and thus no inner cavity is produced. The structure evolves to a shape of uniform stress.

- *Reduction of stress concentration*: shapes of cut-out, hole, joint, etc. are optimised in order to reduce the maximum stress.
- *Thermal stress optimisation*: to obtain the optimum design of uniform stress under the thermal load conditions (Li *et al.* 1997).
- *Elastic contact*: the contacting profile of several separate bodies is optimised to reduce the maximum contact stress (Li *et al.* 1998).
- *Nonlinear problems*: structures with material and geometric nonlinearities are investigated where the strain energy density is used as the evolution criterion (Querin *et al.* 1996).

In the class of ESO based on the *sensitivity number*, the element removal is based on the value of element sensitivity, defined as the change in objective functions/constraints as a result of element to be removed. It is calculated by structural sensitivity analysis on the finite element model, such as the mean compliance sensitivity and eigenvalue sensitivity. This means that the general solution routine of ESO can be applied to problems of different objectives/constraints. Indeed, the range of problems solved by ESO includes the stiffness/displacement (Chu 1997), natural frequency (Xie and Steven 1994), structural vibration (Rong *et al.* 2001a) and structural buckling (Manickarajah *et al.* 1998). Furthermore, different structural systems have been accommodated including 2D and 3D discrete structure, 2D plate and 2D and 3D continuum. It is also noted that size, shape and topology optimisation can be addressed respectively or simultaneously.

One improvement of ESO is its extension to bi-directional ESO (BESO). This is to allow for both element removal and addition (Querin 1997). It has the advantage of correcting some prematurely removed elements or admitting new elements. As such, it can start from a small initial design instead of an over-sized ground structure. This can save computing cost of finite element analysis.

To include non-structure constraint is a recent development of ESO/BESO. The ICC (intelligent cavity control) method can effectively control the number of cavities in structures and reduce the structural complexity (Kim *et al.* 2000). The structural

complexity can be alternatively controlled by bounding the structural perimeter and this is one topic of this thesis.

- *Reverse Adaptivity (RA)*

The method is based on the same principles as ESO of stress criteria, i.e. removal of low-stress elements (Reynolds *et al.* 1999). Its added feature is that procedures of finite element subdivision and mesh refinement are involved during evolution. The term 'reverse' is used because the subdivision is carried out in the element of low stress element, as opposed to the conventional finite element adaptivity in region of high stress. After each finite element analysis, a certain averaged stress is calculated at each element. The total elements are sorted in a stress-ascending order until the r percent of the material is reached and the corresponding stress is the 'cut-off' stress. The elements with stress smaller than the cut-off stress are then subdivided. The subdivision is based on the element edge length of evolving boundary which is calculated from the area of the current design and a user-specified number of elements. Take a triangular element for example, the two element bisection algorithms are adopted for subdivision. The structure is re-analysed based on the refined model and low stressed elements are re-identified and removed.

Use of an adaptive mesh has a few advantages over the ESO method. Firstly, the mesh refinement helps to increase the accuracy of structural response calculation. Although the structure becomes smaller and smaller during evolution, RA ensures that there are sufficient number of elements to represent the structure. Furthermore, one can start with a relatively coarse mesh and then successively refine it. This means a much smaller scale of finite element problems than simply defining a fine mesh from the out-set. Additionally, the element refinement results in a fairly smooth structural boundary which make the design highly practical.

The RA algorithms can be semi-automatic or fully automatic. The former includes the Interactive Design Refinement procedure (IDR) (Christie *et al.* 1998). It mainly involves plotting the stress contour, then defining the structural boundary and remeshing

within it. These procedures are conducted automatically in the fully automatic RA. It has the added capability of judging and handling structural integrity and maintaining structural symmetry. The most recent improvement in RA is introducing material addition procedure and this technique is called evolutionary material translation (EMT) (Reynolds *et al.* 2001). It is similar in principle to BESO but possesses the advantages of RA. Additionally, in the ground structure, as the solution is a sub-domain of the ground structure, it can be non-optimal if the ground structure is under-defined. However, the design domain in EMT can be unbounded instead of being confined to the ground structure. This reduces the dependency of solutions on the initial structural definition.

- *Metamorphic Development (MD)*

The basic idea of ‘development’ or evolution is same as ESO/BESO for stiffness optimisation (Liu *et al.* 1999). It is characterised by the element modification strategy. Firstly, the element efficiency is judged by both the stress and strain energy. Secondly, instead of removing or adding a single element, the modified entities are in groups. Elements are added around some types of ‘growth cone’, defined according to the stress/strain energy distribution pattern. Typically, the added element group consists of a series of rectangular elements in the middle and triangular elements at ends (i.e. the so-called ‘bus’ pattern). This helps to fillet or align the structural boundary thus reduces the jag-saw feature. Like the EMT method, MD can use an unbounded design domain.

For the above-mentioned methods for topology optimisation, each has its strength and weakness. The homogenisation based methods are more mathematically rigorous with issues regarding the existence of solution and convergence well addressed. As the element material is orthotropic, the topology can form toward the lines of the force transmission and the convergence can be rapid. The disadvantage is that more design variables are involved. An element with a rectangular void, for example, has two void dimension variables and one orientation angle variable. In contrast, SIMP uses only one design variable, i.e. material density. This also makes SIMP more general in implementation.

Although evolution-based method, typically ESO, was initially based on heuristics for stress-related problem, sensitivity analysis and gradient search form indispensable features for other problems. The strength of these methods is that they generate more appealing engineering designs. To relate the structural optimisation and engineering design practice, the common design stage of conceptual-preliminary-detail stage can correspond to the topology-shape-size optimisation. Topology optimisation to yield the best conceptual design is at a critical phase. The optimal topology, which may not be unique in most cases, should have such features as being easy to be interpreted for detailed structural sizing. This is a feature of the evolution-based methods as design is distinctly black-and-white. In the meantime, as for the various design requirements, the ESO/BESO method has a systematic routine, which is easy to understand and implement.

To date, various computer packages for structural optimisation have been developed. A certain optimisation algorithm can be embedded in some commercial fine element analysis packages such as *ASPTROS*, *Genesis*, *NASTRAN* and *ANSYS*. There are also specific packages with more sophisticated functions of size, shape and/or topology optimisation such as *Reshape*, *OptiStruct* and *HyperShape*. This is a natural outcome of the extensive research in these fields. Structural optimisation, developed from an academic topic, is gradually establishing itself as a design tool serving the practical design of industries and engineering.

ESO and BESO for Stiffness Optimisation

This chapter presents the basic concept and implementation of the ESO and BESO methods. The theoretical aspects are first discussed including the problem statement, optimal criteria and sensitivity analysis. Then procedures for computer implementation are presented and applied to a number of 3D examples. Results are discussed and compared in terms of optimal design and computational efficiency. Although this chapter is focused on stiffness optimisation of 3D structures, the fundamental idea and notations can be easily generalised for a wide range of problems, and employed in chapters followed with only minor modifications.

3.1. Mathematical Background

3.1.1 Problem Statement

From the elementary continuum mechanics, for an admissible displacement field, the potential energy in a linearly elastic body can be expressed as (Cook *et al.* 1989)

$$\Pi = \int \frac{1}{2} \boldsymbol{\varepsilon}^T \mathbf{E} \boldsymbol{\varepsilon} dV - \int \mathbf{u}^T \mathbf{F} dV - \int \mathbf{u}^T \mathbf{T} dS - \mathbf{D}^T \mathbf{Q}, \quad (3.1)$$

where

- $\boldsymbol{\varepsilon}$ = the strain field.
- \mathbf{E} = the material property matrix.
- \mathbf{u} = the displacement field.

- F** = body forces.
T = surface tractions.
D = discrete displacement of the structure.
Q = discrete external loads.
 V, S = volume and surface area of the structure, respectively.

Using the finite element procedure, Eq. (3.1) becomes

$$\Pi = \frac{1}{2} \mathbf{D}^T \mathbf{K} \mathbf{D} - \mathbf{D}^T \mathbf{P}, \quad (3.2)$$

where **K** is the global stiffness matrix, **P** is the assembled load matrix, consisting of original nodal loads and the contribution of body forces and surface tractions, i.e.

$$\mathbf{P} = \mathbf{Q} + \mathbf{R}, \quad (3.3)$$

where $\mathbf{R} = \sum_{i=1}^{i=n} \mathbf{r}_e^i$

and $\mathbf{r}_e = \int_{V_e} \mathbf{N}^T \mathbf{F} dV + \int_{S_e} \mathbf{N}^T \mathbf{T} dS,$

where **N** is the shape function matrix, V_e and S_e are the element volume and area, respectively, and n is the total number of structural elements.

The static equilibrium equation is:

$$\mathbf{K} \mathbf{D} = \mathbf{P}.$$

To be consistent with the conventional notations in this thesis, we replace **D** with **u**, i.e.

$$\mathbf{K} \mathbf{u} = \mathbf{P}, \quad (3.4)$$

where **u** is the *nodal* displacement vector (rather than the continuous displacement field in Eq. (3.1)).

The overall stiffness of a structure can be evaluated by the mean compliance, i.e. the external work of loads \mathbf{P} done with the real displacement \mathbf{u} . Maximising the structural stiffness is equivalent to minimising the mean compliance. Therefore, the problem statement of stiffness optimisation can be written as

$$\text{Minimise } f = C(\mathbf{x}) = \mathbf{P}^T \mathbf{u}. \quad (3.5a)$$

$$\text{Subject to } g = W^* - \sum_{i=1}^n W_i x_i = 0, \quad (3.5b)$$

$$x_i \in \{0,1\}. \quad (3.5c)$$

Where W_i is the weight of an individual element and W^* the prescribed total structural weight. The binary design variable $\{0,1\}$ declares the absence (0) or presence (1) of an element.

Note that

$$\mathbf{P}^T \mathbf{u} = \mathbf{u}^T \mathbf{K} \mathbf{u}. \quad (3.6)$$

The mean compliance can be written as the summary of contribution of each single elements as follows:

$$C = \mathbf{u}^T \mathbf{K} \mathbf{u} = \sum_{i=1}^n (\mathbf{u}_i^T \mathbf{K}_i \mathbf{u}_i) = \sum_{i=1}^n 2C_i, \quad (3.7)$$

where \mathbf{K}_i and \mathbf{u}_i are the stiffness matrix and displacement vector of the i th element.

$C_i = \frac{1}{2} \mathbf{u}_i^T \mathbf{K}_i \mathbf{u}_i$ is the element strain energy.

3.1.2 Evolution Criteria

3.1.2.1 Sensitivity analysis

In evolution algorithm, the evolution proceeds in the gradient direction and thus requires the sensitivity of the objective function and constraints. A presentation of sensitivity analysis is given in this section based on which the optimality criteria are derived.

The mean compliance is

$$C = \mathbf{P}^T \mathbf{u}. \quad (3.8)$$

Supposing that there is a change in structure, the resultant change in the mean compliance is

$$\Delta C = \mathbf{P}^T \Delta \mathbf{u} + \Delta \mathbf{P}^T \mathbf{u}. \quad (3.9)$$

So far we assume that structural modification has no effect in loading conditions, i.e.

$\Delta \mathbf{P} = \{0\}$, thus

$$\Delta C = \mathbf{P}^T \Delta \mathbf{u}. \quad (3.10)$$

From the equilibrium equation together with the assumption of $\Delta \mathbf{P} = \{0\}$, it follows

$$\Delta \mathbf{K} \mathbf{u} + \mathbf{K} \Delta \mathbf{u} = 0. \quad (3.11)$$

Pre-multiplying the above by $\mathbf{P}^T \mathbf{K}^{-1}$ (i.e. \mathbf{u}^T) leads to

$$\mathbf{P}^T \mathbf{K}^{-1} \mathbf{K} \Delta \mathbf{u} = -\mathbf{u}^T \Delta \mathbf{K} \mathbf{u}. \quad (3.12)$$

Referring to equation (3.10), the derivative of the mean compliance is

$$\Delta C = \mathbf{P}^T \Delta \mathbf{u} = -\mathbf{u}^T \Delta \mathbf{K} \mathbf{u}. \quad (3.13)$$

Supposing that the modification is due to removal of an element, i.e., $\Delta\mathbf{K} = -\mathbf{K}_i$, Eq. (3.13) becomes

$$\Delta C = \mathbf{u}_i^T \mathbf{K}_i \mathbf{u}_i = 2C_i, \quad (3.14)$$

where all entities are at an element level.

3.1.2.2 Optimal criteria

The Lagrangian function for problem (3.5) is

$$\begin{aligned} L(\mathbf{x}, \lambda) &= f - \lambda g \\ &= C(\mathbf{x}) - \lambda(W^* - \sum_{i=1}^n W_i x_i), \end{aligned} \quad (3.15)$$

where λ is the Lagrangian multiplier.

The optimality criterion for problem of continuous design variables is

$$\frac{\partial L}{\partial x_i} = \frac{\partial f}{\partial x_i} - \lambda \frac{\partial g}{\partial x_i} = 0, \quad i = 1, \dots, n. \quad (3.16)$$

However, as the design variable is discrete in ESO/BESO, the derivative in equation (3.16) is replaced with the function increment, i.e.

$$\Delta L_i = \frac{\partial L}{\partial x_i} \Delta x_i = \frac{\partial f}{\partial x_i} \Delta x_i - \lambda \frac{\partial g}{\partial x_i} \Delta x_i = 0, \quad i = 1, \dots, n. \quad (3.17)$$

Recalling Eq. (3.14):

$$\frac{\partial f}{\partial x_i} \Delta x_i = \Delta C = 2C_i, \quad \text{and} \quad (3.18a)$$

$$\frac{\partial g}{\partial x_i} \Delta x_i = -\Delta W = W_i, \quad i = 1, \dots, n. \quad (3.18b)$$

Substituting Eqs. 3.18(a) & (b) into Eq. (3.17) results in

$$2C_i - \lambda W_i = 0, \text{ or} \quad (3.19)$$

$$\lambda = \frac{2C_i}{W_i}.$$

Eq. (3.19) is the optimality criterion on stiffness of the evolutionary algorithm. It is consistent with the well-known condition regarding the overall stiffness optimisation. That is, at an optimum the ratio of element strain energy to its weight is the same for all structural elements (Venkayya *et al.* 1973; Morris 1982). In other words, the final optimum is an idealised status of uniform strain energy with respect to the element weight. To reach or approach such a state requiring re-distributing the strain energy by strengthening areas of high strain energy and/or shrinking areas of low energy. As a special problem of distinct design variable in evolutionary method, this is simply a procedure of adding and/or removing elements according to its strain energy/weight ratio. Using Eq. (3.14), Eq. (3.19) can be re-written as

$$\alpha_i = \frac{\mathbf{u}_i^T \mathbf{K}_i \mathbf{u}_i}{W_i}, \quad (3.20)$$

which is defined as *element sensitivity number*. It is the indicator of element efficiency.

3.2 Implementation of ESO and BESO

3.2.1. Procedures of ESO

In brief, the evolution procedure consists of two modulus, namely, structural analysis and structural modification. They are performed in an iterative manner. The structural modification module is to implement functions of sensitivity analysis as presented above and of removing and/or adding elements. In ESO, only removal procedure is employed and it proceeds as follows.

1. For the given boundary and loading conditions, define the ground structure.
2. Perform FE analysis to obtain information on displacement and/or stress.
3. Calculate the sensitivity number α_e for all elements from Eq. (3.20).
4. Remove elements of the smallest α_e .
5. Repeat Steps 2 to 4 until the structure reaches the prescribed weight.

In the above procedure, the evolution starts with a ground structure which includes all potential elements and nodes. It is a fixed mesh as no new nodes (d.o.f.s) are introduced during evolution, thus it is basically a large, finely-discretised domain. The ground structure has effects on the final design and this aspect will be discussed in Chapter 7.

As for step 4, the sensitivity analysis assumes that changes in structural properties and response are small. Therefore, only a very small fraction of elements are modified and it is determined by a parameter called “modification ratio” (MR) and a reference structure. For example, if $MR=1\%$ is assumed and the current structure with 1000 elements is taken as the reference, totally $1000 \times 0.01 = 10$ elements will be removed at the current iteration. A reference structure can be either the current structure or the initial structure.

3.2.2. Procedures of BESO

BESO involves an element addition procedure. It was originally intended to address the following two problems: to recover prematurely removed elements and to save computational time. These two advantages have been observed in most, if not all, of the applications in 2D problems (Querin 1997; Querin *et al.* 1998; Yang *et al.* 1999a). More recent use of BESO has the added advantage of addressing numerical instability and Chapter 7 is to discuss this in detail.

The procedure of BESO is as follows:

1. Within a ground structure, define the *initial structure*. This can be a very small portion of the design domain which consists of the loading and boundary conditions.
2. Perform FE analysis.
3. Calculate the sensitivity number α_e from Eq. (3.20).

4. Remove elements of the smallest α_e and at the same time, add elements around those of the highest α_e .
5. Repeat Steps 2 to 4 until the structure reaches the prescribed weight.

There are two other parameters involved in BESO, namely, *Addition Ratio* (AR) and *Stage Ratio* (SR). Using the previous example and we define $AR=0.3$, then there are totally 10 elements modified, among which $10 \times 0.3=3$ are added and the other seven removed. It is obvious that $AR<0.5$ will see structure “shrinking” and $AR>0.5$ growing.

As the initial structure is normally very small compared to the target weight, BESO proceeds in such a way that a structure first grows up to a certain point before it decreases, i.e. $AR>0.5$ at early stages then $AR<0.5$. There are two ways to decide this turning point.

The first is to define a Performance Index (PI) and the turning is decided at the point when PI reaches a maximum. This measure has been used for 2D plane stress and truss structure as these kinds of finite elements are ‘scalable’ (Chu 1997; Yang *et al.* 1999a; Liang 2001). For example, for a structure divided by 2D plane stress elements, suppose the design has a weight W_r and mean compliance C_r at the r th iteration, and W_s and C_s at the s th iteration. If $W_r=W_s$, the comparison between these two topologies is straightforward, i.e. the design has the smaller mean compliance is better. However, to make designs of different weights and mean compliances comparable, we need to set one quantity the same and simply compare the other. Keeping this in mind, we scale the structure thickness of different weights to a same target weight by a scaling factor W^*/W_r or W^*/W_s while retaining the current structure topology. As the element stiffness matrix is linear to the thickness ($\mathbf{K} = f(t')$), and all elements are scaled by the same factor, the global stiffness matrix is changed to:

$$\mathbf{K}_{scale}^r = \frac{W^*}{W_r} \mathbf{K}_r, \quad (3.21a)$$

and the displacement vector is

$$\mathbf{u}_{scale}^r = \frac{W_r}{W^*} \mathbf{u}_r, \quad (3.21b)$$

As a result, the mean compliance of the scaled structure is

$$C_{scale}^r = \mathbf{P}^T \mathbf{u}_{scale}^r = \frac{W_r}{W^*} \mathbf{P}^T \mathbf{u}_r = \frac{W_r}{W^*} C^r. \quad (3.22)$$

By this means, the topology at different iterations i are compared in terms of the ‘scaled’ mean compliance C_{scale}^i . The topology with a smaller value of C_{scale}^i is a ‘better’ design. It is noted that the above scaling procedure is the similar to that adopted in the Optimality Criteria method, which is used to scale the design to the constraint boundary.

For the sake of convenience, the scaled mean compliance C_{scale}^i can be made non-dimensional by choosing a reference structure, say, a ground structure or initial structure, and the performance index PI is defined as

$$PI = \frac{C_{scale}^{ref}}{C_{scale}^i} = \frac{W_{ref} \times C_{ref}}{W_i \times C_i}, \quad (3.23)$$

where the target weight W^* has vanished. Apparently, a larger value of PI corresponds to a better design.

For a 3D brick element, however, there is not clear physical meaning of scaling and of PI , thus an alternative *Stage Ratio* is used. For example, a value of $SR=50\%$ means the structure keeps growing up to 50% of the ground structure before starting decreasing.

Elements are added around the structural boundary, i.e. elements with free sides or surfaces can be attached with additional elements, as sketched in Fig. 3.1.

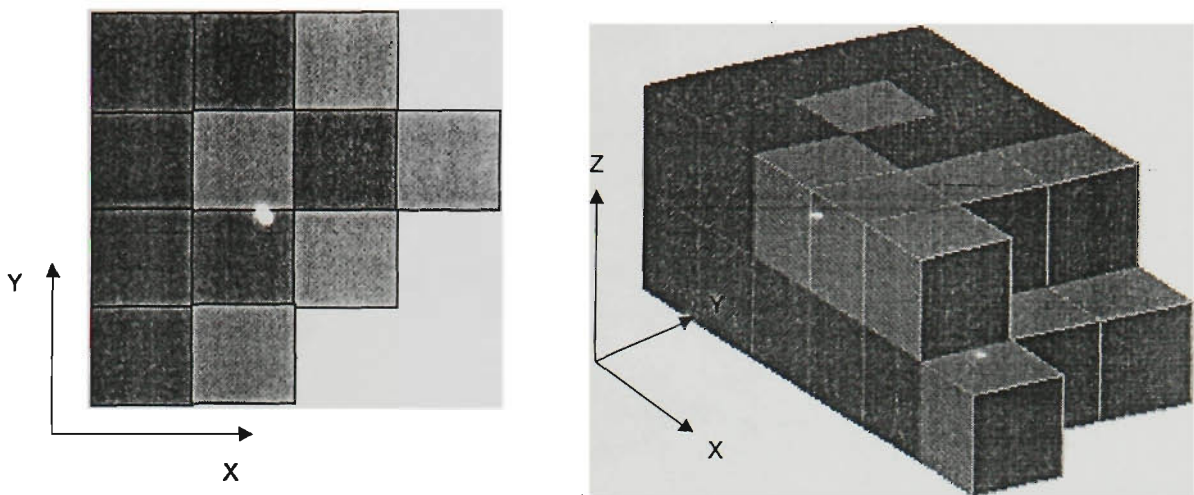


Fig. 3.1. Elements added around the boundary (2D & 3D). The elements in dark are currently existing ones, and those in grey are potentially added elements.

The procedures of ESO and BESO are summarised in a flowchart in Fig. 3.2. As for the finite element analysis shown in the flowchart, one can choose to write the code for this function or use commercial software. The FEA analysis engine employed here is a software package STRAND6 due to its easy handling of element status in the FE model. Similar to the binary representation of design variables, STRAND6 records an existing element as 1 and an absent one 0 and thus change in the element status is as simple as a switch-off or switch-on operation. This saves the effort in mesh re-generation or node and element re-numbering. Based on the result of finite element analysis, a FORTRAN code ESOBRK is written to perform the sensitivity analysis and element removal/addition. Commands of FE analysis and ESOBRK are then written into a batch file and an evolution is performed automatically. It is noted that there are some alternative choices of implementation. Indeed, a similar method called meta-morphic development (MD) using ABAQUS and Unix platform has been working equally well (Liu *et al.* 1999; Liu *et al.* 2000).

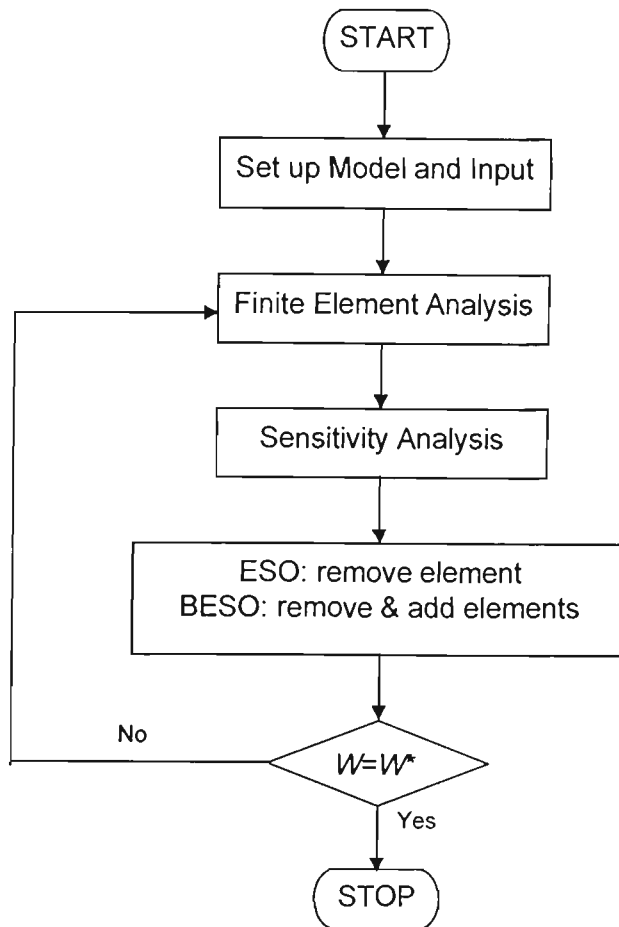


Fig. 3.2. Flow chart of ESO/BESO procedure.

3.2.3. Suppression of Checkerboard Pattern

The checkerboard pattern is a region where solid and void elements distribute in an alternating manner. Designs with checkerboard patterns are unrealistic and undesirable in practice. One effective way to suppress it is the noise filter technique where the checkerboard is analogously treated as unwanted noises (Sigmund 1994) thus signal processing technique can be applied. In ESO and BESO, a similar technique is used called the *average sensitivity method*.

The common feature of the above two techniques is to take the contribution of the neighbourhood element into account thus the strain energy is smeared in a local area.

Firstly, the element sensitivity number calculated from Eq. (3.20) is assigned to each node, thus the *nodal sensitivity number* is calculated from

$$\alpha_{node}^j = \frac{\sum_{i=1}^{n^e} x_i \alpha_i}{\sum_{i=1}^{n^e} x_i}, \quad (3.24)$$

where x_i is the design variable in Eq. 3.5(c) and is equal to either 0 or 1. n^e is the maximum number of elements shared the node j , which is generally equal to the number of sides or surfaces of the employed finite element. For example, for a mesh uniformly divided by linear elements, $n^e=4$ for 4-node elements and $n^e=8$ for 8-node brick elements. α_i is the sensitivity number of the elements joined at node j .

Subsequently, the nodal sensitivity is assigned back to all the sharing elements. For example, a four-node element has four nodal sensitivity numbers α_{node}^1 , α_{node}^2 , α_{node}^3 and α_{node}^4 . Its new sensitivity is worked out by taking an average, i.e.

$$\alpha_e = \frac{\sum_{j=1}^{n^e} \alpha_{node}^j}{n^e}. \quad (3.25)$$

The above technique is included in the application of 2D plane stress problems and proves to be very effective (Yang *et al.* 1999a).

Another way to eliminate checkerboard pattern is to use elements of higher order, such as 8-node quadrilateral elements (Manickarajah *et al.* 1998). However it is not as efficient as the above average method because of high cost of running FEM. This thesis adopts the average sensitivity technique.

3.2.4. Maintaining the Structural Symmetry

For a symmetric structure, it is usual to define a symmetric finite element model. If the structure is symmetric in all respects including the material, geometry, boundary and loading conditions, the symmetry can be generally maintained during the evolution process as well as in the final optimal design. In a structure with one symmetric axis, for example, the symmetry can be kept by simply modifying an even number of elements. However, if there are elements lying on the axis of symmetry, this measure will become ineffective as modifying element on the axis will violate the above ‘even number rule’. In such a case, an alternative check-up measure is used. At the current iteration, after say, 20 elements have been removed as calculated by the modification ratio, record the sensitivity number α_i of the last modified element (i.e. 20th). This number is then compared to the sensitivity number of the remaining elements. Elements with the same value (judged by a relative difference smaller than 10^{-6}) are regarded as being symmetric to the last one and are removed accordingly.

In some cases, the structure may be geometrically symmetrical but loading and restraints are asymmetric. It is often expected that the geometry symmetry can be retained in the optimal topology. However, as the sensitivity numbers of geometrically symmetrical elements are not equal, i.e. $\alpha_{e_1} \neq \alpha_{e_2} \neq \dots \alpha_{e_{n_s}}$, where n_s is the total number of symmetrical elements, the structure would lose the symmetry from the very beginning if elements were removed according to their individual sensitivity number. Therefore, it is necessary to define a common ‘group’ sensitivity number for all symmetrical elements. The procedure is as follows:

1. Record the symmetric information, i.e. an array containing the information of the corresponding symmetric elements. This is done once only at the first iteration.
2. At each iteration, read the symmetric information. After calculating the sensitivity using Eq. (3.20) and Eqs. (3.24) & (3.25), average the sensitivity among the symmetric elements, i.e.

$$\alpha_{e_{sym}} = \frac{\sum_{j=1}^{j=n_s} \alpha_{e_j}}{n_s}. \quad (3.26)$$

3. Assign the $\alpha_{e_{sym}}$ to each symmetrical element in the group, i.e. replace $\alpha_{e_1}, \alpha_{e_2}, \dots, \alpha_{e_{n_s}}$ with $\alpha_{e_{sym}}$, thus all symmetrical elements have a same group sensitivity number $\alpha_{e_{sym}}$. In the subsequent element modification, if the i th symmetrical group has the largest sensitivity number $\alpha_{i_{sym}}$, all elements in the group are removed. This is the same with the addition procedure.

3.3. Examples

In this section, the ESO and BESO methods are applied to two examples of 3D continuum structures. The finite element used here is 8-node brick element and computer time is referred to that of running on Pentium 533 MHz PC. ESO and BESO are performed comparatively. In BESO, addition ratio $AR=0.25$ (or 0.75) and state ratio $SR=50\%$ are used unless otherwise specified. In presenting the numerical results, the structural weight W and mean compliance are set dimensionless by scaling with respect to the corresponding values of the ground structure W_0 and C_0 , respectively.

Example 3.3.1 A deep beam.

As shown in Fig. 3.3, a deep beam of box shaped cross section is the design domain. The beam is clamped at one end and a point load $P=1.0 \times 10^3$ kN acts at the centroid of the free end. The elastic modulus $E=210$ GPa and Poisson's ratio $\nu=0.3$ are assumed.

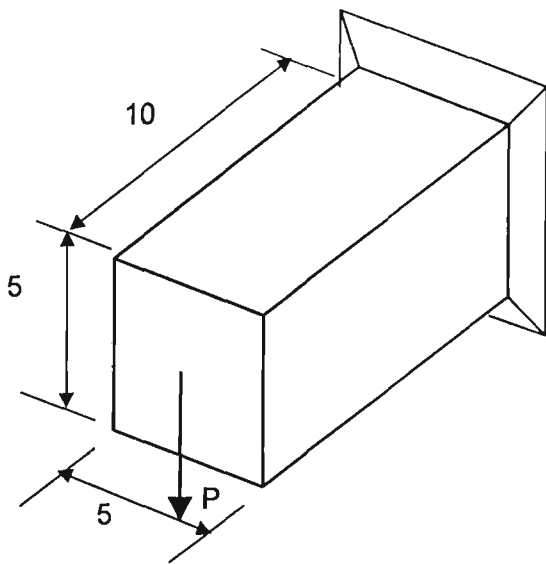


Fig. 3.3. A deep beam.

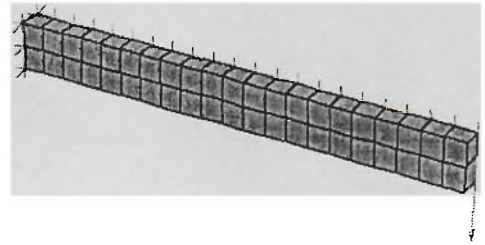
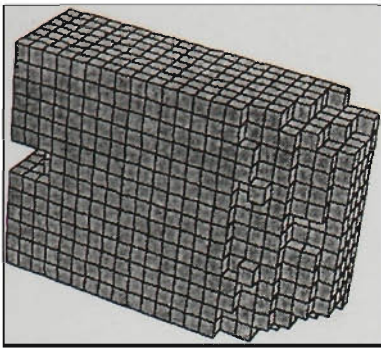


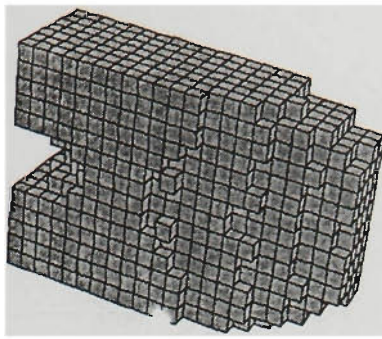
Fig. 3.4. Finite element model, initial design of BESO, half model.

A finite element mesh of $21 \times 14 \times 7 = 2058$ is used to divide the domain and this is a half model due to symmetry with respect to the mid-plane. BESO defines a sub-domain of a small cantilever beam as the initial design, as shown in Fig. 3.4. The crossed area at the back is the plane of symmetry. Two cases are studied: (1) $W^* = 40\%W_0$ and (2) $W^* = 10\%W_0$. A modification ratio $MR = 2\%$ is used for ESO and BESO, and the stage ratio is $SR = 60\%$.

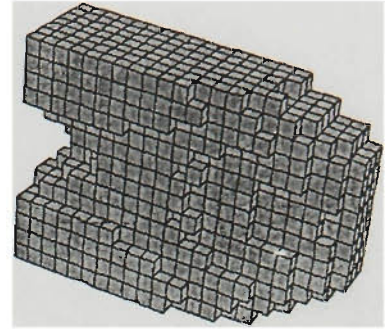
The evolution history of ESO is shown in Fig. 3.5. The element removal starts from the top and bottom of the free end, then extends to the middle of the beam and to the supporting edges. The later stages see the emergence of a Michell type structure in the plane and an I shaped beam section.



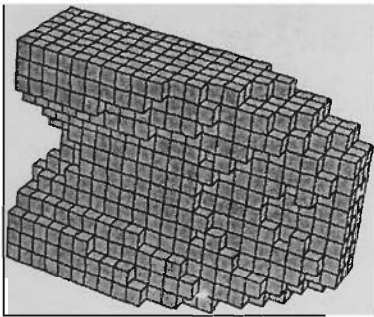
(a) $W/W_0=90\%$, iteration 5.



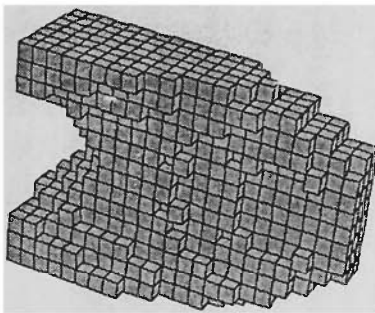
(b) $W/W_0=80\%$, iteration 11.



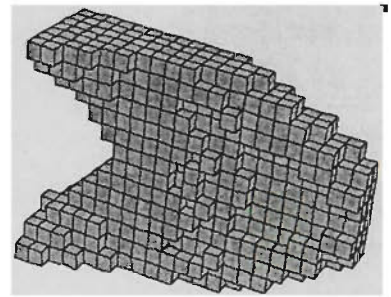
(c) $W/W_0=70\%$, iteration 17.



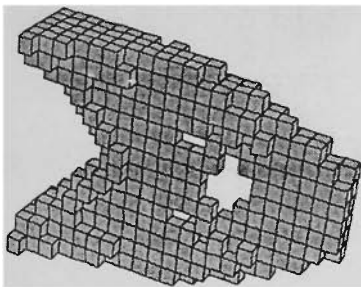
(d) $W/W_0=60\%$, iteration 24.



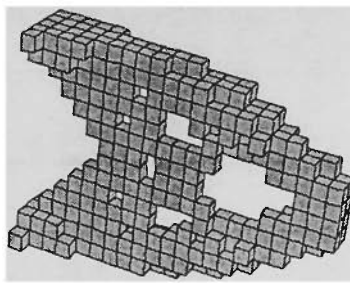
(e) $W/W_0=50\%$, iteration 33.



(f) $W/W_0=30\%$, iteration 57.



(g) $W/W_0=20\%$, iteration 75.



(h) $W/W_0=15\%$, iteration 99.

Fig. 3.5. Iteration history of ESO.

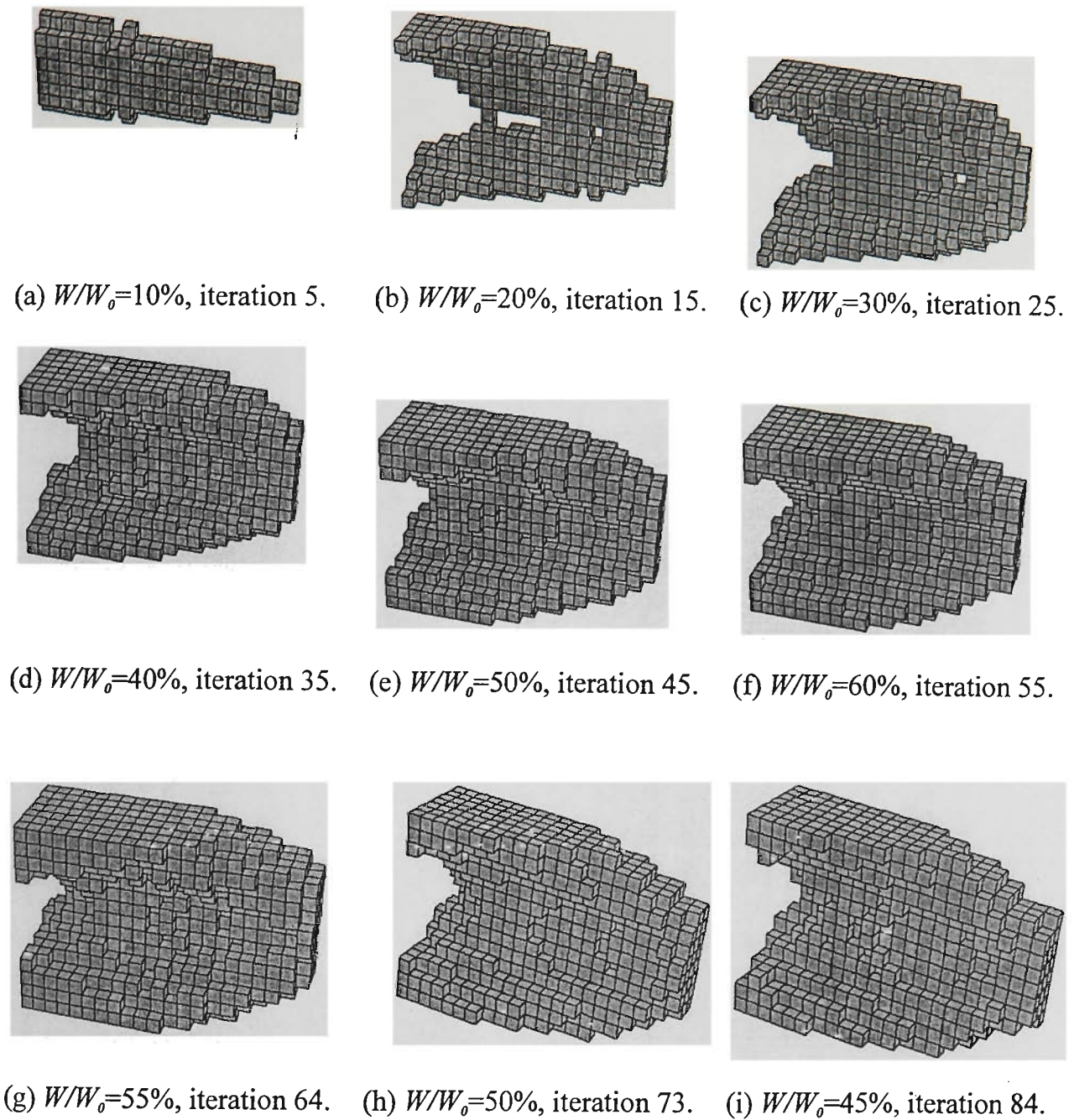
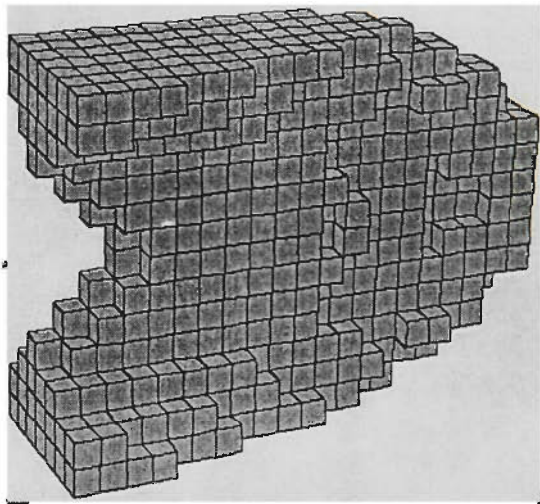
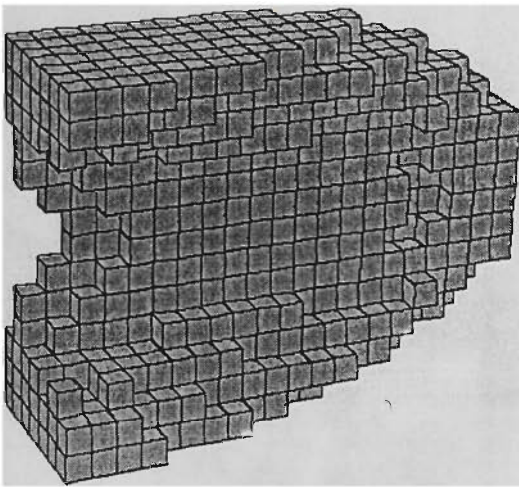


Fig. 3.6. Iteration history of BESO.

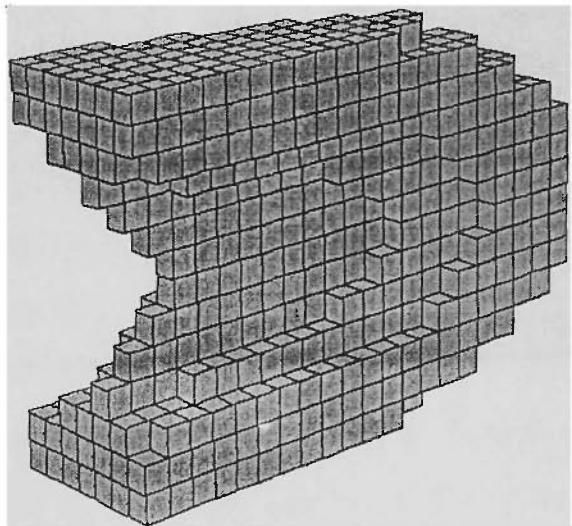
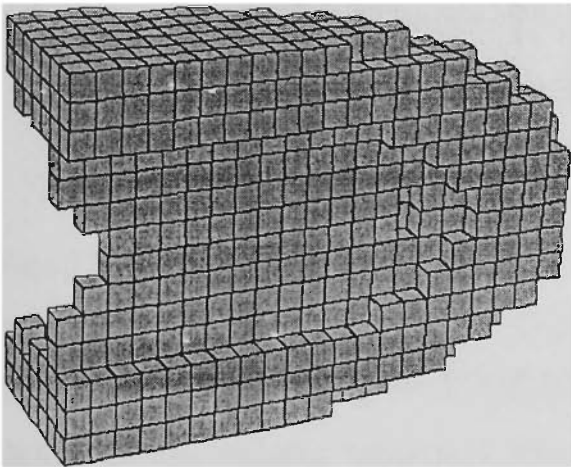
The evolution history of BESO is shown in Fig. 3.6. Figs.3.6(a)~(f) see structure growing and 5(g)~(i) structure decreasing. Initially, the structure grows more in the height because it has more significant contribution to the flexural stiffness ($I \propto h^3$ compared to $I \propto b$). The flexural behaviour is further reflected by tapering with the beam outer shape and the emergence of an I-shaped cross section. Fig. 3.6(f) is the structure with the largest weight throughout iterations $W=60\%W_0$. Fig. 3.6(e) and (h)

correspond to each other with an almost equal weight (50.34% vs. 49.97%), but the latter has a smaller mean compliance 47.55 N.m, compared to 47.81 N.m for the former. This means a structure is normally better developed after the largest design is reached (60% in this example). Indeed, optimum solutions are generally sought in the decreasing stage.

From front



From back

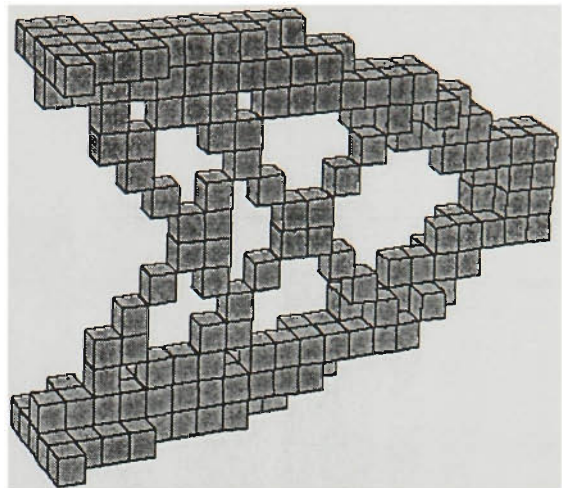
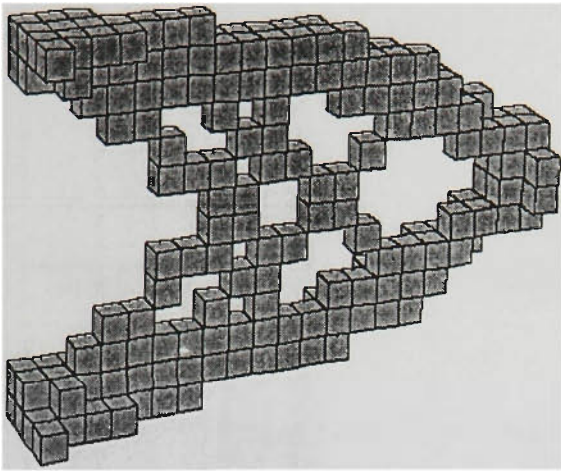


(a) BESO.

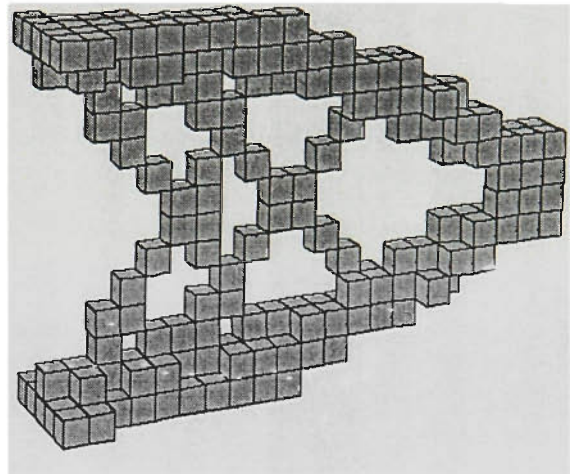
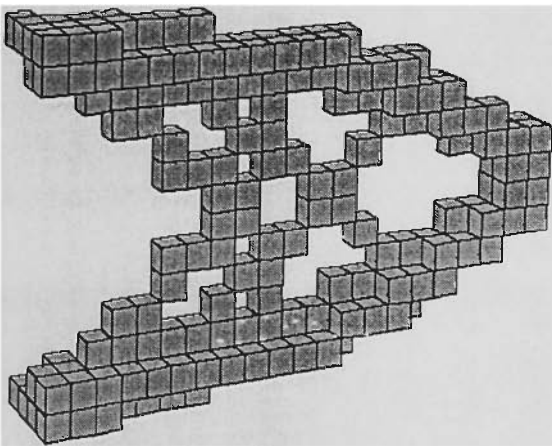
(b) ESO.

Fig.3.7. Optimal topologies: $W/W_0 = 40\%$.

From front



From back



(a) BESO.

(b) ESO.

Fig.3.8. Optimal topologies: $W/W_0=10\%$.

Figs.3.7~3.8 are the optimal topologies for the two prescribed weights. Comparison between the columns shows that though there are differences in inner configuration details, the two methods generate topologies of similar outer shapes and profiles. For a design of low volume fraction, a truss configuration is evolved which reveals the analytical solution reasonably well and agrees well with its equivalent 2D structure (Michell 1904; Xie and Steven 1997).

From Table 3.1, it is seen that the corresponding mean compliance by the two methods is very close and BESO solution is slightly better. This can be explained by BESO's

ability to admit more elements at any stage of evolution. However, as BESO involves two stages which take far more iterations than ESO (almost twice in this example), the solution time is longer than ESO.

Table 3.1. ESO & BESO Results (Example 3.3.1)

Prescribed W^*/W_0		Iteration	Computing time (Min.: Sec.)	Mean Compliance C/C_0
40%	ESO	44	19:14	1.419
	BESO	98	22:22	1.406
10%	ESO	127	30:01	4.859
	BESO	262	50:40	4.696

Example 3.3.2. A cubic block subjected to inclined pull-out forces.

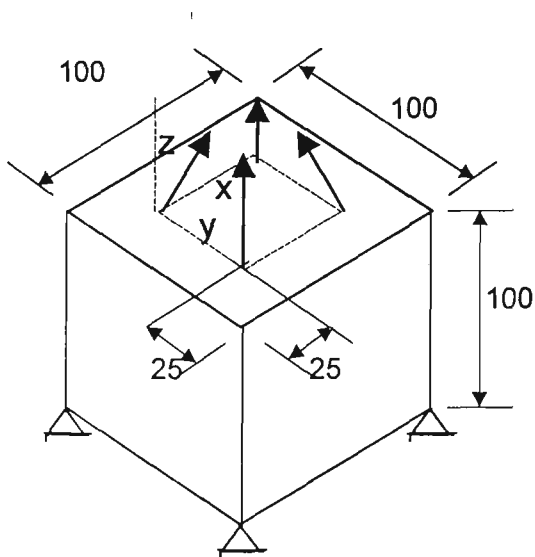


Fig. 3.9. A block applied with point loads.

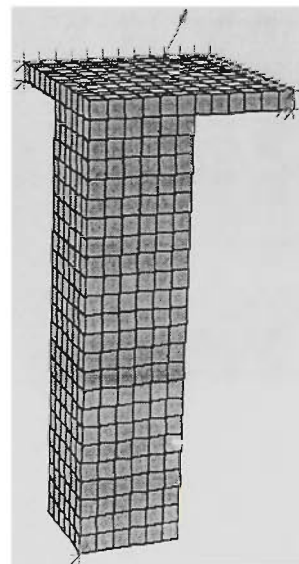
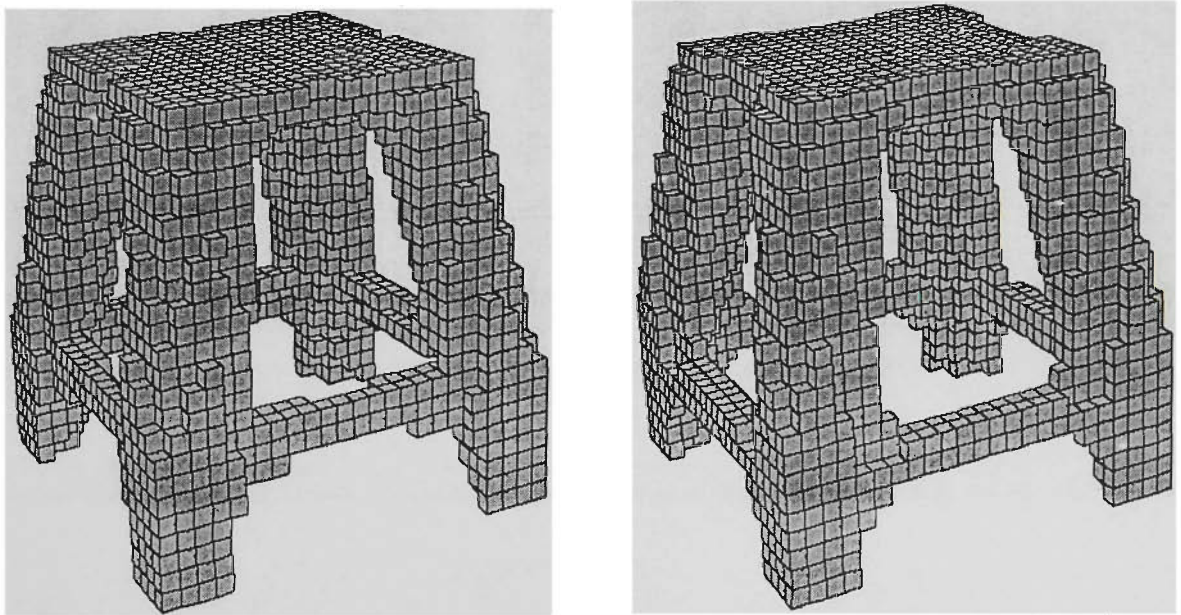


Fig. 3.10. Initial design of BESO.

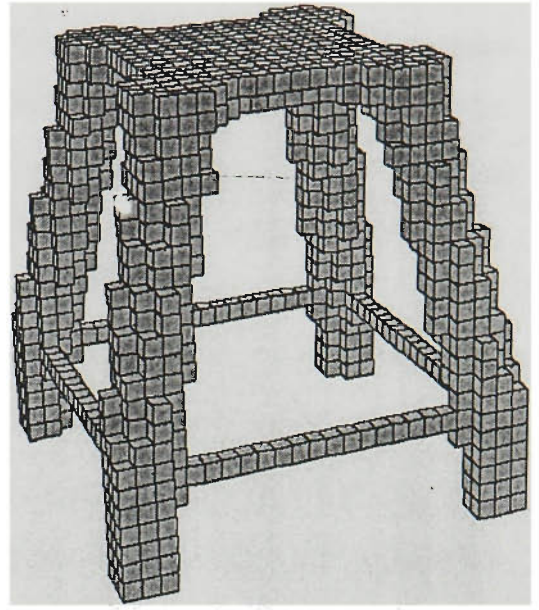
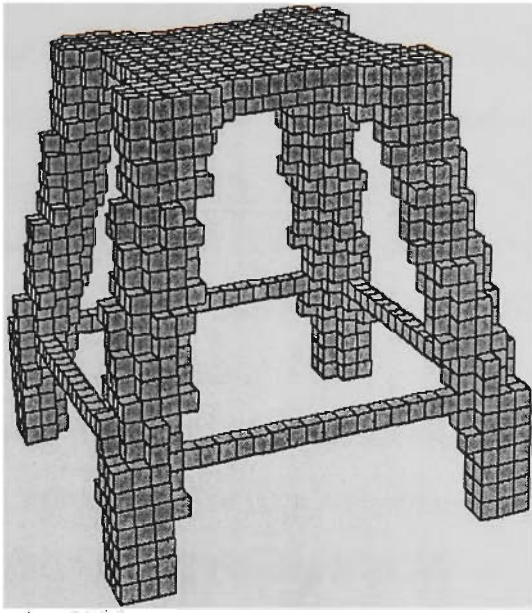
Fig. 3.9 shows a cubic block fixed at its four corners at the bottom. It is subjected to four diagonal pull-out forces at the top. Each point load is at an angle of 45° to the x , y and z axes and three load components are $P_x=P_y=P_z=10$ kN respectively. The elastic modulus $E=210$ GPa and Poisson's ratio $\nu=0.3$ are assumed. A quarter model divided by $12 \times 12 \times 24=3456$ elements is used. The initial design for BESO is shown in Fig. 3.10. A larger modification ratio $MR=4\%$ is used in BESO as compared to $MR=2\%$ in ESO.

Fig. 3.11 gives the topologies of three prescribed weights. The left column is solutions by ESO and the right by BESO. A quadropod stool is obtained which consists of four big legs connecting loads with the nearest supports. Interconnections between the bottom of neighbouring legs are present in Figs. 3.11(a) & 3.11(b) which transfer the shear force as a component of the diagonal loading. The shear force may be insignificant as the connection is removed when the structure weight becomes smaller, as shown in Fig. 3.11(c).

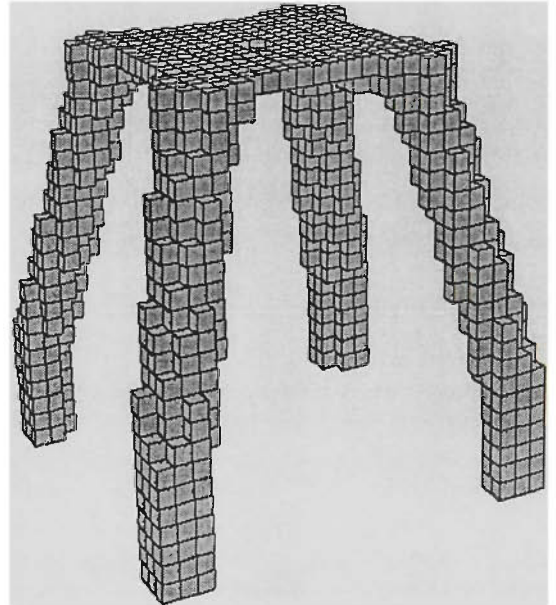
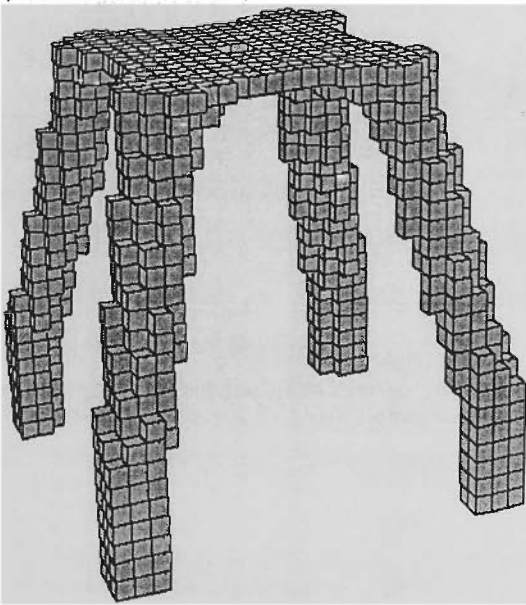


(a) $W^*=40\%W_0$

Fig. 3.11. Topologies from ESO and BESO.



(b) $W^*=10\%W_0$



(c) $W^*=8\%W_0$

ESO.

BESO.

Fig. 3.11. (cont.) Topologies from ESO and BESO.

From Table 3.2, it is seen that BESO has a slightly larger mean compliance than ESO which may be mainly due to a larger value of MR . However, the savings in computer time due to BESO are significant. The time is primarily divided by running FE analysis and structural modification. In most situations the former is much higher than the latter. This is particularly true in this example because of a larger number of finite elements and a large bandwidth in solving the equilibrium equations. Using a twice as large MR , BESO takes a more or less equal iterations but only half of the solution time.

It is noted that a similar problem was investigated by Olhoff *et al.* (1998) where a the applied force was vertical in direction instead of an inclined one. Fig. 3.11(c) is similar to their topology but direct comparison is not available. In fact, ESO/BESO generates distinctly black-and-white topology but solutions based on the homogenisation of composite material or SIMP present grey area. In the reference, the resulting topology is a design with material density less than 0.8 removed by using some penalty techniques.

Table 3.2. Results of ESO & BESO (Example 3.3.2)

Prescribed W^*/W_0		Iteration	Computing time (Min.: Sec.)	Mean Compliance C/C_0
20%	ESO	82	2:18	1.073
	BESO	70	0:46	1.076
10%	ESO	145	2:29	1.214
	BESO	164	1:03	1.216
8%	ESO	163	2:32	1.288
	BESO	184	1:05	1.293

3.4. Conclusions

The basic form of ESO/BESO is presented in this chapter. It can be mathematically regarded as optimal criteria method and the sensitivity analysis gives the search/evolution direction. The evolution is then conducted in an iterative manner by removing and/or adding elements.

The application to 3D problem is successfully. Together with the experience with 2D continuum and discrete structures (truss and frame), it can be said that ESO/BESO are effective methods for a range of structural systems. In fact, as the structural analysis can be conducted by any FEA package, the implementation of ESO/BESO is almost similar for different structures, consisting of calculation of sensitivity analysis and element removal/addition.

Moreover, ESO/BESO is not restricted to the stiffness optimisation. It can be easily extended to different design objectives and this will be detailed in later chapters. For stiffness compliance design itself, it is not restricted to single loading conditions or to global stiffness. In fact, multiple load cases and local stiffness (e.g. individual displacement) have been studied on 2D continuum structures (Chu 1997; Yang 1999). By using virtual load technique, the sensitivity analysis on the mean compliance and on a concerned nodal displacement has a similar form. For multiple load cases, the sensitivity takes the average of contribution of all active load cases. These can be equally applied to 3D continuum structures.

For 3D problems, the computing cost is more critical than for 2D because of larger finite element problems. The BESO method is proposed to improve the algorithm efficiency by means of using a smaller FE model. With the same value of modification ratio MR , there may be not much difference in the solution time of ESO and BESO. However, BESO has the flexibility to use a larger value of MR without losing the solution quality, and significantly saves solution time. The formulation BESO verifies the feasibility of evolutionary algorithms as ESO and BESO converges to similar results.

On Topology Optimisation with Design Dependent Loading

This chapter carries on the investigation into stiffness optimisation of the last chapter but involves more complicated cases where the loading condition is not fixed and needs some degree of optimisation. The uncertainty in loading can be due to the dependency of loading location on the structural topology or profile, such is the cases of so-called transmissible loads and surface loading. Another case is the inclusion of self-gravity in structural analysis. The ESO/BESO routine as detailed previously can be used to handle these three special cases only with a minor modification or amendment. In considering the transmissible load, the transmissible condition is treated as an additional constraint and a simple form of optimal criteria is derived. Modifications are introduced in the finite element model and the original ESO/BESO methodology is followed. In dealing with the surface loading and gravity loading, the methodology is modified in sensitivity calculation by including an additional term considering loading contribution. A range of examples of 2D and 3D structures are tested with the proposed techniques. It is concluded that ESO/BESO can be well adapted to this category of load-dependent problems.

4.1. Introduction

The problem formulation of a basic topology optimisation consists of a permissible design domain, prescribed supporting conditions and given loading conditions.

However, there are many situations where the loading conditions are not prescribed and needs some degree of optimisation. In designing an arch bridge, for example, the self-weight is a major concern and an important component in the load combinations. The final optimum design thus includes information on physical configuration as well as the body force as a part of global load conditions. Apart from the structural gravity, the external load can be uncertain and depends on the design shape or topology, such as the wind and snow loading on a building roof, the water pressure applied to a dam or other underwater constructions/vehicles, the flow considered in turbo machinery or aircraft design.

Topology optimisation of load dependent problems was first dealt with by analytical solution and the results were the so called 'Prager structures' (Rozvany and Prager 1979). They are basically Michell type structures (Michell 1904) which is the least-weight solution with stress-constraints (e.g. fully stressed). The load applying position is not prescribed but allowed to move along a prescribed 'action line' and the load is thus referred to as 'movable' or 'transmissible'. The optimal solution presents the optimal load applying location, and constitutes a solution of the main bearing structures. An arch bridge is cited by Fuchs and Moses (2000) for example to describe this point. The bridge consists of an arch (primary bearing part), deck (load applying part) and spokes between them (load transferring part). The arch usually accounts for a significant proportion of structural weight, being it an upper-deck or lower deck bridge. This gives rise to the idea that one forgets about the exact loading location but only allows for the primary bearing structure to emerge which finally gives the optimal loading location.

It is noted that transmissible loading is such that only the location changes with the design. It is natural if one allows for both location and direction changing. This extension leads to the topology design subject to pressure loadings, as the pressure direction is normal to the structural boundary. Work on this problem is presented by Hammer and Olhoff (2000) on 2D continuum structures, which proves to be feasible and practical.

To some extent, this chapter parallels the work of Fuchs and Moses (2000) and Hammer and Olhoff (2000), and incorporates their concepts into ESO/BESO. The main content consists of three sections, namely, sect. 4.2 for transmissible loading, sect. 4.3 for gravity loading and sect. 4.4 for surface load. In each section, the problem statement is given first. Then the methodology of ESO/BESO is presented including sensitivity analysis and algorithms. Examples are given for verifications.

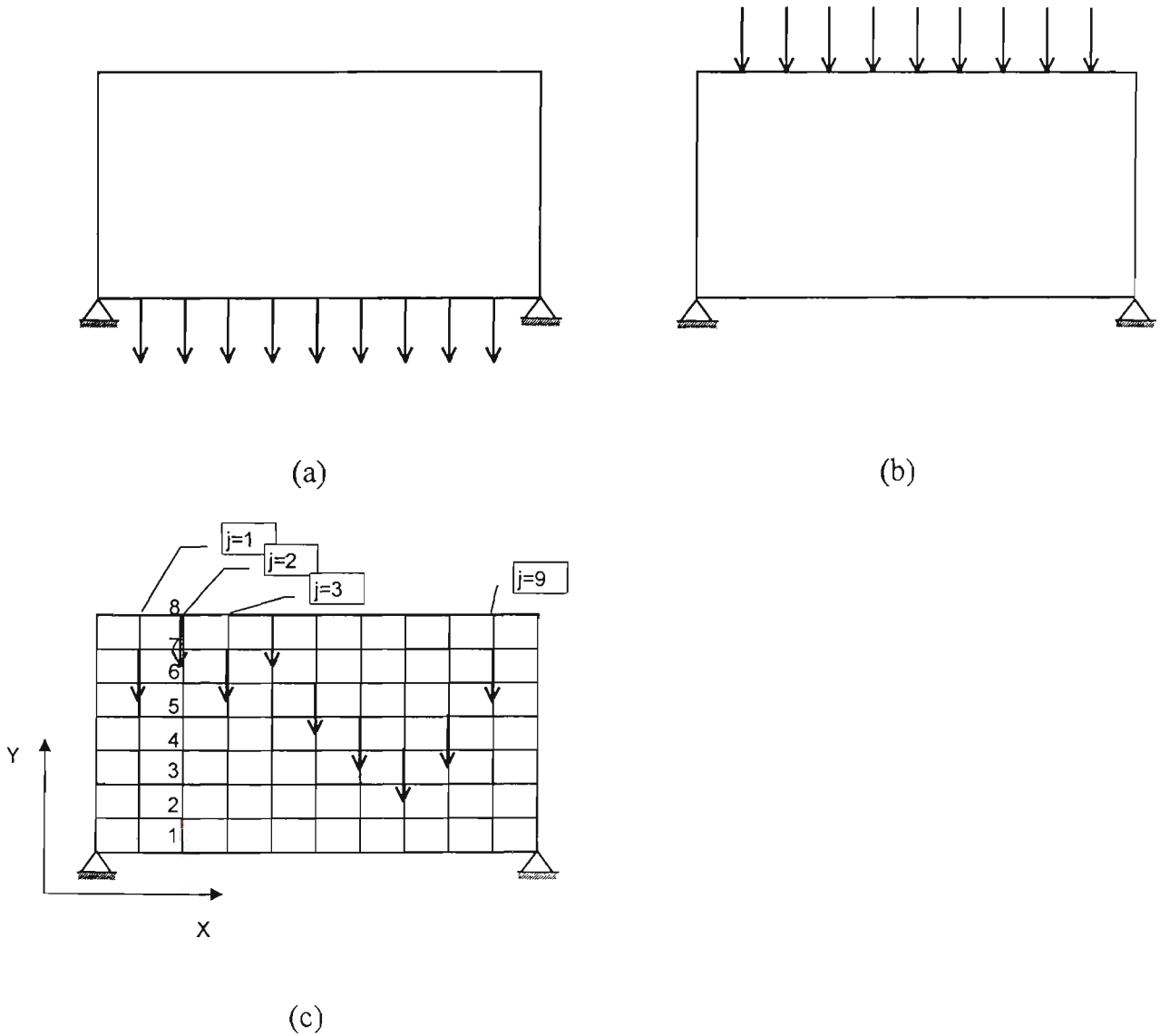


Fig. 4.1. Illustration of sliding loads compared to fixed loading (Fuchs and Moses 2000).

4.2. Topology Optimisation with Transmissible Loads

A transmissible load is a load of given magnitude and direction which can be applied at any point along the load action line (Fuchs and Moses 2000). An illustrative example is given in Fig. 4.1. In comparison to Fig. 1(a) or 1(b) where a series of point loads are applied on the top or bottom, each load can slide along a vertical action line. Based on such a definition, we first present the problem statement of stiffness optimisation, then derive the optimality criteria. ESO/BESO procedure in corporation with the criteria is presented and tested by a few examples.

4.2.1 Problem Statement

We assume that the transmissible loads are aligned with the global coordinate system, and use Fig. 4.1(c) as illustration. Adding the transmissible condition to the basic problem statement in Eq. (3.5), it follows:

$$\text{Minimise } f = C(\mathbf{x}) = \mathbf{P}^T \mathbf{u} . \quad (4.1a)$$

$$\text{Subject to } g = W^* - \sum_{i=1}^n W_i x_i = 0, \quad (4.1b)$$

$$x_i \in \{0,1\} , \quad (4.1c)$$

$$\sum_{m \in M} p_{jm} - p_j = 0, \quad j \in I, \quad (4.1d)$$

where I is the total number of transmissible loads and M is the number of nodes along each line of action, for example, in Fig. (1c), $I=9$ and $M=8$.

The Lagrangian function is

$$L(\mathbf{x}, \lambda, \mu_j, p_{jm}) = C(\mathbf{x}) - \lambda (W^* - \sum_{i=1}^n W_i x_i) - \sum_{j \in I} \mu_j (\sum_{m \in M} p_{jm} - p_j) . \quad (4.2)$$

Taking derivatives with respect to λ and μ_j results in Eq. (4.1b) and (4.1d), respectively. Further, from chapter 3, taking derivative with respect to x_i leads to

$$\frac{\partial L}{\partial x_i} \Delta x_i = 2C_i - \lambda W_i, \quad (4.3)$$

and taking derivative with respect to p_{jm} results in

$$\frac{\partial L}{\partial p_{jm}} = \frac{\partial C}{\partial p_{jm}} - \mu_j = 0, \quad (4.4)$$

where

$$\begin{aligned} \frac{\partial C}{\partial p_{jm}} &= \left(\frac{\partial \mathbf{P}^T}{\partial p_{jm}} \right) \mathbf{u} + \mathbf{P}^T \left(\frac{\partial \mathbf{u}}{\partial p_{jm}} \right) \\ &= \left(\frac{\partial \mathbf{P}^T}{\partial p_{jm}} \right) \mathbf{u} + \mathbf{P}^T \left(\mathbf{K}^{-1} \frac{\partial \mathbf{P}}{\partial p_{jm}} \right) \\ &= 2 \left(\frac{\partial \mathbf{P}^T}{\partial p_{jm}} \right) \mathbf{u} \end{aligned} \quad (4.5)$$

From Eq. (4.1d)

$$\left(\frac{\partial \mathbf{P}^T}{\partial p_{jm}} \right) = (0, 0, \dots, \frac{d p_j}{d p_{jm}}, 0, 0) = (0, 0, \dots, 1, 0, 0), \quad (4.6)$$

which only has one non-zero component at the d.o.f. corresponding to the load p_{jm} .

Denote the displacement at this d.o.f. as $\frac{\partial \mathbf{P}^T}{\partial p_{jm}} \mathbf{u} = u_{jm}$. Submitting Eqs. (4.5)&(4.6) into

(4.4) leads to

$$u_{jm} = \frac{1}{2} \mu_j. \quad (4.7)$$

As pointed out by Fuchs and Moses (2000), Eq. (4.7) means that by introducing transmissible loads, one assumes that the d.o.f. at the action line has a uniform displacement.

4.2.2 Evolution Procedure

We find from the last section that optimisation related to transmissible loads is largely the same as the basic optimisation and difference is the introduction of uniform displacement on the action line. In finite element model, *constraints* are usually used to impose a relationship among d.o.f.s, which can be single-point (i.e. prescribe the value of displacement), or multiple-point. A uniform displacement condition as considered here invokes a multiple-point constraint, i.e. among the action line :

$$\begin{aligned} Dy(2) &= Dy(1) \\ Dy(3) &= Dy(1) \\ &\vdots \\ Dy(8) &= Dy(1) \end{aligned} \tag{4.8}$$

where Dy is the nodal displacement at y direction (global system) and node 1 is chosen as the *master node*. Many FEM packages have the capability of including constraint by different methods, such as coordinate transformation, Lagrange multipliers and penalty functions.

Therefore, in building the FE model in the design domain, a set of initial constraint functions is input. During the evolution, some functions may need updating due to the removal of the master node, otherwise, the evolution procedure is the same as those outlined in Sect. 3.2. The flowchart for the procedure is shown in Fig. 4.2. Items in shaded frames are features different from the basic ESO/BESO procedure.

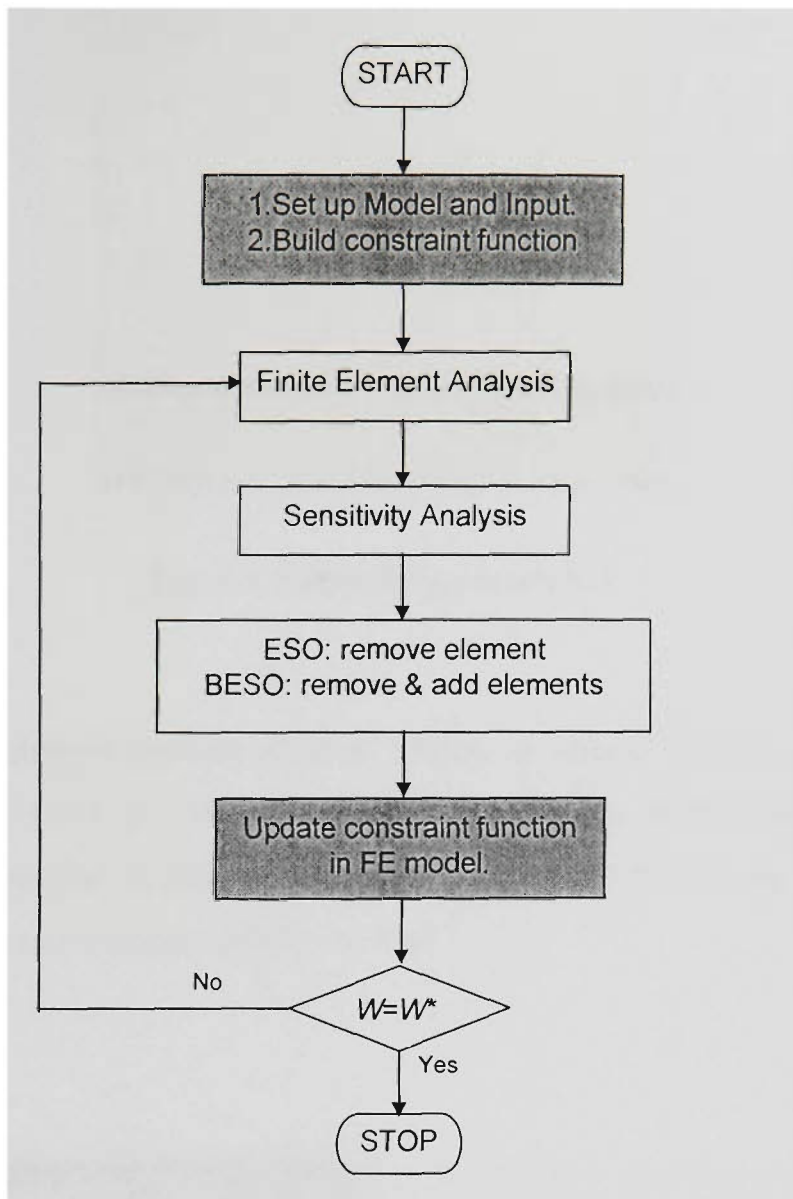


Fig. 4.2. Flowchart: ESO/BESO procedure for optimisation considering transmissible loading.

4.2.3 Examples

Example 1 4.2.3.1 A hinged beam structure.

Take the 2D design in Fig. 4.1(c) for example, where the rectangular area of $5\text{m} \times 2.5\text{m}$ is divided by $1250 = 50 \times 25$ 4-node square finite elements. $E = 210$ GPa, $\nu = 0.3$ and the plane stress condition are assumed. The prescribed weight is $W^*/W_0 = 20\%$. The initial structure for BESO is a thin bar of one layer of elements connecting the two endpoints, as shown in Fig. 4.3.

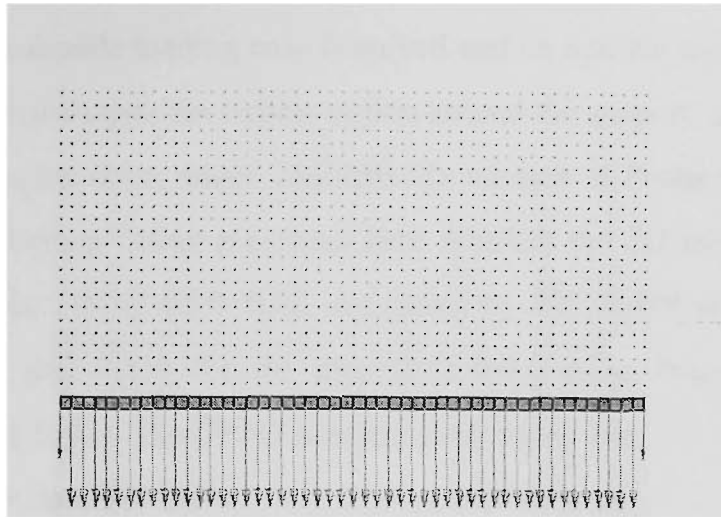


Fig. 4.3. Initial design for BESO.

Firstly, the optimisation problem of fixed loading as defined in Figs. 4.1(a)&(b) are solved. From Fig. 4.4, it is evident that the top-loaded bridge has the load transfer zone as struts in compression, and the bottom-loaded bridge has it as ties in tension. An arch-like primary structure is distinct in both designs.

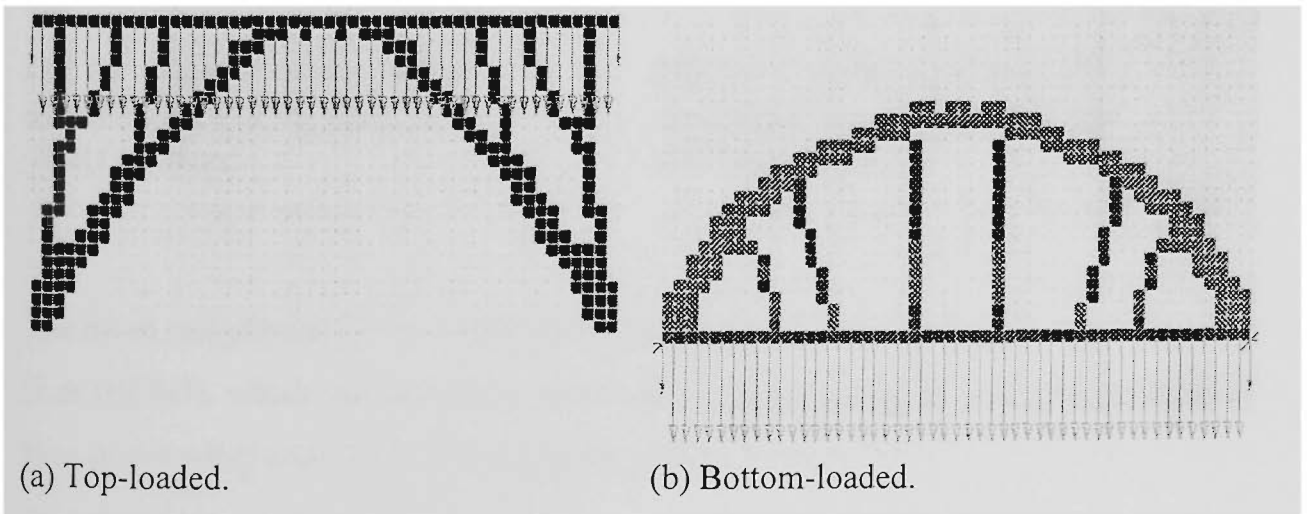


Fig. 4.4. Optimal topologies for fixed loading conditions (ESO solution).

Secondly, the transmissible loading case is solved and an optimal topology is shown in Fig. 4.5. It is seen that despite the hollow region around the support, an arch assuming a parabolic profile is quite clear, which confirms the solution of Fuchs and Moses (2000). Indeed, parabolic curving fitting presented here matches the 2D model well. It has a height-to-length ratio $H/L=2.4/5.0=0.48$, compared to $H/L=0.479$ in reference (Fuchs and Moses 2000), and 0.433 for the analytical solution as Prager arch structures (Rozvany and Wang 1983). The BESO solution is shown in Fig. 4.6, which is similar to that of ESO and also has $H/L=0.48$.

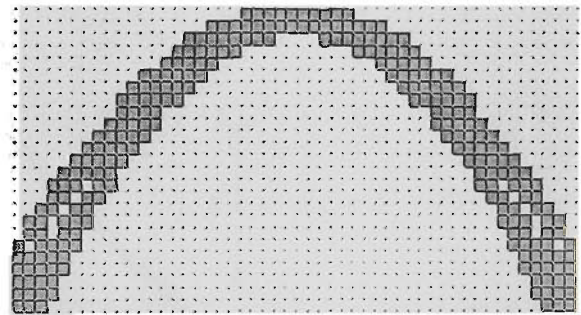
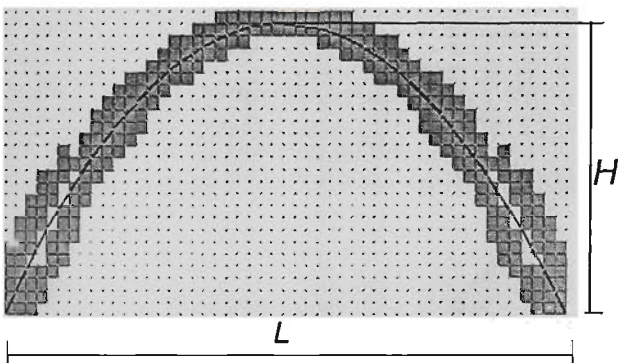


Fig. 4.5. Optimal topologies for transmissible loading conditions. (ESO solution).

Fig. 4.6. Optimal topologies for transmissible loading conditions (BESO solution).

The mean compliance for the transmissible loading is $C=13.82$ N.m (ESO) and $C=13.97$ N.m (BESO), which are compared favourably to the fix loading case where $C=45.06$ N.m (top loaded) and $C=51.79$ N.m (bottom loaded), respectively.

Now we replace the distributed loading with a point load at the mid-span, as shown in Fig. 4.7. Results for BESO procedure are shown in Fig. 4.8. It again predicts a 2-bar Prager structure, with each bar having an angle to the horizontal line equal to 45° . The truss interpretation is given in Fig. 4.9.

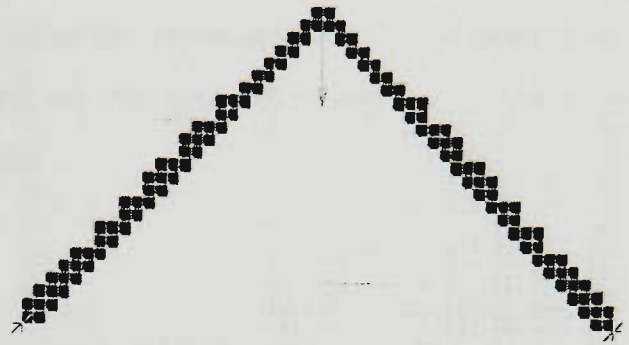
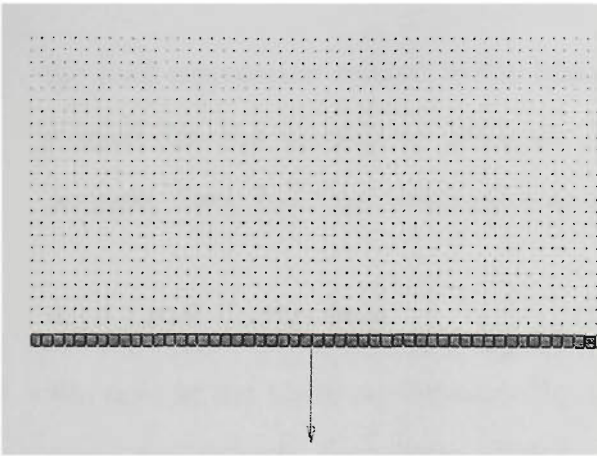


Fig. 4.7. Initial design for BESO.

Fig. 4.8. Optimal topologies for transmissible loading conditions (BESO solution).

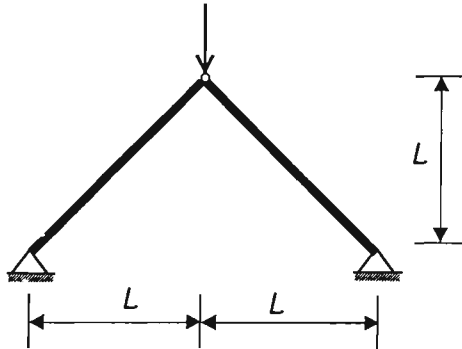


Fig. 4.9. Truss interpretation from 2D continuum design.

From the above theoretical and numerical exploration, it is demonstrated that ESO and BESO are feasible and easily adapted to the problem considering transmissible loading.

4.3. Topology Optimisation with Gravity Loading

When the gravity loading is included in finite element analysis, removing/adding an element may lead to changes in the loading vector, thus it is necessary to include its contribution to the mean compliance sensitivity with respect to the design variable. Sensitivity analysis is dealt with in Sect. 4.3.2. Sect. 4.3.1 presents an introduction to

the load conversion related to the body force as the expression of the load derivative is needed for the sensitivity analysis. Based on the theoretical aspects of these two sections, Sect. 4.3.3 provides a few examples.

4.3.1 Load Conversion

We note in the static equilibrium Eq. (3.3) that the global load vector \mathbf{P} consists of the actual nodal loads, equivalent loads produced by body force and by surface traction. Eq. (3.3) is derived on the principle of work equivalence, and results in consistent loads as it is based on the same shape function as used to derive the stiffness matrix. Consistent load conversion is the most commonly used one and is also adopted in this thesis.

The topic on load conversion can be readily found in the literature on the finite element method (e.g. Cook *et al.* 1989). We hereby briefly present the expression from Eq. (3.3) for some cases as considered in this chapter. Take an 8-node solid isoparametric element for example, it has the shape functions:

$$N_i = \frac{1}{8}(1 + \xi_i \xi)(1 + \eta_i \eta)(1 + \zeta_i \zeta), \quad (4.9)$$

where ξ , η and ζ are dimensionless Cartesian coordinates, and $\xi_i = \pm 1$, $\eta_i = \pm 1$ and $\zeta_i = \pm 1$.

Suppose the body force is due to the gravity of constant intensity q and its direction aligns with the global Z axis. Consider the loads distributed on Node 1 for example.

$$r_e^1 = \int_0^1 N_1 q dV = \int_0^1 N_1 q J d\xi d\eta d\zeta, \quad (4.10)$$

where J is the determinant of the Jacobian matrix. It is in general a function of ξ , η and ζ . For special solid elements which have all its six faces as rectangles (e.g. 8-node brick elements), it is a constant and $J = \frac{1}{8}V_e$. Therefore, Eq. (4.10) becomes

$$r_e^1 = \frac{1}{8} q V_e \int_0^1 N_1 d\xi d\eta d\zeta = \frac{1}{8} q V_e, \quad (4.11)$$

which means that the element body force is equally distributed to each individual node.

Similarly, it can be found that for a 4-node rectangular element under plane stress condition, each node carries a quarter of the total body force, i.e. $\mathbf{r}_e = \frac{1}{4} q V_e$.

4.3.2 Sensitivity Analysis

The static equilibrium in an incremental form is

$$(\mathbf{K} + \Delta\mathbf{K})(\mathbf{u} + \Delta\mathbf{u}) = \mathbf{P} + \Delta\mathbf{P} . \quad (4.12)$$

Ignoring the second-order terms,

$$\Delta\mathbf{K}\mathbf{u} + \mathbf{K}\Delta\mathbf{u} = \Delta\mathbf{P} .$$

Thus

$$\mathbf{P}^T \mathbf{K}^{-1} \Delta\mathbf{K}\mathbf{u} + \mathbf{P}^T \mathbf{K}^{-1} \mathbf{K} \Delta\mathbf{u} = \mathbf{P}^T \mathbf{K}^{-1} \Delta\mathbf{P} ,$$

$$\mathbf{u}^T \Delta\mathbf{K}\mathbf{u} + \mathbf{P}^T \Delta\mathbf{u} = \mathbf{u}^T \Delta\mathbf{P} ,$$

$$\mathbf{P}^T \Delta\mathbf{u} = \mathbf{u}^T \Delta\mathbf{P} - \mathbf{u}^T \Delta\mathbf{K}\mathbf{u} . \quad (4.13)$$

The increment of mean compliance C is

$$\Delta C = \mathbf{P}^T \Delta\mathbf{u} + \Delta\mathbf{P}^T \mathbf{u} . \quad (4.14)$$

From Eq. (4.13),

$$\Delta C = 2\Delta\mathbf{P}^T \mathbf{u} - \mathbf{u}^T \Delta\mathbf{K}\mathbf{u} , \quad (4.15)$$

which consists of an addition term compared to Eq. (3.13).

1. Removal Criteria

Recalling Eq.(4.11), if an 8-node solid rectangular element is removed, the change in load vector $\Delta\mathbf{P}$ can be written as

$$\Delta\mathbf{P}_i = \{0,0,-\frac{1}{8}qV,0,0,-\frac{1}{8}qV,\dots\}_{24 \times 1}^T, \quad (4.16)$$

where it is again assumed that the gravity is in line with the global z direction. Therefore, for the three d.o.f. s at x, y, z of each node, only the component at the z direction is non-zero. Obviously, $\Delta\mathbf{P}_i$ can be calculated at the element level. From Eqs. (4.15)&(4.16) and recalling Eq. (3.20) and that $\Delta\mathbf{K} = -\mathbf{K}_i$, we define the element sensitivity number as

$$\alpha_i = \frac{\mathbf{u}_i^T \mathbf{K}_i \mathbf{u}_i + 2\Delta\mathbf{P}_i^T \mathbf{u}_i}{W_i}. \quad (4.17)$$

The first term in the numerator representing the strain energy is always positive. The second term is equal to $-2\mathbf{P}_i^T \mathbf{u}_i$. As \mathbf{u}_i is usually in the same direction as \mathbf{P}_i , this term is negative in most cases.

2. Addition Criteria

There are two alternative ways to consider the addition criteria. The first one is that adopted in the basic BESO, i.e. adding elements around the elements of the *largest strain energy* (i.e. $\mathbf{u}_i^T \mathbf{K}_i \mathbf{u}_i$). This will in general help to disperse the strain energy and make a more uniform distribution. However, it is only an approximate means as the change in the load vector induced by the addition is ignored. The accuracy is acceptable if the change is small but not for the case of large changes. Meanwhile, how significant the change is can be uncertain and problem dependent.

The second way is to directly calculate the sensitivity number for *potentially added elements* using Eq. (4.15) or (4.17) with some variations in the signs of $\Delta\mathbf{K}_i$ and $\Delta\mathbf{P}_i$.

However, it is noted that the displacement of a potential added element is to be extrapolated according to the assumed displacement field. For incompatible 2D or 3D elements as adopted in this thesis, the extrapolation for one node is not unique and varies with the nodes employed as the base displacements. In this respect, an average value can be taken but it raises the same question of accuracy as concerned in the first way.

For the above arguments, we exclude the addition criteria for the problem considering self weight, i.e. ignore BESO and only ESO is performed. This is acceptable as the role of BESO is not indispensable but complements the ESO and serves as an alternative way. The ESO procedure is present in the flowchart in Fig. 4.10.

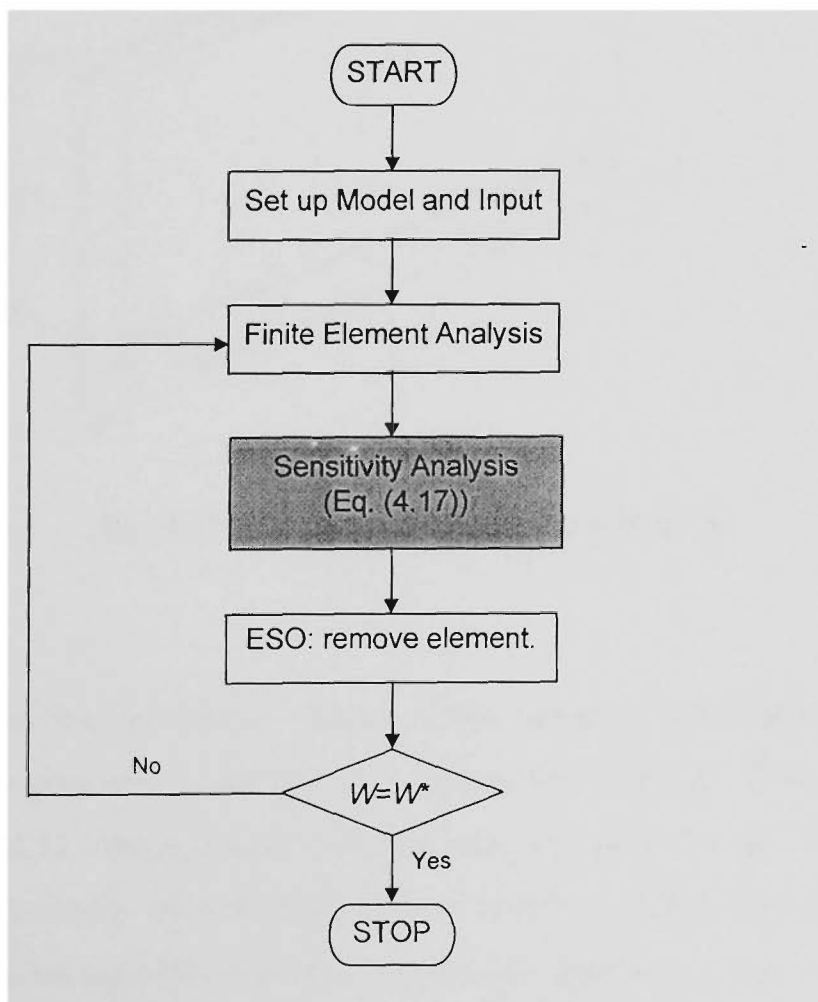


Fig. 4.10. Flowchart: ESO procedure for optimisation considering gravity loading.

4.3.3 Examples

Example 4.3.3.1 A 3D arch bridge.

A 3D version of arch bridge is shown in Fig. 4.11. The design domain is a rectangular block of dimensions of $L \times H \times B = 1.2\text{m} \times 0.6\text{m} \times 0.2\text{m}$. Its two end sides are hinged to supports. $E = 210 \text{ GPa}$, $\nu = 0.3$ and density of $\rho = 2700 \text{ kg/m}^3$ are assumed. The design objective is to minimise the mean compliance under gravity loading only for a given weight $W^*/W_0 = 15\%$. A half model is divided by $3375 = 50 \times 25 \times 3$ 8-node brick elements.

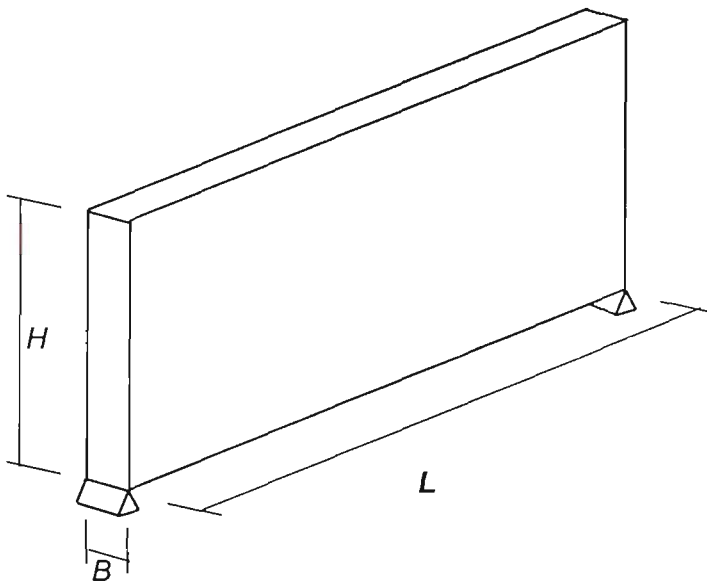


Fig. 4.11. Design domain under gravity loads.

It is well known that the ‘optimal’ design in this case is an arch bridge. Following the ESO procedure presented in the previous section, we obtain an optimum topology as shown in Fig. 4.12, which is quite different from our prediction of an arch. However, such a design is exactly what the optimisation intends to. In fact, the stiffest solution is two columns on the top of the end supports. As each support only has one row of nodes, the columns would tumble inwards. The small arch joining the columns is thus presented to prevent the tumbling.

This can be explained further from the calculation of mean compliance. Examining the expression, $\sum_{i=1}^n \mathbf{P}_i \mathbf{u}_i$, can be written as $\sum_{i=1}^n \frac{1}{8} qV(u_1 + u_2 \dots + u_8)_i$. As the converted gravity nodal load $\frac{1}{8} qV$ is the same for all elements, the contribution of each element is largely determined by the displacements $u_1, u_2 \dots u_8$. (which are in the same direction as the gravity load in most cases). Elements in the mid-span, for example, have the largest displacement, thus contributing the most to the mean compliance. The elements around the supports, however, have the smallest displacement so their contribution is small. This may explain the tendency of accumulating material towards the supports region. On the other hand, the material in the support region has very low stress, so it is expected that it would have been removed on a stress criteria. To verify this point, an optimisation based on stress criteria is performed.

As presented in Chapter 2, stress based optimisation was the very first attempt of ESO based on which a systematic method has been developed (Xie and Steven 1997). Its fundamental idea is that by slowly removing elements of low stress, the stress distribution in the structure becomes more uniform. For static determinate structure, the solution has all its element/member with the same stress, and is a full-stressed design (FSD), as pointed by many researchers (Rozvany and Prager 1979; Haftka and Gürdal 1992).

In this example, instead of removing elements of the lowest sensitivity number of mean compliance, the element efficiency is measured by a von Mises stress. The resulting topology optimum is shown in Fig. 4.12, which is a 3D arch bridge as expected with a height-to-length ratio $H/L=0.42$. Table 4.1 compares the mean compliance and stress for solutions obtained by stiffness (case 1) and stress-based (case 2) optimisation. The stress uniformity is evaluated by a simple measure as ratio of the minimum stress to the maximum one (Xie and Steven 1997). It is observed that:

1. In terms of the maximum element von Mises stress σ_{\max}^{VM} , the stress-based case has a lower value than the stiffness case, and a much higher value of stress ratio. This

conforms to the optimisation objective as obtaining a more uniform stress distribution.

2. In terms of mean compliance, the stiffness-based case has a smaller value than the stress-based one. This verifies the design objective of stiffness optimisation.

Therefore, it can be said that the solution is in line with its intended design objective.

Table 4.1. Comparison of Example 4.3.3.1

	Stiffness optim.	Stress-based optim.
W	14.99%	15.04%
σ_{\max}^{VM} (Pa)	0.72802×10^5	0.68268×10^5
σ_{\min}^{VM} (Pa)	0.41769×10^3	0.11924×10^5
$\sigma_{\min}^{VM} / \sigma_{\max}^{VM}$	0.57%	17.46%
C (N.m)	0.1534×10^{-4}	0.1680×10^{-4}

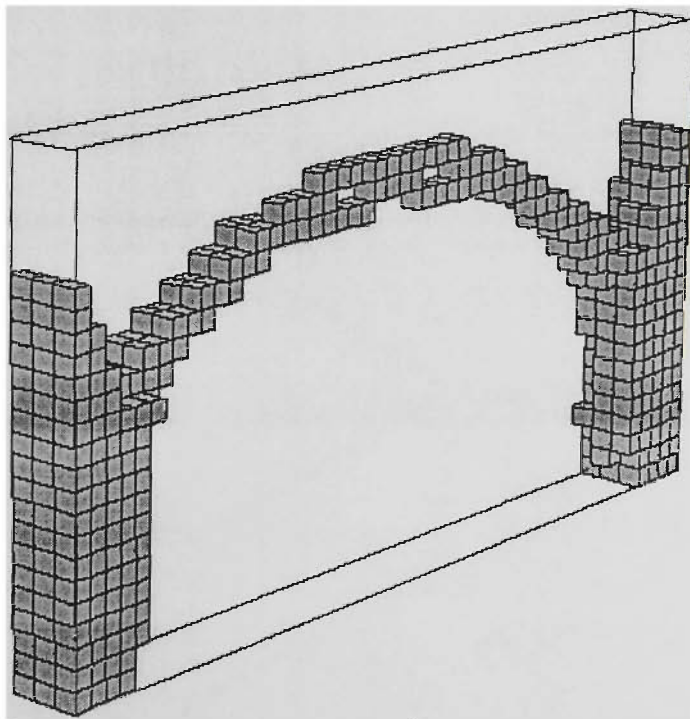


Fig. 4.12. Topology design (stiffness optimisation).

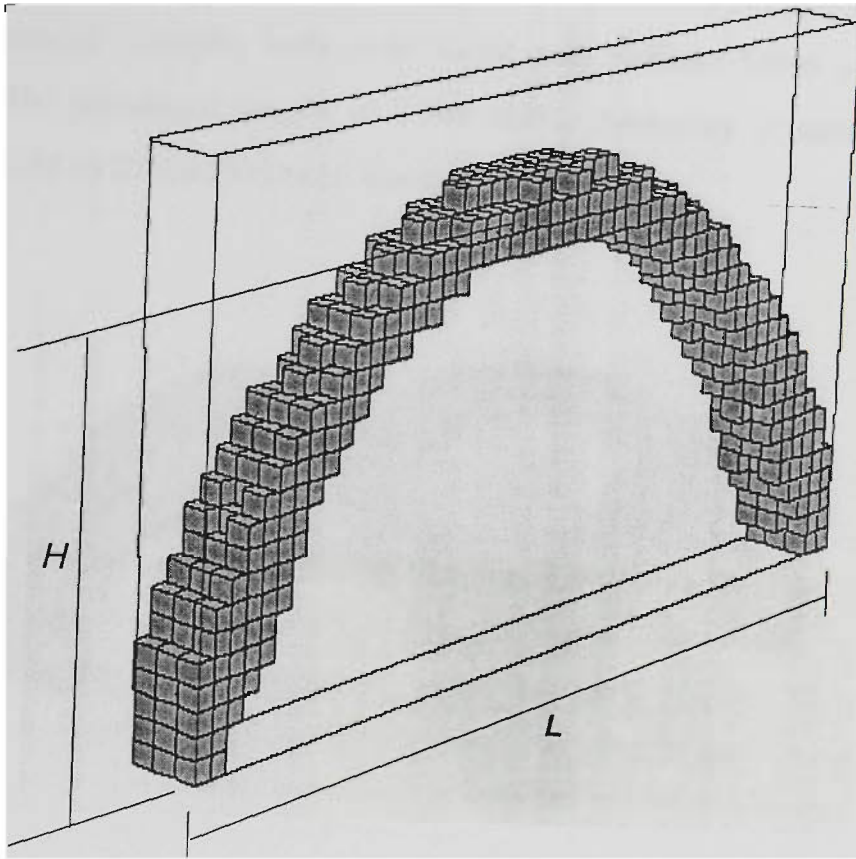


Fig. 4.13. Topology design (stress-based optimisation), $H/L=0.42$.

Example 4.3.3.2 A box block.

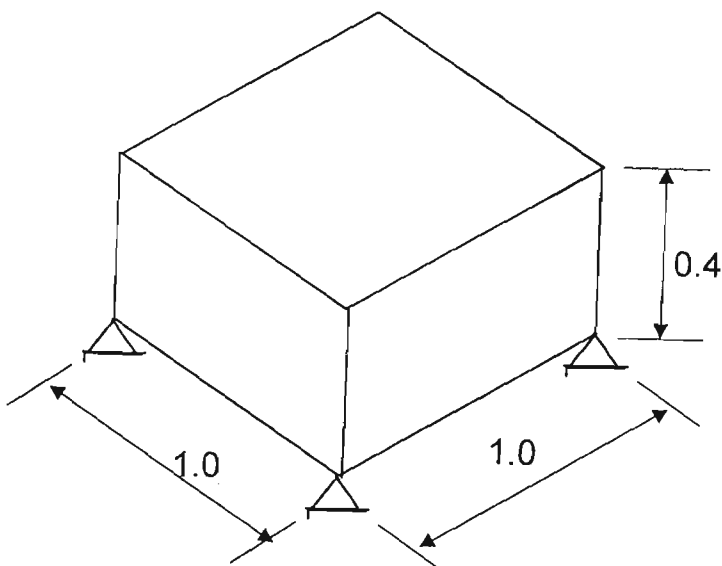


Fig. 4.14. Design domain of a box block.

As shown in Fig. 4.14, the design domain is a solid block fixed at four bottom corners. $E=210$ GPa, $\nu=0.3$ and $\rho =2700$ kg/m³ are assumed. Gravity loading is applied only. Like the previous example, both stress-based and stiffness based optimisation are performed. The prescribed weight is $W^*/W_0=10\%$. Symmetry is used and a quarter model is divided by 3375= $15\times 15\times 15$ 8-node brick elements.

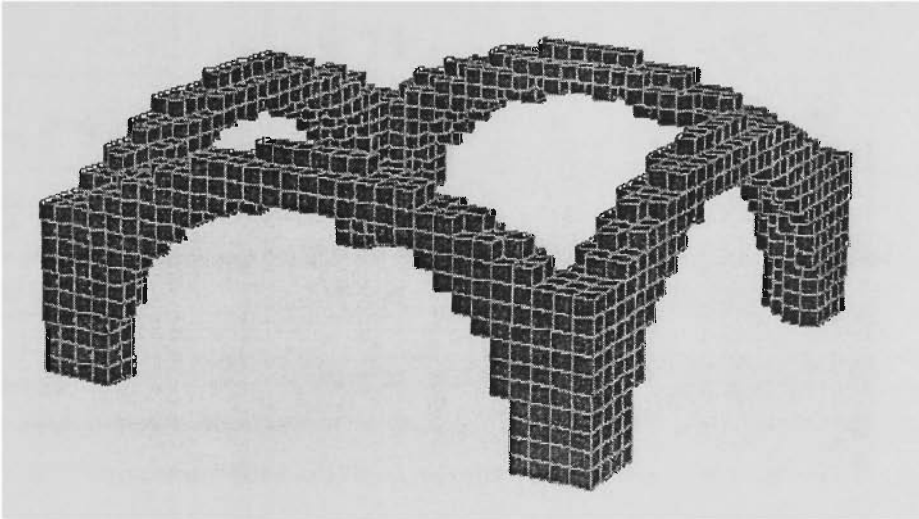


Fig. 4.15. Topology design (stiffness optimisation).



Fig. 4.16. Topology design (stress-based optimisation).

In Fig. 4.15, the design of minimum mean compliance is quadrilateral court enclosed by combinations of four arches. In comparison, stress-based design is a dome like structure where the central top roof is connected to the closest supports. Table 4.2 compares the

mean compliance and stress of these two designs. The same observations as in Example 4.3.3.1 can be made.

Table 4.2. Comparison of Example 4.3.3.2

	Stiffness Optim.	Stress-based Optim.
W	10.01%	10.01%
σ_{\max}^{VM} (Pa)	0.492532×10^6	0.490792×10^6
σ_{\min}^{VM} (Pa)	0.300505×10^4	0.105779×10^5
$\sigma_{\min}^{VM} / \sigma_{\max}^{VM}$	0.610%	2.155%
C (N.m)	0.8019×10^{-4}	0.8662×10^{-4}

Example 4.3.3.3 A cable bridge.

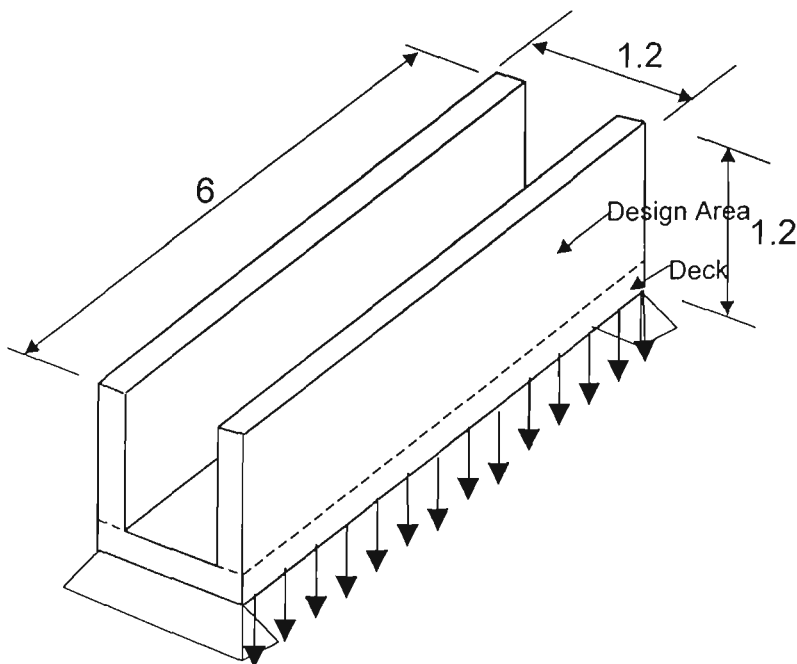


Fig. 4.17. The design area.

As shown in Fig. 4.17, A box beam is fixed at two supports. $E=210$ GPa and $\nu=0.3$ are assumed. A combination of gravity loading and external loads are considered, with density of $\rho=2700$ kg/m³ and distributed loading of intensity $q=0.094$ MPa. These values are such that the work done by these two load components in the ground structure is almost equal.

Due to symmetry, a quarter model is used and the quarter domain is divided by a mesh of $45 \times 18 \times 9$. Fig.4.18 shows the optimal design in a form of cable bridge. It has a mean compliance of $C=0.575$ N.m.

In comparison, a case considering only the external loading is solved and the topology is shown in Fig. 4. 19. Its mean compliance is $C=0.274$ N.m.

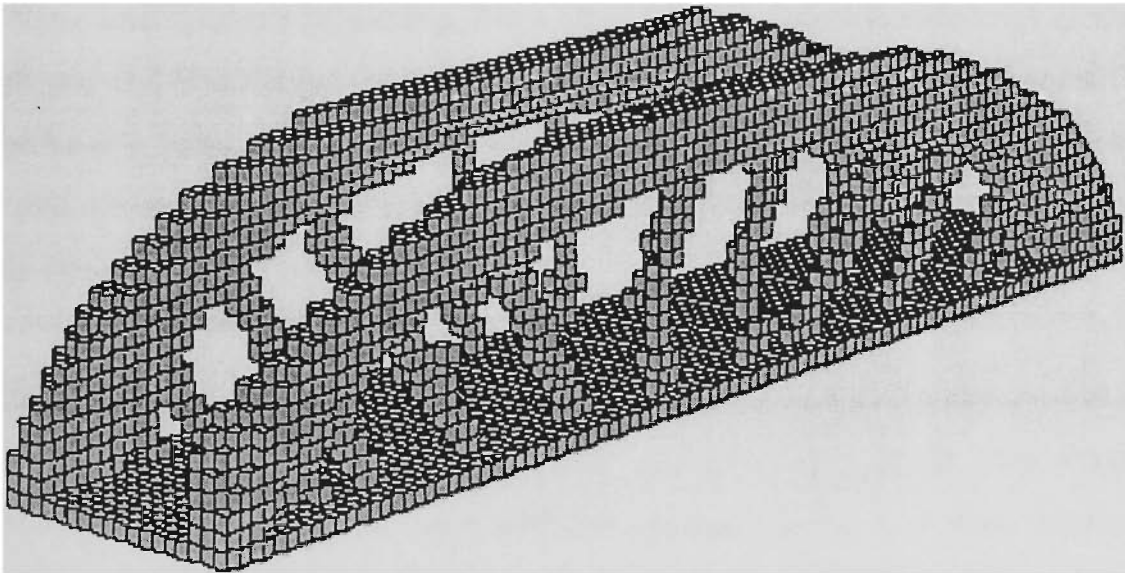


Fig. 4.18. Topology design (including gravity).

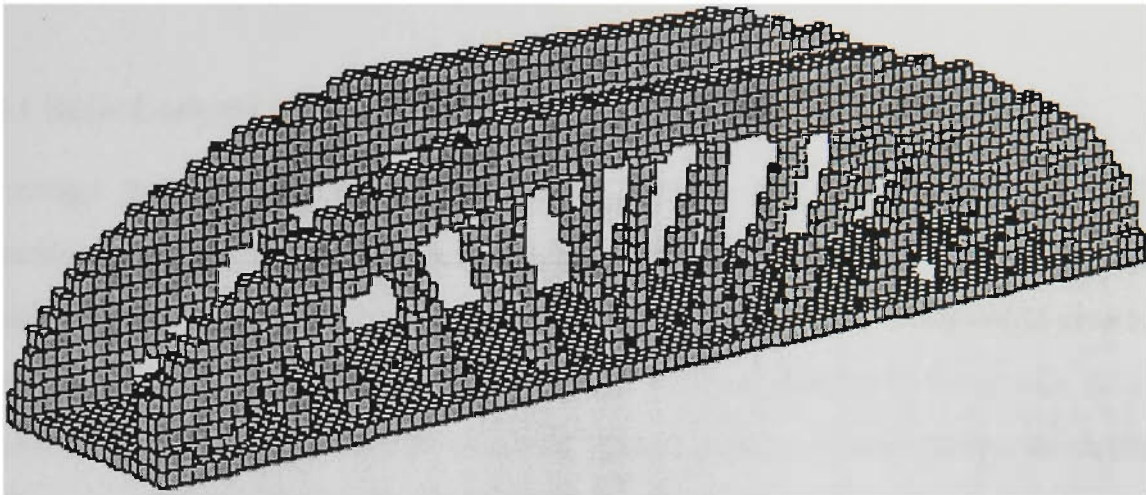


Fig. 4.19. Topology design (external loading only).

In the above examples, the ESO method has effectively found optimal solutions to problems including gravity loading. For a 3D element, a simple 8-node brick element is employed as it is sufficient for the concerned design problems and is much more cost – effective (e.g. compared to 20-node element). If other kinds of elements are employed, the load conversion becomes more involved, but the expression for sensitivity analysis is the same.

Stiffness and stress-based problems can be largely equivalent which is observed in many ESO applications (Li *et al.* 1999). In some special cases such as truss structures (2D&3D), they are exactly the same with the optimal solution as a static determinate structure. Despite differences in these two optimisation problems observed in 3D continuum, comparisons show the solution of each optimisation case fulfils its intended design objective.

4.4 Topology Optimisation with Surface Loading

4.4.1 Basic Concept

Topology optimisation considering surface loading was successfully addressed by Hammer and Olhoff (2000). The loads are pressures applied to a subdomain surface which connects some defined points or points allowed to move along some prescribed lines. Based on the SIMP algorithm where the element density is the design variable, iso-volumetric density spline curves are defined to make a smooth surface for applying the pressure. The pressure is then converted to consistent nodal loads at each element.

Defining the iso-volumetric density curves in the above procedure adds considerable complexity to the optimisation problem. As an initial investigation of surface loads using ESO/BESO, we may simplify the problem and assume that the load only changes at the applying location but keeps its direction. As shown in Fig.4.20(a), vertical downward pressures are applied at the upper surface of the structure (xy plane). If the design changes to Fig. 4. 20(b) after removing element R1, R2 & R3, the pressure will be still vertical downward, and applied to the new surface, precisely, the segment of local xy plane of each element. This implies that the total external loads are constant and equal to the summation of loads carried by individual surface. Understandably, if one loaded element is removed at one step, the loads will *move along its direction* to the element connecting to and closest to it, and be applied at the corresponding face (or edge), for example, the upper face of elements R1, R2&R3 vs. the upper face of elements 4, 5&6. It is the same with the case of 2D element, as shown in Fig. 4.21.

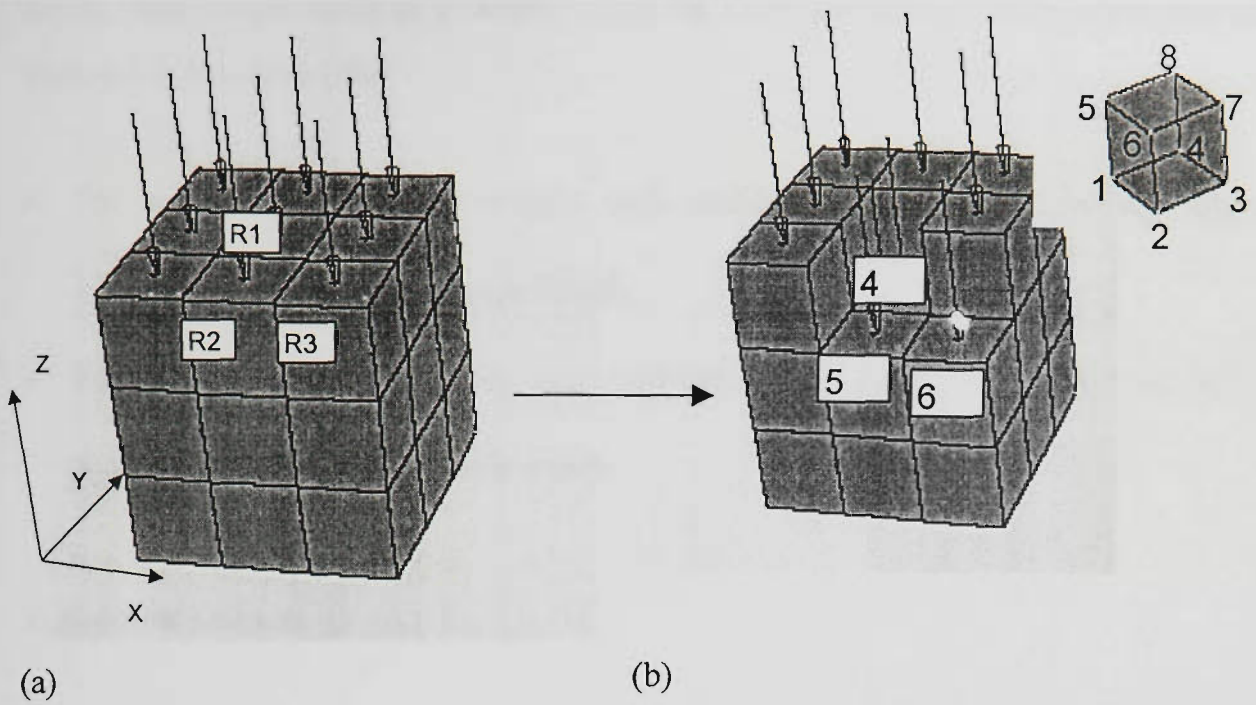


Fig. 4.20. Moving of surface loading (3D).

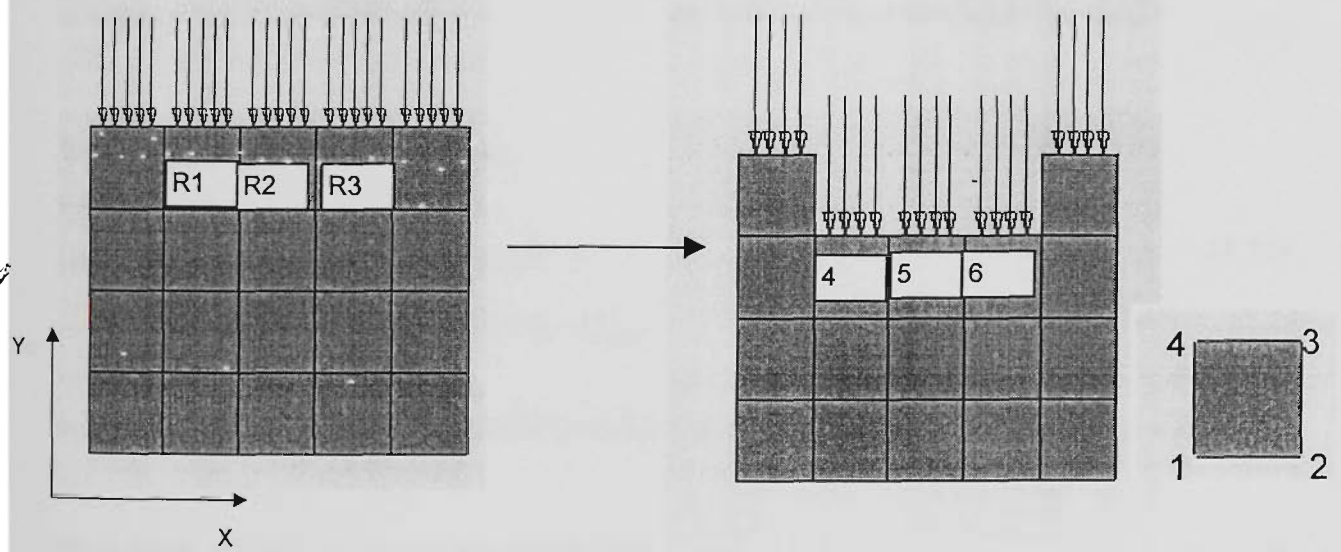


Fig. 4.21. Moving of surface loading (2D).

4.4.2 Sensitivity Analysis

Similar to the case of gravity loading, we shall first convert the surface loading to nodal loads, then the change in global load vector is to be addressed.

Again, take simple cases as example, using Eq. (3.3) and follow similar procedure to Sect. 4.3.2, it is found that

- For a 4-node rectangular element with uniform normal stress q at one edge, $\mathbf{r}_e = \frac{1}{2}qL_e$, where L_e is the edge length.
- For an 8-node brick element with uniform normal stress T on one face only, $\mathbf{r}_e = \frac{1}{4}TA_e$ where A_e is the surface area.

1. Removal criteria

In Figs. 4.20 and 4.21, for a 4-node element to be removed, if it is a loaded element, removing cause change in load vector

$$\Delta \mathbf{P}_i = \frac{1}{2}qL\{0,1,0,1,0,-1,0,-1\}_{8 \times 1}^T \quad (4.18)$$

Similarly, for an 8-node element,

$$\Delta \mathbf{P}_i = \frac{1}{4}qA\{0,0, 1,0,0, 1,0,0, 1,0,0, 1,0,0,-1,0,0,-1,0,0,-1,0,0,-1\}_{24 \times 1}^T \quad (4.19)$$

where the nodes of one element follows the numbering rules as shown in Fig. 4.20&21.

Therefore, all are known in calculating the element sensitivity number. In summary, for elements with applied loads, using Eq. (4.17); for elements without loads, simply using Eq. (3.20).

It is worth noting that the sensitivity analysis is based on the assumption that the change in the physical modification and load fields is very small. To ensure a sufficient load change, we introduce two heuristic rules:

1. Only shape optimisation is performed, i.e. materials are nibbled away from the structural boundary, thus the load changes between corresponding elements are gradual, i.e. layer by layer, as shown in Figs 4.20 & 21.
2. In the case where topology optimisation is performed, if the element has no element connected in the load direction (i.e. there is a gap between two elements), as elements 1&2 in Fig. 4.22, they are kept unchanged and removal are not allowed. In fact, the sensitivity calculation from Eq. (4.17) is no longer applicable in this case.

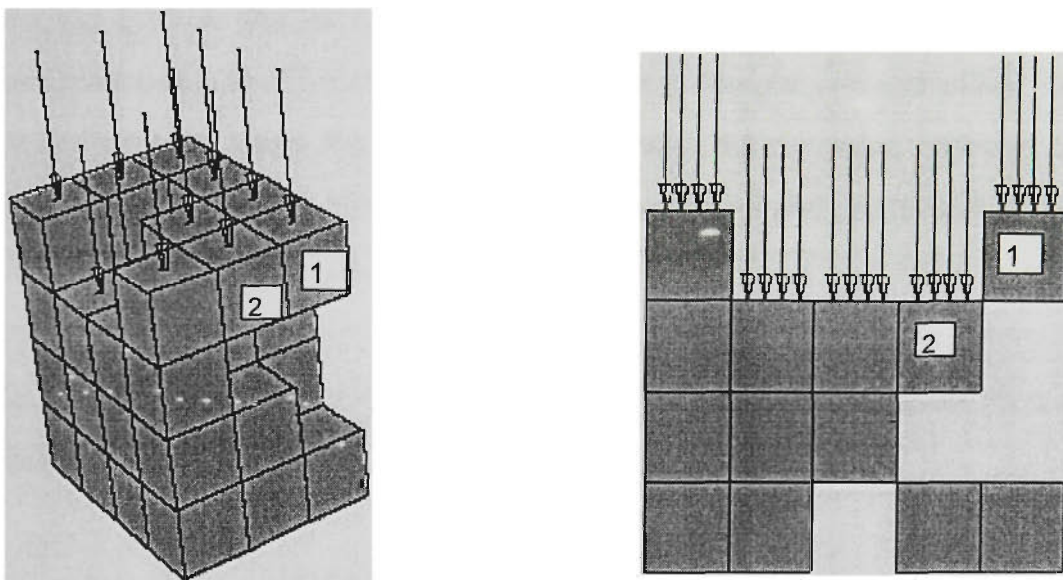


Fig. 4.22. Special types of elements which are kept unchanged.

2. Addition criteria

As discussed in Sect. 4.3.2, changes in load vector make sensitivity analysis for added elements difficult, be it a gravity load or surface load. However, there are differences in these two cases. While gravity load is in general applied to each node of the whole structures, the surface load can act on part of structure only and not all nodes have to be involved. Given the simple case as studied in this section, it is assumed that the structure is only applied with surface loading in one plane which is the projection of one

of xy , yz or zx planes. Therefore, for a 3D element, one element is either free or loaded at only one face. By using some measures, it is possible to keep the load vector unchanged when adding elements:

Firstly, for load-free elements, addition will not affect the load vector. For this kind of element, *one* sensitivity number is calculated using Eq. (3.20) and it is used for *both* the removal and addition criteria, i.e. if the number is among the smallest, it is removed; if being the largest one, extra elements are added around.

Secondly, for loaded elements, it is specified that the elements are only added around the load-free faces so that the load vector will not change. For this kind of elements, *two* sensitivity numbers are calculated and used *separately* for removal and addition criteria. First, calculate No.1 using Eq. (4.17) and check with the removing criterion. Second, calculate No.2 using Eq. (3.20) (i.e. element strain energy) and check with the addition criterion. A problem associated with using different removal and addition sensitivity numbers is that one element can be in both pools and eligible for removing *and* addition. Though very rare in practice, this case is handled with a conservative rule by choosing an addition operation.

Therefore, both ESO and BESO can be applied for optimisation with surface loading. The flowchart is shown in Fig. 4.23.

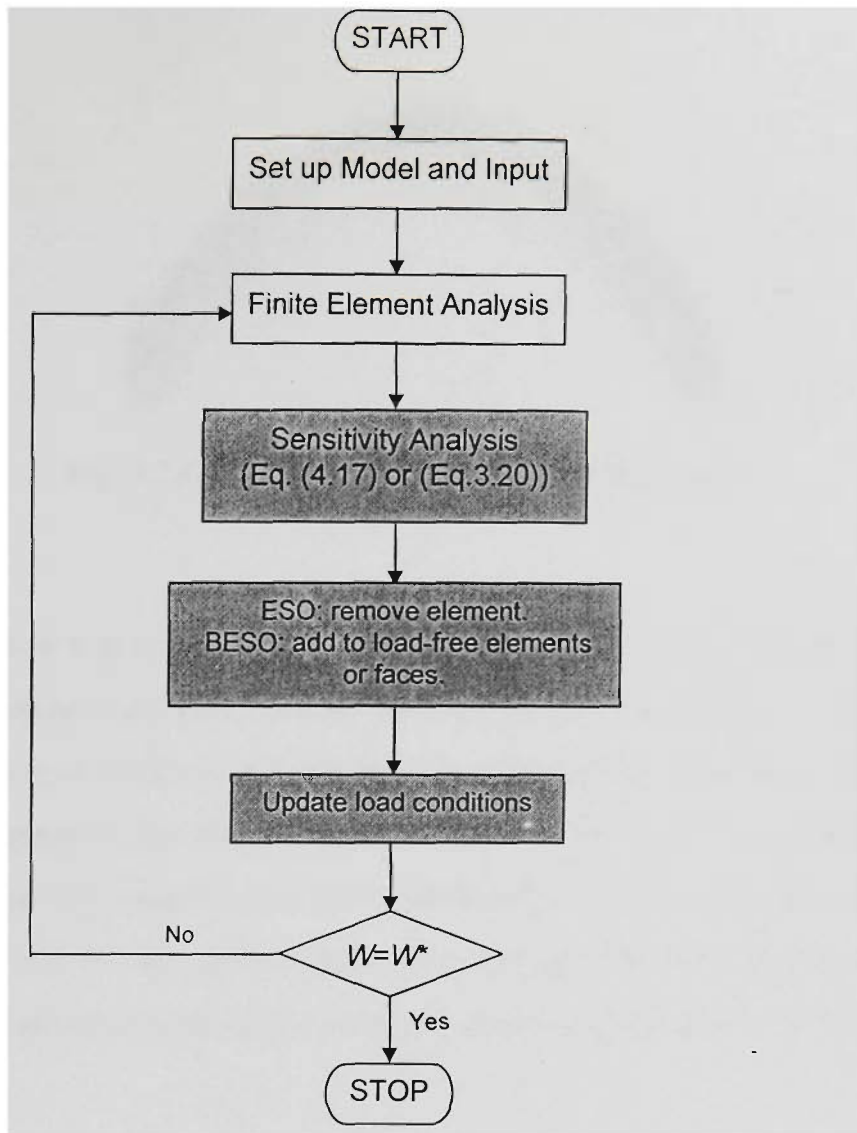


Fig. 4.23. Flowchart: ESO/BESO procedure for optimisation considering surface loading.

4.4.3 Examples

Example 4.4.3.1 2D arch bridge.

The optimal design carrying the transmissible loading has studied in Sect. 4.2.3. As an extension, we change the problem to finding the optimal topology that carries the downward surface loading at the top. ESO procedure is used. The final design is shown in Fig. 4.24.

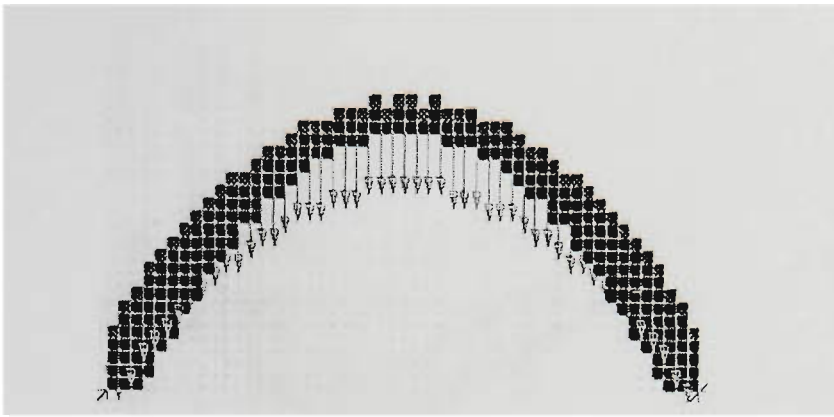


Fig. 4.24. Optimum topologies for surface loading.

The design has a mean compliance $C=24.7$ N.m, which is between $C=13.7$ N.m for transmissible loading and $C=51.0$ N.m for fixed loads. For surface loading, while the load location is optimised compared to the case of fixed case, the extent of optimisation cannot be compared to the case of transmissible loading. In fact, there are many other possibilities regarding how the load can be allocated along the action line, instead of just imposing the load on one surface node. The transmissible loading can be the ‘best’ possibility as it allows for the largest extent of relaxation on loading conditions.

Example 4.4.3.2 A block supporting pressure.

This example is inspired by the work of Fuchs and Moses (2000), as shown in Fig. 4.25. The block is hinged at four bottom supports and the top surface is subjected to the uniformly distributed pressure.

The problem is treated in the reference as a transmissible loading case. In the same attempt to solve it by using ESO and BESO, it is found the running time for finite element analysis is prohibitively high due to the introduction of a large number of constraint equations (e.g. for a mesh of $15 \times 15 \times 15$, $16 \times 16 \times 15 = 3840$) equations in the ground structure). Formulating the problem as surface loading, however, adds no extra cost in finite element analysis thus a computationally more feasible way for this example. Both ESO and BESO are performed, $MR=2\%$ for ESO, and $MR=4\%$, $AR=0.33$ and $SR=0.50$ for BESO.

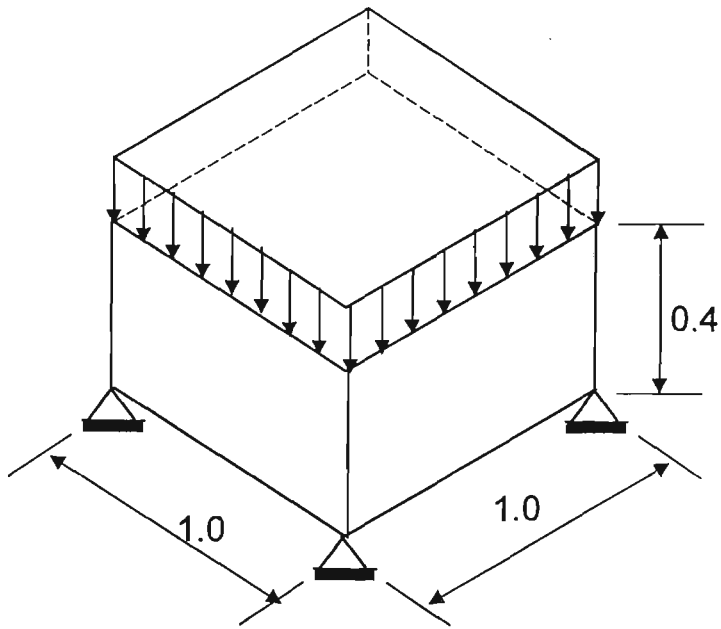


Fig. 4.25. Design domain of a rectangular block, uniform pressure at the top face.

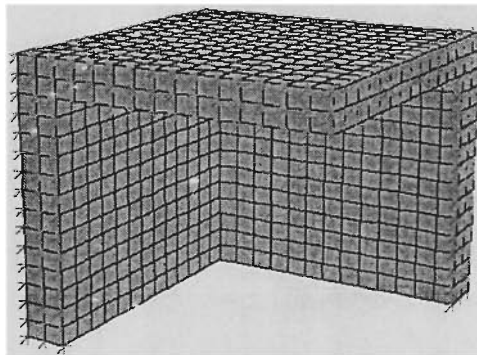
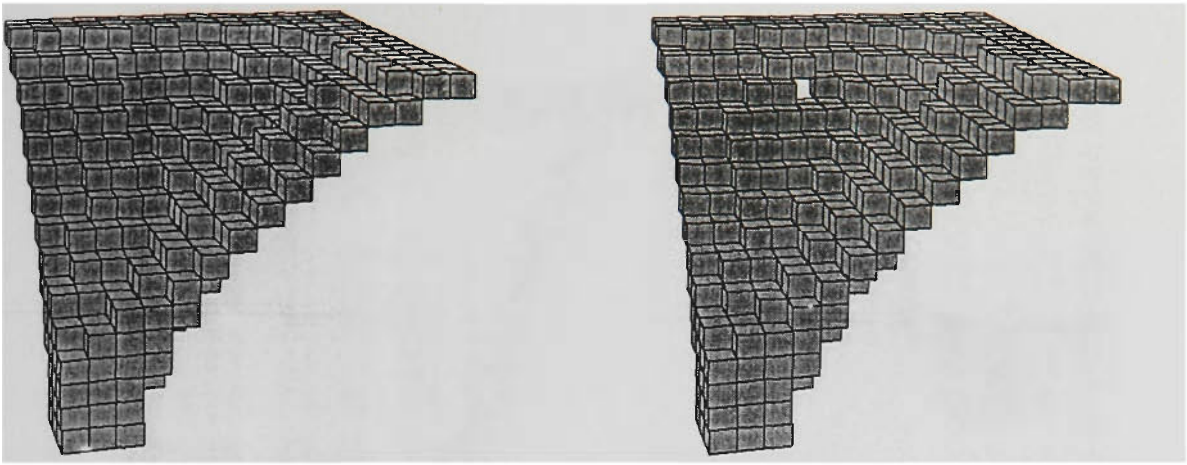


Fig. 4.26. Initial design for BESO, quarter model, hatched areas are symmetric surface.

Only a quarter of model is used due to symmetry and it consists of $15 \times 15 \times 15 = 3375$ elements. The initial design for BESO is shown in Fig. 4.26. The optimal designs with 10% of the weight by ESO and BESO are shown in Fig. 4.27. They are very much the same. A full model of BESO design is shown in Fig. 4.28. A shape resembling a gothic vaulting emerges, clearly revealing the arches between adjacent supports and two arches supported diagonally (Fig. 4.29).



(a) ESO.

(b) BESO.

Fig. 4.27. Optimal topologies (quarter model).

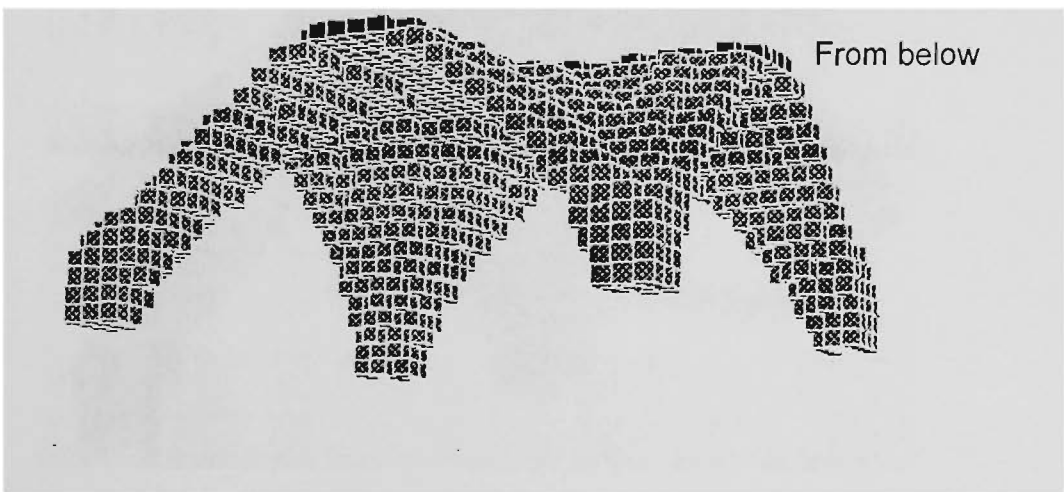
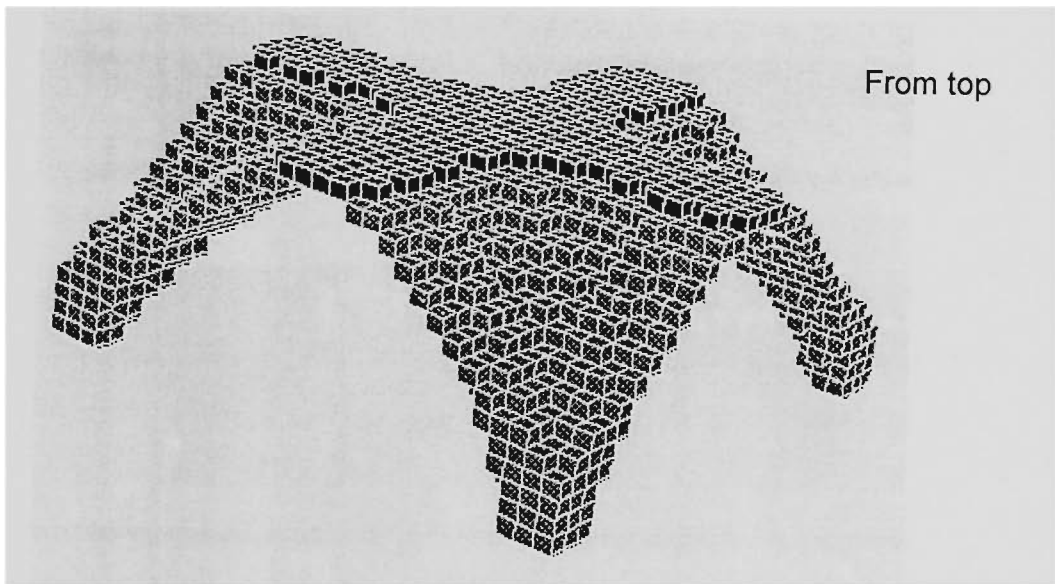


Fig. 4.28. Optimal topologies (full model of BESO result).

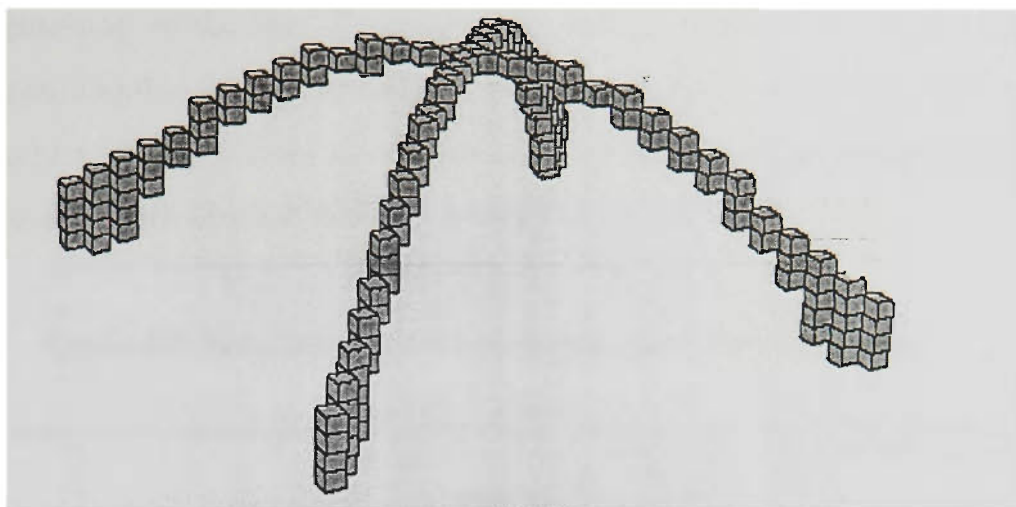


Fig. 4.29. Extract of a diagonal arch from the full model.

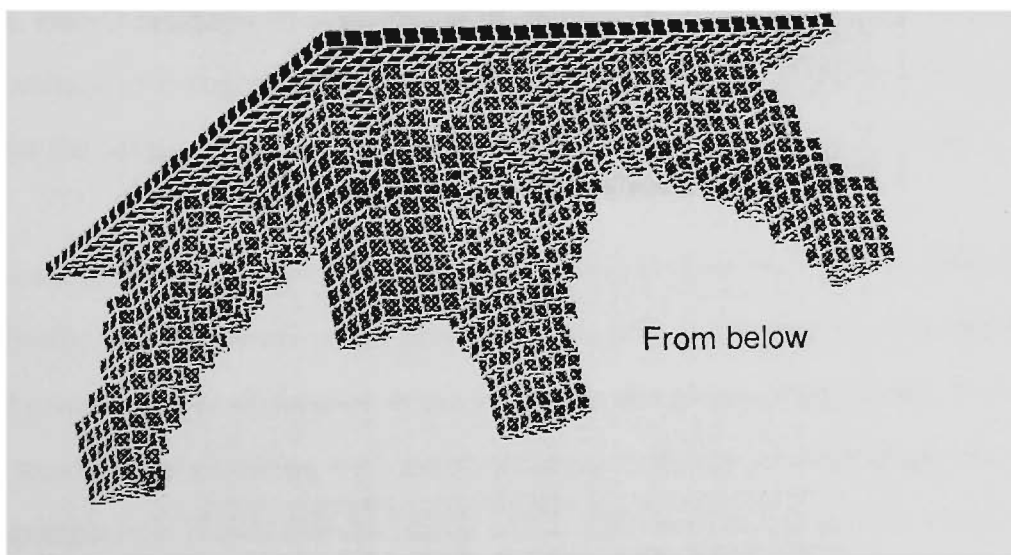
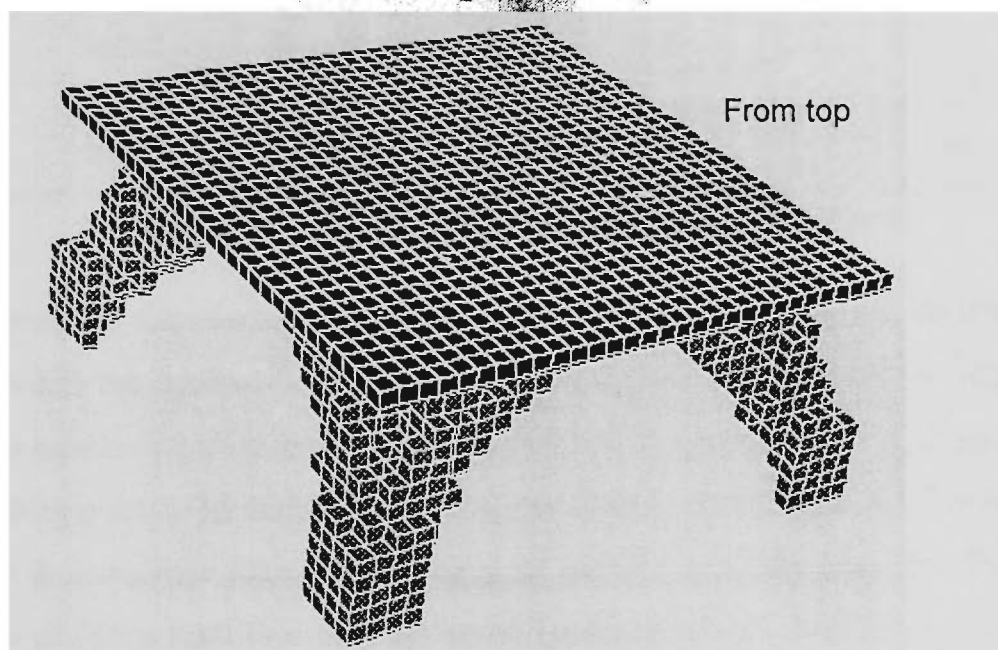


Fig. 4.30. Topology of design supporting top pressure.

It is natural to compare the above result with cases of fixed load location, i.e., the pressure remaining on the top. The loaded top layer is assigned non-design elements which are not modified during evolution. The optimal design is presented in Fig. 4.30. It turns out to be a table like structure with the top face, four main legs transferring load to the supports and zones of small bars connecting the top and legs.

Table 4.3. Results on Surface Loading and Fixed Loading

Cases		WW*	Iteration	Computing Time (Hour: Min.)	Mean Compliance C/C ₀
Fixed loading	ESO	15.29%	146	8:50	1.380
	BESO	15.47%	116	3:57	1.379
Surface loading	ESO	10.4%	145	7:16	1.380
	BESO	10.1%	145	2:58	1.379

Table 4.3 provides the numerical results for two cases by both ESO and BESO. It is noted that while the optimal designs for fixed loading and transmissible loading have more or less equal value of mean compliance, the latter has a much smaller weight (10% to 15%), which point to its strength in finding an ‘optimum’ load locations. Further, the comparison in computing time sees BESO is far more efficient for this case. Firstly, a larger value of MR is used thus the number of iterations in ESO and BESO are almost comparable. BESO normally uses a smaller FE model than ESO at each iteration, which results in savings in computing efforts. At the same time, the solution quality is not sacrificed for the savings, as the values of mean compliance are almost the same.

Quantitative comparisons to other benchmark solutions (Fuchs and Moses 2000) are not available, firstly due to variations in problem formulation (surface vs. transmissible), and secondly due to slight difference in the geometry and physical properties. However, as cases of transmissible loading and surface loading is similar in a non-rigorous sense, qualitative comparison shows that the image of the topology design as a 3D vault agrees reasonably well.

4.5 Conclusions

The basic ESO/BESO is extended to solve optimisation problem considering load variations. The transmissible loading is considered as a constraint on uniform displacement among the action line. The gravity and surface loading has an effect on the sensitivity analysis. Apart from these aspects, the procedure and computer algorithms are almost the same as those for basic ESO/BESO. This demonstrates that the evolutionary algorithms are easy to generalise and adapt.

Comparing to fixed loading conditions, designs allowing for surface loading provides a better solution because the load location is optimised to some extent. Transmissible loading, which allows for the largest degree of relaxation on loading conditions, is the 'best' design and able to reveal a clear pattern of loading bearing structure. For optimisation including self-weight, differences are observed in stiffness and stress-based topologies. It is verified that they are the optimal solutions for each intended problem formulations.

As observed in Chapter 3, BESO can be computationally more efficient than ESO for a large FE problem.

ESO and BESO for Frequency Optimisation

This chapter applies ESO and BESO to frequency optimisation of 2D and 3D structures. The basic problem statement is presented with respect to objective functions of single frequency and multiple frequencies. Sensitivity analysis of objective function is performed and element sensitivity number is derived. The ESO and BESO procedures are proposed which are similar to those for static problems. Several issues related to frequency optimisation are discussed, including repeated eigenvalues, closely-spaced eigenvalues and optimisation of a desired mode shape. They are incorporated into the ESO/BESO methods with minor modifications. A range of 2D and 3D examples are given for verification.

5.1. Introduction

Structural dynamic design and optimisation are of great importance in various fields, such as aircraft flutter control, aseismic design of high rise building, and the design of space structure and their control system. The objective functions and constraints in dynamic optimisation can be dynamic displacement or stress and natural frequency.

When the optimisation is focused on direct dynamic response, the dynamic behavior can be analyzed in either frequency or time domain, depending on the nature of the loading. The former has been effective in addressing optimisation of systems under harmonic excitation or random excitation and the latter for transient response under impact loading. In dealing with the frequency response problem, the objective can be the

response amplitude and the stress (Sadek 1995), or equivalent dynamic mean compliance corresponding to a single excitation frequency or over a frequency spectrum (Ma *et al.* 1993). In optimal design under random excitation, the mean square response can be taken as the constraint (Rong *et al.* 2001a). Time domain analysis is less popular due to the high cost associated with numerical integration of a large scale problem. The most recent results might be on the transient response under impulsive loadings where the design objective is the mean dynamic compliance within a specified time integral (Min *et al.* 1999). Explicit direct integration is used to solve the transient problem. Alternatively, the impact-type dynamic loading can be transformed to the equivalent static loading on the principle of same displacement pattern. Then the optimisation routine for static problems can be followed (Kang *et al.* 2001).

Dynamic response is significantly affected by the natural frequencies in many ways. Excessive response will be caused if the structural frequency is close to the excitation frequency. It is also desirable that the frequencies be sufficiently spaced for some wide spectrum excitation. In some situation such as designing a bell, the first several frequencies are rigorously specified and such a shape design poses a real challenge. There has been extensive research on natural frequency optimisation and a survey by Grandhi (1993) gives a list of bibliography, covering the problem statement, algorithms and sensitivity analysis. The objective functions/constraints are normally maximising a single or multiple eigenvalues. The sensitivity analysis for distinct frequencies has been well addressed (Fox and Kapoor 1968) and much effort has been devoted to non-distinct or repeated frequency (see Seyranian *et al.* 1994 for a survey). As for eigenvector sensitivities, there are Nelson's method (Nelson 1986), the modal method (Mills-Curran 1988), an improved modal method (Ojvalvo 1988; Wang 1991) and modal truncation method (Liu *et al.* 1994).

It is noted that there have been great advances in dynamic optimisation by changing topologies, compared to the previous size and shape optimisation. The homogenisation methods together with its variants, for example, have solved frequency optimisation for 2D and 3D structures, with single and multiple frequencies (Díaz and Kikuchi 1992;

Tenek and Hagiwara 1993; Ma *et al.* 1993; Ma *et al.* 1995; Mijar *et al.* 1998). In ESO/BESO, results have been obtained on 2D structures with the natural frequency or random response being the design objective (Xie and Steven 1994; Xie and Steven 1996; Yang *et al.* 1999b; Rong *et al.* 2001a).

Based on the above ESO/BESO research, this chapter presents the frequency optimisation on 2D and 3D structures. It is organised as follows: Sect. 5.2 presents the problem statement and sensitivity analysis, followed by proposing the ESO/BESO procedures. Three special issues are dealt with in Sect. 5.3, namely, repeated eigenvalues, closely-spaced eigenvalues and keeping tracking of a desired mode shapes using a modal assurance criterion (MAC). Sect. 5.4. provides a range of examples covering problems of single frequency, multiple frequencies, closely-spaced frequencies and mode tracking. Both ESO and BESO are performed and results are compared.

5.2. Basic Concepts

5.2.1. Problems Statement

In a finite element model, the vibration of a free, undamped elastic structure system is governed by an eigenvalue equation:

$$(\mathbf{K} - \lambda^j \mathbf{M})\phi^j = \mathbf{0}, \quad (5.1)$$

where \mathbf{K} and \mathbf{M} are global stiffness and mass matrices, and λ^j and ϕ^j are the j th eigenvalue and eigenvector, respectively.

The optimisation problem can be stated as

$$\text{Maximise } f = \lambda^j. \quad (5.2a)$$

$$\text{Subject to } g = W * -\sum_{i=1}^n W_i x_i = 0, \quad (5.2b)$$

$$x_i \in \{0,1\}. \quad (5.2c)$$

There are a few variations based on the above formulations. In some cases, a problem is presented as to satisfy a given individual or series of eigenvalues (or circular frequency in Radial) $\omega^{*j_0}, \omega^{*(j_0+1)}, \dots, \omega^{*j_n}$. To consider such a multiple objective function, a function is built as the average distance between the actual and target circular frequencies:

$$\text{Minimise } f = \sum_{k=j_0}^{k=j_n} c_k \frac{(\omega^k - \omega^{*k})^2}{(\omega^{*k})^2}, \quad (5.3)$$

where c_k is some user-defined weight coefficient.

The above definition can also be applicable for maximising a set of frequencies, where the target frequencies are given by the maximum obtained by optimising each single frequency as stated in Eq. (5.2).

5.2.2. Sensitivity Analysis

By applying variation operations on Eq. (5.1), the eigenvalue sensitivity is calculated by the following equation (Fox and Kapoor 1968):

$$\Delta\lambda^j = \frac{\phi^{jT} (\Delta\mathbf{K} - \lambda^j \Delta\mathbf{M}) \phi^j}{\phi^{jT} \mathbf{M} \phi^j}. \quad (5.4)$$

It is common that mode shapes are orthogonal with respect to the global mass matrix, i.e. $\phi^{jT} \mathbf{M} \phi^j = 1$. And also, when removing one element i , the change in the stiffness and mass matrices are $\Delta\mathbf{K} = -\mathbf{K}_i$ and $\Delta\mathbf{M} = -\mathbf{M}_i$, respectively. Therefore, Eq. (5.4) becomes

$$\alpha_i^j = \Delta\lambda_i^j = \phi_i^{jT} (\lambda^j \mathbf{M}_i - \mathbf{K}_i) \phi_i^j, \quad (5.5)$$

Where α_i^j is the sensitivity number of the j th eigenvalue due to the removal of element i . ϕ_i^j is the eigenvector with only the element entities. Theoretically, removing an element of positive sensitivity will increase the frequency and removing the largest one will be the most efficient. To be consistent with the presentation on the stiffness optimisation in the previous chapters and the statement that the removal is first conducted on the *smallest* sensitivity, we define the element sensitivity number as

$$\gamma_i^j = -\alpha_i^j = -\Delta\lambda_i^j = \phi_i^{jT} (\mathbf{K}_i - \lambda^j \mathbf{M}_i) \phi_i^j . \quad (5.6)$$

Furthermore, for multiple frequency optimisation of Eq. (5.3), the sensitivity of objective function in is

$$\gamma_f = \Delta f_i = \sum_{k=j_0}^{k=j_n} c_k \frac{2(\omega^k - \omega^{*k})}{(\omega^{*k})^2} \Delta\omega^k = \sum_{k=j_0}^{k=j_n} c_k \frac{(\omega^k - \omega^{*k})}{(\omega^{*k})^2 \omega^k} \Delta(\omega^{k^2}) = \sum_{k=j_0}^{k=j_n} c_k b_k \alpha_i^k , \quad (5.7)$$

$$\text{where } b_k = \frac{(\omega^k - \omega^{*k})}{(\omega^{*k})^2 \omega^k} .$$

5.2.3. Evolutionary Procedures

1. Define the ground structure and initial structure (BESO only).
2. Perform dynamic analysis to obtain eigenvalues and eigenvectors.
3. Calculate the element sensitivity number γ_i^j or γ_i using Eq. (5.6) or (5.7).
4. Removing elements of the smallest sensitivity number and adding elements around those of largest ones. Parameters such as modification ratio MR and addition ration AR are used in deciding the number of removed and/or added elements.
5. Repeated Steps 2-4 until the prescribed weight is reached, or the improvement in frequency or objective functions is very small.

5.3. Special Issues Related to Frequency Optimisation

5.3.1. Optimisation Involving Repeated Eigenvalues

Sensitivity of repeated eigenvalues has been a subject of extensive research (Choi *et al.* 1983; Bartholomew and Pitcher 1984; Cher 1993). As the eigenvectors associated with the repeated eigenvalues are not unique but can be any linear combination of the involved eigenvectors, the sensitivities cannot be determined uniquely using the formulas of Eq.(5.4). Instead, the following sub-problem is to be solved.

$$\left\{ \Phi^T \left(\frac{\partial \mathbf{K}}{\partial x_i} - \lambda^m \frac{\partial \mathbf{M}}{\partial x_i} \right) \Phi + \frac{\partial \lambda^m}{\partial x_i} [I] \right\} \mathbf{a}_m = \mathbf{0}, \quad (5.8)$$

where Φ consists of the original orthogonal eigenvectors that are associated with the same repeated eigenvalue λ^m , and $[I]$ is the identity matrix with a dimension corresponding to the multiplicity (r) of the repeated eigenvalues.

Eq. (5.8) is apparently an eigensystem with the repeated eigenvalue sensitivity $\partial \lambda^m / \partial x_i$ being its eigenvalue and \mathbf{a}_m the corresponding eigenvector. If the eigenvalues of this smaller eigensystem are distinct, the unique eigenvector \mathbf{a}_m can be used to determine the unique eigenvectors that is associated with the repeated eigenvalues by the following linear combination of eigenvectors:

$$\bar{\phi}^m = \Phi \mathbf{a}_m. \quad (5.9)$$

After determining the unique eigenvectors for the repeated eigenvalues, Eq. (5.4) can be used again to calculate the eigenvalue sensitivities for those repeated eigenvalues, although the solutions have already been found by solving the eigensystem of Eq. (5.8).

Based on the above sub-eigenvalue approach to repeated eigenvalue sensitivities, some simplification techniques have been proposed. Equation (5.8), can be written as an increment form:

$$\{A + \Delta\lambda^m\} \mathbf{a}_m = \mathbf{0}, \quad (5.10a)$$

where

$$A = \begin{bmatrix} k_{11} & k_{12} & \dots & k_{1r} \\ k_{21} & k_{22} & \dots & k_{2r} \\ \dots & \dots & \dots & \dots \\ k_{r1} & k_{r2} & \dots & k_{rr} \end{bmatrix}, \quad (5.10b)$$

$$\text{and } k_{st} = \phi^{sT} (\Delta\mathbf{K} - \lambda^m \Delta\mathbf{M}) \phi^t \quad (s = 1, 2, \dots, r; t = 1, 2, \dots, r). \quad (5.10c)$$

It is found that if all the off-diagonal elements are zero, the eigenvalue sensitivity increment is in a simplified form, i.e.

$$\text{If } k_{st} = 0, s \neq t, s, t = 1, 2, \dots, r, \quad (5.11a)$$

$$\Delta\lambda_j = k_{jj}, j=1, 2, \dots, r. \quad (5.11b)$$

Eq. (5.11b) is similar to Eq. (5.4), thus the distinct and repeated eigenvalue problems have the identical formulae of eigenvalue sensitivities. This simplification is obviously hinged to the satisfaction of Eq. (5.11a) which can be realised in some cases. For example, for 2D plate bending problem where the symmetry nature of structure incurs repeated eigenvalues, Eq. (5.11a) can be enforced as an additional constraint in the optimisation problem statement which means that $\Delta\mathbf{K}$ and $\Delta\mathbf{M}$ (basically, increment in design variable $\Delta\mathbf{x}_j$) are forced to fulfil Eq. (5.11a) (Krog and Olhoff 1999). Alternatively, by reducing the design space of a symmetric plate using a symmetry reduction methods (Kosaka and Swan 1999), Eq. (5.11a) can be automatically satisfied.

5.3.2. Optimisation Involving Closely-Spaced Eigenvalues

Repeated frequencies are inherent for symmetric structures and are most encountered in the size optimisation of discrete truss or frame structures and optimal plate bending designs. While in most situations the nature of repeated eigenvalues can be predicted from the outset by using the symmetric information, the occurrence of closely-spaced eigenvalues is more uncertain. In maximising one frequency, for example, the frequency of interest can be increased up to the point of its neighbour frequencies and the structure becomes ‘multi-modal’. Then the mode shape may interfere with each other and evolution can be discontinuous.

Closely-spaced eigenvalues can be generally considered in the problems statement. For example, instead of maximising a single eigenvalue, all multiple closely-spaced eigenvalues of r are needed to be optimised. Those multiple objective functions are accounted for by a simple average technique, i.e. Eq. (5.2a) is replaced with

$$\text{Maximise } f = \frac{1}{r} \sum_{s=1}^{s=r} \lambda^s . \quad (5.12)$$

Accordingly, the sensitivity of the objective function is

$$\gamma_i = \frac{1}{r} \sum_{s=1}^{s=r} \alpha_i^s . \quad (5.13)$$

While intending to increase the average of all participating eigenvalues, it is not guaranteed in the above average technique that *each* frequency is increased or the eigenvalues $\lambda^{k+1}, \dots, \lambda^{k+r}$ are kept over λ^k in the next iteration. This consideration has given rise to an improved strategy which defines a set of element ‘eligible’ for modifying by taking account of the distance between the closely-spaced eigenvalues $\lambda^{k+1} - \lambda^k, \dots$ and $\lambda^{k+r} - \lambda^k$. Reported results have shown moderate improvement (less than 3%) over the average method (Rong *et al.* 2001b).

In this chapter, close eigenvalues are handled by the average methods for its effectiveness and relative simplicity, which has demonstrated in many applications (Ma *et al.* 1995; Xie and Steven 1997).

5.3.3. Optimisation Considering Mode-Tracking

One difficulty associated with frequency optimisation is the swap of the mode shapes during iterations. The evolution may not follow the same mode shape during structural modification. In some design problems, a desired mode is of particular interest and calls for tracking the mode during the course of evolution.

There are several ways of mode-tracking, such as higher order eigenpair perturbations, the cross-orthogonality checks and modal assurance criterion (MAC) (Eldred *et al.* 1993; Ting *et al.* 1993). The inclusion of mode-tracking in topology optimisation has been effective, based on a MAC technique (Kim & Kim 2000). As pointed out in their application, MAC has a few features appealing to the application of topology optimisation. Firstly, it does not involve orthogonality thus considerably reduces the computing time. Secondly, despite the decreasing number of nodes or d.o.fs., MAC can be calculated with satisfactory accuracy. Thirdly, MAC needs not to be included in the objective function or constraints thus simplifying the algorithm routine.

In view of the above advantages of MAC, this section studies its incorporation to ESO/BESO to address optimisation of a specific mode shape. MAC is defined as

$$\text{MAC}(\phi^a, \phi^b) = \frac{|\phi^{aT} \phi^b|^2}{(\phi^{aT} \phi^a)(\phi^{bT} \phi^b)}, \quad (5.14)$$

where ϕ^a and ϕ^b are the modes to be correlated. MAC has also been widely used to check the correlation between the numerical results and experimental data.

To realise a mode tracking capability for ESO and BESO, a reference mode ϕ_{ref} is firstly defined. It is usually based on the the ground structure as it consists of the largest number of nodes. At each iteration, all the calculated modes (say, the first eight) are checked in terms of MAC based on ϕ_{ref} . The one with the largest MAC is regarded as the desired mode shape which shares the most similarity to the reference. Then the sensitivity analysis using Eq. (5.4) are conducted on this mode. In fact, the general problem statement and procedures are the same as the basic frequency optimisation but only an additional procedure to identify the mode of interest is introduced.

It is noted that multiple frequencies can occur in the case of mode tracking. This is dealt with using the same strategies as presented in section 5.3.2.

5.4. Examples

Six examples of 2D plane stress and 3D continuum structures are presented in this section. 4-node rectangular elements and 8-node brick elements are used, respectively. The following data apply to all examples unless otherwise specified: the modification ratio MR , addition ratio AR and stage ration SR are 1%, 0.25 and 50%, respectively, the weight coefficient c_i in Eq. (5.3) is 1.0 where applicable. All 2D examples are conducted on a Pentium 233 PC, and 3D examples on a Pentium 533 PC.

Example 5.4.1. A frame to be reinforced.

As shown in Fig. 5.1, a two-bar truss is to be reinforced by adding material in the rectangular domain to increase its first frequency. For simplicity, the Young's modulus $E = 100$, Poisson's ratio $\nu = 0.3$, thickness $t = 0.001$ and density $\rho = 1$ are assumed. A mesh of 64×40 square elements is used. The initial 2D continuum model shown in Fig. 5.2, covers 23.6% of the full design domain and it has the first eigenvalue, $\lambda_0 = 0.177 \times 10^3$.

Four cases are studied where the relative volume of the added material V^+ is specified respectively as 6.4%, 11.4%, 21.4% and 31.4% of the volume of the full design domain. To solve the reinforcement problem by using BESO, the evolution starts from the original frame. Once the structure grows to the target volume, it is modified by adding and removing the same number of elements to keep the volume constant. The results are shown in Fig. 5.2.

For comparison, topologies obtained by ESO for the first two cases are shown in Fig. 5.3. Clearly, ESO solution with two bars intersecting with each other provides a better reinforcement effect, as seen in the value of eigenvalues in Table 5.1. Though BESO has the strength of adding elements, they can be added only around the structural boundary and this to some extent limits the design domain for addition. The diagonal cross in Fig. 5.3 can be only evolved after the structure is fully developed, which is not the case in this example as the structure only grows to its target weight which is relatively low. As a higher target weight is used, the difference in solutions by the two methods becomes smaller, as also seen in Table 5.4.1.

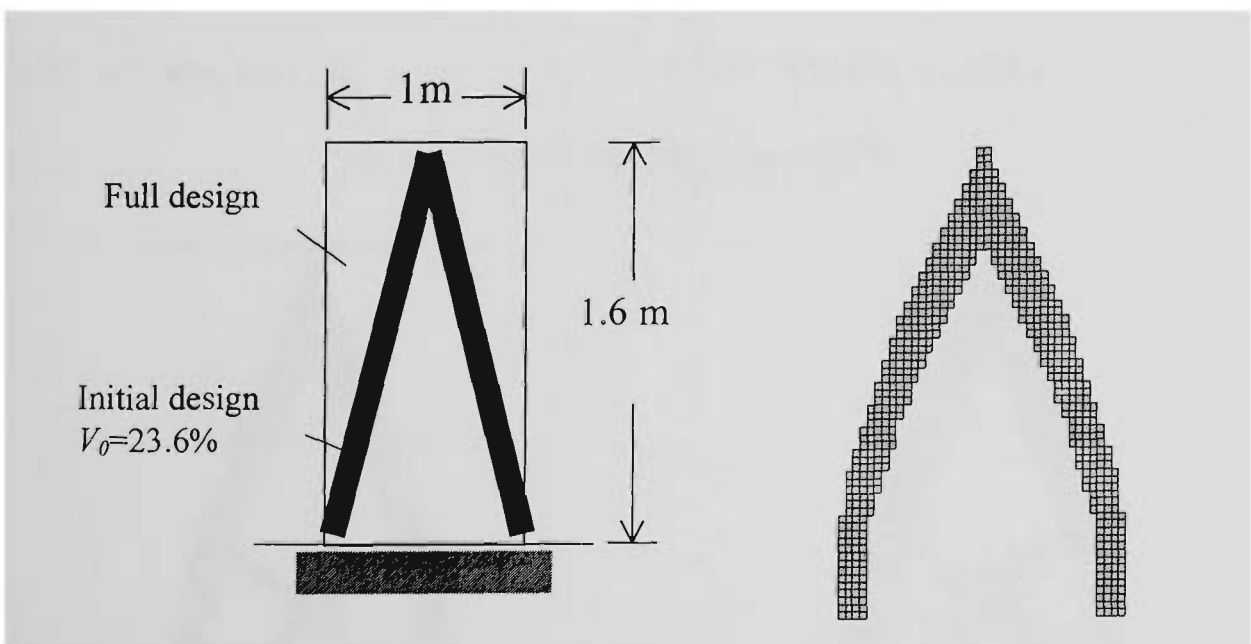
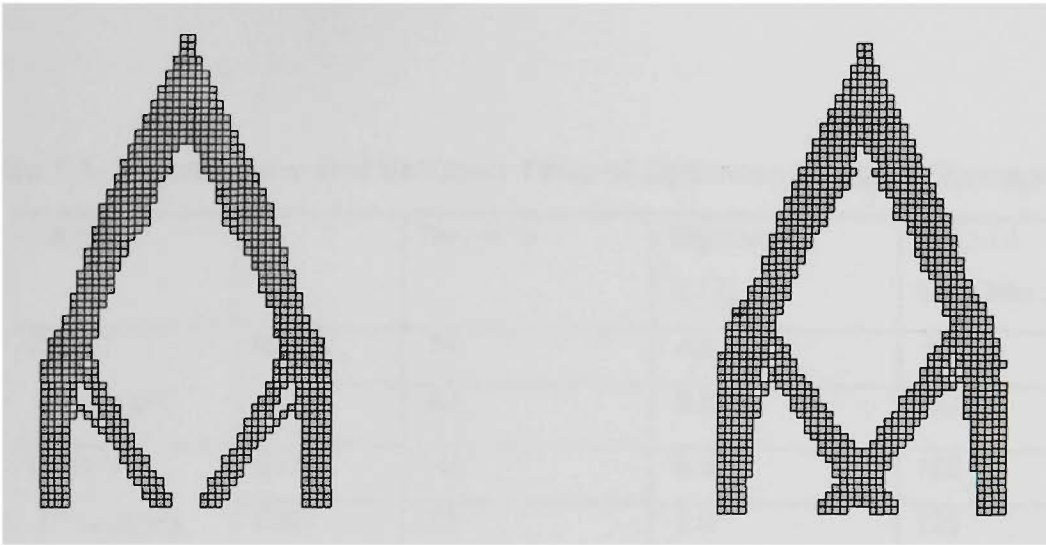


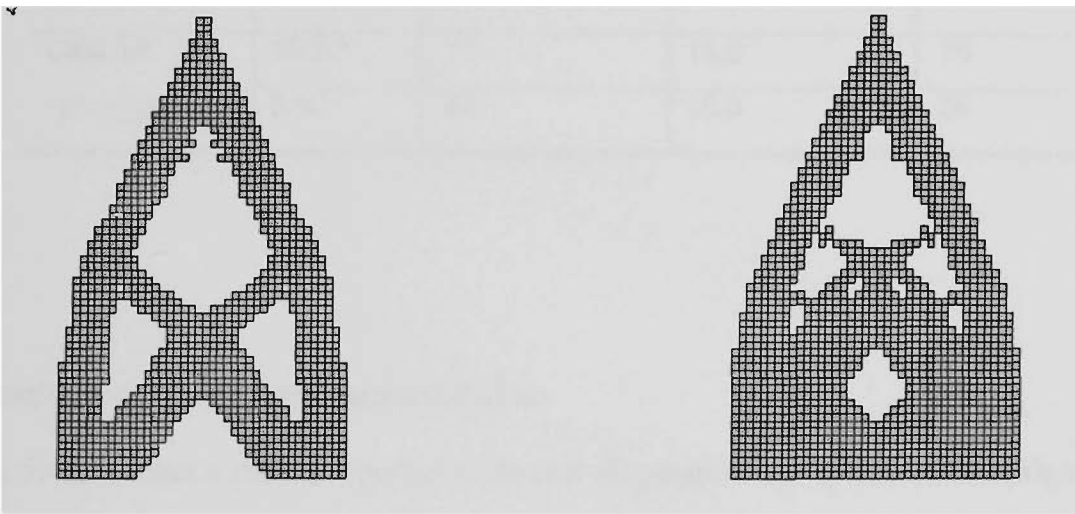
Fig. 5.1(a). A two-bar truss.

Fig. 5.1(b). Finite element model.



(a) $V^+ = 6.4\%$, $\lambda = 4.5\lambda_0$.

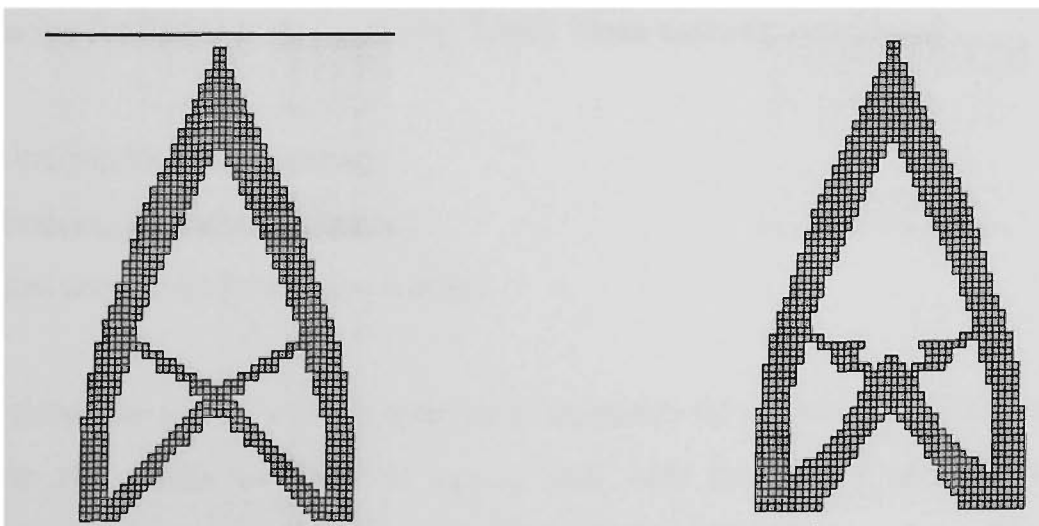
(b) $V^+ = 11.4\%$, $\lambda = 6.9\lambda_0$.



(c) $V^+ = 21.4\%$, $\lambda = 11.1\lambda_0$.

(d) $V^+ = 31.4\%$, $\lambda = 13.8\lambda_0$.

Fig. 5.2. Optimal topologies for BESO.



(a) $V^+ = 6.4\%$, $\lambda = 4.5\lambda_0$.

(b) $V^+ = 11.4\%$, $\lambda = 6.9\lambda_0$.

Fig. 5.3. Optimal topologies for ESO.

Table 5.1. Eigenvalues and Solution Time of Optimum Designs (Example 5.4.1)

Cases		Iterations	Eigenvalue λ / λ_0	Solution time (Min.)
Case I $V^+ = 6.4\%$	BESO	74	4.5	60
	ESO	89	6.0	137
Case II $V^+ = 11.4\%$	BESO	146	6.9	120
	ESO	73	7.0	125
Case III $V^+ = 21.4\%$	BESO	109	11.1	135
	ESO	53	12.7	110
Case IV $V^+ = 31.4\%$	BESO	71	13.8	70
	ESO	44	15.0	95

Example 5.4.2 A diagonal supported plate.

Fig. 5.4(a) shows a plate supported at its two diagonal corners with a full design domain of dimensions $0.15 \text{ m} \times 0.1 \text{ m}$. The Young's modulus $E = 70 \text{ GPa}$, Poisson's ratio $\nu = 0.3$, thickness $t = 0.01 \text{ m}$ and density $\rho = 2700 \text{ kg/m}^3$ are assumed. The design domain is divided into 50×50 rectangular elements. The prescribed weight is $W^* = 50\%W_0$. The initial design for BESO is shown in Fig. 5.4(b). Three cases are considered:

- I. Maximising the first frequency;
- II. Maximising the second frequency;
- III. Maximising the first three frequencies.

Fig. 5.5 shows the topology of the optimum 1st frequency by performing BESO, which is similar to the results of ESO. It agrees well with the design obtained by the homogenisation methods (Tenek and Hagivara 1993). The history of the first three

frequencies is shown in Fig. 5.6. A constant increase in the first frequency is seen through the evolution and the second and third drop in the later iterations.

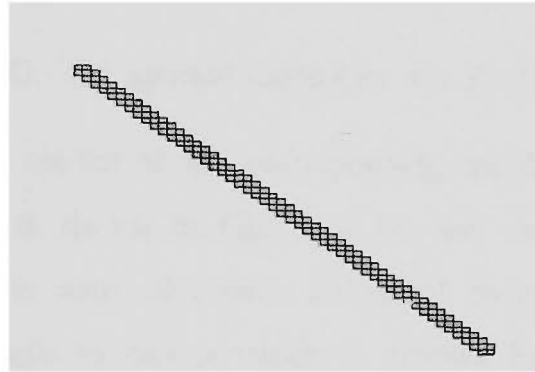
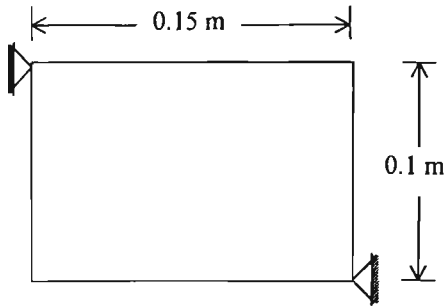


Fig. 5.4(a). A diagonally supported plate.

Fig. 5.4(b). Initial design for BESO.

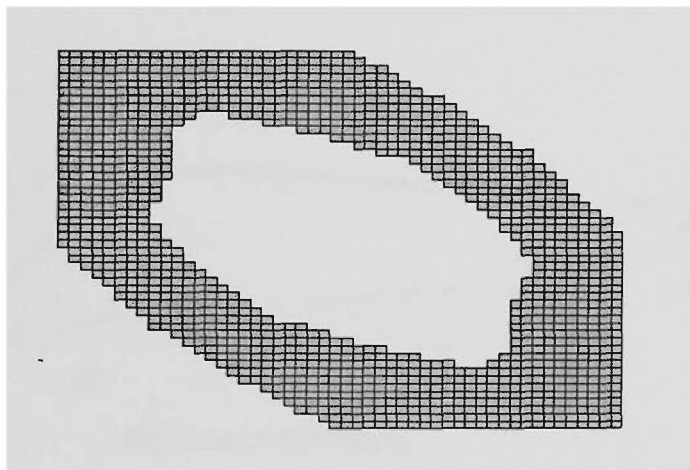


Fig. 5.5. Optimal design of maximising the first frequency.

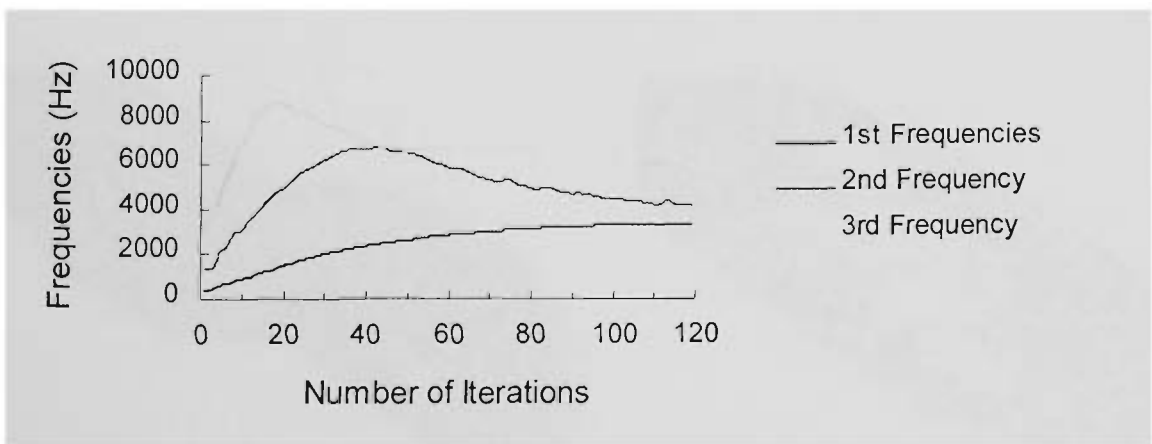


Fig. 5.6. Evolutionary history of the first three frequencies: maximising first frequency.

In maximising the second frequency, as shown in Fig. 5.7, the second and third frequencies become close at later stages. Then the new element sensitivity number is calculated by $\frac{1}{2}(\alpha_i^{(2)} + \alpha_i^{(3)})$ using Eq. (5.13). The optimal topologies for BESO are given in Figs. 5.8 and Fig. 5.9. They are similar to the corresponding topologies obtained by ESO. The frequency history is shown in Fig. 5.10 for the case of maximising the first three frequencies. It is noted that each individual frequency gradually approaches the corresponding single maximum which is denoted by the horizontal lines.

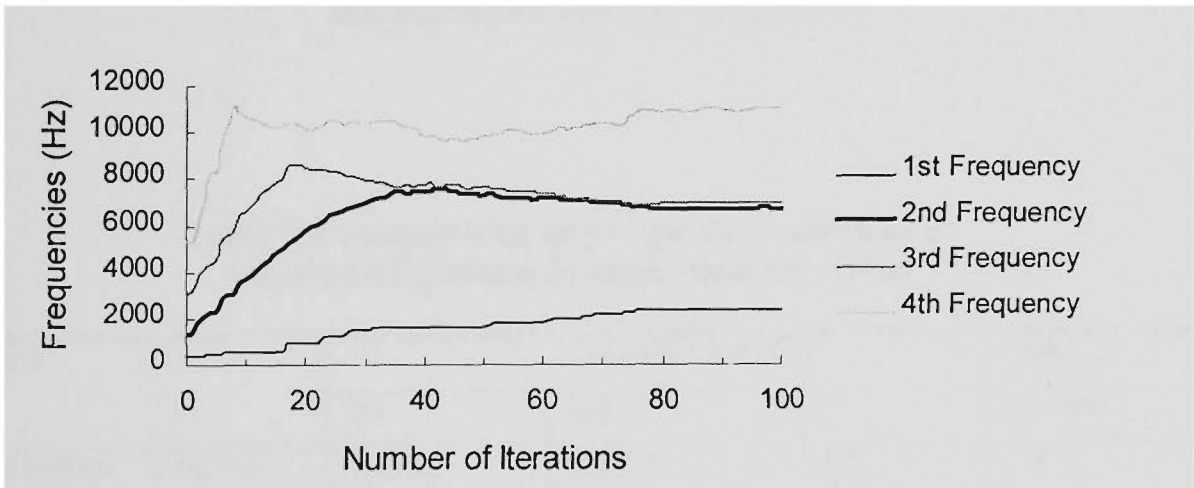


Fig. 5.7. Evolutionary history of the first four frequencies: maximising second frequency.

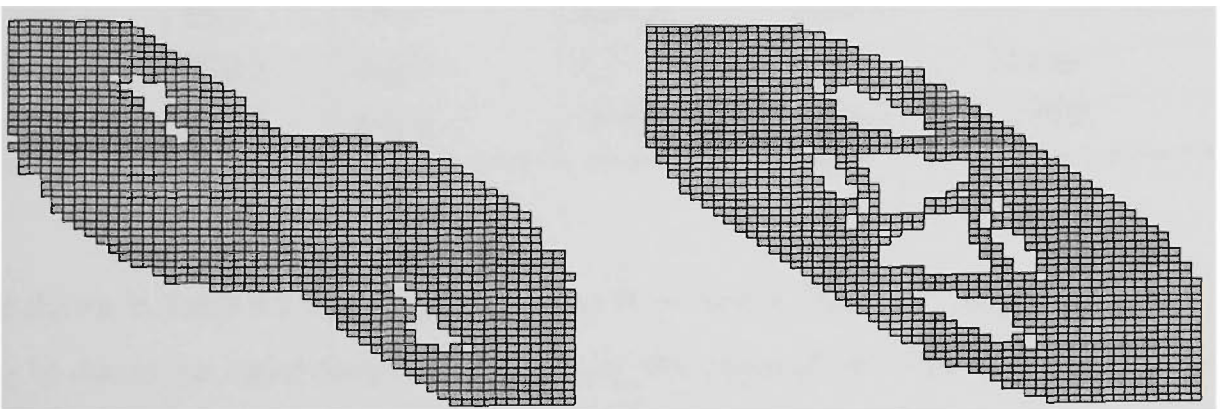


Fig. 5.8. Optimal design of maximising the second frequency.

Fig. 5.9. Optimal design of maximising the first three frequencies.

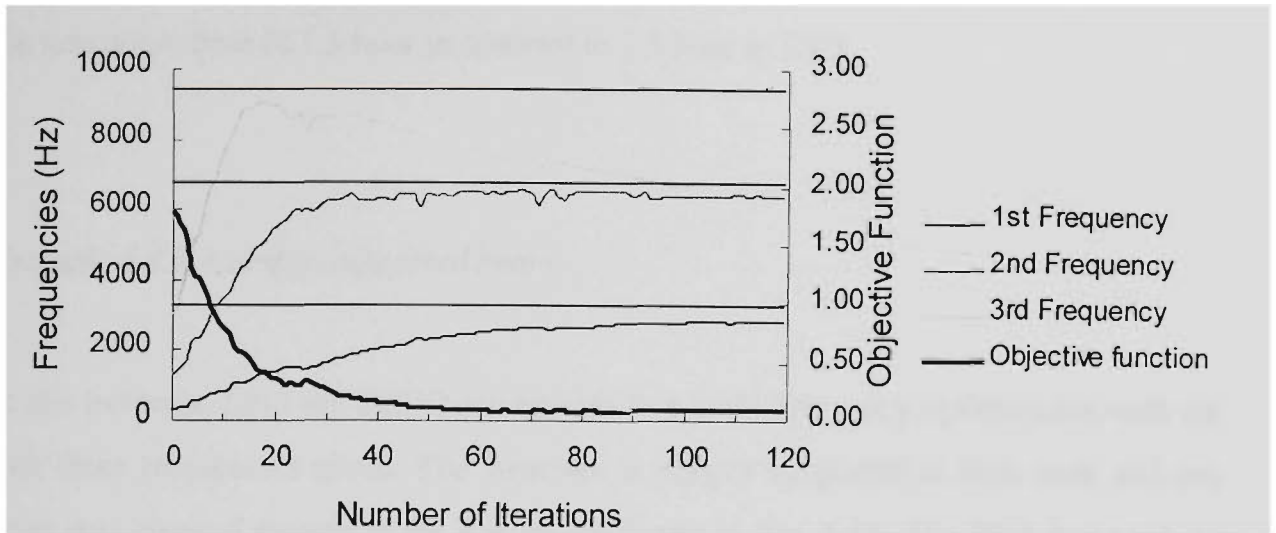


Fig. 5.10. Evolutionary history of the first four frequencies: maximising the first three frequencies.

Table 5.2. Frequencies and Objective Functions of Initial and Optimum Designs (Example 5.4.2)

Cases		Frequencies f (Hz)			Objective
		1st	2nd	3rd	Function f
Initial Design	BESO	340.2	1352.8	3015.2	1.9071
	ESO	2361.6	4671.3	4750.8	0.3748
Case I	BESO	3293.7	4204.2	6026.3	--
	ESO	3283.7	4188.1	5988.6	--
Case II	BESO	2372.3	6780.1	6922.0	--
	ESO	1749.3	6026.2	6209.1	--
Case III	BESO	2845.5	6376.6	6768.4	0.0887
	ESO	2667.6	5906.5	7265.5	0.0952

It is shown in Table 5.2 that ESO does not work as well as BESO in this example. This may be due to the initial design which has very close second and third frequencies. The structure becomes multi-modal from the outset and both frequencies can only increase slowly. Such a problem can be circumvented by using BESO which can flexibly choose

the initial structure definition. Also, BESO takes less solution time in both cases with the maximum time of 1.5 hour in contrast to 2.5 hour in ESO.

Example 5.4.3 A simply supported beam.

In this example, ESO and BESO are applied to a multi-frequency optimization with the first three frequencies given. The structure is simply supported at both ends and has three concentrated masses at the bottom, as shown in Fig. 5.11. The final design is to have 34% of the weight of the rectangular design area. The initial design of one row of element connecting the two supports is adopted in BESO, as shown in Fig. 5.12. Five cases are considered:

Cases I, II and III: Maximizing the first, second and third frequency, respectively.

Cases IV and V: Specifying the first three frequencies: (a) $f_1^* = 80$ Hz, $f_2^* = 130$ Hz and $f_3^* = 160$ Hz; and (b) $f_1^* = 50$ Hz, $f_2^* = 130$ Hz and $f_3^* = 210$ Hz.

As shown in Table 5.3, BESO yields better results than ESO in the first three cases. The topologies by two methods are given in Fig. 5.13. Designs by ESO cover a larger space while those by BESO only grow to about half the total allowable height. Additionally, as ESO involves an oversized design domain, it tends to produce structure with skeletal representations if the target weight is small (say 35%). Nonetheless, The corresponding designs share some similarity in external shape and internal configurations.

In cases IV and V, it is noticed that though frequencies oscillate around the target values, the objective functions generally converge to nearly-zero, as shown in Fig. 5.14. Two topologies of the specified frequencies are given in Fig. 5.15. The average computational times in five cases for BESO and ESO are 30 minutes and 90 minutes, respectively.

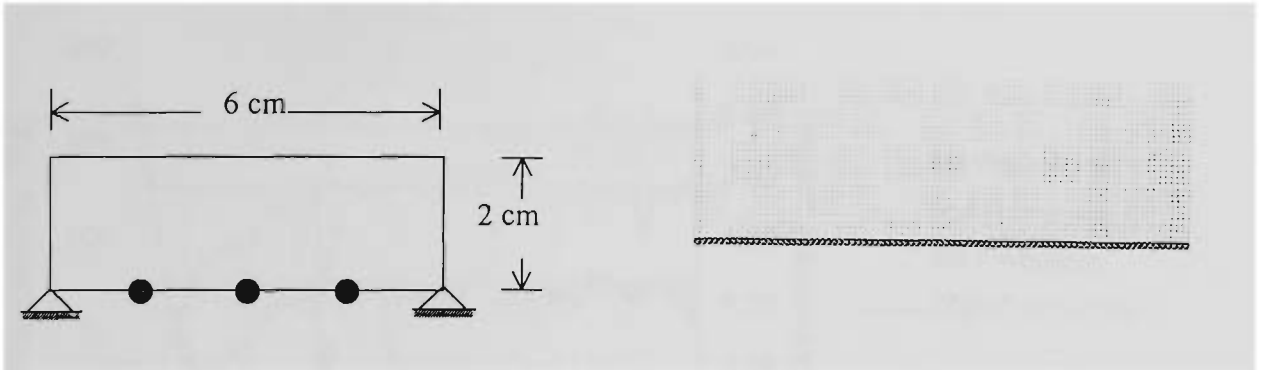


Fig. 5.11. The design area of a simply supported beam.



Fig. 5.12. Initial design for BESO.

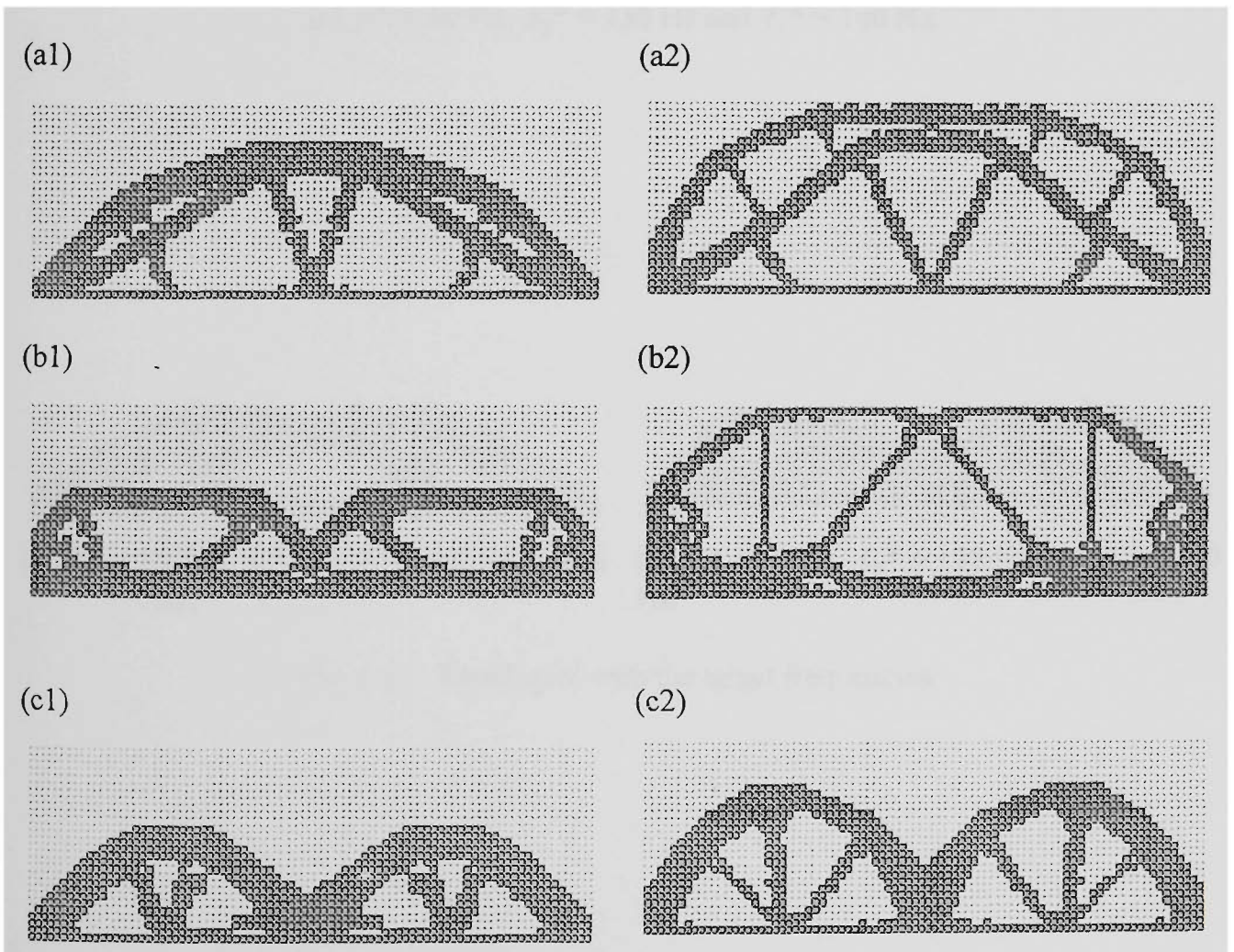


Fig. 5.13. Topologies of independently maximised single frequencies, comparison of BESO and ESO:

- (a1 & a2) Maximising the first frequency: BESO and ESO.
- (b1 & b2) Maximising the second frequency: BESO and ESO.
- (c1 & c2) Maximising the third frequency: BESO and ESO.

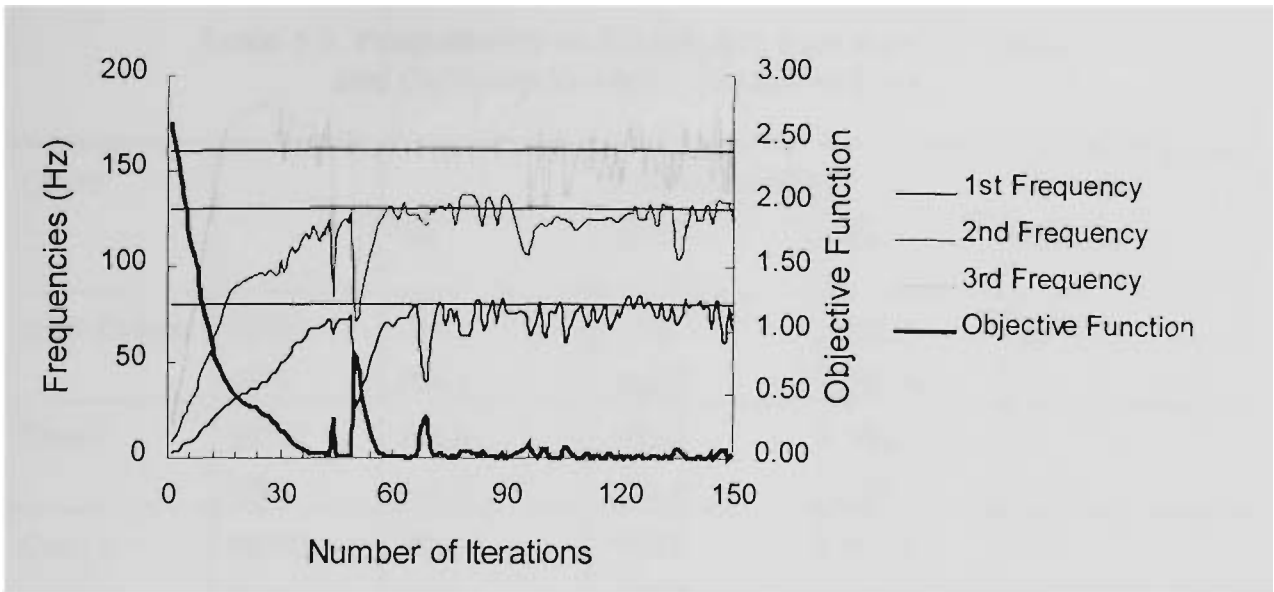
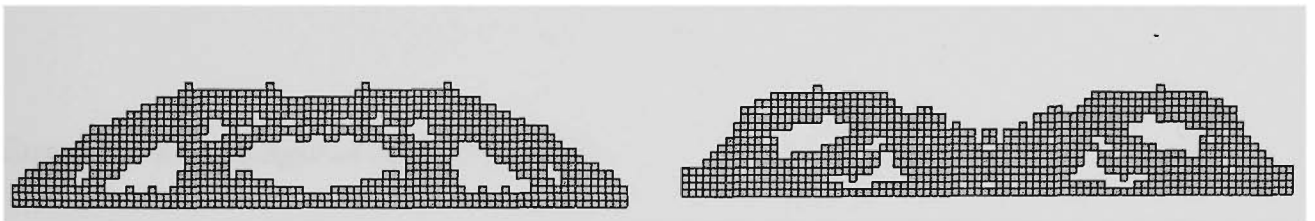


Fig. 5.14. Evolutionary history of the first three frequencies:
 (a) $f_1^* = 80$ Hz, $f_2^* = 130$ Hz and $f_3^* = 160$ Hz.



(a) $f_1^* = 80$ Hz, $f_2^* = 130$ Hz and $f_3^* = 160$ Hz;
 (b) $f_1^* = 50$ Hz, $f_2^* = 130$ Hz and $f_3^* = 210$ Hz.

Fig. 5.15. Topologies with the target frequencies.

Table 5.3. Frequencies and Objective Functions of Initial and Optimum Designs (Example 5.4.3)

Cases		Frequencies f (Hz)			Objective Function f
		1st	2nd	3rd	
Initial Design	BESO	2.6	7.4	15.8	2.6300
	ESO	154.2	166.2	332.4	--
Case I	BESO	121.0	123.4	150.9	--
	ESO	114.7	120.2	137.5	--
Case II	BESO	39.2	166.7	218.2	--
	ESO	44.3	160.6	167.9	--
Case III	BESO	47.0	127.0	318.1	--
	ESO	49.2	124.3	295.7	--
Case IV	BESO	79.6	131.4	161.2	0.0002
		(80.0)*	(130.0)	(160.0)	
Case V	BESO	48.5	130.7	208.8	0.001
		(50.0)	(130.0)	(210.0)	

* The number in parenthesis is the frequency target f^* .

Example 5.4.4 A diagonally supported block.

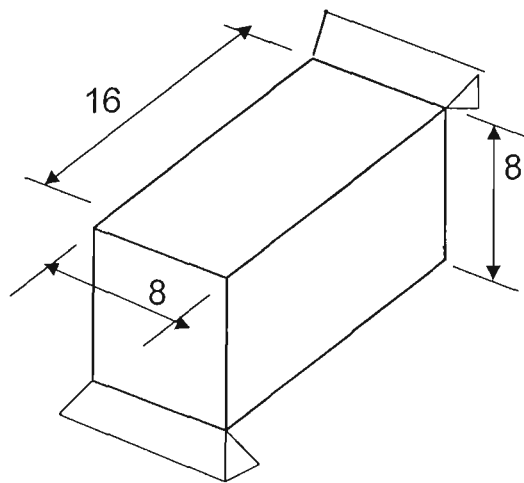


Fig. 5.16. A diagonally supported block.

Study a 3D version of Example 5.4.2, as shown in Fig. 5.16. It has the first frequency $f_1 = 68.05$ Hz. The initial design for BESO (not shown here) is an empty box connecting the two diagonal edges with $f_1 = 45.25$ Hz. Optimal designs for $W^* = 30\%W_0$ are shown in Fig. 5.17. They are similar to their 2D counterparts as shown in Fig. 5.5. Fig. 5.18 gives the frequency history during optimisation. Multi-modal eigenvalues are observed in the later iterations.

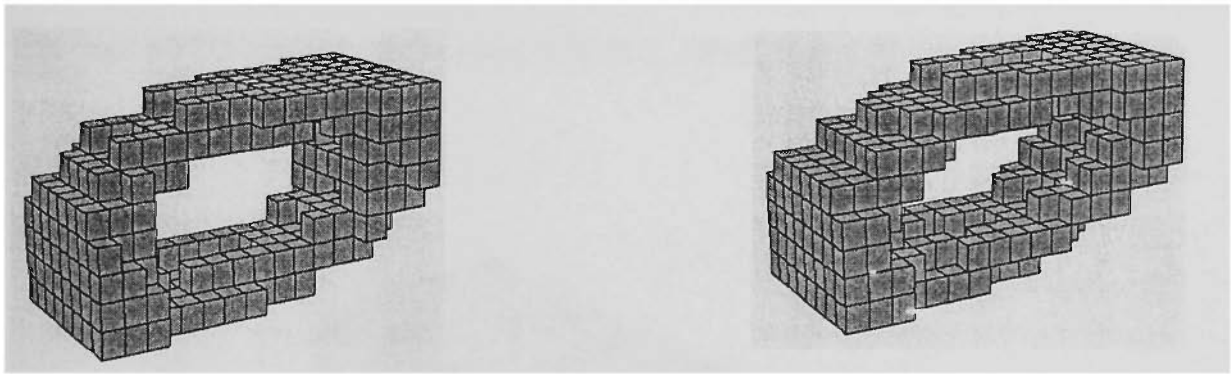
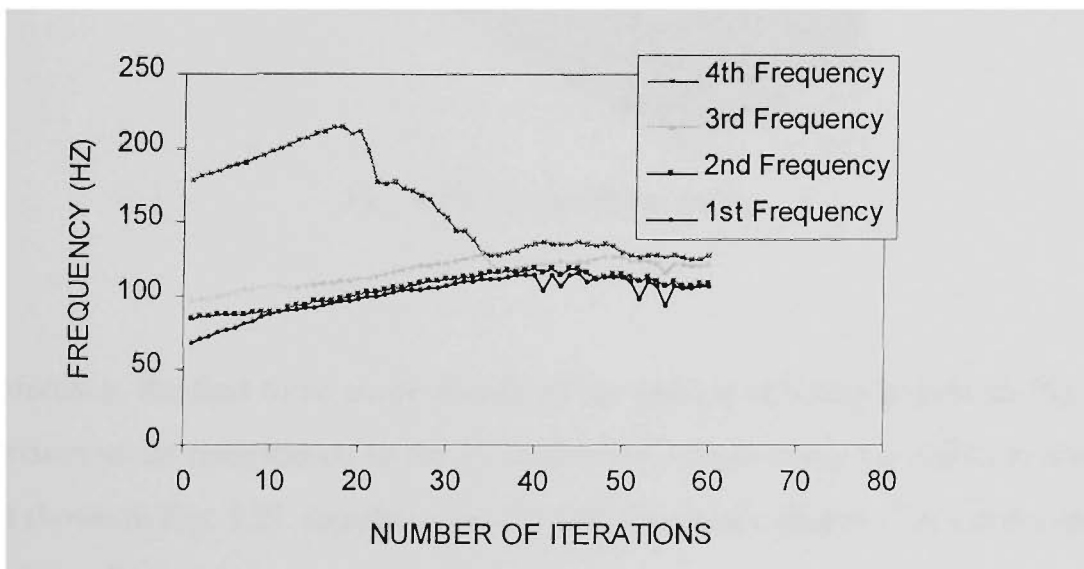
(a) ESO: $f_1 = 113.13$ Hz.(b) BESO: $f_1 = 116.73$ Hz.Fig. 5.17. Optimal topologies: $W^* = 30\%W_0$.

Fig. 5.18. Evolutionary history of the first four frequencies.

The following are two examples on optimisation of a desired mode shape using MAC mode-track method.

Example 5.4.5 A cantilever beam: to track the torsion mode.

Fig. 5.19 gives a 3D cantilever beam of box section with four lumped masses attached at the end. The dimensions are $L \times H \times B = 30 \times 10 \times 0.8$ and $E = 210$ GPa, $\nu = 0.3$ and $\rho = 2700$ kg/m³ are used. To simulate an actuation suspension, the design objective is to maximise the frequency of torsional mode and the target weight is $W^*/W_0 = 50\%$. Both ESO and BESO methods are applied. $MR = 0.2$, $AR = 0.25$ and $SR = 50\%$ are used.

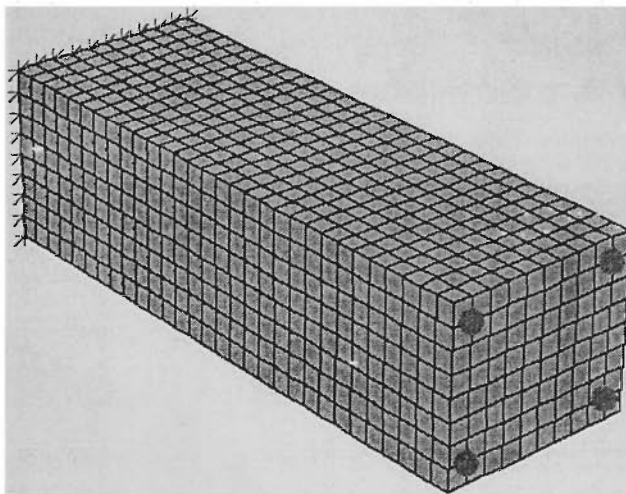


Fig. 5.19. A cantilever beam.

For reference, the first three mode shapes of the ground structure is give in Fig. 5.20. The torsion mode corresponds to the 3rd mode. The initial design for BESO is a hollow box as shown in Fig. 5.21, together with the first four mode shapes. The torsion mode is ordered the 4th.

In Table 5.4, it is seen that the torsion mode remains the third in ESO with a few times when the 5th mode has the largest MAC, as shown in the MAC history in Fig. 5.22. In

BESO, the mode switches from 4 to 3 in the final optimum. In fact, the 3rd mode takes over at a very early stage and dominates onward, as seen in Fig. 5.23. The history of the first eight frequencies is given in Fig.5.24 and 5.25 where the 3rd and 4th mode have very close frequency at the optimum. Fig. 5.26 gives the topologies and corresponding mode shapes for ESO and BESO. They are very similar to each other. In Table 5.5 it is seen that the results and solution time are comparable in the two methods.

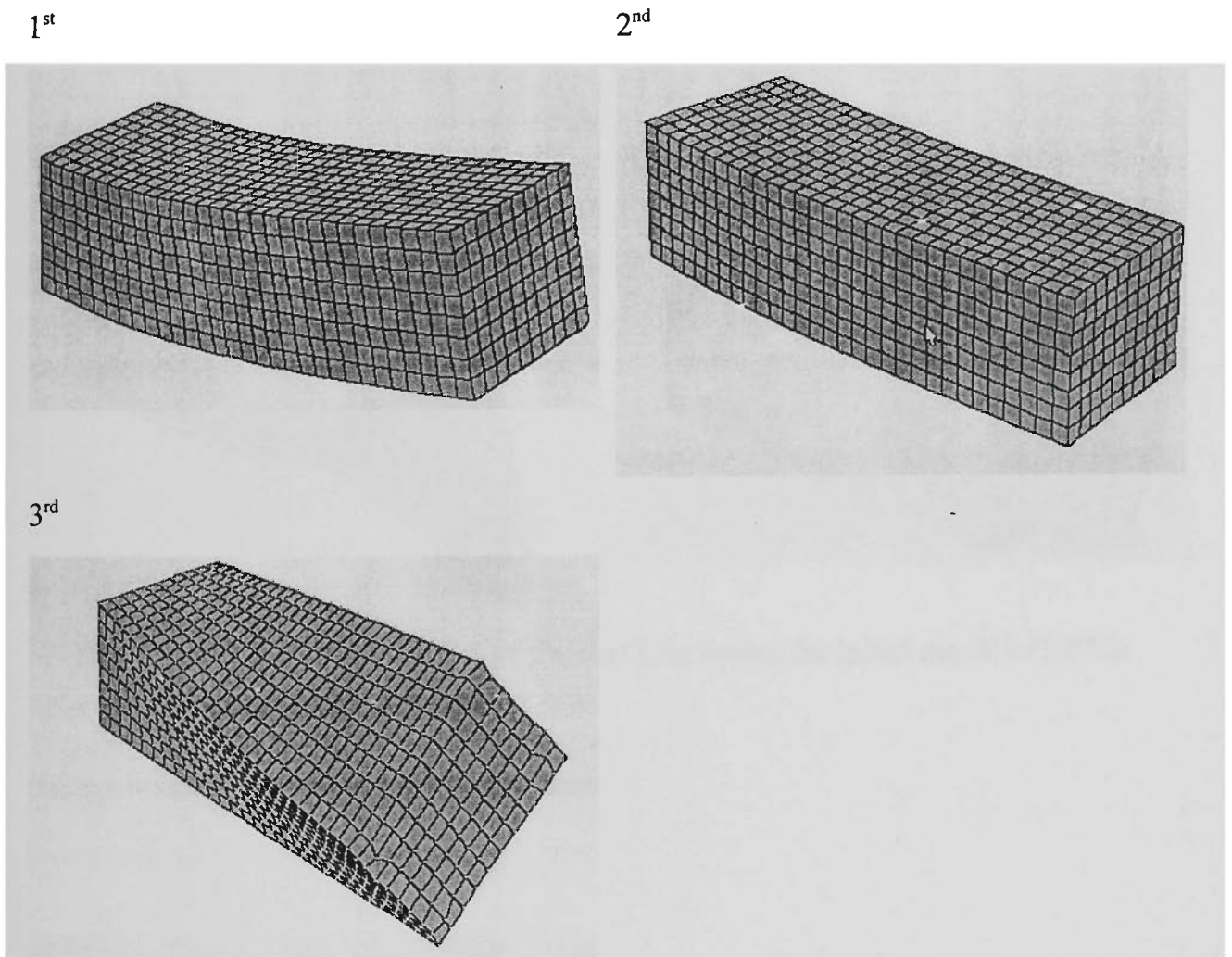


Fig. 5.20. Mode shapes of the first three modes for reference.

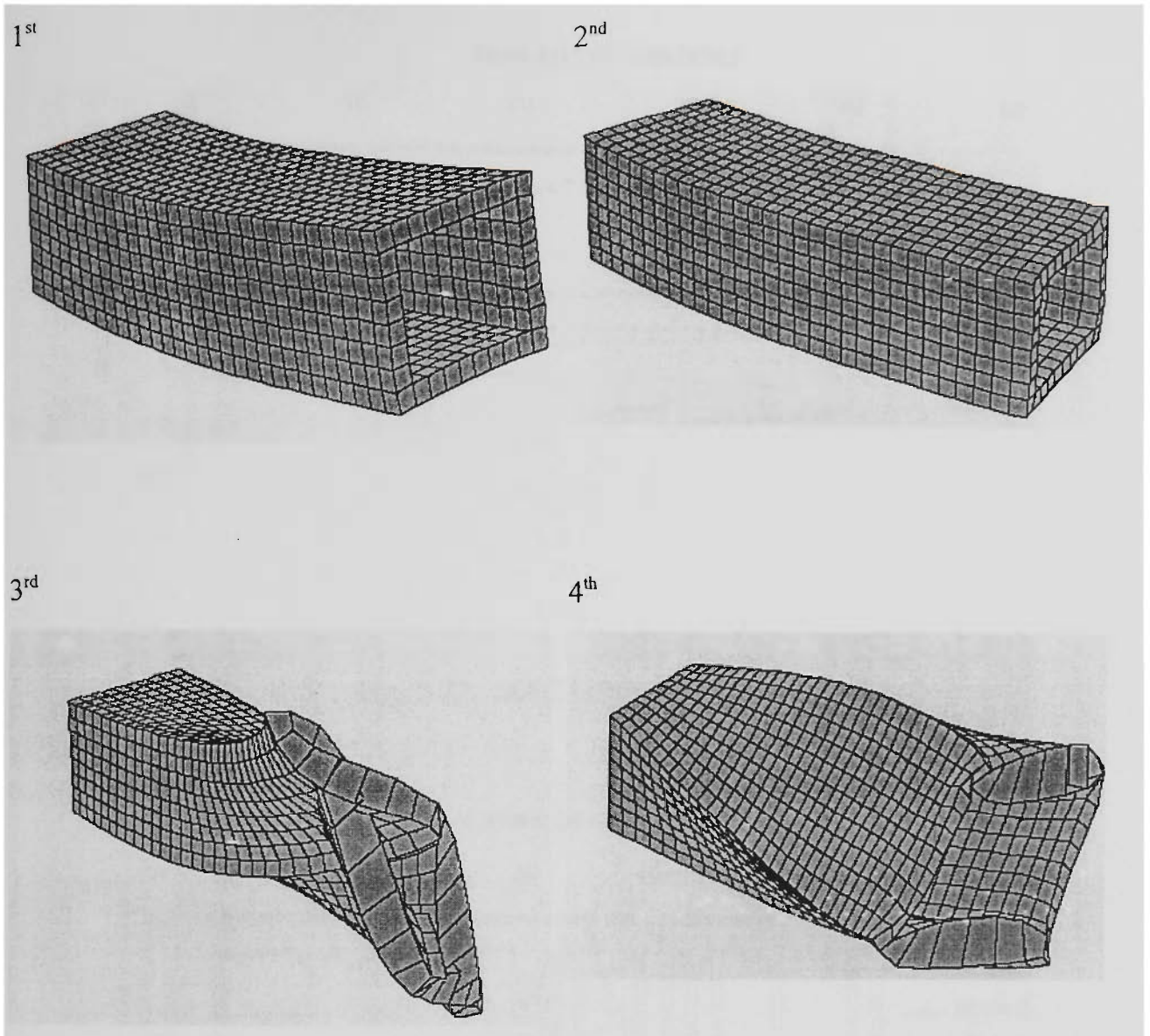


Fig. 5.21 (Cont.). Mode shapes of the first four modes for initial model of BESO.

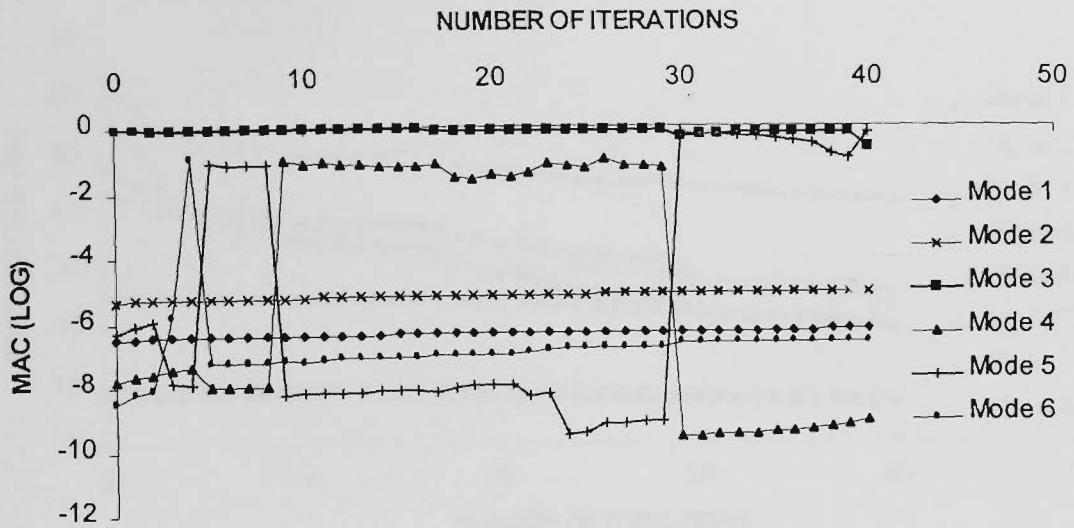


Fig. 5.22. MAC history: ESO.

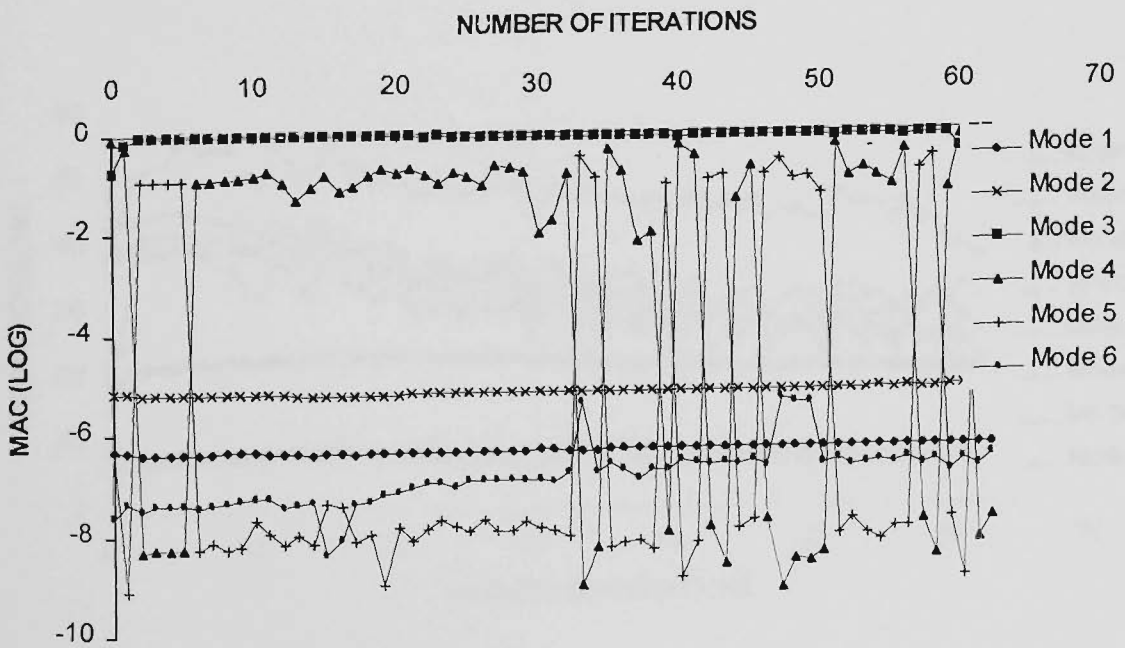


Fig. 5.23. MAC history: BESO.

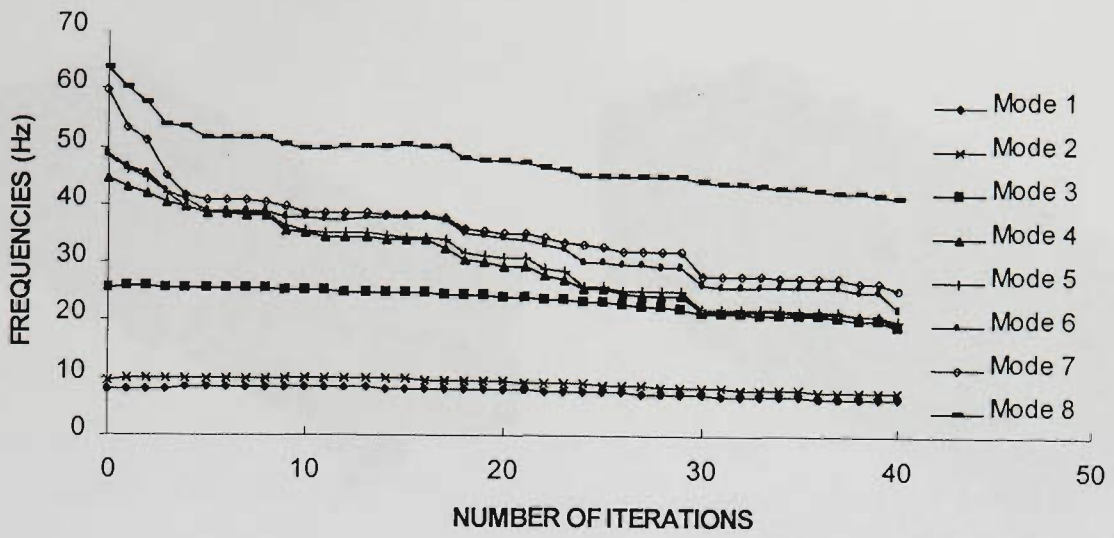


Fig. 5.24. History of the first eight frequencies: ESO.

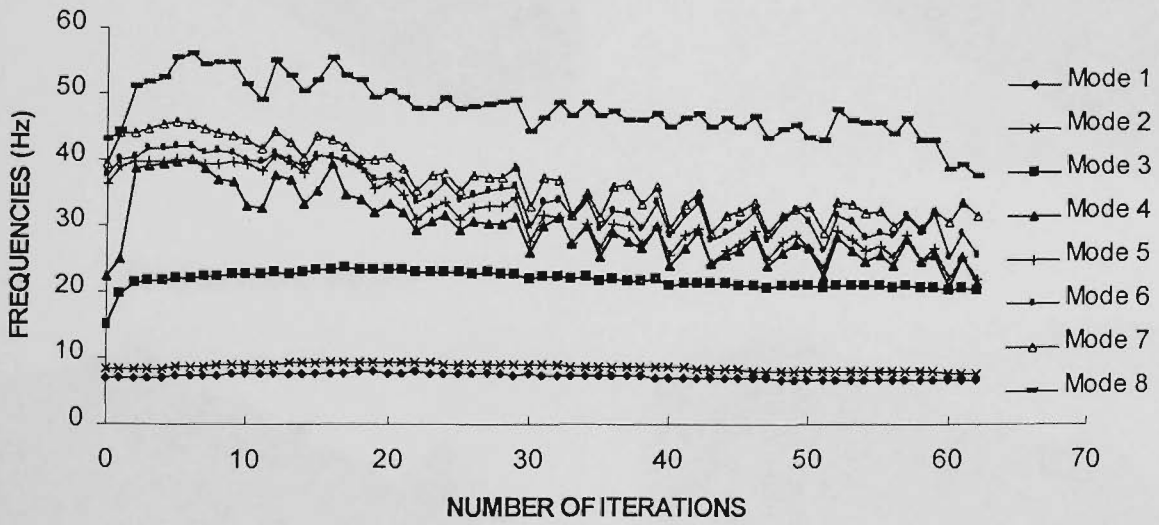


Fig. 5.25. History of the first eight frequencies: BESO.

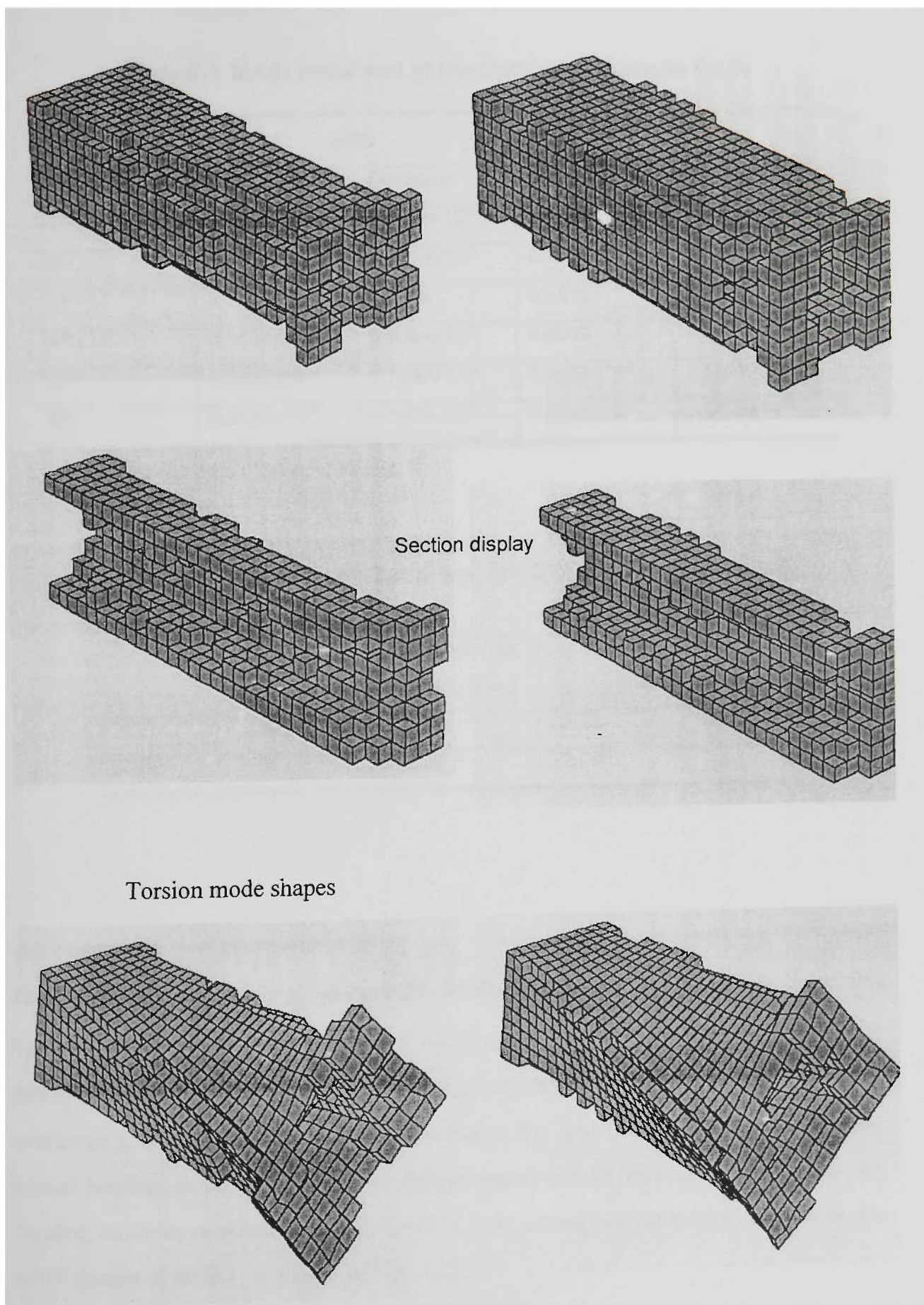


Fig. 5.26. Optimum topologies.

Table 5.4. MAC: Initial and at the Optimum (Example 5.4.5)

Mode orders	ESO		BESO	
	Initial	Optimum	Initial	Optimum
1 st	0.3170×10^{-6}	0.4505×10^{-6}	0.4798×10^{-6}	0.4341×10^{-6}
2 nd	0.4757×10^{-5}	0.6616×10^{-5}	0.7207×10^{-5}	0.6464×10^{-5}
3 rd	1	0.7064	0.1816	0.8260
4 th	0.1483×10^{-7}	0.5094×10^{-1}	0.8082	0.1575
5 th	0.5022×10^{-6}	0.7520×10^{-9}	0.4453×10^{-6}	0.5631×10^{-8}
6 th	0.3445×10^{-8}	0.1460×10^{-6}	0.2468×10^{-7}	0.1711×10^{-6}

Table 5.5. Frequency at Optimum, $W=50\%W_0$ (Example 5.4.5)

	Iteration	Compt. time (Min.: Sec.)	3 rd Frequency (Hz)
ESO	29	2:30	22.23
BESO	36	2:23	22.09

Example 5.4.6 A hinged block: to track the bending mode.

The previous example is used again but the block is hinged at its bottom corners. The first four mode shapes for the ground structure are shown in Fig. 5.27, representing the overturning, the first bending mode in yz plane, the first bending in xy plan and the second bending mode in yz plane. The design objective is to track and optimise the first bending mode in yz plane with $W^*/W_0=45\%$. It is corresponding to the 1st mode in the initial design of BESO, as shown in Fig. 5.28.

From Table 5.6, it is seen that at the optimum, the desired bending modes are the 3rd in both ESO and BESO. From the MAC history of ESO in Fig. 5.29, it is seen that the early stage sees swaps between the 2nd and 3rd and then the 3rd dominates towards the end, with a few occasions of switching to the 4th. In Fig. 5.30 for BESO (MAC 10^{-14} is not shown), the bending mode is the 1st in the beginning, switches to 2nd for a few iterations and ends up with 3rd. The change course is clearly reflected in the frequency history, as shown in Figs. 5.31 and 5.32. Fig. 5.33 displays the optimal topologies and corresponding torsion mode shapes. Table 5.7 compares the frequencies obtained by ESO and BESO. ESO has a better solution but BESO takes much less time.

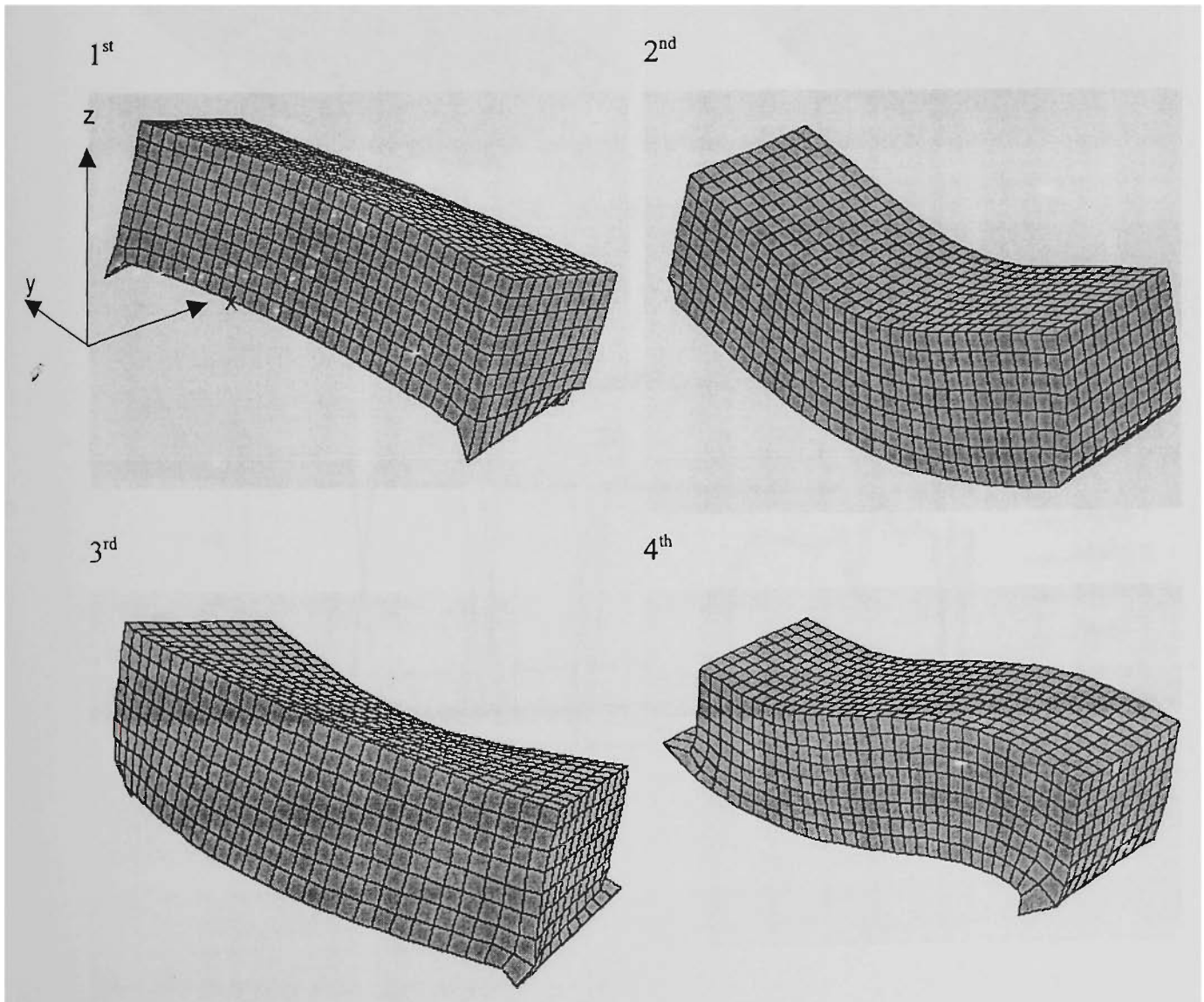


Fig. 5.27. Mode shapes: ESO.

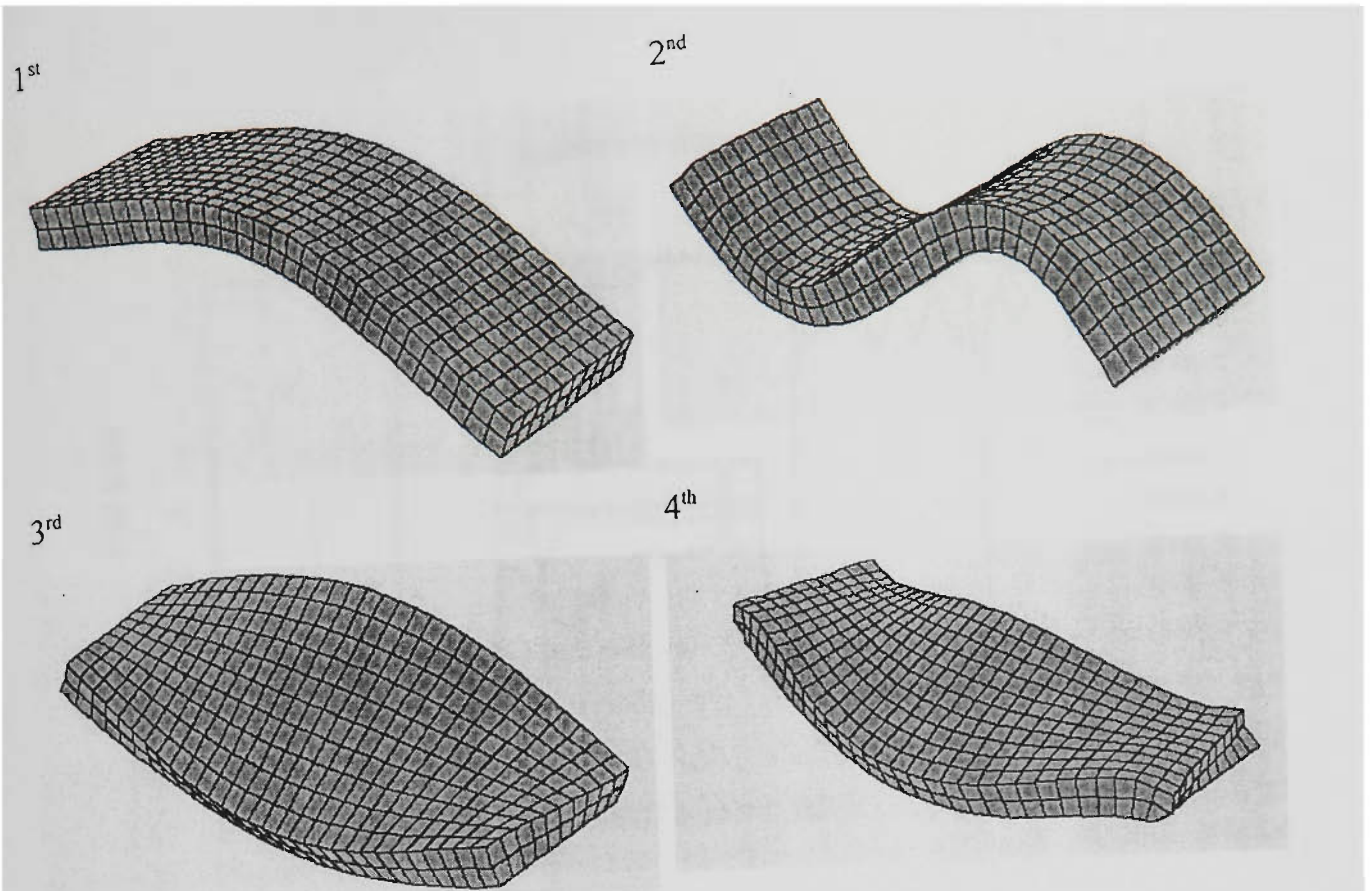


Fig. 5.28. Mode shapes: BESO.

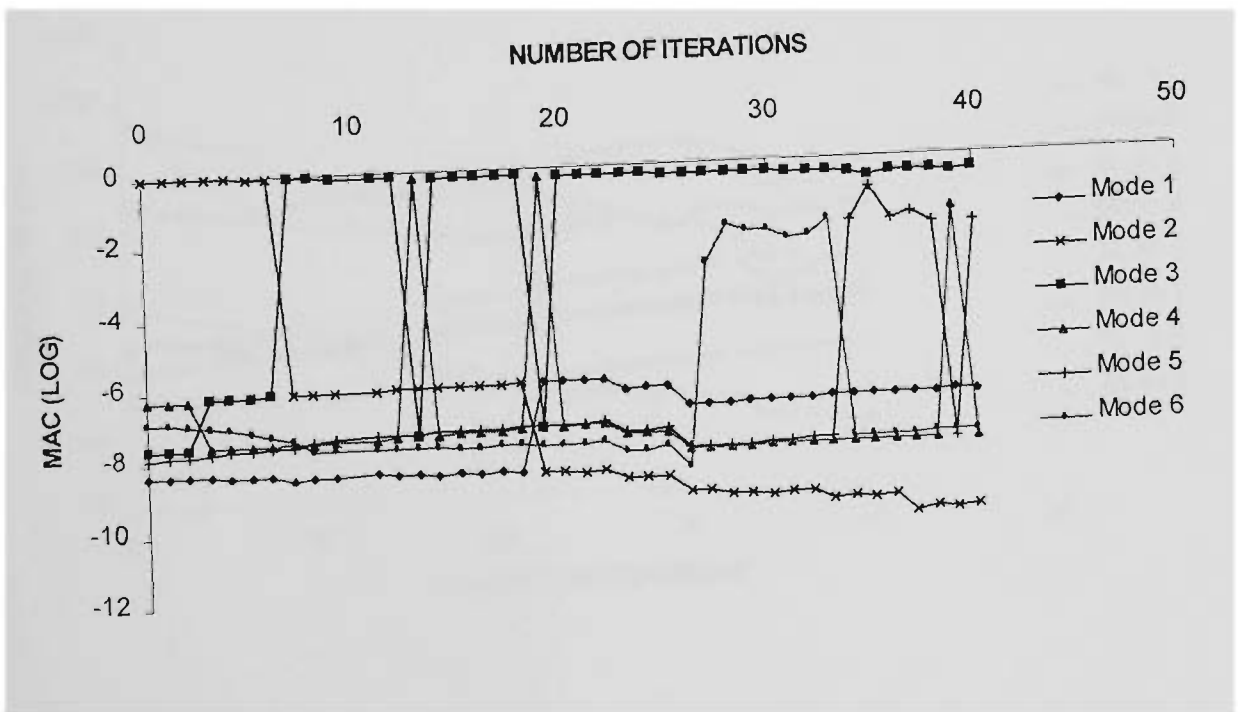


Fig. 5.29. MAC history: ESO.

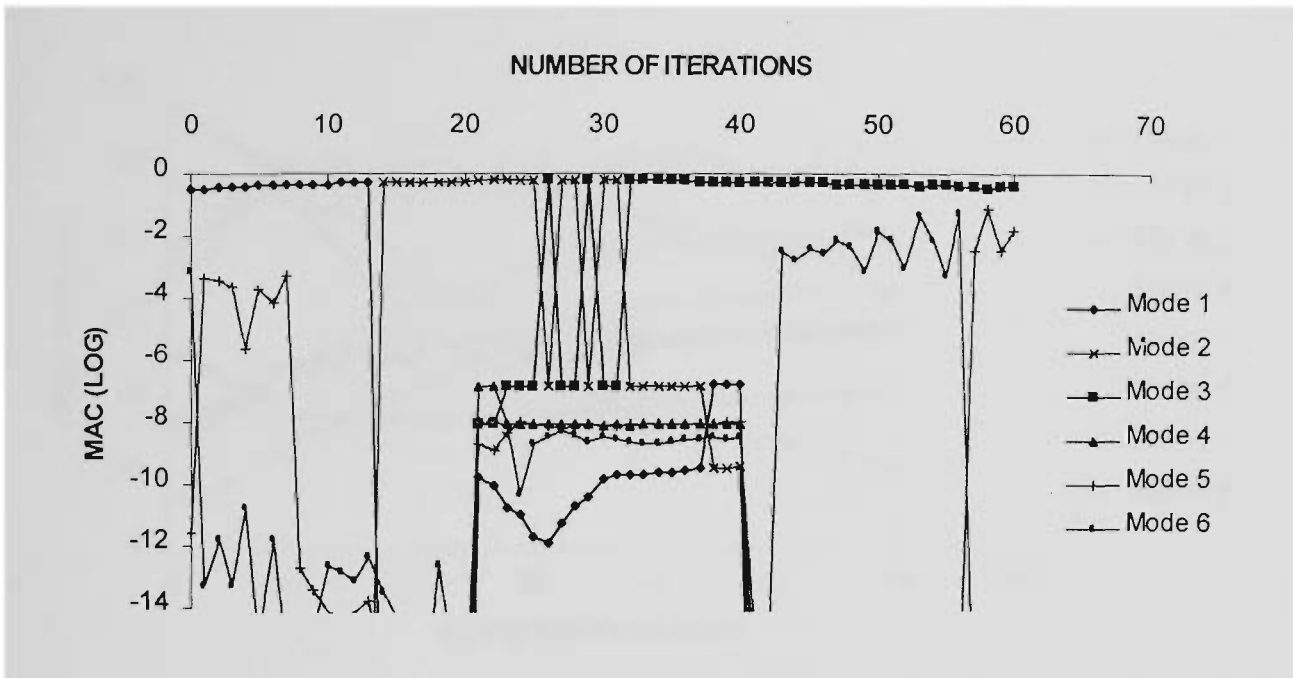


Fig. 5.30. MAC history: BESO.

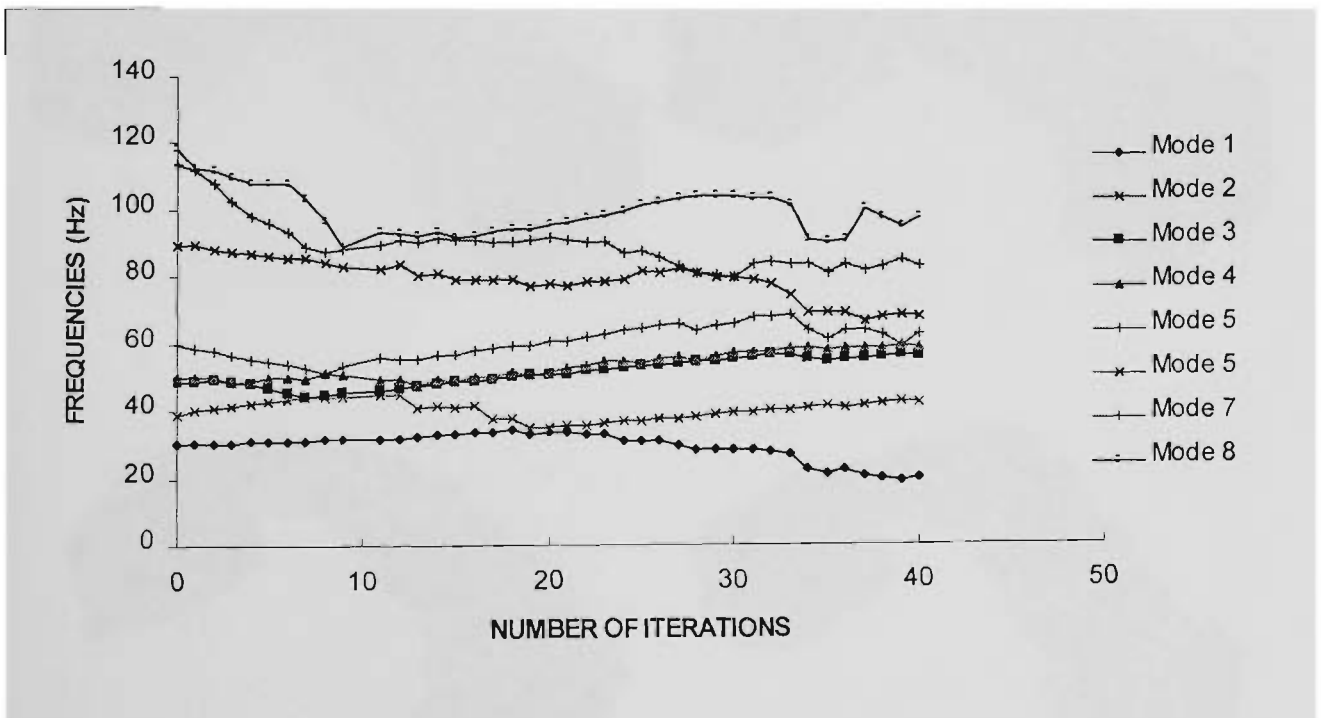


Fig. 5.31. History of the first eight frequencies: ESO.

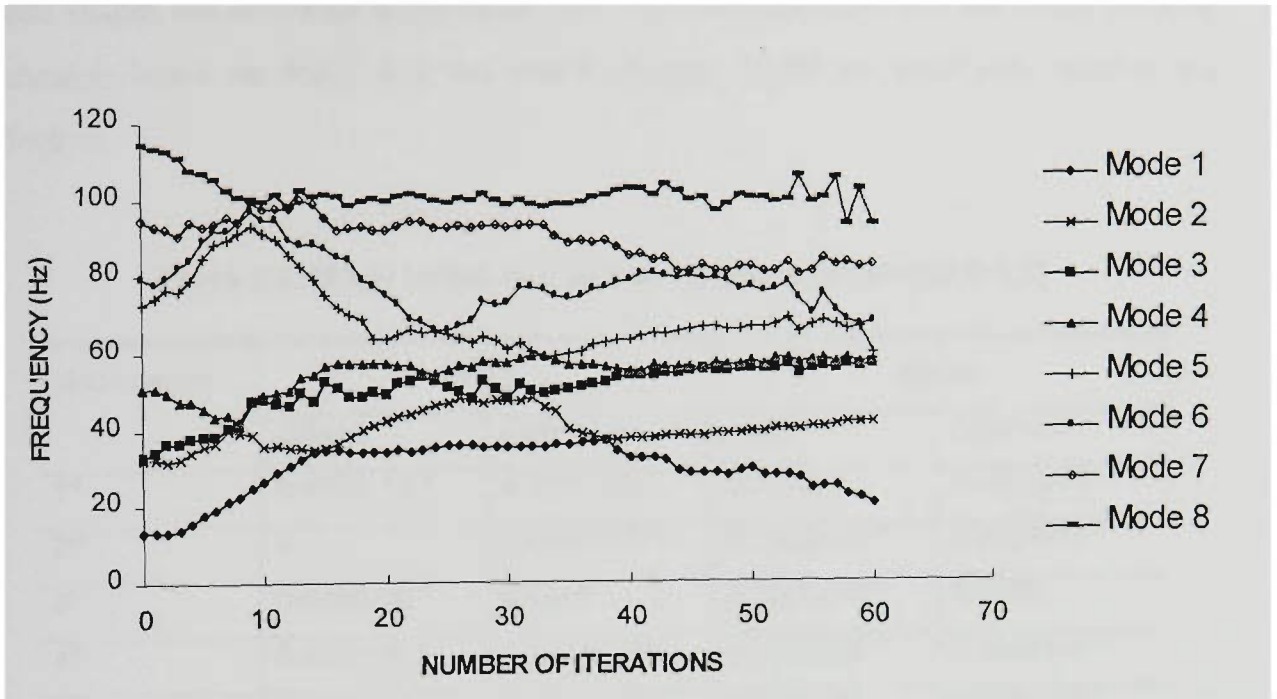


Fig. 5.32. History of the first eight frequencies: BESO.

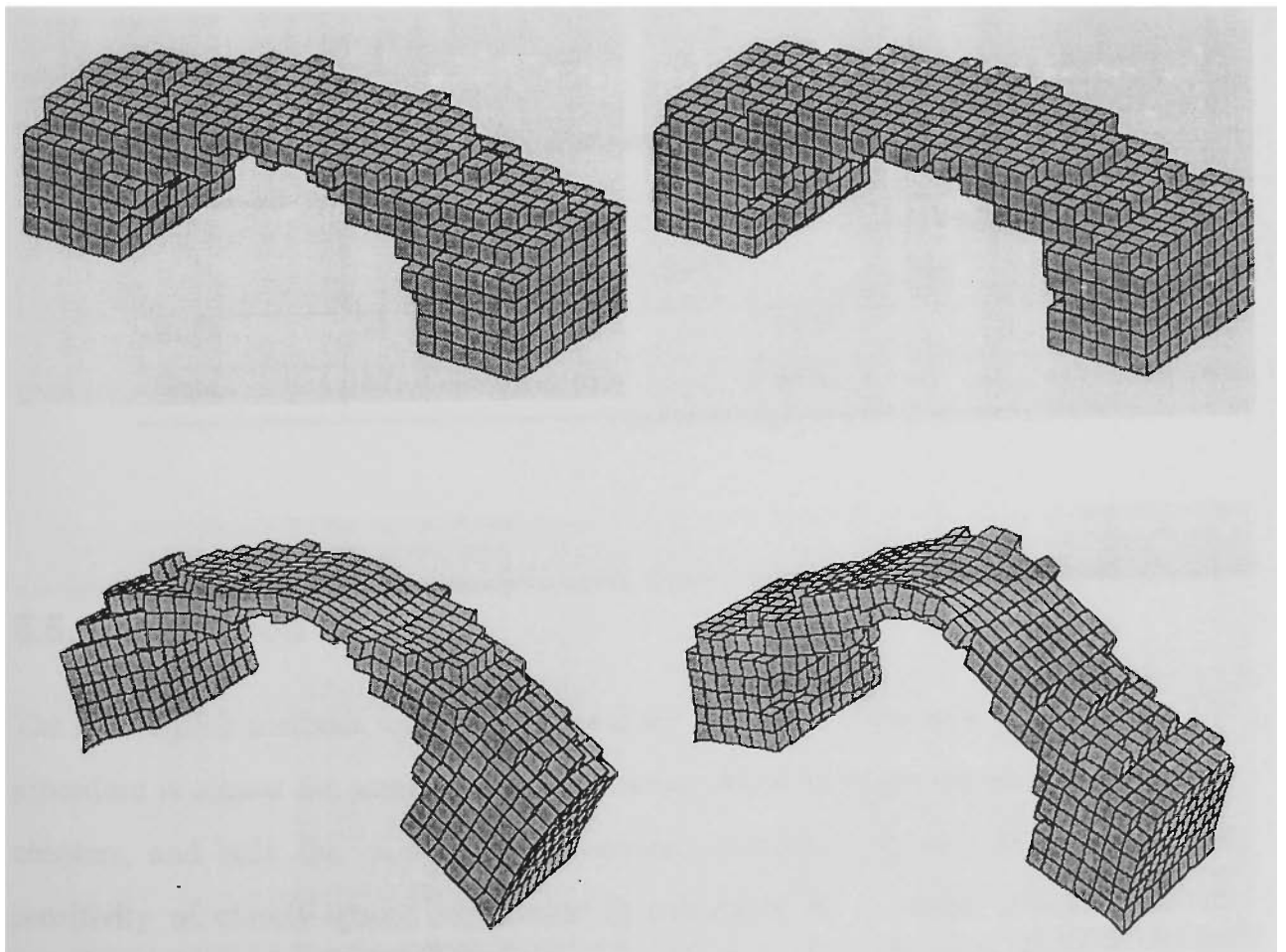


Fig. 5.33. Optimum topologies.

In this example, as in the previous one, ESO and BESO start from the different order of mode shapes but converge to the same one. This demonstrates that the mode tracking technique based on MAC and the search strategy based on sensitivity number are effective.

Table 5.6. MAC: Initial and at the Optimum (Example 5.4.6)

Mode orders	ESO		BESO	
	Initial	Optimum	Initial	Optimum
1 st	0.4750×10^{-8}	0.1661×10^{-6}	0.3168	0.1573×10^{-6}
2 nd	1	0.6487×10^{-9}	0.7770×10^{-15}	0.2304×10^{-9}
3 rd	0.2488×10^{-7}	0.5018	0.1032×10^{-16}	0.5186
4 th	0.5469×10^{-6}	0.9284×10^{-8}	0.9836×10^{-14}	0.8106×10^{-8}
5 th	0.1426×10^{-7}	0.1026×10^{-7}	0.2305×10^{-11}	0.9263×10^{-8}
6 th	0.1449×10^{-6}	0.1436×10^{-2}	0.9406×10^{-3}	0.2872×10^{-8}

Table 5.7. Frequency at Optimum, $W=45\%W_0$ (Example 5.4.6)

	Iteration	Compt. time (Min.: Sec.)	3 RD Frequency (Hz)
ESO	27	2:24	54.16
BESO	40	1:28	53.5

5.5. Conclusion

The ESO/BESO methods are easily generalised to natural frequency optimisation. The procedure is almost the same as those for static problems as presented in the previous chapters, and only the module for calculating sensitivity number is different. The sensitivity of closely-spaced eigenvalue is calculated by a simple average method, which is easy to understand and implement and proves to be effective. To optimise and

keep track of a desired mode, a procedure for identifying the mode shape of interest based on MAC is incorporated into ESO/BESO and its effectiveness is verified.

ESO and BESO in most cases converge to very close results. BESO can be computationally more efficient in most 2D cases.

Various Aspects of Numerical Implementation and Image Processing

While Chapters 3 to 5 develop the ESO/BESO methods and focus on different design objectives in static and dynamic behaviours, this chapter deals with aspects associated with the evolutionary method in general. The accuracy of sensitivity calculation is first studied and measures to ensure the reliability are introduced. Then the effect of parameters on solutions is studied, including the modification ratio in both ESO and BESO, and addition ratio, stage ratio and initial design in BESO. As the two methods are both based on a finite element model, an initial attempt on post-processing the results is made using AutoCAD. The objective of this chapter is to increase the reliability of the ESO/BESO methods, to provide user guidelines as to parameters selection as well as to enhance the method capability as a viable computer aided design tool.

6.1. Introduction

A numerical method can be evaluated in various aspects, such as:

1. Reliability

In ESO and BESO, the algorithm reliability is primarily dependent on the so-called element sensitivity number, which is the criterion driving the evolution process. There are many reasons that the calculation will lose its accuracy. Firstly, the sensitivity

analysis does not assume a continuous change but a jump in design variables (0 to 1 or 1 to 0), which may cause abnormal changes in the objective function. Secondly, the sensitivity analysis is largely based on the linear expansion of the objective function, i.e. the first order. There is the possibility that a higher order of expansion should be considered.

One sign of inaccurate sensitivity is the jump in the objective function, as opposed to the assumption that it would change smoothly. If such a big jump is observed at an iteration, the evolution needs to be reversed at this point to avoid being misled. This is a simple operation of cancelling the last structural modification and restoring the mesh, i.e. deleting the added elements and recovering the removed elements. To allow the evolution to continue, those elements should be excluded from modification for some times.

The above technique is effective in correcting the inaccuracy of sensitivity analysis and finding a smooth search path to the optimum. However, there are some cases where the inaccuracy is irreparable because of inherent features of a particular problem. A typical example is given in a discussion paper (Zhou and Rozvany 2001), which cannot be solved by the present ESO/BESO due to the specifications of extreme loading and supporting conditions. Though regarded as an isolated case, this reminds us that like any other method, ESO/BESO has its own limitations. However, for ordinary problems encountered in practical engineering design, the feasibility and effectiveness have been well demonstrated.

2. Stability

Despite the extensive research on topology optimisation, study of numerical instability is limited. A systematic survey is given by Sigmund and Petersson (1998) summarising various aspects of the issues and solutions. The instability can be stated as the checkerboards, mesh-dependencies and local minima. The following briefly describes these aspects and adds to the features associated with ESO/BESO.

- Checkerboard

Checkerboard, as detailed in Chapter 3 (Sect.3.2.3), refers to regions of alternative solid and empty material distributing like a checkerboard pattern. The underlying mathematical reason for it may be the nonconvergence of the FE solution. The checkerboard is prone to appear in a coarse mesh and/or a mesh of lower order of elements. In homogenisation based topology optimisation or SIMP, procedures to control or reduce the checkerboard are proposed, such as the use of higher order finite elements, patches, noise filtering or imposing extra constraints.

ESO/BESO deals with the checkerboard pattern using a technique similar to the noise filtering and involves averaging the sensitivity in a neighbourhood. In the application on problems of 2D plane stress, plate bending and 3D solid elements, the averaging technique proves to be effective in preventing the formation of checkerboard and is also computationally efficient. In fact, only negligible amount of computing is involved.

- Mesh dependence

It refers to generating qualitatively different solution from different finite element grids. While a finer mesh is expected to reveal a design at a higher resolution, it actually produces designs with more configuration details. There are two categories of mesh dependency problems. The first one is due to the nonexistence of solution for the inherent 0-1 discrete problems. Same techniques for checkerboard suppression can be adopted to remedy this kind of problems, such as the filtering and perimeter control. The second category is the non-uniqueness of solution and a typical example is a bar under uni-axis tension. Manufacturing constraints such as bounding the area can be a solution to this category.

In ESO/BESO method, the mesh dependency can be remedied by a perimeter control method. This topic is left in the next chapter for a detailed presentation.

- Local minimum

Topology optimisation problems normally have many local minima, and different solution can be obtained by changing algorithm parameters or initial conditions. In the simplest case as a single-variable function with the range of the variable being given, the condition of a global optimum which can be searched in the gradient direction is that the function is convex with respect to the variable. For the 2D plane stress condition, if we take the plate thickness t as the design variable and the mean compliance C as the objective function, it is found that C is not convex as $C = f(t^{-1})$. Thus it is likely that a search method based on the sensitivity analysis may not find a global optimum. This is further complicated by the fact that the design variable is not single but multiple as a structure is normally has more than one element. In this case, each design variable is updated respectively instead of by the same magnitude. For the above reasons, an optimisation algorithm is highly likely to end up with a nearby stationary point or local minimum. In the mathematical programming (MP) algorithm, for example, the solution is susceptible to the change in parameters such as move limits, definition of design domain and penalty power.

While local minimum solutions are not desirable from the mathematical point of view, they represent feasible designs and provide useful design options to engineer. It is then up to the engineer to decide which design addresses the requirements best, e.g. by taking into account of other factors (such as manufacture or assembly).

The local minimum in ESO/BESO can be due to variations in parameters such as the ground structure and initial structure (BESO), modification ratio, addition ratio and stage ratio (the last two for BESO only). Parameter effects on ESO/BESO have been studied in many literatures (Chu 1997; Yang 1999), covering different structure systems and objective functions. This chapter intends thus for continuum structures where mean compliance/frequency is the objective, as complementary to the previous study.

Apart from the above mentioned various numerical aspect, this chapter also suggests a possible way of post-processing. Based on a fixed finite element model, there is a gap between the actual analysis model and final design draft. Switching between these two

models is critical in practical engineering design. Some complete packages incorporating post-processing to topology optimisation have been developed, such as FIDO by the ADOPT research Group (Hinton *et al.* 1998). Using the 2D and 3D continuum finite element models, image extraction techniques such as boundary surface fitting or skeleton thinning are used to process the finite optimum topologies.

Post-processing for ESO/BESO is largely based on the use of available software, such as SolidWorks and AutoCAD. This chapter presents a few results of 3D continuum post-processed by AutoCAD.

6.2. Verification of Sensitivity Analysis

6.2.1 Measure of Accuracy

- ε_1 -Change between two cycles.

The sensitivity analysis is valid when the change between two cycles is small. As the first measure, we define

$$\varepsilon_1 = \frac{f^{(m)} - f^{(m-1)}}{f^{(m)}}, \quad (6.1)$$

where f denotes the objective function which can be the mean compliance, single or multiple eigenvalues. The superscript in brackets denotes the iteration cycle.

- ε_2 -Difference in the predicted and actual objective functions.

To complement the above measure, we examine the predicted value of the objective function:

$$f^{(m)} = f^{(m-1)} + \Delta f^{(m-1)}, \quad (6.2)$$

where $\Delta f^{(m-1)}$ is the predicted increment in the objective function, which is the sum of the sensitivity number for all removed elements, i.e.

$$\Delta f^{(m-1)} = \sum_{i=1}^{Nr} \alpha_i, \quad (6.3)$$

where Nr is the total number of removed elements.

We compare the value of the objective function predicted from the current iteration with the actual value, and define

$$\varepsilon_2 = \frac{f^{(m)} - f^{(m-1)}}{f^{(m)}}. \quad (6.4)$$

Ideally, ε_2 is equal to 0, or as small as possible. It is noted that BESO has ε_1 and ESO has both ε_1 and ε_2 .

In frequency optimisation, ε_2 is defined only when the optimisation problem is exactly the same between two neighbour iterations. This is because that the predicted value is based on the same order of eigenvalues and its sensitivities. Therefore, ε_2 measure is not activated in such situations: the mode shapes swap orders, the structure becomes multi-modal from 'single' modal (or single to multiple), or the multiplicity changes.

6.2.2 Numerical Implementation

At each iteration, the two measures ε_1 and ε_2 are checked up against its prescribed limit:

$$|\varepsilon_1| \leq \bar{\varepsilon}_1, \quad (6.5a)$$

$$|\varepsilon_2| \leq \bar{\varepsilon}_2. \quad (6.5b)$$

From experience, $\bar{\varepsilon}_1 = 5\%$ and $\bar{\varepsilon}_2 = 2\%$ can be used. If *both* of the above expressions are satisfied in ESO, or the first is satisfied in BESO, the evolution goes ahead without interruption. Otherwise, it is regarded that a ‘sharp’ change has happened, most possibly due to inaccurate evaluation of the sensitivity analysis. The first step is to resume the structure to its previous configuration by cancelling the last iteration, i.e. removed elements are reinstated and added elements are excluded. To avoid repeating modifying these elements at an immediate iteration, they are set as temporarily ‘frozen’ for the next few iterations, denoted by N_f . It is noted that a too small N_f will cause oscillation in the designs, for an extreme case, $N_f = 0$ means the iteration just repeat itself and cannot go any further. On the other hand, those elements cannot be frozen too long, as this assumes a reduced set of design domain. The experience shows that $N_f = 3$ works effectively, i.e. after 3 cycles after the sharp changes happen, the temporarily unavailable elements are unfrozen.

This measure is effective in getting over the local anomalies and allowing the evolution to proceed. However, if very frequent sharp changes happen and the design just oscillates around a point, it is regarded that no further improvement can be achieved by modifying the structure, and the evolution comes to a termination. Namely, the accumulated occurrence of sharp change N_{osc} exceeds a prescribed upper bound \bar{N}_{osc} , which is usually taken as 15.

The above check-up procedure can be written into the ESO/BESO procedure as a small loop, as shown in the flowchart of Fig. 6.1.

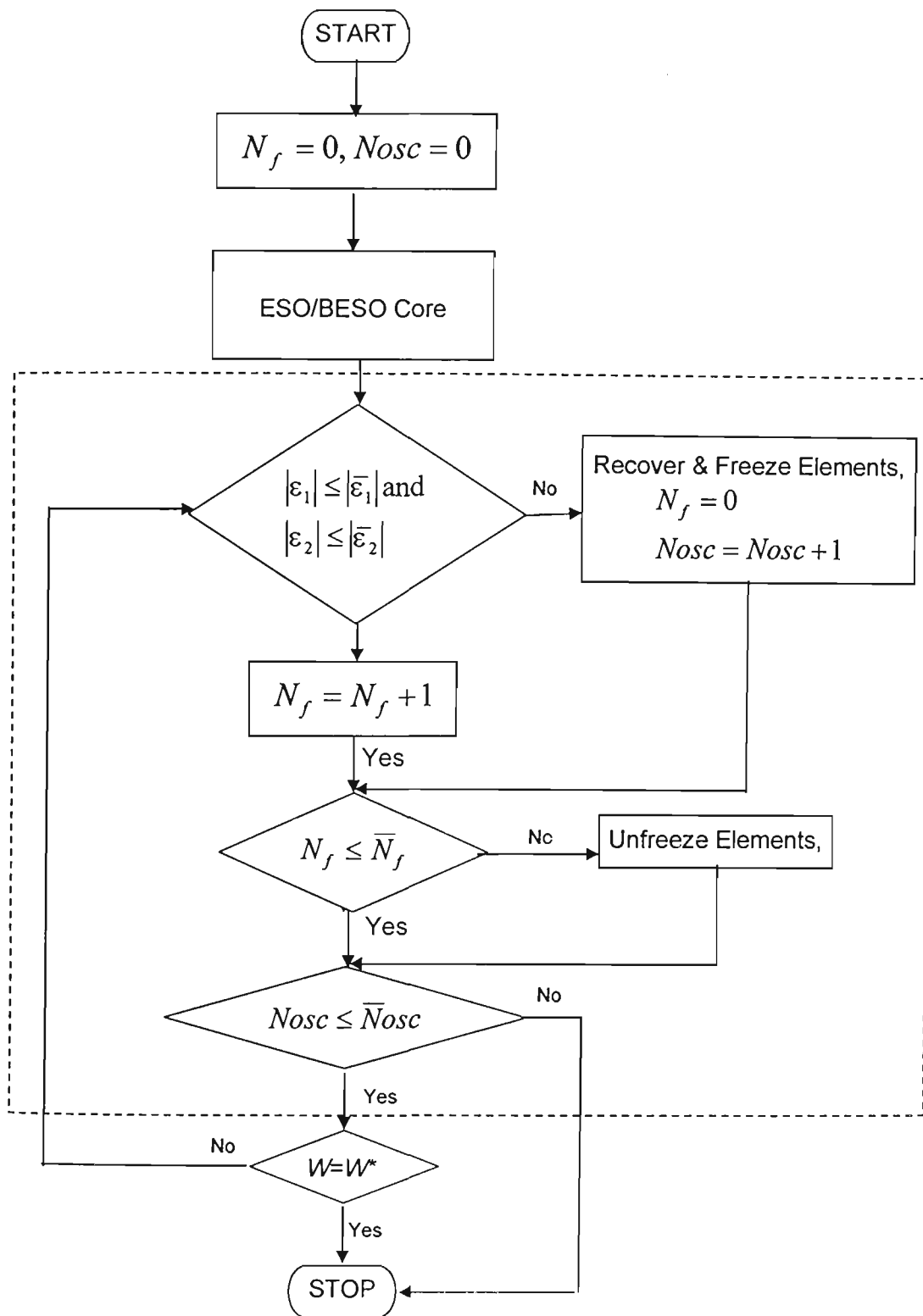


Fig. 6.1. Flow chart: procedure dealing with sharp changes:
Checkup-recover-freeze-unfreeze.

6.2.3 Examples

Examples in this section are chosen from chapters 4~6 for verifying the sensitivity analysis and demonstrating the above proposed procedures. All physical and geometry properties and design parameters are as previously given. In the chart or table demonstration, the mean compliance is given in percentage related to the ground structure, i.e. C/C_0 . Only ESO is considered for it includes both measures of errors.

6.2.3.1 Basic Stiffness Optimisation: External Loading Only.

Example 4.3.3 as a cable bridge is studied for this purpose. Fig. 6.2 shows the evolution history of 300 iterations and the structural weight is from 100% to 14%. The left axis is for the errors ε_1 and ε_2 , and the right axis is for the relative mean compliance.

It is seen that the mean compliance gradually increases as the structure degenerates. The evolution is rather smooth in the first 100 iterations or so before the structure reduces to 17%. Then sharp changes are frequently observed, initially with an interval of around 10 iterations and later becoming oscillating. All sharp changes have ε_1 going beyond the limit (denoted by the horizontal dashed line), with some occasions of ε_2 also exceeding its bound. Checking the structural behaviour during those iterations, it is found that in many occasions two major parts of structure are connected only by one element at its diagonal side. This produces a weak link and decreases the structural integrity. As elements are recovered to strengthen the link and the evolution is reversed, the overall history is gradual and smooth.

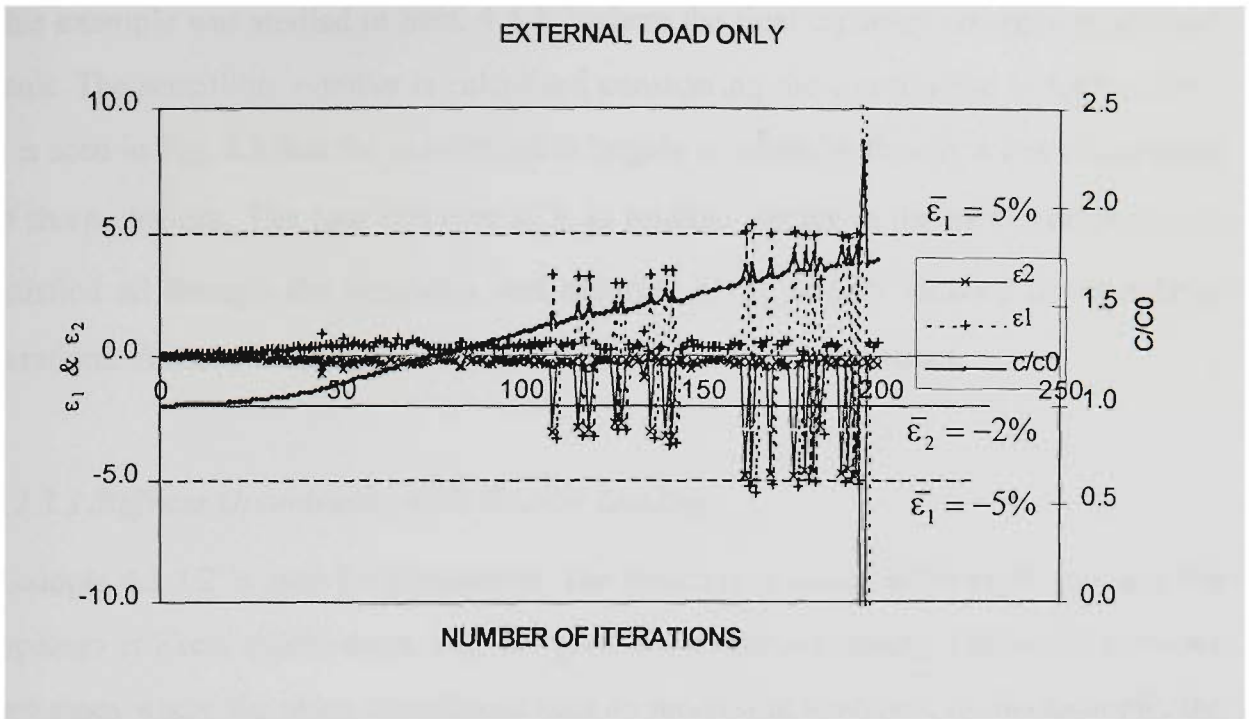


Fig. 6.2. Iteration history of the mean compliance and two measures of errors: basic stiffness optimisation.

6.2.3.2 Stiffness Optimisation with Surface Loading.

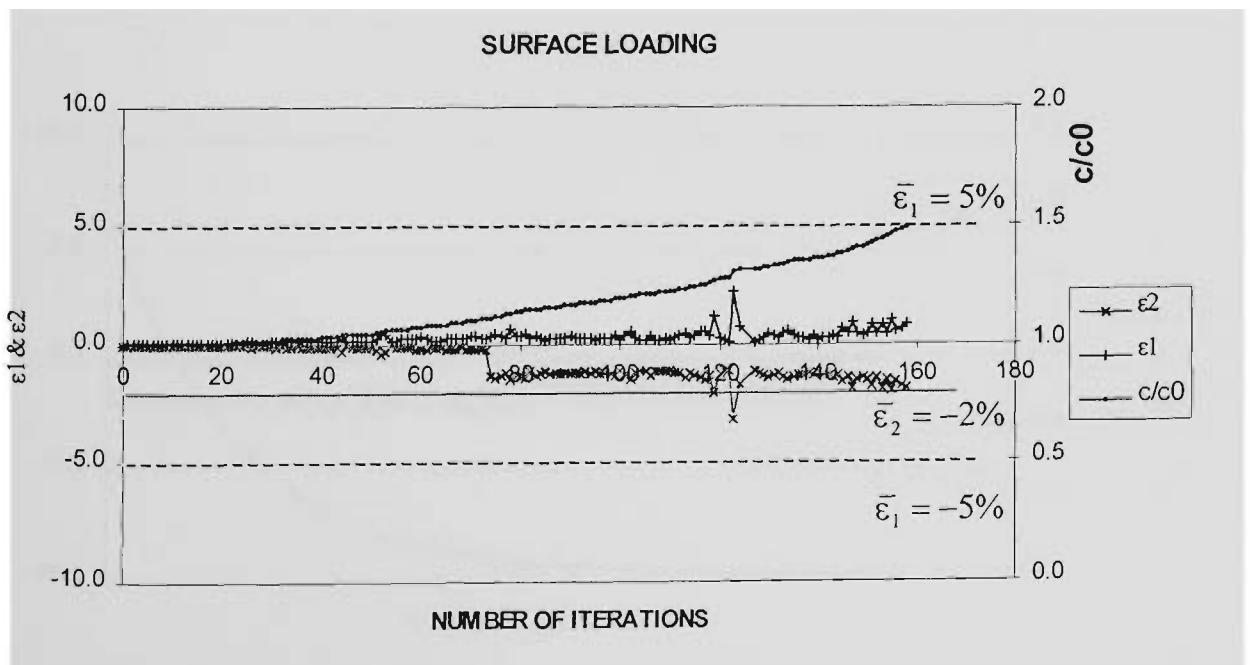


Fig. 6.3. Iteration history of the mean compliance and two measures of errors: surface loading.

This example was studied in Sect. 4.4.3.2 where the final topology emerges as a church vault. The sensitivity number is calculated considering the contribution in load vectors. It is seen in Fig. 6.3 that the calculation is largely accurate, with only a few occurrences of sharp changes. The first criterion of ε_1 as relative change in the mean compliance is satisfied all through the iterations, and criterion of ε_2 is only violated in some latter iterations. A smooth change in the mean compliance is rather distinct.

6.2.3.3 Stiffness Optimisation with Gravity Loading.

Example 4.3.3.2 is used for illustration. The structure is under self-weight only and the topology is like a quadri-court. Fig. 6.4 gives the evolution history. Unlike the previous two cases where the mean compliance sees an increasing tendency, in this example, the mean compliance decreases as the structure reduces its weight. This is evident as the overall loading is also decreased during the course. Both measures ε_1 and ε_2 are well below the prescribed limit and no sharp changes are observed.

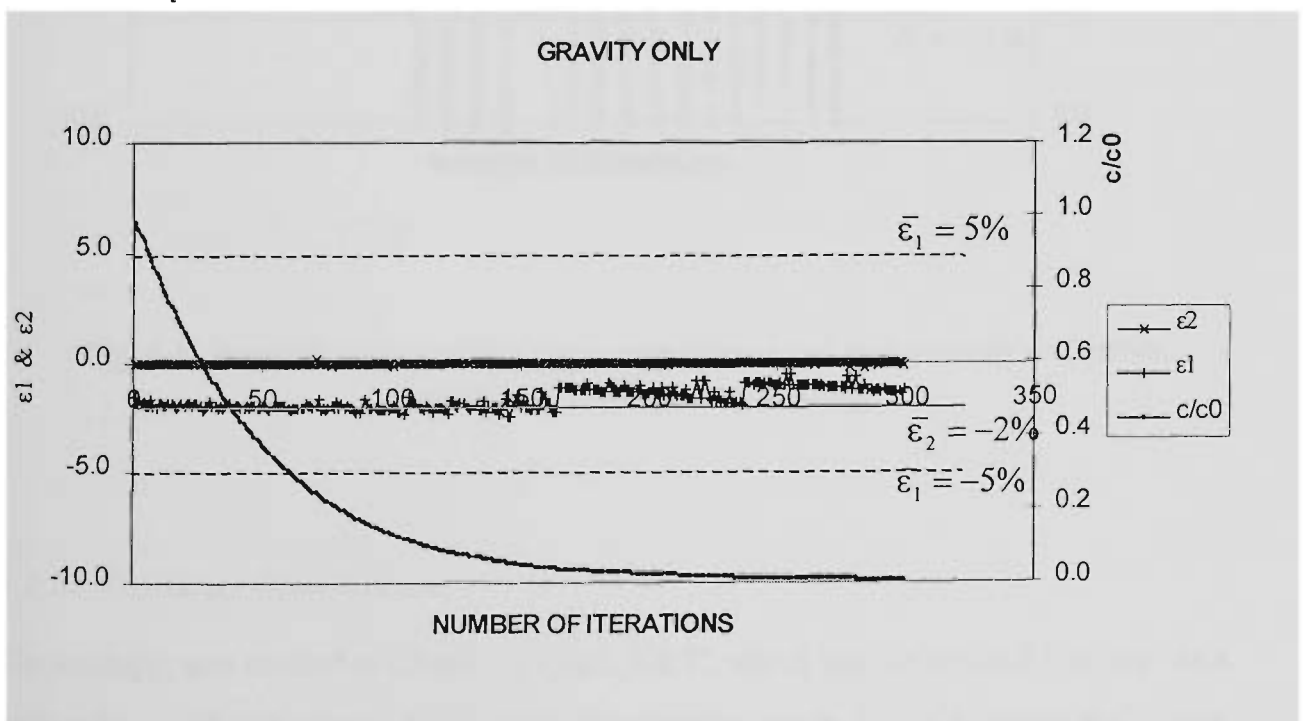


Fig. 6.4. Iteration history of the mean compliance and two measures of errors: gravity loading only.

6.2.3.4 Stiffness Optimisation with Combination of External Loads and Gravity.

Same as in Sect 6.2.3.1, we again use Example 4.3.3.3. The load combination is as per Chapter 3. Comparing Figs. 6.5 to 6.2, it is seen that adding the gravity to the combination causes higher rate of sharp changes and the magnitude of the change is much larger. This may be because that the change in the mean compliance is not monotonic, as seen in the history. By using the proposed checkup-recover-freeze-unfreeze technique, an overall stable convergence is observed.

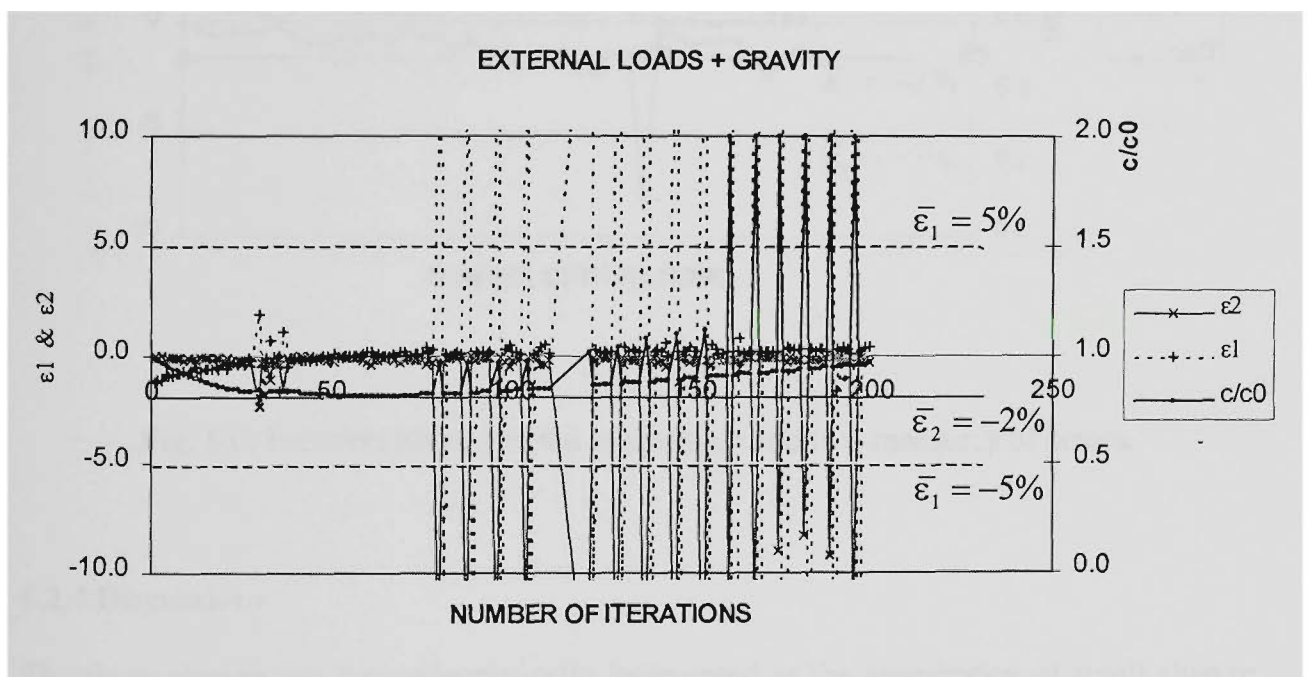


Fig. 6.5. Iteration history of the mean compliance and two measures of errors: external loads plus gravity loading.

6.2.3.5 Frequency Optimisation.

The example was studied in Chapter 5 (Sect. 5.4.5), which has the optimal topology as a hollow box with a maximised frequency for a torsion mode. Fig. 6.6 gives the history of natural frequency associated with the torsion mode shape tracked from the ground structure. It is noted in the foregoing minimisation problems that the stiffness optimisation always has $\varepsilon_2 < 0.0$, i.e. the predicted value of mean compliance is smaller

than the actual one. Likewise, for a maximisation problem as in this example, the predicted frequency increase is normally overestimated as $\varepsilon_2 > 0$. As the later stage sees multi-modal phenomenon, ε_2 is no longer defined. Meanwhile, ε_2 is below the limit except at one or two locations, which corresponds to a sharp decrease in the eigenvalue.

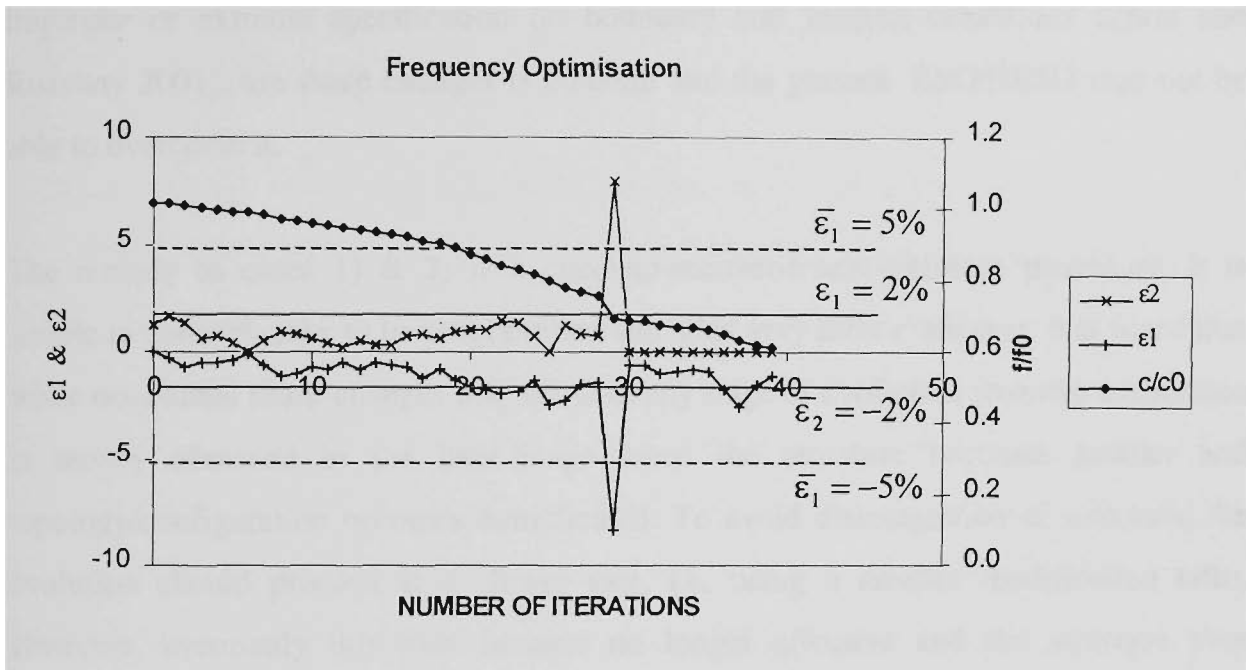


Fig. 6.6. Iteration history of the eigenvalue and two measures of errors.

6.2.4 Discussions

The sharp change can be mathematically interpreted as the assumption of small change in sensitivity analysis being violated. Physically, this situation can be caused by:

- 1) The structure is disintegrated after removing some particular elements, which is the most common case in the example provided above. For example, the truss has one of its member cut in the middle, and the connection between the load and supports or main structure becomes very weak.
- 2) The structure integrity is maintained, but there is significant change in the stress/strain energy or load path due to element removal. This can be: a) a much complicated stress/strain energy field which may underestimate the element sensitivity;

b) A reliable sensitivity but too many elements removed at once whose accumulated effect becomes significant.

3) As a very special case, if the stress/strain energy is too complicated due to an improper or extreme specification on boundary and loading conditions (Zhou and Rozvany 2001), the sharp changes is inherent and the present ESO/BESO may not be able to overcome it.

The remedy to cases 1) & 2) is a checkup-recover-freeze-unfreeze procedure. It is simple in concept, easy to be programmed and adds very little extra cost. It is noted that while occasional sharp changes may occur at any stage of evolution, frequent occurrence is mostly observed in the later stage when the structure becomes smaller and topology/configuration becomes complicated. To avoid disintegration of structure, the evolution should proceed at a slower rate, i.e. using a smaller modification ratio. However, eventually this may become no longer effective and the structure may oscillate around a weight for a number of iterations (say 15). This implies that no further modification can be made without causing disintegration of the structure, and the structure is to be left as it is and the evolution be terminated.

6.3. Parameter Studies

The major parameters involved in ESO and BESO are modification ratio, the initial design, addition ratio and stage ratio. From detailed parameter studies for 2D continuum structures (Chu 1997; Yang 1999), the following observations are made:

1. In both ESO and BESO, different topologies are obtained by changing the modification ratio MR . However, the structural performance is close, such as the mean compliance, natural frequencies or performance index PI , with a average difference of 3%. The recommended value for MR is 1%~5%.
2. BESO is less sensitive to the addition ratio AR than to the modification ratio MR . Two usual values are $AR = 0.33$ and $AR=0.25$. No distinct difference in topology optimisation is observed when varying AR .

3. In BESO, the solution is also affected by the initial design. A definition fully interpreting the support and load conditions and having longer boundaries can be more advantageous.

When studying whether the above guidelines are applicable to 3D problems, it is worth noting the following points.

Firstly, those guidelines are summarised based on a very fine mesh on a 2D domain. Let us take example 4.2.3.1 (Chapter 4, 2D arch bridge) to describe the level of mesh discretising. A mesh of 50×25 is used in this example, which is considered as relatively fine only, as a similar problem was previously studied using a much finer meshes, e.g. 80×40 (Yang *et al.* 1999). Further, consider a corresponding 3D arch bridge in Example 4.3.3.1, a mesh of $50 \times 25 \times 3$ is used. This is also deemed as relatively fine, as the same mesh of 50×25 is used in dividing the plane, with 3 layers in thickness. Use of a very fine mesh for 3D problems requires higher computing costs, and is also subjected to the capacity of the codes performing ESO/BESO. For this consideration, most 3D problems use only reasonably fine meshes, and it may call for a smaller modification ratio than 2D problems. In the example of previous chapters, normally, 1% and 2% are used for ESO, and sometimes BESO adopts a large value as $MR=4\%$.

Secondly, as mentioned in Chapter 3, the stage ratio is exclusive for 3D. It is heuristic and intuitive, rather than a rigorous definition of a perform index as in 2D problem. A series of study on 3D & 2D continuum is presented as follows.

6.3.1 Modification Ratio (*MR*)

6.3.1.1 Effect on ESO

The example is shown in Fig. 6.7. A 3D thin cantilever beam is applied a point load at the bottom of the free end. $E=210$ GPa and $\nu=0.3$ are assumed. By using the symmetry in the thickness, the half design domain is divided using a mesh of $36 \times 24 \times 3=2592$.

Three cases are studied, $MR=1\%$, $MR=2\%$ and $MR=4\%$. In all cases, there is no particular weight target, but allowing the structure to evolve up to 300 iterations.

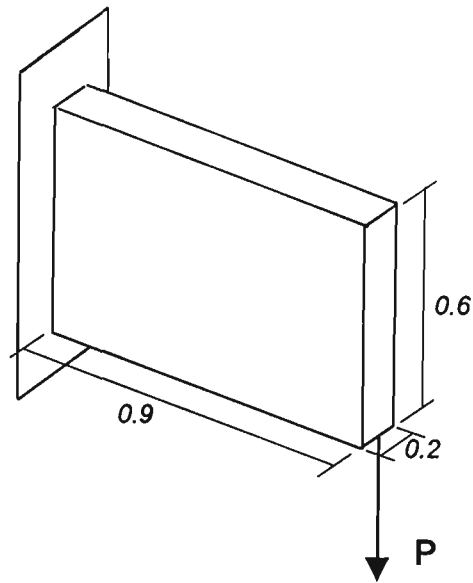


Fig. 6.7. A cantilever beam.

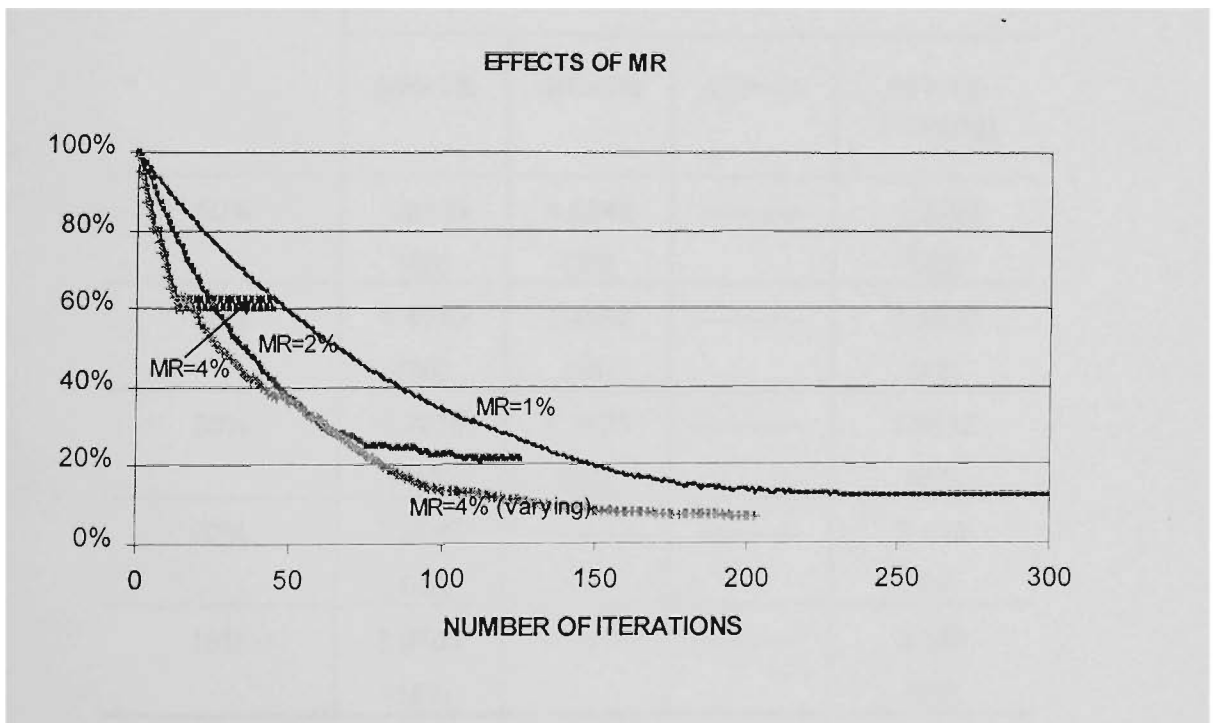


Fig. 6.8. Iteration history of structural weight by different values of MR .

Fig. 6.8 shows the iteration history of the structural weight. In case 1 ($MR=1\%$), the evolution is kept up to the end. However, both case 2 and case 3 are terminated due to the high rate of sharp changes. Case 2 ($MR=2\%$) oscillates around a weight of 22% before the evolution comes to a stop. Case 3 ($MR=4\%$) becomes oscillating at an even higher weight of 60%. For this reason, they are not feasible if the weight target is below those values.

A natural way to get over the oscillation due to a large modification ratio is to decrease the ratio when necessary. In other words, among the whole history, on the first oscillation on a weight W_1 , a smaller MR is used for the iterations onward, say, $0.5MR$. When it comes the second occurrence of oscillation around W_2 , MR is halved again and becomes $0.25MR$, and so on and so forth.

Table 6.1. Comparison of Mean Compliance using Different MR (ESO)

Prescribed Weight W^*/W_0	Mean Compliance C/C_0 (Number of Iterations)			
	$MR=1\%$	$MR=2\%$	$MR=4\%$	$MR=4\%$ (Varying)
50%	1.2419 (66)	1.2842 (35)	-----	1.2993 (28)
40%	1.4075 (86)	1.4582 (46)	-----	1.4926 (42)
30%	1.7076 (113)	1.7725 (60)	-----	1.8112 (63)
20%	2.3647 (149)	-----	-----	2.413 (81)
15%	3.0765 (183)	-----	-----	3.142 (95)

The above technique using a varying modification ratio is applied with an initial value of $MR=4\%$. The history is displayed as in Fig. 6.8, too. It effectively prevents a

premature termination of evolution as the structure well reaches a low weight as 6%. Five times of oscillation happen and the modification ratio changes sequentially as 4%, 2%, 1%, 0.5%, 0.25% and 0.125%. A changing MR has the advantage of saving computing time, as less iterations are involved for a given weight constraint compared to using a fixed small value, say 1%. This is demonstrated in Table 6.1.

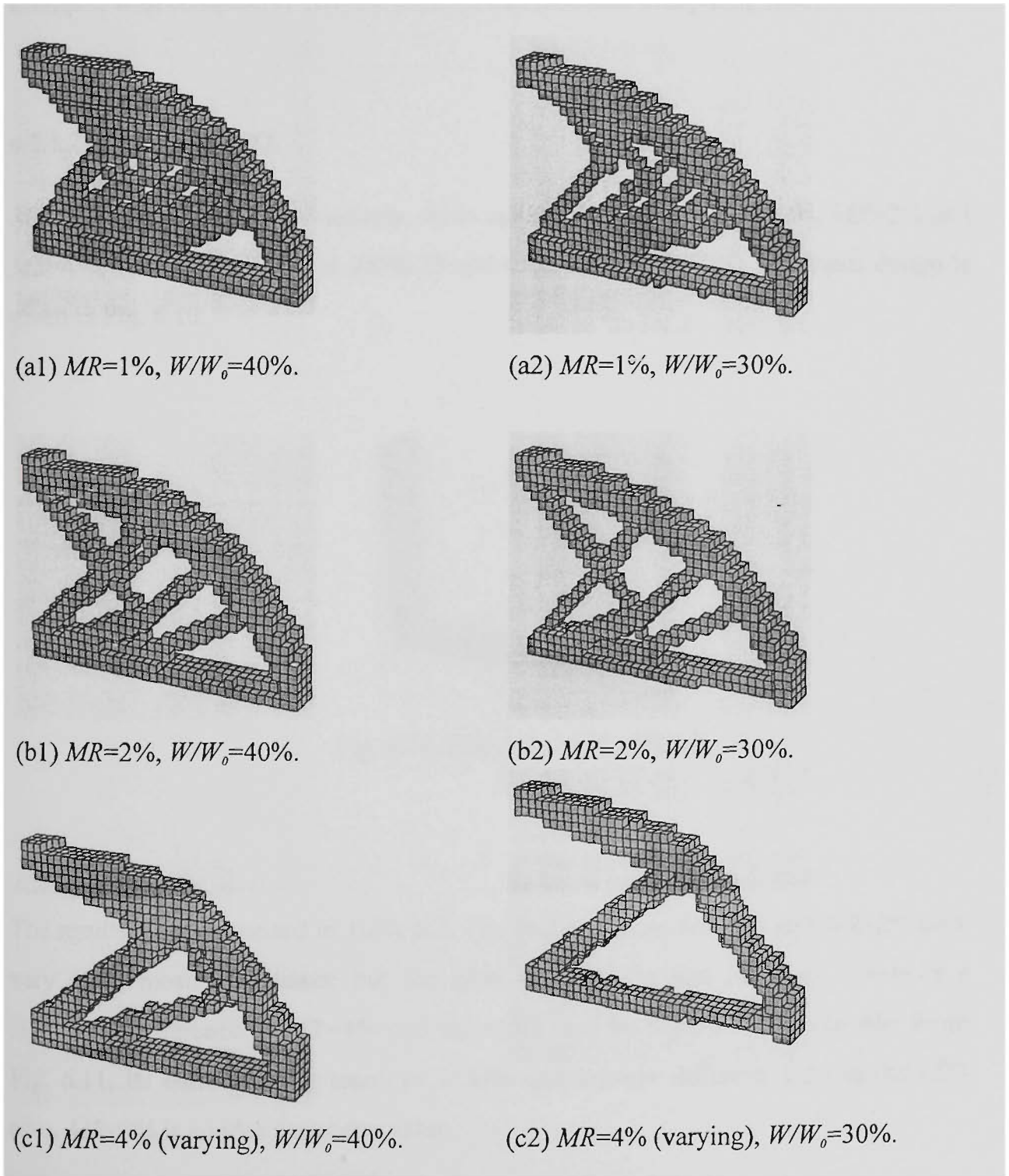


Fig. 6.9. Topologies by different MR (ESO).

Table 6.1 also compares the mean compliance by using different modification ratios. For each given weight percentage, a large value of MR yields a larger mean compliance. The topologies are also different, as shown in Fig. 6.9. All topologies are featured by a half arch between the load point and the top side of supports. Use of a larger modification ratio reduces the internal configuration details. Combining the numerical results in Table 6.1, a value of $MR=2\%$ can be the most suitable parameter for this example, with comparably reliable solution and moderate computing time.

6.3.1.2 Effect on BESO

Still use the last example. Similarly, three cases are considered: $MR=1\%$, $MR=2\%$ and $MR=4\%$. The addition ratio is $AR=0.25$ and stage ration $AR=50\%$. The initial design is given in Fig. 6.10.

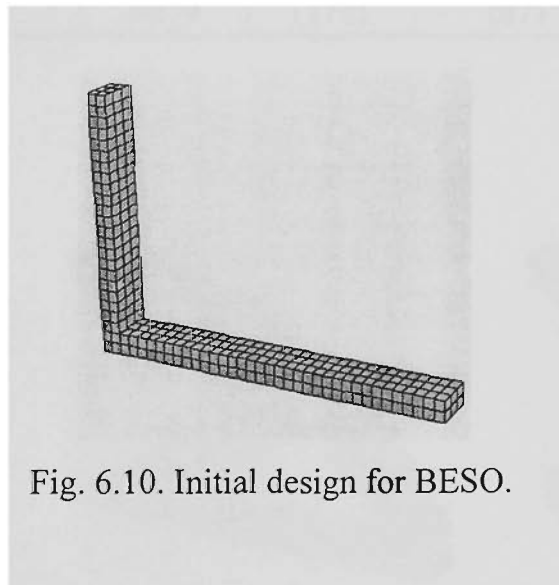
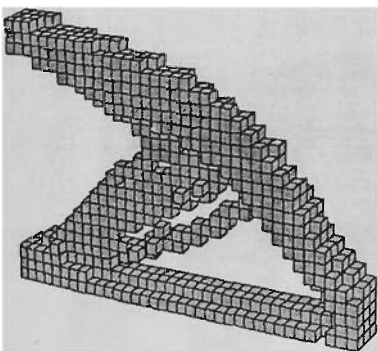
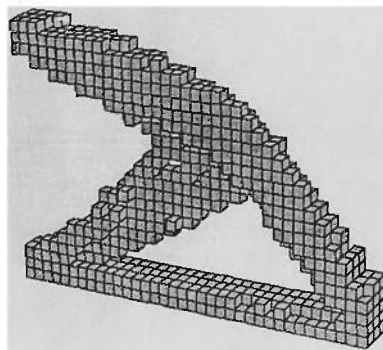
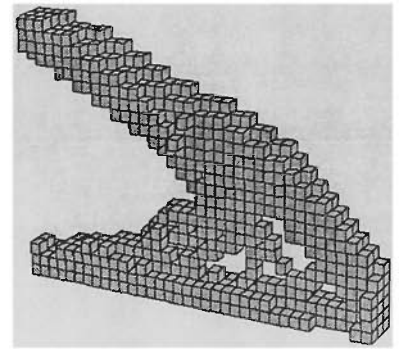


Fig. 6.10. Initial design for BESO.

The results are summarised in Table 6.2. The first two cases $MR=1\%$ and $MR=2\%$ have very close mean compliance but the latter involves far less iterations. There is a significant difference in $MR=4\%$ and the result may be regarded as unreliable. From Fig. 6.11, its corresponding topology is also qualitatively different. Like in the ESO case, $MR=2\%$ is an idea parameter value.

Table 6.2. Comparison of Mean Compliance using Different MR (BESO)

Prescribed Weight W^*/W_0	Mean Compliance C/C_0 (Number of Iterations)		
	$MR=1\%$	$MR=2\%$	$MR=4\%$
50%	1.3405 (72)*	1.4126 (33)	1.6797 (16)
40%	1.4205 (120)	1.4525 (57)	1.6209 (29)
30%	1.7863 (189)	1.7556 (92)	1.8314 (48)
20%	2.3656 (264)	2.4078 (136)	2.4578 (69)
15%	3.1484 (377)	3.1218 (175)	3.3580 (87)

(a) $MR=1\%$.(b) $MR=2\%$.(c) $MR=4\%$.Fig. 6.11. Topologies by different MR (BESO, $W/W_0=30\%$).

Indeed, $MR=2\%$ is the mostly used value in examples of the previous chapters. It is noted that there are cases where a larger value (say, $MR=4\%$) is also used and satisfactory results are obtained, such as in the Example 3.3.2 (stool) and 4.4.3.2 (vault).

Again, let us study Example 3.3.2 and compare the effect of MR ($MR=4\%$ and $MR=2\%$). The result is shown in Table 6.3. It is noted that the corresponding mean compliance is very close. The topologies are also very similar to each other, as shown in Fig. 6.12. It can be said that $MR=4\%$ is a better choice for its computing savings for this example.

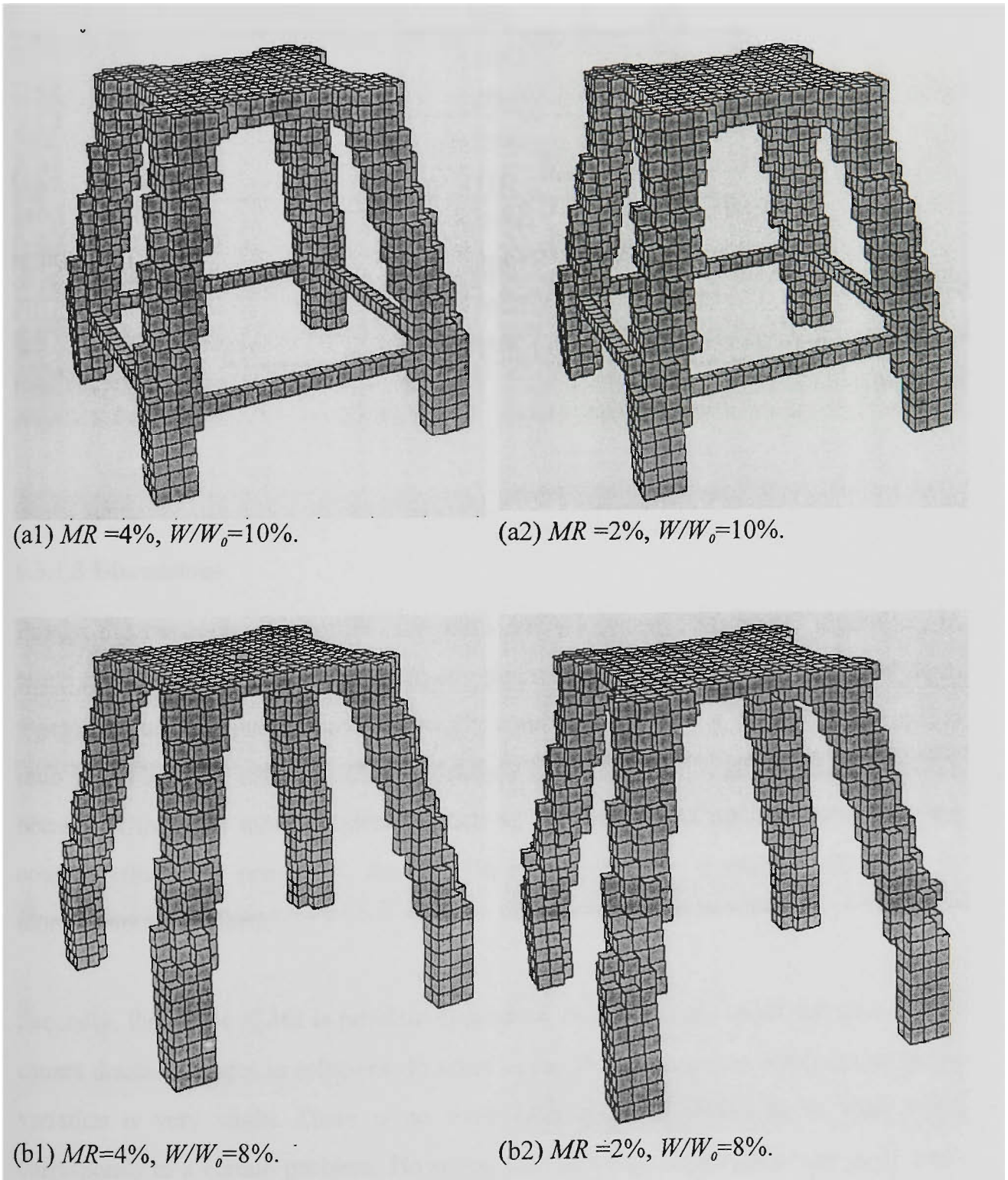


Fig. 6.12. Optimal topologies.

Table 6.3. Comparison of Mean Compliance using Different MR (BESO)

Prescribed Weight W^*/W_0	Mean Compliance C/C_0 (Number of Iterations)	
	$MR=2\%$	$MR=4\%$
40%	1.0197 (49)	1.0212 (30)
30%	1.0353 (80)	1.0361 (46)
20%	1.0732 (127)	1.0760 (70)
10%	1.2184 (288)	1.2160 (164)
8%	1.2939 (336)	1.2930 (184)

6.3.1.3 Discussions

Firstly, the parameter of modification ratio MR affects the ESO/BESO algorithms in terms of structural performance (mean compliances, frequencies or performance index), topologies and computing time. Generally speaking, in ESO, a smaller modification ratio yields a better solution. This correlation is less distinct in BESO, most possibly because it involves more parameters such as stage ratio and addition ratio thus the coupled effect may complicate the case. In both algorithms, a smaller MR results in more computing efforts.

Secondly, the effect of MR is problem dependent. In some cases, small variation in MR causes drastic changes in solutions. In other cases, the difference in solution due to the variation is very slight. There is no fixed rules or clear pattern as to what value corresponds to a certain problem. However, the following observations are made from the experience:

1. If a complicated truss-like topology is expected, a smaller value of MR is recommended. The truss structure has a relatively low fraction of material but a high demand of design resolution. In general, after a structural member (say, a spoke) is formed in a truss, removing it will normally cause big changes in structural performance. Such a qualitative change can easily happen when using a large modification ratio. Though this sharp change can be remedied to some extent by varying the modification ratio, i.e. successively halving the value, precaution should be taken in that any fine change in later stage cannot compensate the premature loss of structural details in the early stage.
2. If the load path is relatively well defined, the modification ratio can be larger. Such is the case of simple space trusses.
3. The design experience can play a role in parameter selection. However, if the situation is difficult to make the judgement, there are the alternative guidelines. If the target weight is a large fraction of the ground structure, say 60% or 50%, a larger modification ratio can be used. And if a small target is the case (<20%), a smaller value is recommended.
4. The recommended range is 1%~4%, and 2% can work well for most, if not all cases.

The modification ratio is a primary parameter affecting the performance of both ESO/BESO. The remainder of this section deals with other parameters involved in BESO only.

6.3.2 Stage Ratio (SR)

Again, let us use the cantilever as example, parameters are set as $MR=2\%$ and $AR=0.25$ and initial design is the one given in Fig. 6.10. Variations on the stage ratio are considered as $SR=60\%$, 50% , 40% and 30% respectively. Results for these four cases are provided in Table 6.4. The advantage of using a larger SR is quite clear. This is simply because that the structure has better developed thus provides a larger design domain before it starts decreasing the weight, as shown in Fig. 6.13. Two cases with $SR=40\%$ and 30% have a much larger value of mean compliance and are considered

unsuitable for this example. Their topologies are also different and clearly indicate a premature design, as shown in Fig. 6.14.

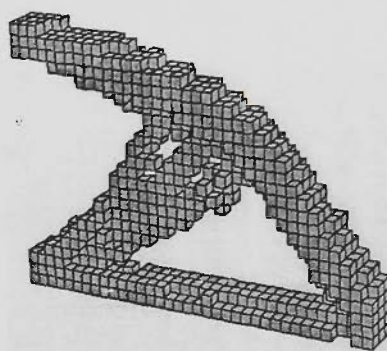
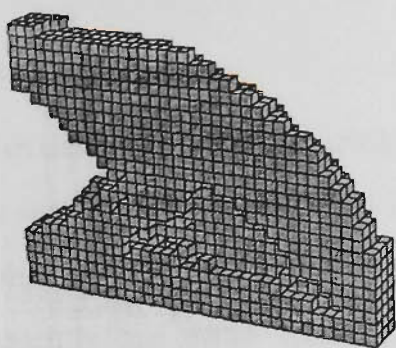
While the other two cases $SR=60\%$ and 50% are feasible parameters, the latter involves fewer iterations. They are the most used values and are recommended for common BESO applications.

Table 6.4. Comparison of Mean Compliance using Different SR

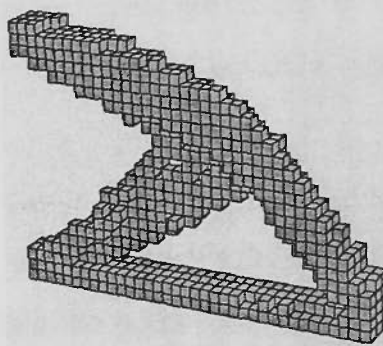
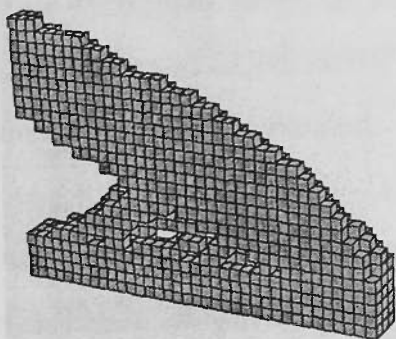
Prescribed Weight W^*/W_0	Mean Compliance C/C_0 (Number of Iterations)			
	$SR=60\%$	$SR=50\%$	$MR=40\%$	$MR=30\%$
Max	1.639	1.4126	2.4042	5.088
50%	1.2514 (65)	1.4126 (33)	-----	-----
40%	1.4275 (89)	1.4525 (57)	2.4042 (22)	-----
30%	1.7782 (123)	1.7556 (92)	1.9476 (55)	5.0881 (17)
20%	2.4075 (168)	2.4078 (136)	2.5744 (102)	3.9394 (56)
15%	3.1204 (207)	3.1218 (175)	3.4485 (150)	4.5003 (91)

It is worth noting that there should be a gap between SR and the target weight fraction, normally 10% or 15%. This is to allow for sufficient iterations and improvement between the structure developing to its maximum and reaching its target. However, if the gap is smaller than 10% or 15%, the usual way is to continue the evolution while keeping the weight constant. Normally, there should be considerable improvement by doing so and the procedure terminates when the improvement become negligible. This is easily realised by just setting $AR=0.5$. It can be certainly applied to cases of any target weight for a possible fine-tuning.

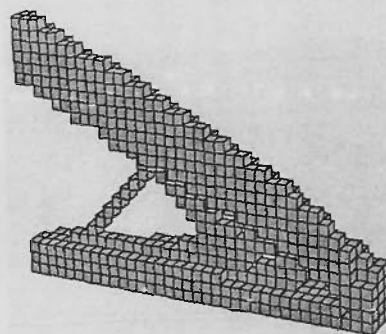
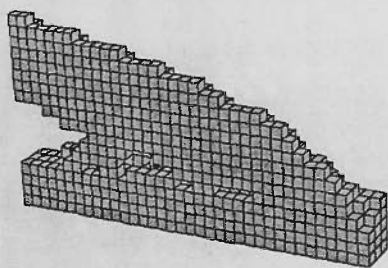
SR=60%:



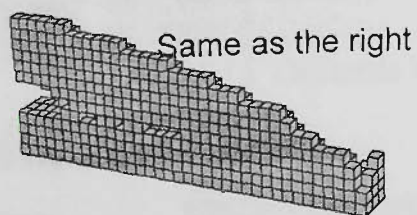
SR=50%:



SR=40%:



SR=30%:



Same as the right

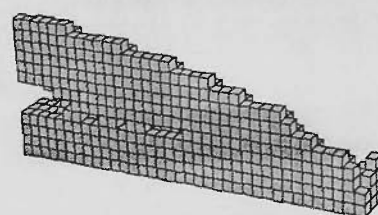


Fig. 6.13. Topology at $W/W_0=SR$.

Fig. 6.14. Optimum topology at $W/W_0=30\%$.

6.3.3 Initial Structure

The simple rules in defining the initial structure can be:

1. Including the necessary supporting and loading conditions to ensure a non-singular structural or rigid body analysis.
2. Being conveniently and easily operated. Based on STRAND6, for example, the initial model (and also ground structure) is defined in its graphic interface. In most cases, a structure of regular shape as rectangle or its combination can be quickly designed using functions as SUBSTRUCTURE or SECTION. If possible, defining a structure element by element is avoided.

Let us look at Example 3.3.1 as a box beam. There can be three definitions of initial design, as shown in Fig. 6.15. All of three accommodate the point load and part of the supporting conditions. The same parameters are applied, with $MR=2\%$, $AR=0.25$ and $SR=0.60$.

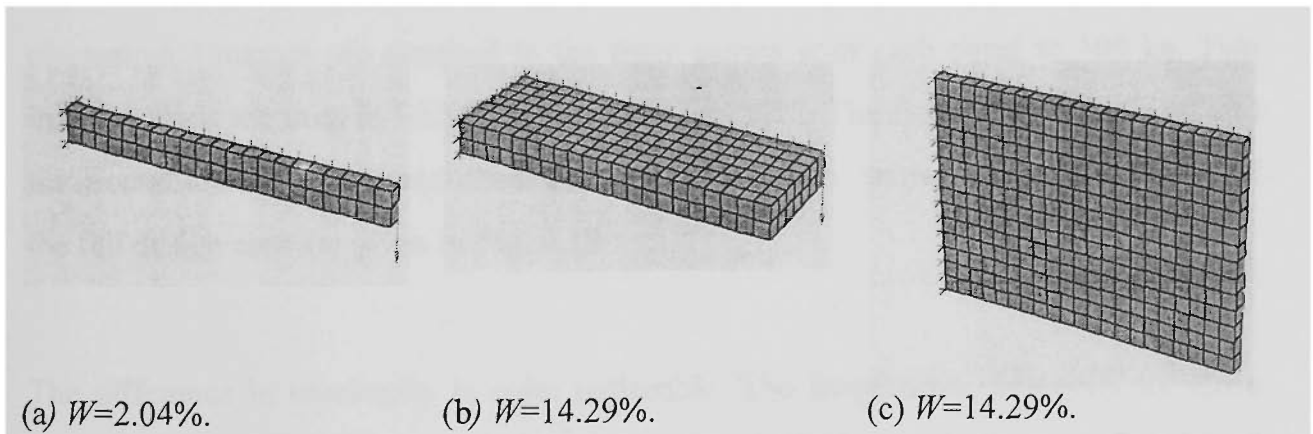


Fig. 6.15. Different initial designs.

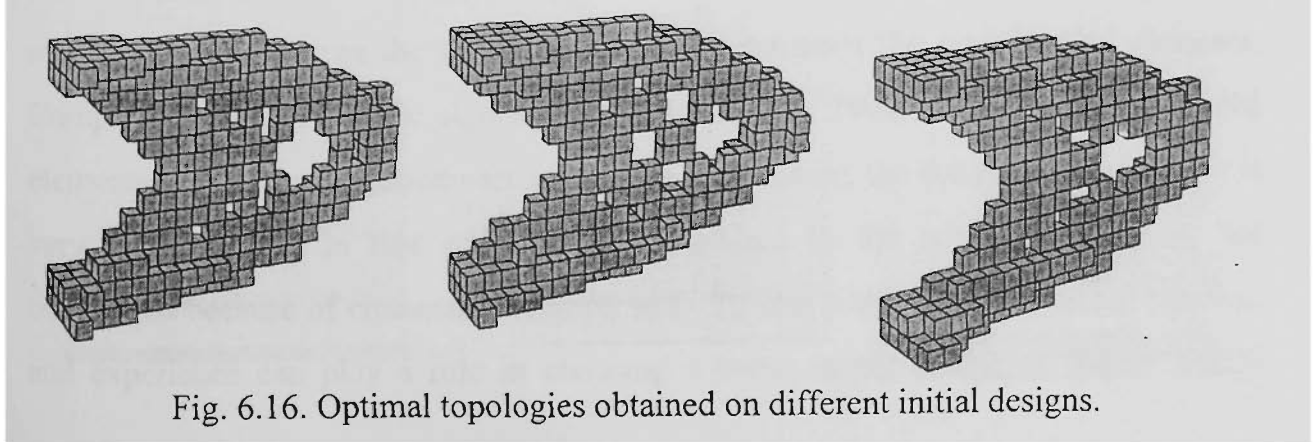


Fig. 6.16. Optimal topologies obtained on different initial designs.

Table 6.5. Comparison of Mean Compliance for Different Initial Designs

Case	W_{ini}/W_0 (%)	Iteration	Mean Compliance C/C_0
A	2.04	172	2.284
B	14.29	161	2.293
C	14.29	162	2.299

The optimal topologies from these initial designs are given in Fig. 6.16. A primary structure as a tapered I beam is distinctly present, and there is only slightly difference in inner details. The values of mean compliance are very close, as shown in Table 6.5. The number of iterations is also comparable.

Let us further study the effect of initial structures on a frequency problem. In Fig. 6.17, a 3-story frame is to be reinforced so as to maximise its first natural frequency. It is modeled by 4-node square elements and covers 14.5% of the full rectangular area. Six concentrated masses are attached to the three stories with each equal to 100 kg. Two initial designs are used in BESO, as shown in Fig. 6.18. The first is the frame itself and the second includes some additional connecting bars. The optima of a weight of 45% of the full design area are given in Fig. 6.19.

The difference in topologies is quite noticeable. The frequencies, however, are close with 30.4 Hz for Fig. 6.19(a) and 30.3 Hz for Fig. 6.19(b). Like in most gradient based methods, there exists the possibility that the search may end up with a local minimum which is close to the initial value. As far as BESO is concerned, the local minimum is more likely to occur as the initial design also determines the set of added elements. Compared to binary genetic algorithms (Chapman *et al.* 1994) where potentially added elements are searched exhaustively in the ground structure, the design space in BESO is very much limited in that only elements attached to the structural boundary are considered because of connection requirements. At this point, the engineering intuition and experience can play a role in choosing a better initial design. A 'better' initial

design may address the most of loading and supporting conditions and has a larger measure of structural boundary/surface. Understandably, a structure with a larger boundary poses a larger design domain where elements can be attached and is more likely to grow effectively.

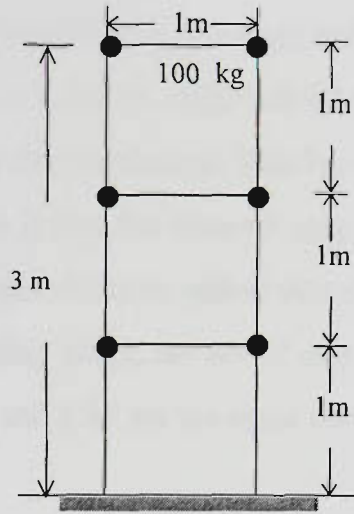
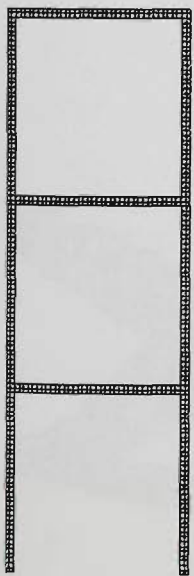
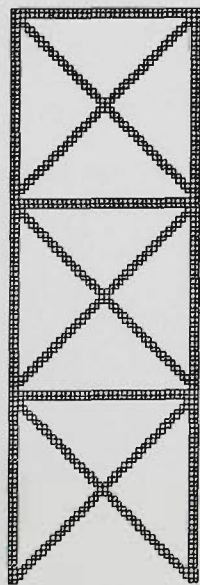


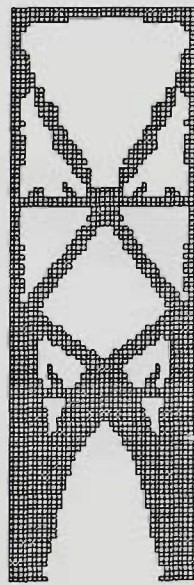
Fig. 6.17. A 3-story frame.



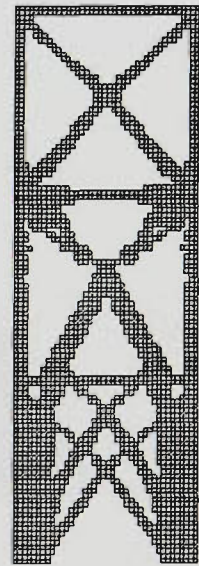
(a)



(b)



(a) $f_1=30.4$ Hz.



(b) $f_1=30.3$ Hz.

Fig. 6.18. Initial designs.

Fig. 6.19. Optimum designs.

6.3.4 Addition Ratio (AR)

This parameter specifies how the modified elements ($MR \times W_{current}$) can be divided between added and removed ones. It can be 1:1 based ($AR=1/2$, ie. 0.5 vs. 0.5), 1:2 ($AR=1/3$, ie. 0.33 vs. 0.67), 1:3 ($AR=1/4$, i.e. 0.25 vs. 0.75). As two extreme cases, $AR=1.0$ means the structure is modified by growing only, and $AR=0$ reduces BESO to ESO. The net change in structure is $|AR-(1-AR)| \times MR = |2AR-1| \times MR$. Clearly, in the range of 0~0.5, a smaller AR means a steeper change. This has the advantage of reach a target weight faster. The disadvantage is that the element may become less 'selective'. In the ascending stage, there are so many elements added that elements of moderate sensitivity may be selected. In the descending stage, the set of element of 'low' stress may be too large. For this reason, $AR=0.25$ and 0.33 are the most used ones.

Still use the cantilever as an example to compare the effects of these two values. $MR=2\%$, $SR=50\%$ and initial design in Fig. 6.10 are used. Table 6.6 summarises the results. As expected, $AR=0.33$ provides a better result than $AR=0.25$ in most cases, and it involves more iterations. Except in dimensions of the diagonal member, no significant difference is presented in optimal designs, as shown in Fig. 6.20.

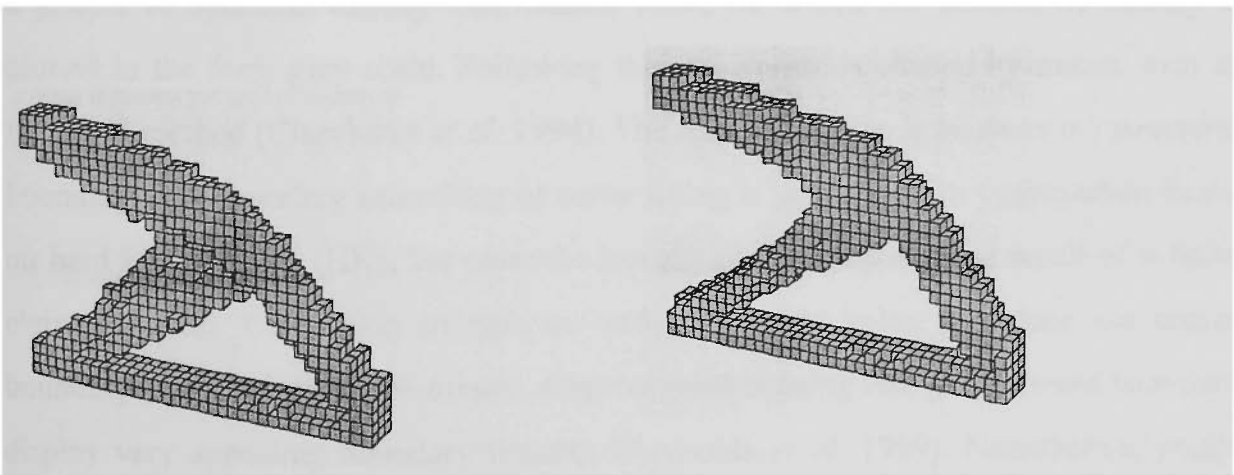


Fig. 6.20. Optimal topologies using different AR , $W/W_0=30\%$.

Table 6.6. Comparison of Mean Compliance using Different AR

Prescribed Weight W^*/W_0	Mean Compliance C/C_0 (Number of Iterations)	
	AR=0.25	AR=0.33
50%	1.4126 (33)	1.2974 (50)
40%	1.4525 (57)	1.4533 (79)
30%	1.7556 (92)	1.7343 (117)
20%	2.4078 (136)	2.3481 (173)
15%	3.1218 (175)	3.0429 (232)

6.4. Design Post-processing

Designs obtained from topology optimisation normally calls for post-processing. In optimisation based on the homogenisation method or SIMP, for example, the solution is a pattern of optimum density distribution, based on which the contour of density is plotted in the form grey scale. Following this, an isoline is chosen by means such as threshold method (Chirehdast *et al.* 1994). The selected isoline is taken as the structural boundary, and boundary smoothing or curve fitting is performed. In optimisation based on hard kill methods (HK), the outcome has zig-zag boundaries as a result of a finite element model. Combining triangle or wedge elements helps to reduce the coarse boundary (Liu *et al.* 1999). Similarly, adaptive meshes using fine grids around boundary display very appealing boundary features (Reynolds *et al.* 1999). Nonetheless, image processing is still necessary, firstly to close the gap between the analysis model and engineering draft, and secondly, to allow for further shape or size optimisation using some alternative methods, such as boundary variation approach.

Post-processing can be incorporated into topology optimisation to form an integral tool kit, such as FIDO (Fully Integrated Design Optimisation) (Hinton *et al.* 1998). It has the functionality of extracting boundary surface using fitting or skeleton thinning techniques. In ESO/BESO, attempts on post-processing are most done by using software packages such as SolidWorks or AutoCAD. The following provide results on 3D images using AutoCAD.

The graphic interface in the FEA package STRAND enables data output in various forms such as ASC, DXF and IGES. The optimal design is firstly output as a DXF file, which is then read by AutoCAD. The compatibility is good between these two packages and the model is automatically regenerated in AutoCAD by simply opening the file. By specifying a few control points, a spline is generated which represents a smooth structure edge. A few edges then form a 3D curved surface by functions such as those for generating ruled surface or Coons surface. This procedure is manually done and it is up to the designer how the final topology can be interpreted and processed. Figs. 6.21~23 give some examples.



Fig. 6.21. Visualisation from AutoCAD, example 4.4.3.2, a vault supporting surface loading.

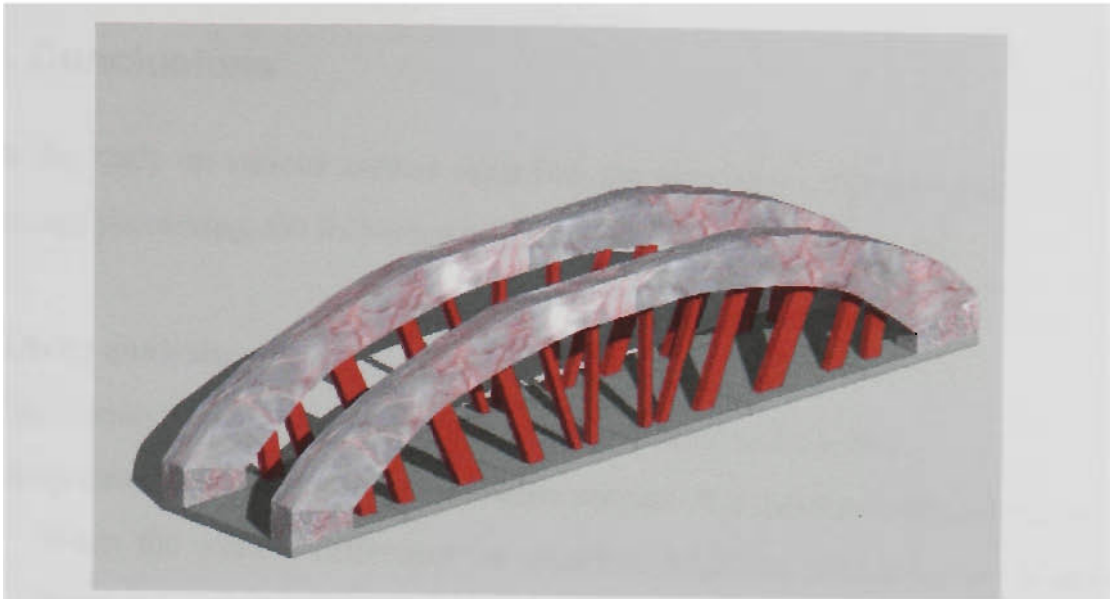


Fig. 6.22. Visualisation from AutoCAD, example 4.3.3.3, a cable bridge, distributing loading on deck.

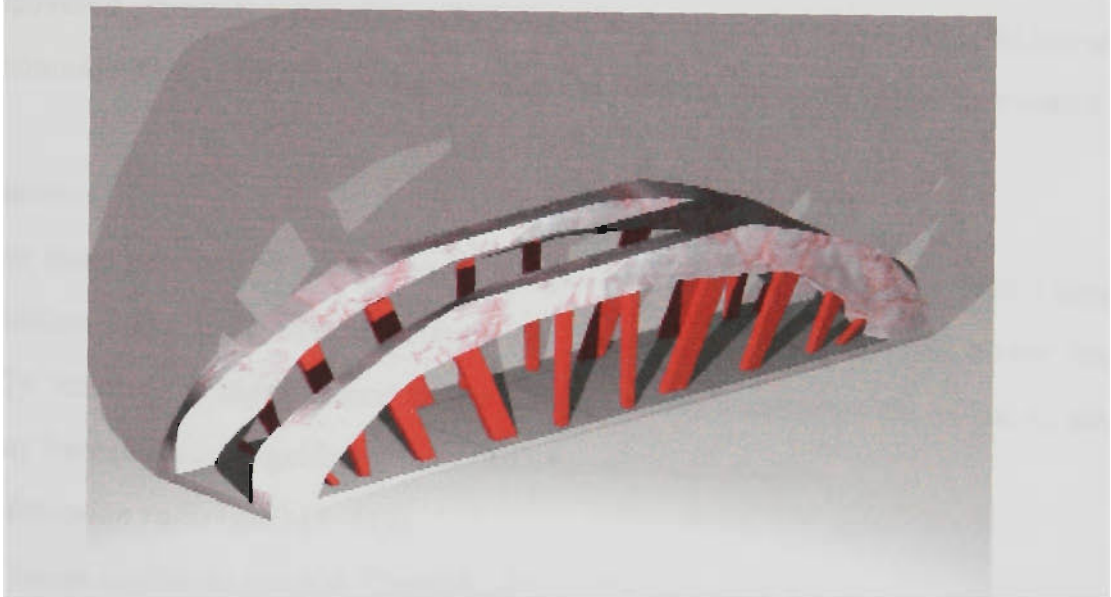


Fig. 6.23. Visualisation from AutoCAD, example 4.3.3.3, a cable bridge, distributing loading on deck plus self-gravity.

6.5. Conclusions

From the study on various aspects regarding the algorithm reliability, parameter effect and image processing, the following remarks and conclusions are made:

Sensitivity analysis:

1. Calculation of element sensitivity is largely accurate and reliable.
2. Sharp changes can occur in the evolution process. It is quantitatively defined as:
 - When the relative difference in objective functions between two consecutive iterations exceeds 5%, and/or
 - When the relative difference in the predicted and actual values of objective function exceeds 2%.
3. Sharp changes are dealt with by a checkup-recovery-freeze-unfreeze procedure. Recovered elements are temporarily frozen for 3 iterations before being unfrozen. If accumulated occurrence of sharp changes exceeds 15, the evolution is terminated.

Parameters:

The four main parameters/factors, namely, modification ratio, stage ratio, initial design and addition ratio have various effects on the optimal solution. The above order generally reflects the significance of the effect, though sometimes the effect of stage ratio may become more significant than that of modification ratio.

1. *Modification ratio (MR)* (1~4%).
 - The range applies in general. Conservatively, 2% can work for most problems with a satisfactory balance between the solution quality and computing cost.
 - A larger value (3~4%) can be used with confidence for structures of clear load path.
 - A smaller value should be applied in cases where: 1) the final design may possess truss features; 2) the solution has a small target weight (<20%). The common practice is to first use 2% as a trial value, if not satisfactory, change to 1%.

2. *Stage ratio (SR)* (50~60%).

It has considerable effect on BESO performance.

- The advised range can be applied in general.
- Again, for problems of possible truss solutions, a larger value 60% is preferred.
- If the gap between the target weight and stage ratio is smaller than 15%, a 'flat' stage is advised when the evolution proceeds while keeping structural weight constant.

3. *Initial structure.*

Using engineering common sense, a favourable initial design:

- Includes information of loading and restraint conditions as much as possible.
- Reflects an effective load path as much as possible.
- Has a large boundary/surface which allows for a large design domain.

In the meantime, it is easy to generate within the finite element model.

Addition ratio (AR) (0.25 or 0.33).

- The advised value can be applied in general.
- A larger value 0.33 is more conservative, and be applicable if the solution is unpredictable or truss solutions are possible.
- For larger finite element problem (e.g. more than 7000 3D elements), a smaller value 0.25 can be used to offset the computing cost.

In summary, cautions are taken when truss-like structures are involved. They normally have a much more complex geometry thus are more susceptible to sharp changes and parameter variations. Consecutive values of all parameters/factors within the given ranges are recommended.

Image Processing:

1. It can be undertaken by any graphic software, providing they are compatible with graphic interface of the FE software. Here we use AutoCAD for its wide engineering application.
2. It is so far done manually. Automatic processing can be explored further.

Perimeter Control for BESO

As a special topic of numerical instability of optimisation algorithms, the mesh dependency is discussed briefly in the last chapter. This chapter addresses this problem in more details and investigates techniques to suppress or reduce the effect of size/shape of finite elements on optimal solutions. Perimeter control technique, as successfully used in SIMP and homogenisation based methods to solve the problem, is incorporated into BESO. A problem statement is first presented and computer algorithms are developed. The technique is then applied to a series of 2D and 3D problems. It is found that bounding the perimeter can be used to control the topology complexity, as a tighter bound normally yields a simpler configuration. Also, for 2D problem, solution converges with respect to the finite element grid. Thus, it is concluded that perimeter control technique improves the numerical stability of the BESO method.

7.1. Introduction

A finite element model has been commonly used topology optimisation. The size or shape of the element usually affects the optimal solution. It is well recognised that the optimal topology varies with the grid discretization in such way that the topology becomes more detailed (often, with more structure members or holes) with mesh refinement. It will eventually end up with a ‘chattering design’ with infinite number of microscopic holes. This may suggest that the optimisation problem should be relaxed from the outset by allowing for microscopic perforated materials. The significance of

relaxation is that it provides a possible lower bound of mean compliance against which some macroscopic design can use as benchmarks. However, unless the composite areas are purposely intended, the solution is hard to appeal to practical manufacturing.

In contrast to the above relaxation, the problem can be restricted to enforce a macroscopic design constraints. Sigmund and Petersson (1998) summarised the restriction as (1) global gradient constraint, (2) local gradient constraint, (3) mesh independent filtering and (4) perimeter control, most of which based on the SIMP approach. The global gradient is defined as the norm of a functional of the design variable density. The local gradient constraint and filter are equivalent to specifying the lower bound of the dimension of a member. For example, it will exclude the formation of very thin bars or spokes. The perimeter is defined as the total variation of the density, which approaches the structural overall perimeter when the design variable is either 1 or 0. The last two restriction techniques have been used most effectively, as the filter technique has addressed the mesh dependency for both 2D and 3D problems (Sigmund 1994; Sigmund *et al.* 1998), so is with the perimeter control method (Haber *et al.* 1996; Fernandes *et al.* 1999). A few variants of the perimeter control technique are proposed recently, such as a dual method (Beckers 1999), a quasi-isotropic perimeter measure (Petersson *et al.* 1999) and a gravity control function (Fujii and Kikuchi 2000). The perimeter control has also been used to exclude or reduce the microscopic perforations and chattering designs in the homogenisation method (Bendsøe 1995).

Adding perimeter control to topology optimisation is simple in concept and easy to implement. A complex or chattering design normally features small and densely distributed holes, isolated elements or structural member of small scale. Those features can be generally reflected in a large measure of structural perimeter. While the measure of perimeter can be very involved in SIMP or homogenisation methods, it can be calculated straightforwardly in ESO/BESO. Therefore, this chapter employs the concept of perimeter control and incorporates it to the ESO/BESO algorithms. The objective is to use the combined algorithm to handle the problems of numerical instability and to realise design complexity control. As for controlling the structural complexity in ESO,

work has been done based on the intelligent cavity creation [ICC] (Kim *et al.* 2000). It is similar to the perimeter control technique but controls the number and scale of structural cavities in an intuitive way. Mesh independency can be expected with the ICC method.

The remainder of this chapter is organised as follows. Sect 7.2 presents the definition and calculation of the perimeter measure in 2D and 3D settings. The concept of characteristic groups is used to distinguish elements according to their contribution to the structural perimeter measure. Sect. 7.3 presents the problem statement of BESO with perimeter bound and proposes the implementation algorithms. Sect. 7.4 applies the proposed methodology to a range of 2D and 3D examples. Each example is studied on different levels of finite element grids as well as with different perimeter bounds. Conclusions are drawn at the end of this chapter.

7.2. Perimeter Measures

7.2.1 Definition

The perimeter is defined as:

- For 2D rectangular elements, the total length of external and internal boundaries.
- For 3D solid elements, the total surface area.

i.e.

$$p_i = \sum_{j=1}^{m_i} l_{ij}, \quad (7.1)$$

where m_i is the number of free edges/surface of element i and l_{ij} is the length/area of its j th free edge/surface. m_i is in a range of 0~4 for 2D rectangular element, and 0-6 for 3D solid element.

At the structural level, the total perimeter measure is

$$P = \sum_{i=1}^n x_i p_i = \sum_{i=1}^n \sum_{j=1}^{m_i} x_i l_{ij}, \quad (7.2)$$

where x_i is the binary design variable.

7.2.2 Characteristic Groups

In a uniform mesh, a quadrilateral element has totally eight neighbour elements, with four attached on edges and four joined at corners, as sketched in Fig. 7.1. Together with the element itself, there are totally $2^8 - 1 = 255$ possibilities of connections (minus 1 because the case of all blank elements are excluded). Though high in number, those cases can be categorised into five groups in terms of perimeter measure p_i , namely, $p_i = 0, 1, 2, 3$ and 4. Selective examples are given in Table 1. For simplicity, the side length l_{ij} is assumed to be equal to 1 in calculating the element perimeter p_i .

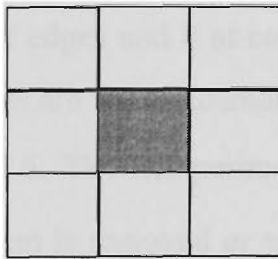
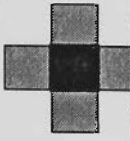
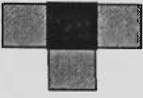
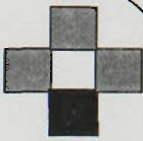


Fig. 7.1. Connection of quadrilateral elements.

If an element of type E4 is removed, for example, a hole is created and the perimeter will increase by 4, i.e. $\Delta p_i = +4$, and if it is added, the open hole is filled and $\Delta p_i = -4$. Thus, from a perimeter control point of view, this type of element is highly undesirable in the case of element removal but strongly preferred for element addition. Element type E2, for another example, can be removed or added without affecting the local perimeter. Similarly, the other three types of element have their own effects.

Table 7.1. Perimeters of All Types of Element ($l_{ij} = 1$)

Group (p_i)	0	1	2	3	4
Examples	 E4	N^+  E3	 E2	N^-  E1	 E0
$4 - p_i$	4	3	2	1	0
Δp_i (if removed)	+4	+2	+0	-2	-4
Δp_i (if added)	-4	-2	0	+2	+4

All the above can be readily extended to 3D brick elements. Such an element has 26 neighbours, with 6 at faces, 12 at edges and 8 at corners. As for the $2^{27} - 1$ connection possibilities, the connection details are not concerned but there are 7 group of perimeter measures, i.e. $p_i = 0, 1, 2, 3, 4, 5$ and 6. The net perimeter change Δp_i for each group is calculated by assuming the element is removed or added. If $\Delta p_i < 0$ they are desired for the modification, and vice versa.

To put in a concise form, we define,

$$N_0 = \{1, 2, \dots, n\}, \quad (7.3a)$$

$$N^+ = \{e \mid \Delta p_e \leq 0, e_{\text{added}} \in N_0\}, \quad (7.3b)$$

$$N^- = \{e \mid \Delta p_e \leq 0, e_{\text{removed}} \in N_0\}, \quad (7.3c)$$

where N_0 is the set of all structural elements. N^+ is the subset of N_0 for which element *addition* will not increase the local perimeter. N^- is the subset of N_0 for which element *removal* will not increase the perimeter. For example, N^+ can include of element types E4, E3 and E2, while N_2^- consists of element types of E2, E1 and E0, as shown in the two ringed areas in Table 7.1.

7.3. Evolutionary Methodology with Perimeter Control

7.3.1 Problem Statement

For optimisation bound on the perimeter measure, an extra constraint is enforced:

$$\text{Minimise or Maximise } f . \quad (7.4a)$$

$$\text{Subject to } g = W^* - \sum_{i=1}^n W_i x_i = 0, \quad (7.4b)$$

$$x_i \in \{0,1\} , \quad (7.4c)$$

$$P = \sum_{i=1}^n \sum_{j=1}^{m_i} x_i l_{ij} \leq P^* . \quad (7.4d)$$

The objective function can vary with the design problems, which can be stiffness problem stated as Eq. (3.5), and frequency problems in Eq. (5.2) or (5.3), or any of their variations presented in the previous chapters.

7.3.2 Implementation

The procedure is similar to the basic BESO:

1. Define the initial structure in the given design domain.
2. Conduct FE analysis.
3. Calculate the sensitivity number and the *overall structural perimeter*.

4. Judge if the perimeter constraint is activated, if yes, restrict the set of elements suitable for modification to N^+ and N^- . Otherwise, all elements are available for modification.
5. Modify elements in the appropriate sets.
6. Repeat Steps 2 to 5 until both the prescribed weight and perimeter requirements are satisfied.

Fig. 7.2 gives the flowchart.

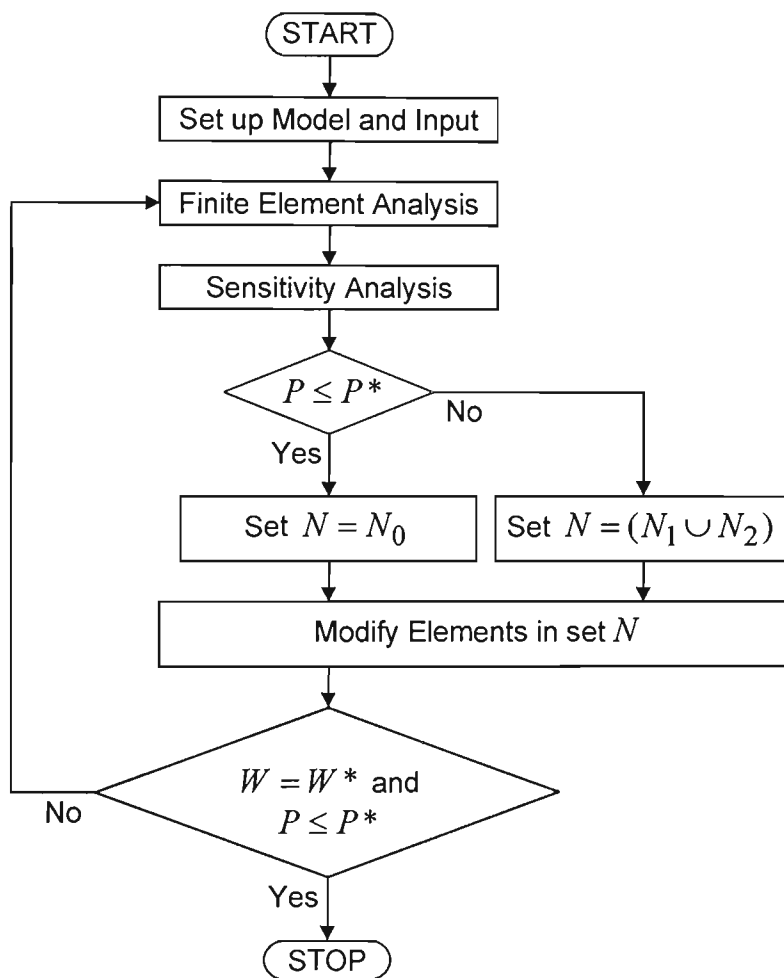


Fig. 7.2. BESO with perimeter control.

To explain some steps in more detail:

- In Step 3, there is a small loop to calculate the perimeter.
 1. In the whole structure, node by node, read into connection information, an array NODECNCT (dimension of 4 or 8) records the elements sharing the node, with absent element recorded as 0.
 2. Take a 2D 4-node element for example. In each element, from NODECNCT for all of its four nodes, if two neighbouring nodes share elements other than the element itself, the edge between these two nodes is attached and not free. The total number of free edges for this element is calculated.

This procedure obviously has a high demand of storage. The array NODECNCT alone needs a space of the total number of nodes multiplied by 4, or by 8. For 3D problems, this sometimes causes insufficient memory problem. An alternative way is thus proposed as follows:

1. Define a regular rectangular block, divide it with a uniform mesh, and number the elements increasingly and consecutively. As sketched in Fig. 7.3, the mesh is numbered element by element in x direction, line by line in y direction, and layer by layer in z direction. The total numbers of elements in the three directions are recorded as MESHX, MESHY and MESHZ, respectively.
2. In the whole structure, element by element, store its property (1 or 0) in array ELEPRP.
3. Element by element, decide the location of each element (say, Lx , Ly and Lz), then decide its neighbours at six faces. Take the element at the top face for example, it has the location coordinators of Lx , Ly and $Lz+1$, from which the number of this element is uniquely decided as NUMELE. Check its status according to ELEPRP(NUMELE). If it is present (1), the top face is bounded; if it is absent (0), the face is free.

It is noted that the above strategy does not mean that the design domain has to be regular. In fact, any variations like holes, cut-out can be represented by simply setting elements in the region a zero property number which means they do not physically exist. And also, it is specified that elements are not to be added in this region.

There are some special cases in perimeter calculation. A most encountered one is using a half or quarter model due to structural symmetry. Faces and edges on the line/plane of symmetry though appearing free, are actually attached with elements.

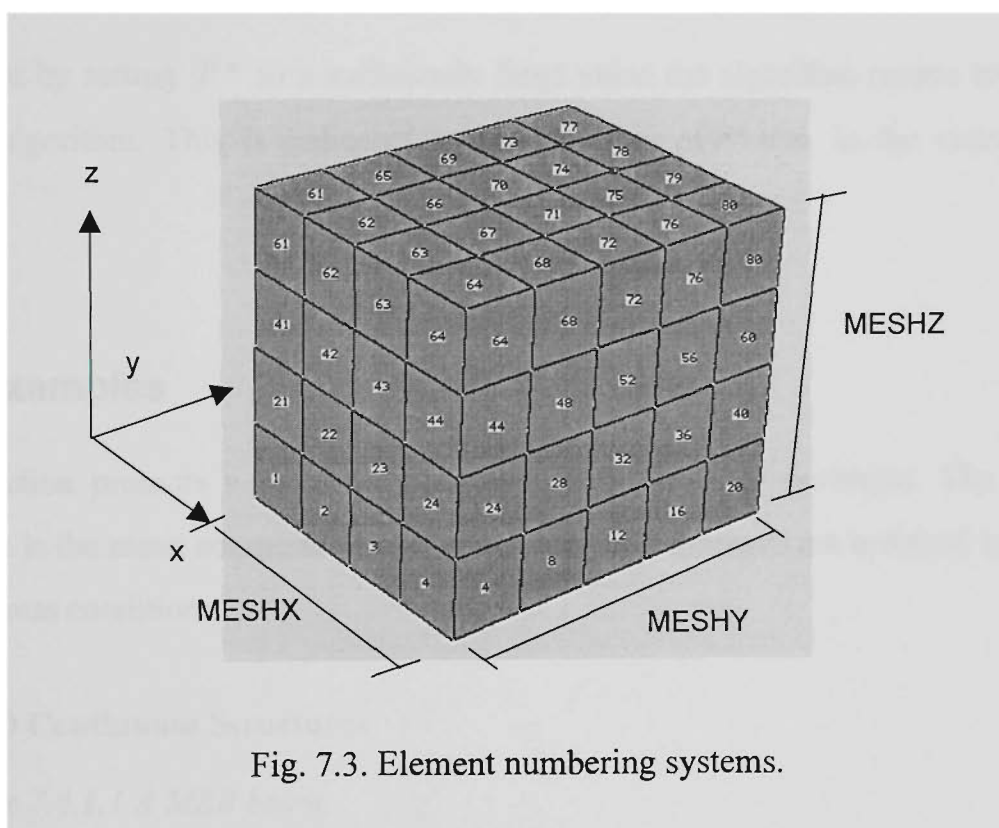


Fig. 7.3. Element numbering systems.

- As for Step 4 judging the perimeter conditions.

This is only carried out in the descending stage of evolution process, i.e. after the structure has grown to the maximum design. The perimeter constraint as a non-structural consideration is regarded as at the second level and subordinate to the mechanical constraint throughout the evolution. Ascending stage sees significant growth in structure. Including the perimeter constraint at this stage may affect or prevent the structure being fully developed.

- As for Step 5 element modification.

Removing or adding one element will change the perimeter of its neighbouring elements. Therefore, the arrays NODECNCT and ELEPRP are updated at each modification.

- As for Step 6 termination conditions.

The target weight can be reached explicitly but perimeter limit is approximated more arbitrarily. In the case where an inappropriate perimeter is specified, there may be not an optimum solution.

Note that by setting P^* to a sufficiently large value the algorithm reverts to the basic BESO algorithm. This is indicated by the notation of $P^* = \infty$ in the examples that follow.

7.4. Examples

This section presents a range of examples of 2D and 3D problems. The objective function is the mean compliance or displacement. 2D elements are assumed to be under plane stress condition.

7.4.1 2D Continuum Structures

Example 7.4.1.1 A MBB beam.

As shown in Fig. 7.4. The beam is simply and roll supported at its ends. A downward point load $F = 5.12 \times 10^6$ kN is applied at the mid-span of the upper frame. The beam's dimensions are $10L \times 2L \times 0.05L$ ($L = 0.2$ m). The outer frame, which is used as the initial design, must be retained during optimisation. The space within the frame is to be optimised so that the displacement at point A is less than $0.07L$ ($u^* = 14$ mm). The following material properties are assumed: Young's modulus $E = 70$ GPa, Poisson's ratio $\nu = 0.25$ and density $\rho = 2800$ kg/m³. The material, geometric and loading conditions are the same as those given by Haber *et al.* (1996).

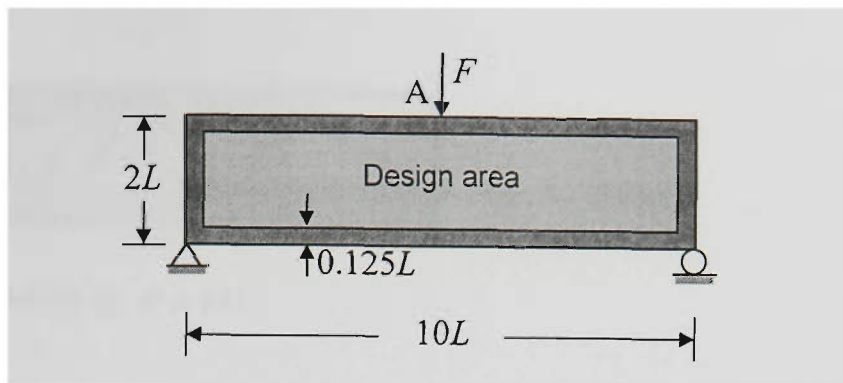


Fig. 7.4. A MBB beam.

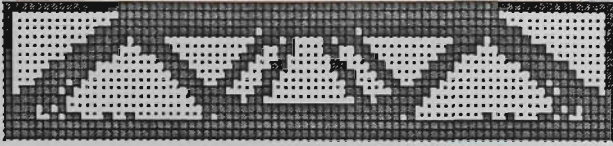
Three meshes are used:

- (A) $0.125L \times 0.125L$,
- (B) $0.125L \times 0.0625L$,
- (C) $0.0625L \times 0.0625L$.

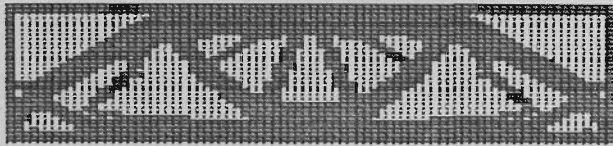
Four perimeter limits are considered:

- (0) $P^* = \infty$,
- (1) $P^* = 81L$,
- (2) $P^* = 72L$,
- (3) $P^* = 68L$.

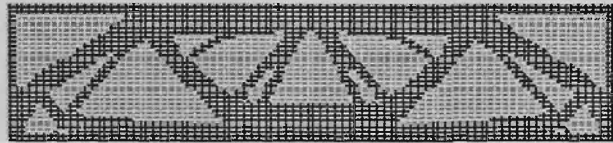
The optimised topologies found are shown in Figs. 7.5 to 7.8. Without perimeter control higher grid refinements generate more complicated designs, as shown in Fig. 7.5(c) where the topology has the largest perimeter of around $90L$. In Figs. 7.6 to 7.8, the topologies generally become simpler than their counterparts in Fig. 7.5. Topologies using different meshes in cases 2 and 3 (Figs. 7.7 and 7.8) are similar in terms of the number of holes and spokes. Thus perimeter control works effectively in these cases to achieve mesh independent solutions. Mesh dependency is still observed in case 1 (Fig. 7.5). This can be due to the relatively large perimeter bound. It is noted that there exist local minima satisfying the structural and perimeter constraints and the possibility to obtain a local minimum may be higher in the case of a loosened perimeter constraint (Haber *et al.* 1996). For the cases examined in this chapter, it is observed that, if a restrictive perimeter constraint is imposed and the same parameter values are used, all meshes normally converge to the same solution.



(a) Mesh A: $P = 81L$.

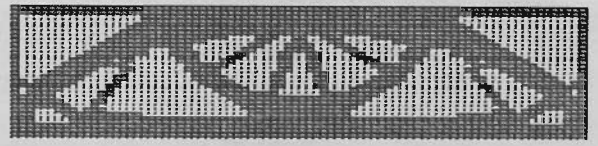


(b) Mesh B: $P = 85.5L$.

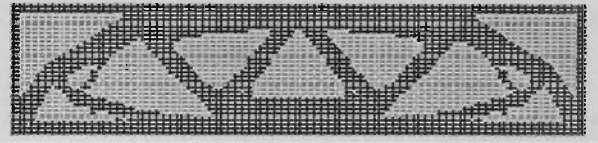


(c) Mesh C: $P = 89.875L$.

Fig. 7.5. Topologies for MBB beam:
case 0, $P^* = \infty$.

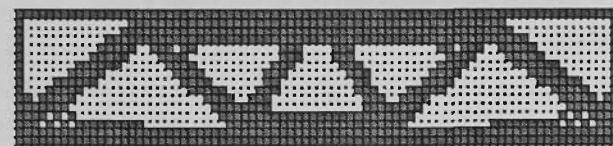


(a) Mesh B: $P = 81L$.

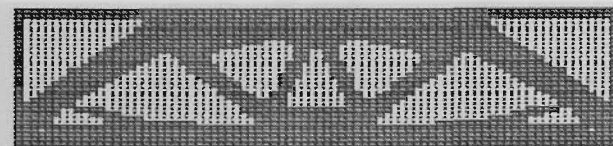


(b) Mesh C: $P = 80.875L$.

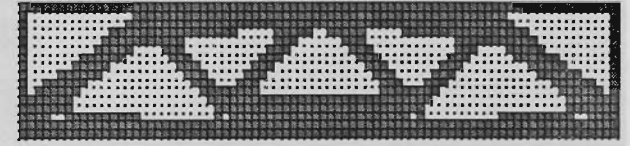
Fig. 7.6. Topologies for MBB beam:
case 1, $P^* = 81L$.



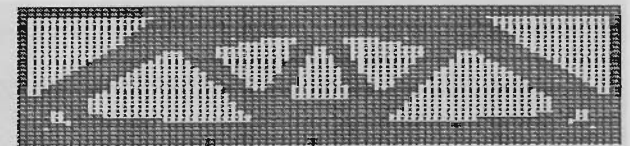
(a) Mesh A: $P = 72L$.



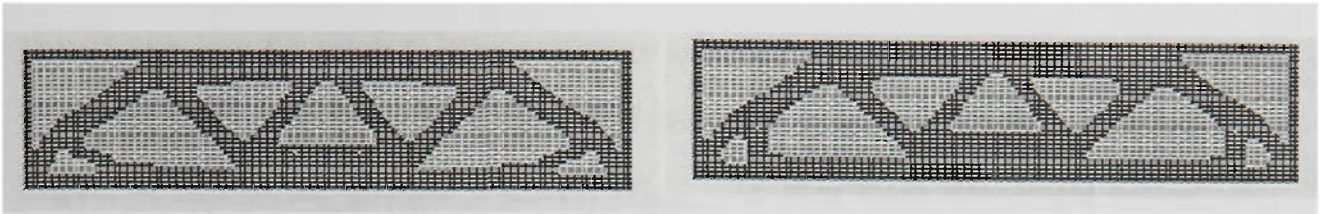
(b) Mesh B: $P = 72L$.



(a) Mesh A: $P = 68L$.



(b) Mesh B: $P = 68L$.



(c) Mesh C: $P = 71.875L$.

(c) Mesh C: $P = 68.125L$.

Fig. 7.7. Topologies for MBB beam:
case 2, $P^* = 72L$.

Fig. 7.8. Topologies for MBB beam:
case 3, $P^* = 68L$.

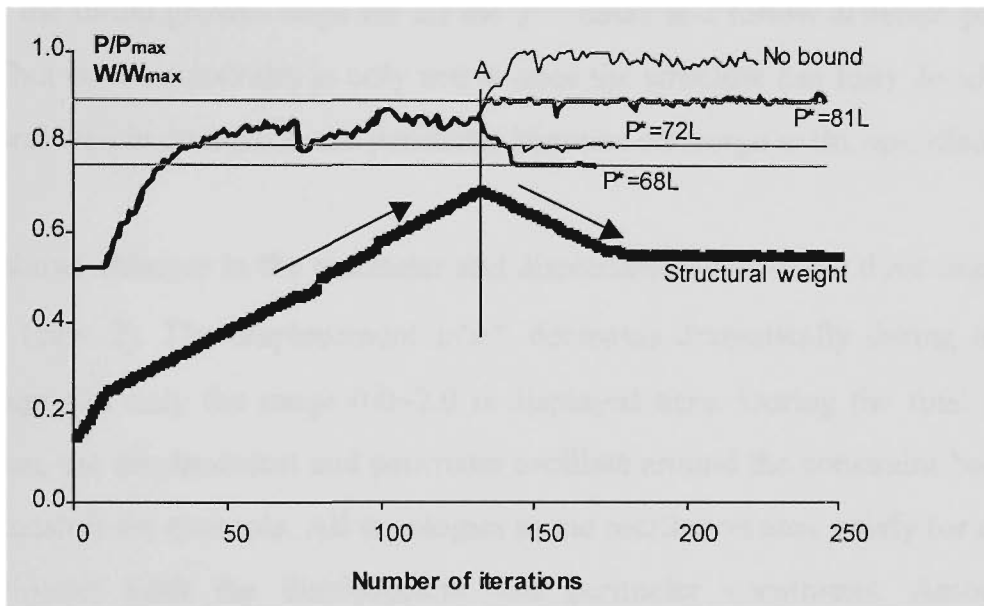


Fig. 7.9. Evolutionary histories of perimeter and structural weight (mesh C).

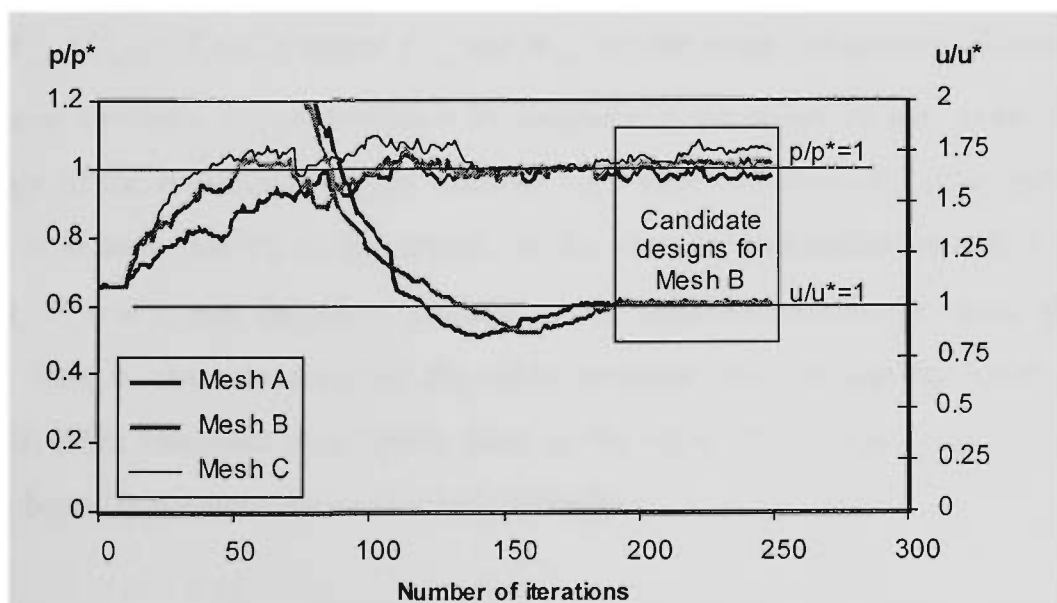


Fig. 7.10. Evolutionary histories of perimeter and displacement (case 2: $P^* = 72L$).

Fig. 7.9 displays the variation of the perimeter (for all four cases) and weight (for case 1) with iteration for mesh C. The perimeter is scaled with respect to P_{\max} , the largest value that occurs during the optimisation of case 0 (no bound); the weight is scaled with respect to that of the ground structure, W_{\max} . As seen from the weight history, by initially using an addition ratio $AR > 0.5$, the structure keeps growing and changes to decrease at point A. As discussed in chapter 3, this turning is decided when the performance index PI reaches a maximum. It is seen that the perimeter histories are the same over the initial growth stage for all the P^* cases and follow different paths from point A. That is, the constraint is only active once the structure has fully developed. As the structural weight decreases, the perimeter histories converge to the specified bounds.

Fig. 7.10 shows changes in the perimeter and displacement for all the three meshes with $P^* = 72L$ (case 2). The displacement u/u^* decreases dramatically during the initial growth stage and only the range 0.0~2.0 is displayed here. During the final stages of optimisation, the displacement and perimeter oscillate around the constraint boundaries. Consider mesh B for example. All topologies in the oscillation area satisfy (or only very slightly violate) both the displacement and perimeter constraints. Among these candidate designs, the one with the largest PI is taken as the final solution.

Table 7.2 lists values of PI for all cases. It is noted that PI is calculated from Eq. (3.23), i.e. $PI = (W_{ref} \times C_{ref}) / (W_i \times C_i)$ where C_{ref} and W_{ref} are the mean compliance and weight of a reference topology. For convenience in comparison, the reference here is taken as the topology of the prescribed weight obtained on a case of unbounded perimeter. In Table 7.2, it is seen that PI is the largest for the case of unbounded perimeter (i.e. $PI=1.0$ for $P^* = \infty$), and decreases slightly as the perimeter bound becomes more restrictive. This is also observed for the other methods that use similar techniques (Haber *et al.* 1996; Fenandes *et al.* 1999). Also, as the structural perimeter takes discrete values, the bound is not necessarily reached precisely.

To further compare the above results with those obtained from alternative methods based on SIMP (Habel *et al.* 1996), it is noted that direct numerical comparison is not feasible. First of all, the volume fraction (or density) is taken as the design variable which is continuous to model a full phases of material as solid. This does not allow a straightforward measure of perimeter as presented in Sect. 7.2, but resorts to some other approximated techniques. In the literature, the perimeter is defined as an integral function of volume fraction, which will reverts to direct perimeter measure only when porous material is not present. Secondly, different models (continuous vs. discrete) also generate variations in the calculation of structure response such as mean compliance. For these reasons, only qualitative comparison is carried out. It is found that the forgoing observations have been confirmed in the literature. Also, topologies in Fig. 7.8 with the lowest perimeter control agree well the reference.

Table 7.2. Perimeter & Performance Index for Different Cases

	Mesh A		Mesh B		Mesh C	
	P ($\times L$)	PI	P ($\times L$)	PI	P ($\times L$)	PI
$P^* = \infty$	81.0	1.0	85.5	1.0	89.875	1.0
$P^* = 81L$	---	---	81.0	0.9925	80.875	0.9996
$P^* = 72L$	72.0	0.9992	72.0	0.9843	71.875	0.9833
$P^* = 68L$	68.0	0.9968	68.0	0.9820	68.125	0.9608

Example 7.4.1.2 Michell type structure

Fig. 7.11 shows an initial design for a simply supported beam. It is allowed to grow upwards, with the upper boundary of the design domain being unlimited. The thickness $t = 4L$ ($L = 0.2$ m), and the same material properties as used in Example 7.4.1.1 are assumed. The objective is to minimise the mean compliance under mid-span loading of a structure with a given weight ($W^* = 14.6$ kg).

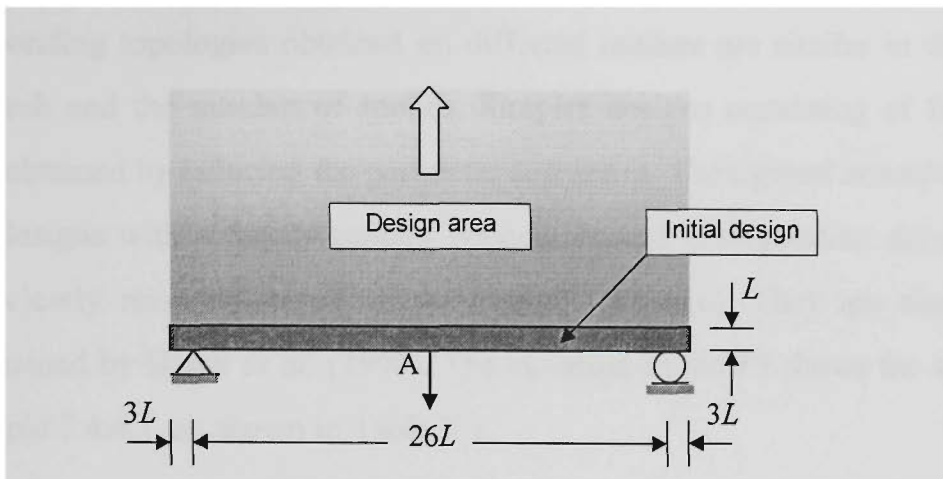


Fig. 7.11. A Michell type structure.

This example has been a classic topology problem and been extensively benchmarked. Based on a microstructure problem, the density grey-scales show heavy density in a shape of half circle in the outer and relatively light design in the radial direction. It can be interpreted as a bicycle wheel with a rigid rim and tension steel spokes. This pattern of design is also quite clear in ESO results (Xie and Steven 1997). It is further studied by BESO with perimeter control as follows.

Three meshes are used:

- (A) $L \times L$,
- (B) $0.5L \times 0.5L$,
- (C) $0.33L \times 0.33L$.

Four perimeter limits are considered:

- (0) $P^* = \infty$,
- (1) $P^* = 214L$,
- (2) $P^* = 192L$,
- (3) $P^* = 160L$.

The optimal topologies found are shown in Figs. 7.12 to 7.15, in which characteristic Michell-type structures are revealed (Michell 1904). The coarse mesh (A) seems unable to adequately resolve the structural configuration. For each perimeter bound (cases 1~3),

the corresponding topologies obtained on different meshes are similar in the shape of the outer arch and the number of spokes. Simpler designs consisting of fewer larger spokes are obtained by reducing the perimeter constraint. The tightest constraint (case 3) results in designs with a highly refined boundaries and configuration details such as fillets are clearly revealed, as shown in Figs. 7.15(b)&(c). They are similar to the designs obtained by Haber *et al.* (1996). The variation in the PI shows the same trends as in Example 7.4.4.1, as shown in Table 7.3.

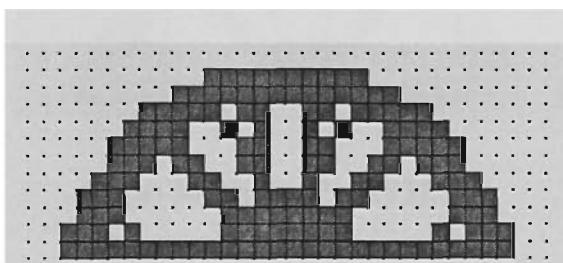
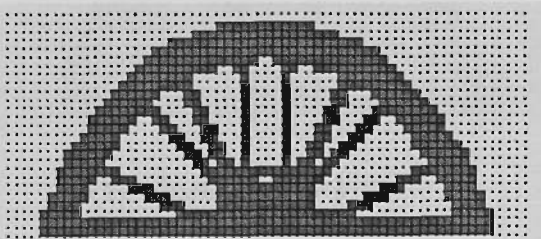
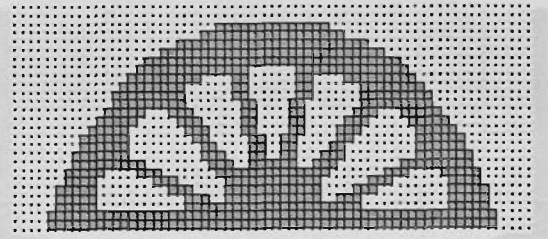
(a) Mesh A: $P = 196L$.(b) Mesh B: $P = 255L$.(c) Mesh C: $P = 262.0L$.(a) Mesh B: $P = 213L$.(b) Mesh C: $P = 210L$.

Fig. 7.12. Topologies for the Michell-type structure: case 0, $P^* = \infty$.

Fig. 7.13. Topologies for the Michell-type structure: case 1, $P^* = 214L$.

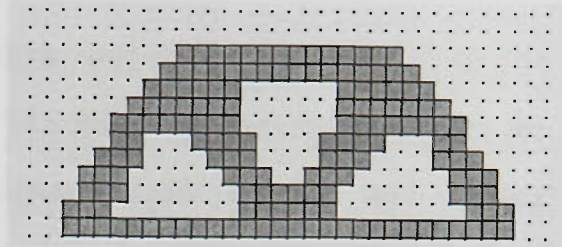
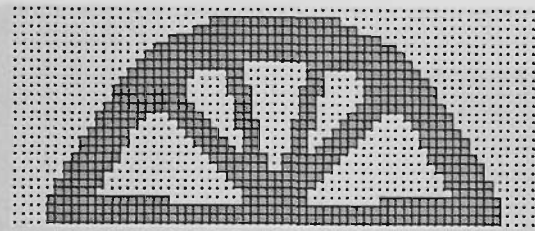
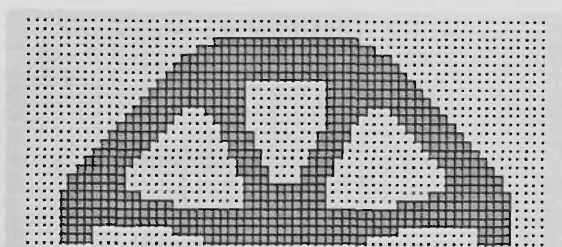
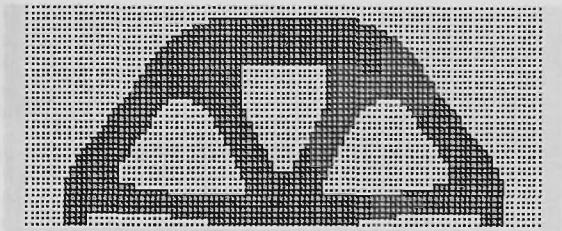
(a) Mesh A: $P = 154L$.(a) Mesh B: $P = 193L$.(b) Mesh B: $P = 160L$.(b) Mesh C: $P = 191.3L$.(c) Mesh C: $P = 159.3L$.Fig. 7.14. Topologies for the Michell-type structure: case 2, $P^* = 192L$.Fig. 7.15. Topologies for the Michell-type structure: case 3, $P^* = 160L$.

Table 7.3. Perimeter & Performance Index for Different Cases (Example 7.4.1.2)

	Mesh A		Mesh B		Mesh C	
	$P (\times L)$	PI	$P (\times L)$	PI	$P (\times L)$	PI
$P^* = \infty$	(196.0)	1.0	255.0	1.0	262.0	1.0
$P^* = 214L$	---	---	213.0	0.9926	210.0	0.9909
$P^* = 192L$	---	---	193.0	0.9909	191.3	0.9829
$P^* = 160L$	154.0	0.9846	160.0	0.9803	159.3	0.9649

Example 7.4.1.3 A shear wall.

The design domain and the initial design of the shear wall are shown in Fig. 7.16. The wall dimensions are $120L \times 60L \times L$ ($L = 0.05\text{ m}$). The following material properties are assumed: Young's modulus $E = 20\text{ GPa}$, Poisson's ratio $\nu = 0.2$ and density $\rho = 2300\text{ kg/m}^3$. The weight constraint is 45% of the maximum possible (obtained when the entire design domain is filled).

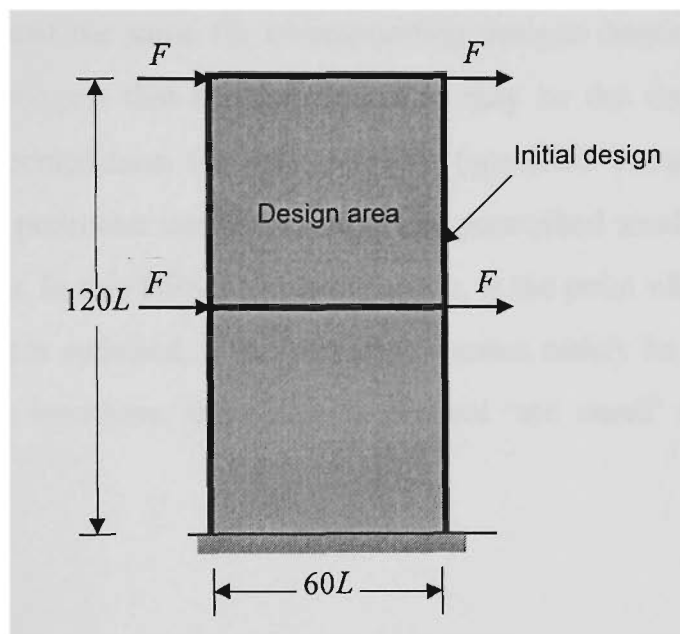


Fig. 7.16. A shear wall.

Three meshes are used:

- (A) $2.5L \times 2.5L$,
- (B) $1.67L \times 1.67L$,
- (C) $1.25L \times 1.25L$.

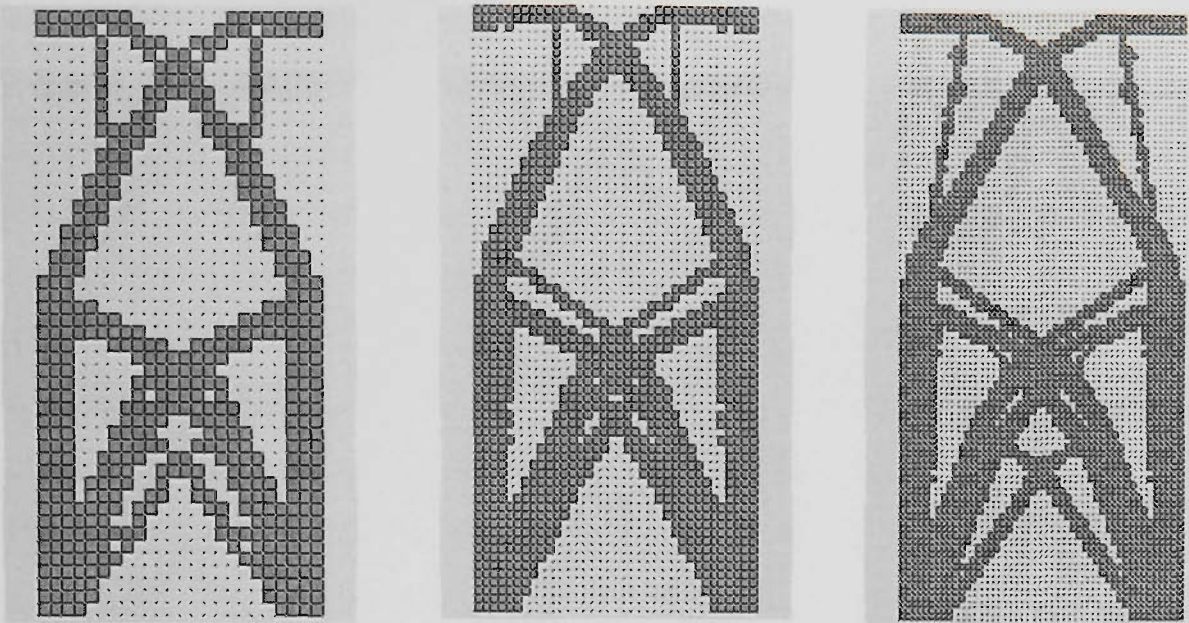
Five perimeter limits are considered:

- (0) $P^* = \infty$,
- (1) $P^* = 1200L$,
- (2) $P^* = 1120L$,
- (3) $P^* = 1050L$,
- (4) $P^* = 970L$.

The solutions found are shown in Figs. 7.17 to 7.21. The variation in the PI shows the same trends as observed for the last two examples, as shown in Table 7.4. Similar solutions are obtained on three meshes for cases 2, 3 and 4. For case 1 the solutions differ somewhat due to the relatively relaxed perimeter constraint, as also observed in Example 7.4.1. By strengthening the perimeter constraint, first, the similarity in topologies on different meshes increases. Second, the topologies become simpler with the elimination or merger of structural members. However, qualitative differences are not observed between the solutions for cases 3 and 4 (Figs. 7.20&21). The inner configuration is almost the same for corresponding designs despite different perimeter bounds. This may suggest that this configuration may be the simplest topology with satisfactory mean compliance for this problem (specified structural weight). Also, understandably, the perimeter constraint cannot be prescribed smaller without changing the weight constraint. In this BESO implementation, at the point where the displacement or weight constraint is satisfied, if the perimeter cannot satisfy its constraint value for, say, 10 consecutive iterations, this value is deemed 'too small' and the process will terminate.

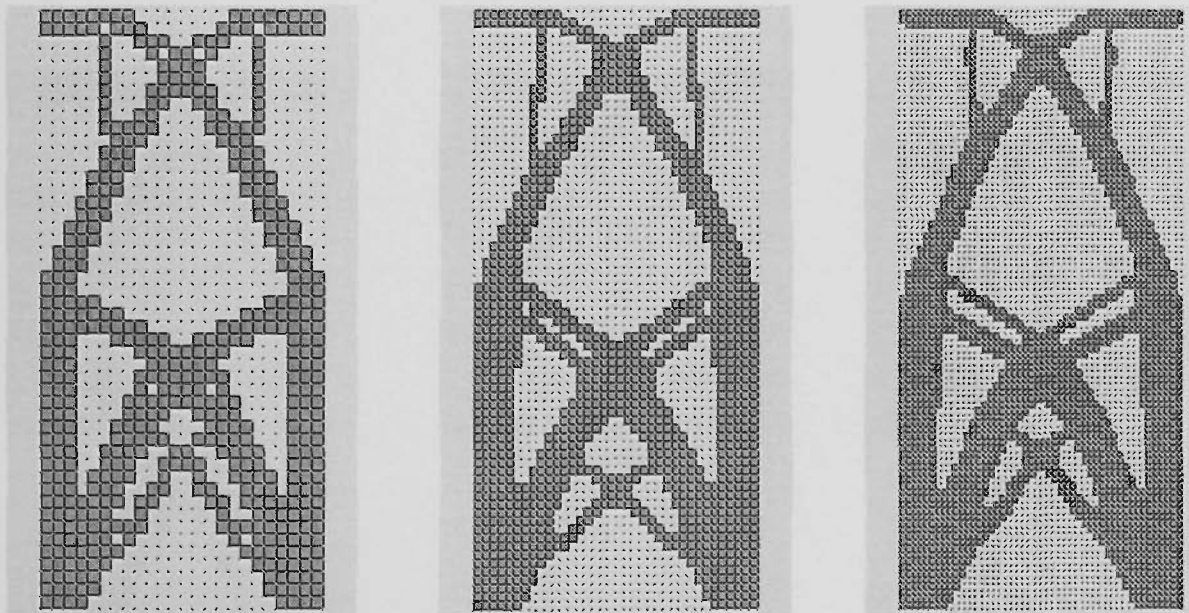
**Table 7.4. Perimeter & Performance Index for Different Cases
(Example 7.4.1.3)**

	Mesh A		Mesh B		Mesh C	
	P ($\times L$)	PI ($\times 10^6$)	P ($\times L$)	PI	P ($\times L$)	PI
$P^* = \infty$	1200	1.0	1212.84	1.0	1297.5	1.0
$P^* = 1200L$	---	---	1202.84	0.9858	1200	0.9860
$P^* = 1120L$	1100	0.9922	1112.86	0.9666	1125	0.9857
$P^* = 1050L$	1035	0.9861	1046.24	0.9644	1050	0.9741
$P^* = 970L$	965	0.9703	972.94	0.9619	972.5	0.9723



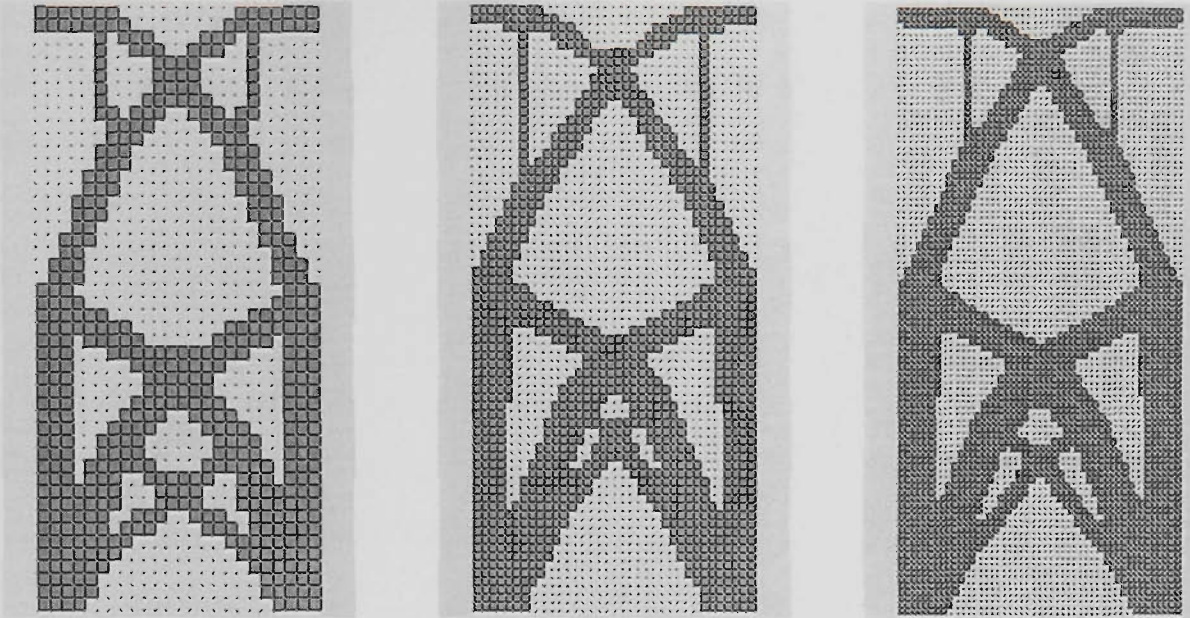
(a) Mesh A, $P = 1200L$. (b) Mesh B, $P = 1212.84L$. (c) Mesh C, $P = 1297.5L$.

Fig. 7.17. Topologies for the shear wall: case 0, $P^* = \infty$.



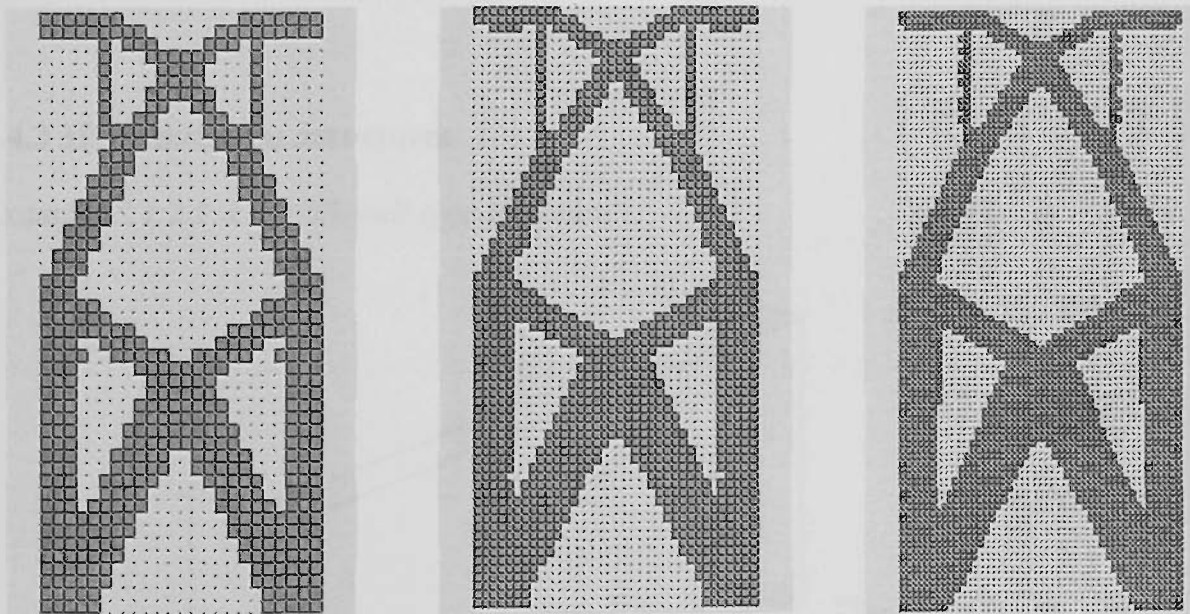
(a) Mesh A, $P = 1200L$. (b) Mesh B, $P = 1202.84L$. (c) Mesh C, $P = 1200L$.

Fig. 7.18. Topologies for the shear wall: case 1, $P^* = 1200L$.



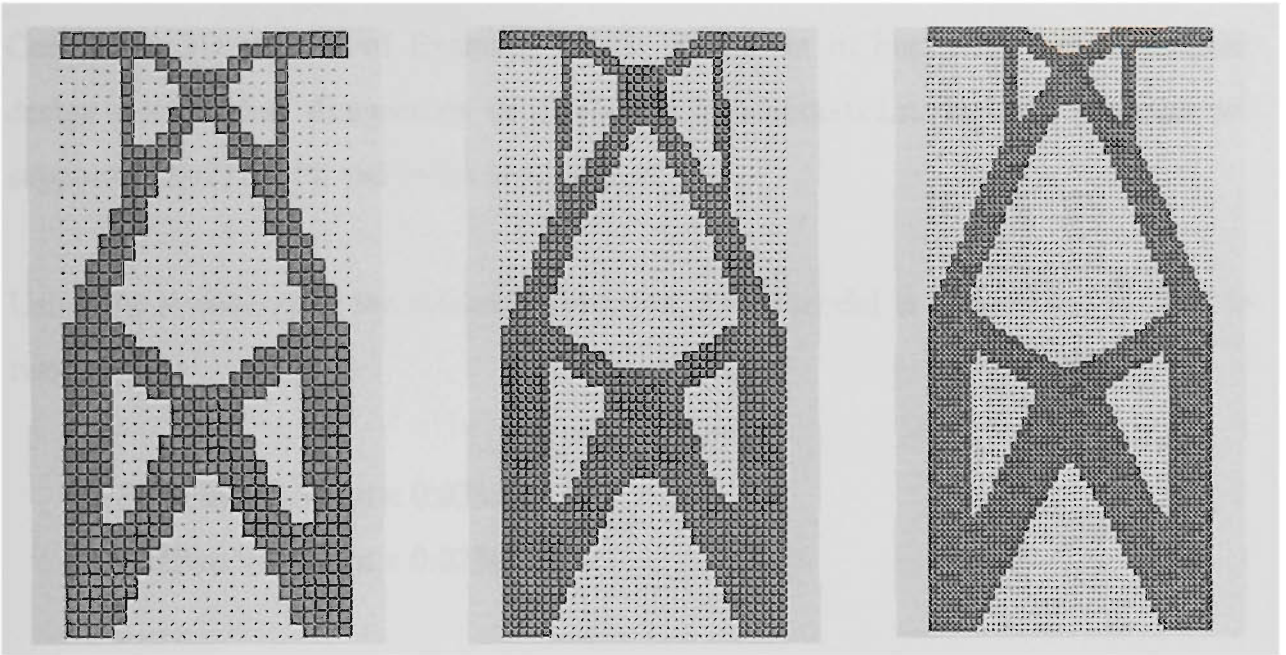
(a) Mesh A, $P = 1100L$. (b) Mesh B, $P = 1112.86L$. (c) Mesh C, $P = 1125L$.

Fig. 7.19. Topologies for the shear wall: case 2, $P^* = 1120L$.



(a) Mesh A, $P = 1035L$. (b) Mesh B, $P = 1046.24L$. (c) Mesh C, $P = 1050L$.

Fig. 7.20. Topologies for the shear wall: case 3, $P^* = 1050L$.



(a) Mesh A, $P = 965L$. (b) Mesh B, $P = 972.94L$. (c) Mesh C, $P = 972.5L$.

Fig. 7.21. Topologies for shear wall: case 4, $P^* = 970L$.

7.4.2 3D Continuum Structures

Example 7.4.2.1 A 3D Michell type structure.

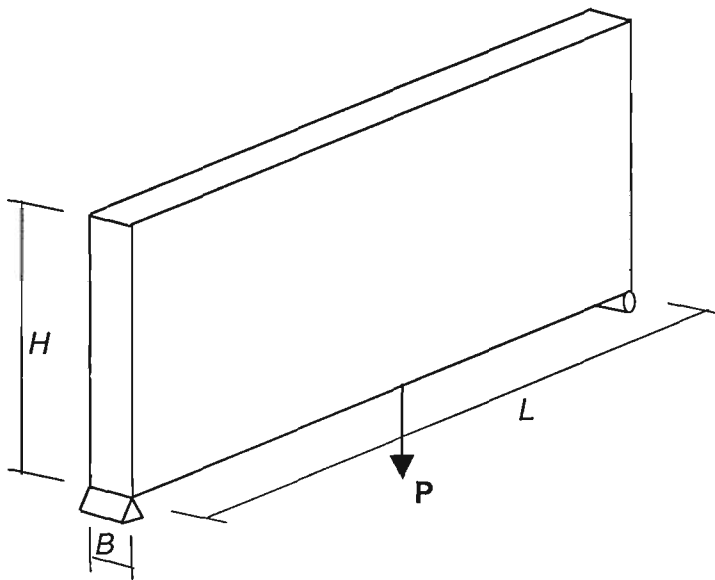


Fig. 7.22. A beam, 3D model.

Consider a 3D version of Example 7.4.1.2, as shown in Fig. 7.22. The rectangular design domain has dimensions of $L \times H \times B = 1.2\text{m} \times 0.6\text{m} \times 0.2\text{m}$. It is simply and roll supported. $E = 210\text{ GPa}$ and $\nu = 0.3$ are assumed.

Using the symmetry in the thickness direction, a half model is defined and divided by two meshes:

(A) $0.033\text{m} \times 0.033\text{m} \times 0.033\text{m}$,

(B) $0.024\text{m} \times 0.024\text{m} \times 0.033\text{m}$.

Two target weights are considered, for $W^*/W_0 = 32.5\%$, four cases of perimeter bound are studied as

(0) $P^* = \infty$, (1) $P^* = 1.22\text{m}$, (2) $P^* = 1.1\text{m}$ and (3) $P^* = 0.95\text{m}$.

For $W^*/W_0 = 25\%$, the perimeter bounds are:

(0) $P^* = \infty$, (1) $P^* = 1.1\text{m}$, (2) $P^* = 1.0\text{m}$ and (3) $P^* = 0.95\text{m}$.

Firstly, BESO without perimeter control, i.e. case 0 is conducted on the coarse mesh A and the topologies are shown in Figs. 7.23 & 7.24. The hatched area represents the plane of symmetry. It is worth noting there exist in two designs hollow regions which are not viable or convenient for manufacture. Results on the perimeter and mean compliance of the two target weights are given in Table 7.5.

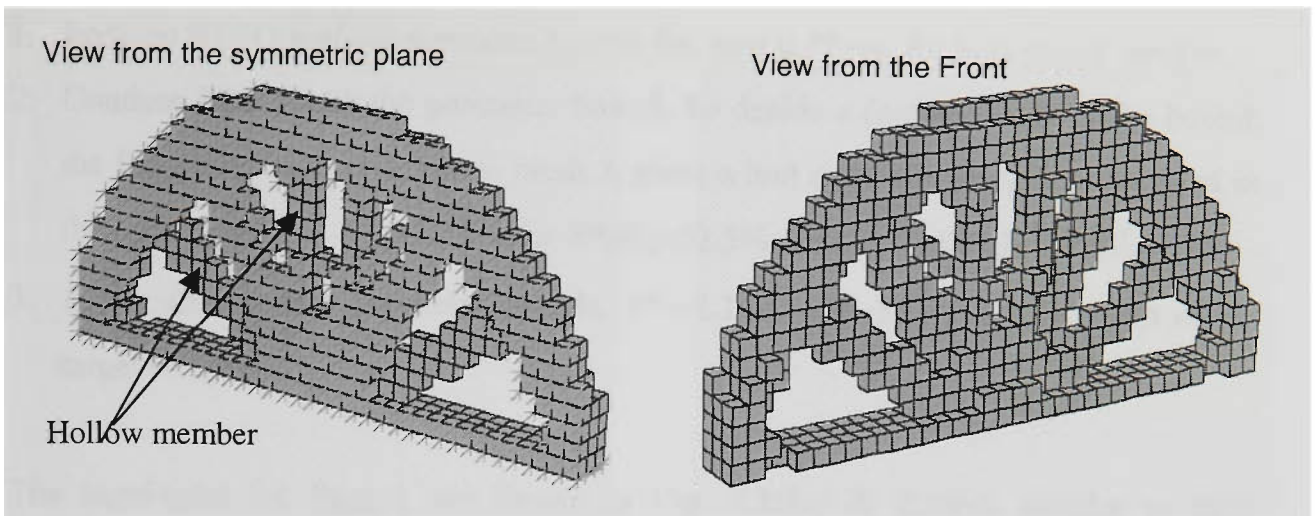


Fig.7.23. Optimal topology on Mesh A, $W^*/W_0=32.5\%$, $P=1.211\text{m}$.

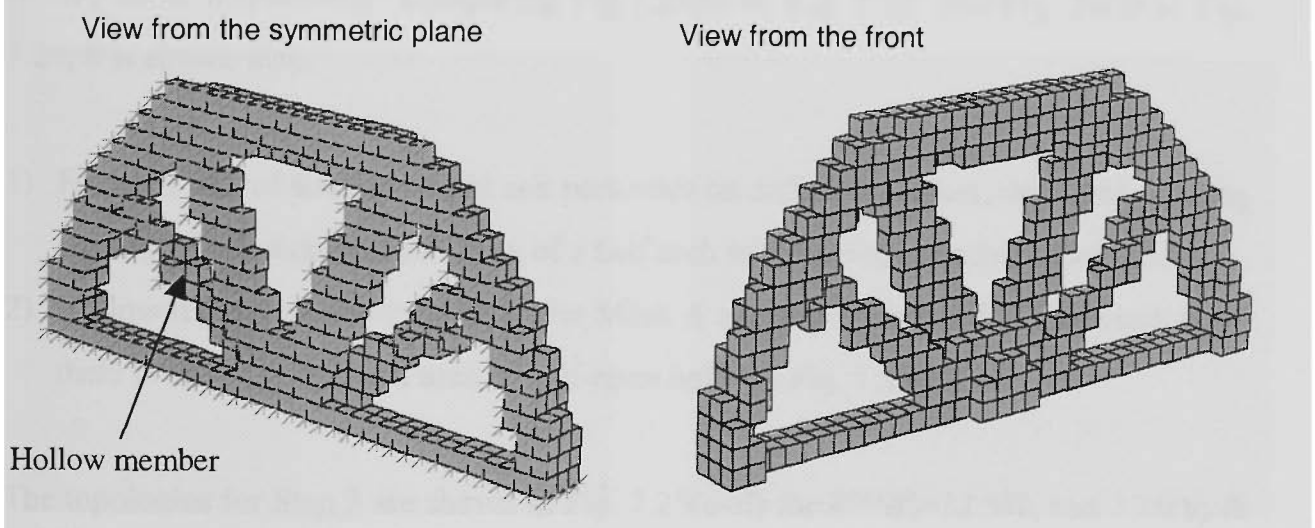


Fig.7.24. Optimal topology on Mesh A, $W^*/W_0=25\%$, $P=1.00\text{m}$.

**Table 7.5. Results on Mesh A, Case 0
(Example 7.4.2.1)**

	W	Perimeter	Mean Compliance C (N.m)
$W^*=32.5\%$	32.41%	1.2110	0.124381
$W^*=25\%$	25.00%	1.0024	0.155770

Secondly, experiments on the fine mesh B is conducted as follows:

1. Perform BESO *without* perimeter bound, i.e. case 0 $P^*=\infty$, for both target weights.
2. Conduct BESO *with* the perimeter bound. To decide a feasible value of the bound, the forgoing study on a *coarse* mesh A gives a hint and their perimeters are used as the initial trial, i.e. $P^* = 1.22$ m for $W^*/W_0=32.5\%$ and $P^* = 1.0$ m for $W^*/W_0=25\%$.
3. Apply another two perimeter bounds, $P^* = 1.10$ m and $P^* = 0.95$ m for both of the target weights.

The topologies for Step 1 are shown in Fig. 7.25(a) & 7.26(a). Similar to their counterparts on the coarse mesh A, there presents hollow regions or hidden holes.

The topologies for Step 2 are shown in Fig. 7.25(b) for $W^*/W_0=32.5\%$, and 7.26(c) for $W^*/W_0=25\%$, respectively. Comparing Fig.7.25(b) to Fig. 7.23, and Fig. 26(c) to Fig. 7.24, it is shown that:

- 1) For each pair of similar weight and perimeter on different meshes, the corresponding topologies are similar, consisting of a half arch and the same number of spokes.
- 2) Hollow regions as observed in coarse Mesh A are largely reduced in fine mesh B, as there is only a very small area of half-open holes in Fig. 7.25(b).

The topologies for Step 3 are shown in Fig. 7.25(c~d) for $W^*/W_0=32.5\%$, and 7.26(b) & (d). Look through columns of these two figures, it is observed that:

- 1) Topologies bounded with perimeter are free of hollow regions or hidden holes (except in Fig. 7.25(b)).
- 2) As the perimeter is more strictly bound, fewer spokes are present and they tend to be have a larger width. This tendency is however, reversed in 7.26(c~d). To explain this, it is noted that the integer perimeter measure consists of the number of surfaces in the xz , yz , and xy plane, .i.e. $P=P_{xz}+P_{yz}+P_{yx}$. In Fig. 7.26(c~d), the proportions are $1408=522+338+540$ and $1360=542+274+544$, respectively. The increase in P_{xz} from 522 to 542 reflects the number of spokes from 4 to 6, however, the increase is

totally offset by the dramatic decrease in P_{yz} from 338 to 274, witnessed by the bottom tie which is rough and irregular in Fig. 7.26(c) and becomes highly smooth in Fig.7.26(d).

The results on perimeter and mean compliance for the above experiments are summarised in Tables 7.6 and 7.7. There is an arbitrary change in the mean compliance with the value of perimeter bound, as opposed to a clear pattern of a more restrictive bound corresponding to a larger mean compliance (i.e. less optimal). It may be explained as follows.

In BESO considering the perimeter control, there are two criteria for the element addition, i.e. the sensitivity number and the perimeter contribution. Suppose a core element, say E0, has the largest sensitivity and has, say, four free faces. Therefore, for the sensitivity criterion, four elements E1, E2, E3 and E4 are all eligible for addition. However, they can be different for the perimeter criterion. For example, elements, say E2 and E3, whose addition would have increased the perimeter will not be actually added. Therefore, the final result is that only two elements E1 and E4 are added.

In BESO without perimeter control, however, only the sensitivity criterion is used. It is noted that the sensitivity is that of the core element E0, but not that of elements E1, E2, E3 or E4. In fact, these four eligible elements can have different sensitivity contributions. For example, adding E1 or E4 may significantly increase the structural stiffness, but adding E2 and E3 may only has moderate or little contribution. What actually happen, however, is that all elements E1, E2, E3 and E4 are treated equally and added at once, instead of only adding E1 and E4. In this case, the result (4 elements added) is not as good as the previous result (2 elements added) of using perimeter control.

For 2D structures, it can be said that the contribution of the added elements to the same core element be more similar, as compared to 3D structures. The latter case involves a complex stress field. For the present example, it is easily understood that the six stress

components at one point can be very different in magnitude, with the in-plane stress components dominating those in the thickness direction.

**Table 7.6. Perimeter & Mean Compliance
(Example 7.4.2.1, $W^*=32.5\%$)**

	W	Perimeter (m)	Mean Compliance C (N.m)
$P^* = \infty$	32.43%	1.3970	0.138775
$P^* = 1.22$ m	32.43%	1.2161	0.136476
$P^* = 1.1$ m	32.43%	1.1032	0.134928
$P^* = 0.95$	32.43%	0.9584	0.138505

**Table 7.7. Perimeter & Mean Compliance
(Example 7.4.2.1, $W^*=25\%$)**

	W	Perimeter (m)	Mean Compliance C (N.m)
$P^* = \infty$	25.01%	1.2648	0.162881
$P^* = 1.1$ m	25.01%	1.1040	0.160933
$P^* = 1.0$ m	25.01%	1.0088	0.162884
$P^* = 0.95$	25.01%	0.9659	0.161971

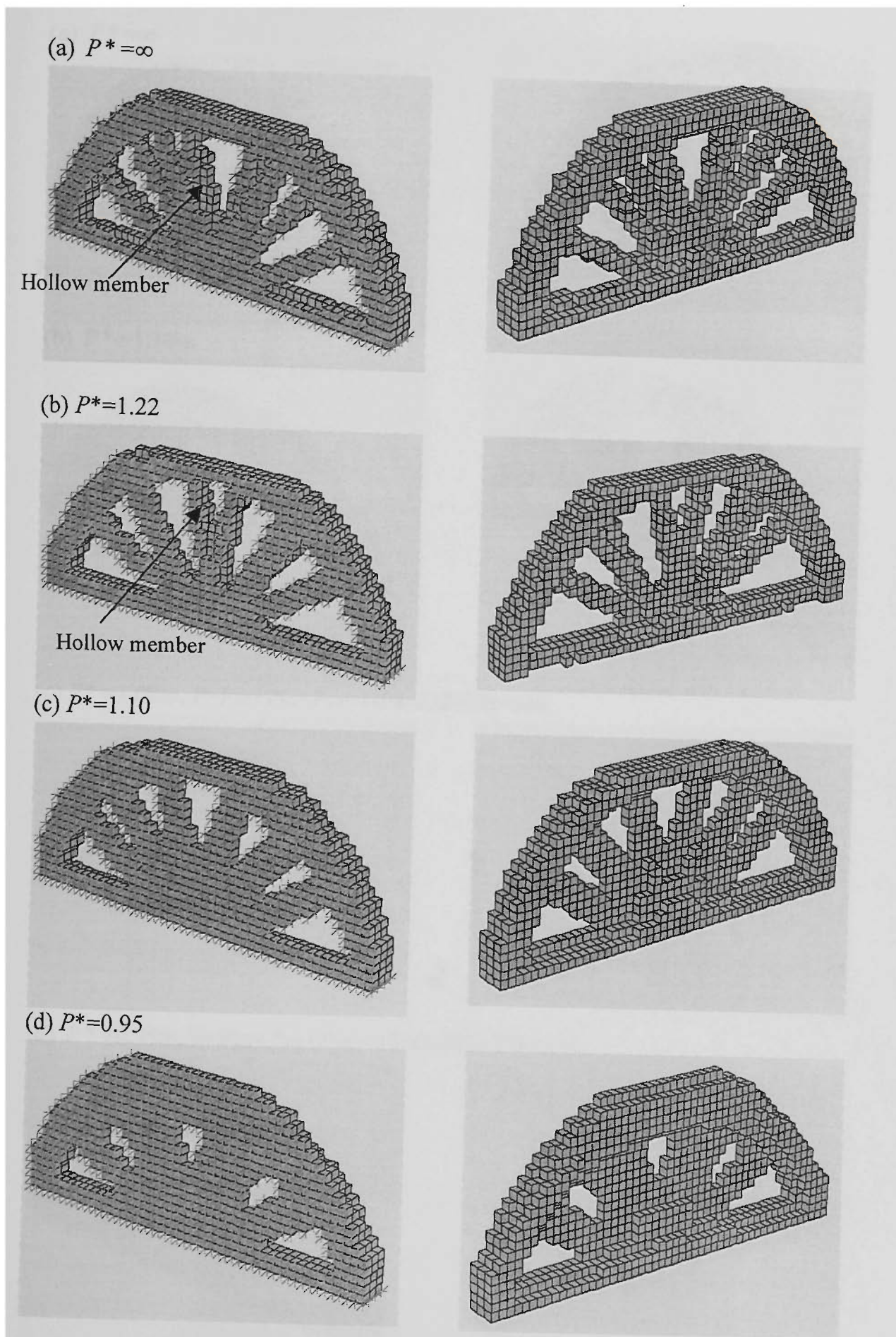
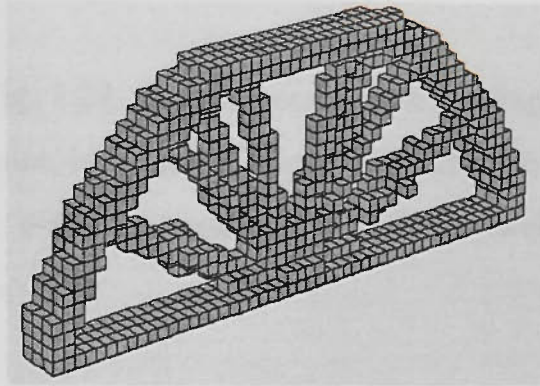
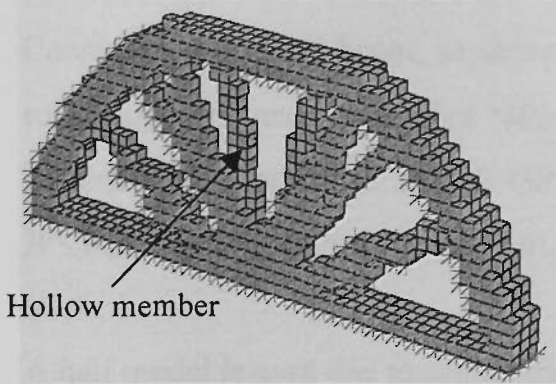
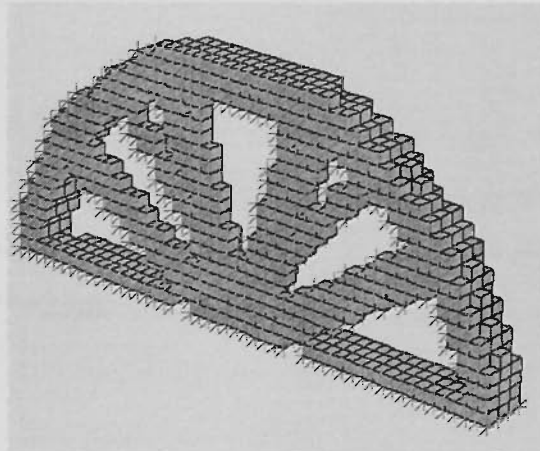
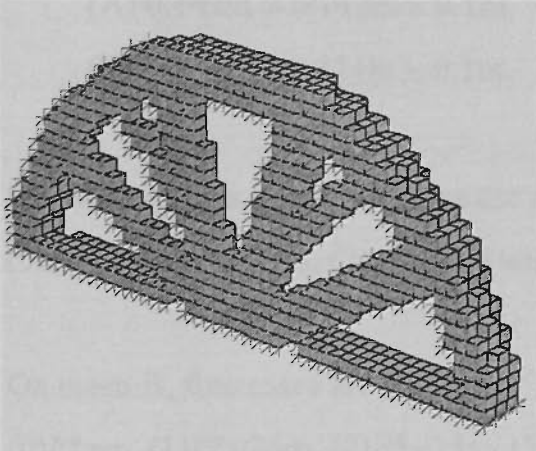
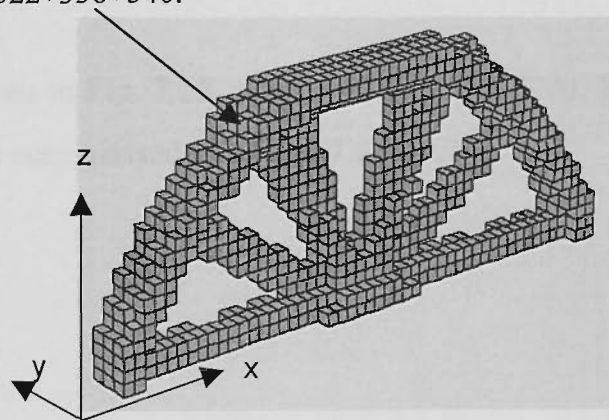
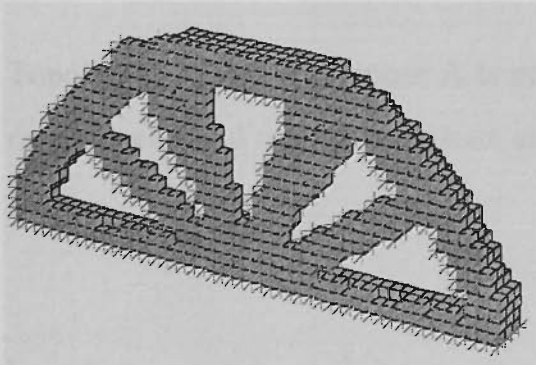
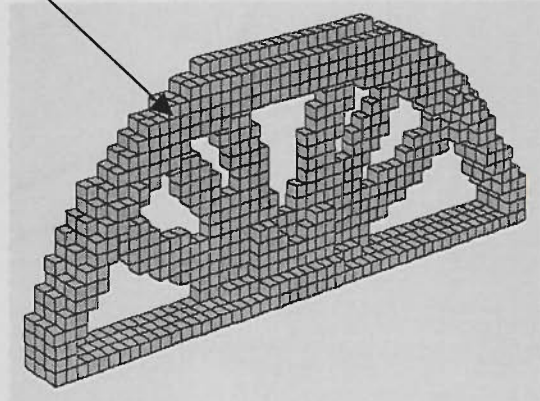
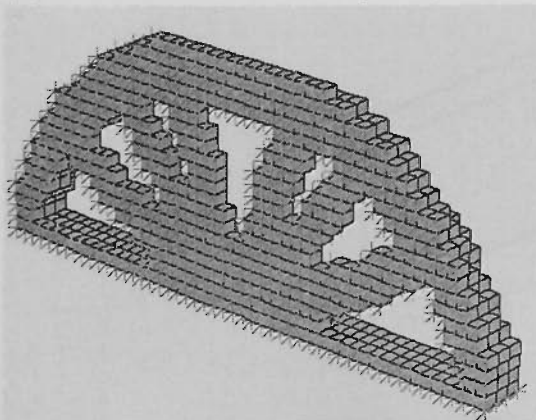


Fig. 7.25. Optimal topology on Mesh B, $W^*/W_0 \approx 32.5\%$.

(a) $P^* = \infty$ (b) $P^* = 1.10\text{m}$ (c) $P^* = 1.00\text{m}$, $P = P_{xz} + P_{yz} + P_{yx} = 1408 = 522 + 338 + 540$.(d) $P^* = 0.95\text{m}$, $P = P_{xz} + P_{yz} + P_{yx} = 1360 = 542 + 274 + 544$.Fig. 7.26. Optimal topology on Mesh B, $W^*/W_0 = 25.0\%$.

Example 7.4.2.2 A 3D MBB beam

Consider a 3D MBB beam, as shown in Fig. 7.27. The long-span beam is simply and roll supported and is applied with a point load at the top. The dimensions are $L \times H \times B = 10\text{m} \times 2\text{m} \times 0.6\text{m}$. $E = 210\text{ GPa}$ and $\nu = 0.3$ are assumed. The target weight is $W^*/W_0 = 30\%$. All regions are open to design.

A half model is used due to symmetry. Two meshes are:

(A) $0.142\text{m} \times 0.142\text{m} \times 0.1\text{m}$,

(B) $0.111\text{m} \times 0.111\text{m} \times 0.1\text{m}$.

On mesh A, four perimeter cases are studied:

(0) $P^* = \infty$, (1) $P^* = 25\text{m}$, (2) $P^* = 24\text{m}$ and (4) $P^* = 23\text{m}$.

On mesh B, five cases are studied:

(0) $P^* = \infty$, (1) $P^* = 26\text{m}$, (2) $P^* = 25\text{m}$, (3) $P^* = 24\text{m}$ and (4) $P^* = 23\text{m}$.

Topologies obtained on mesh A is given in Fig. 7.28, and mesh B in Fig. 7.29. Results on perimeter and mean compliance are summarised in Tables 7.8 & 7.9.

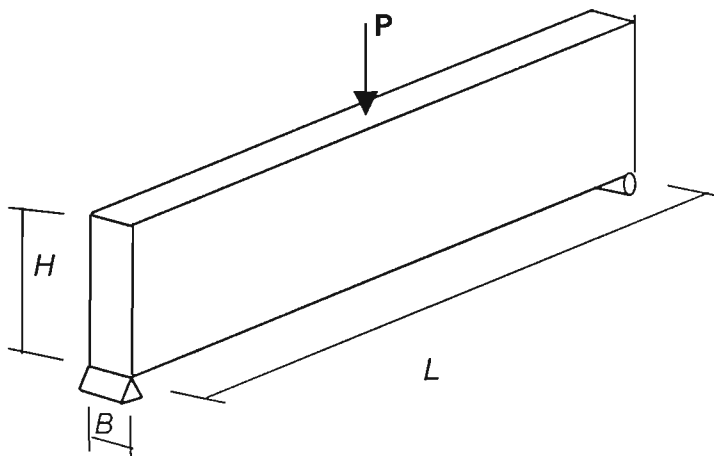


Fig. 7.27. A 3D MBB.

The following observations are made:

1. From Fig. 7.28 (coarse mesh A), the tendency can be seen that the structure becomes less complicated in xy plane and/or the boundary in each xy , yz or zx plane becomes more regular.
2. Note the change from Figs. 7.28(c) to (d) ($P^*=24\text{m}$ to $P^*=23\text{m}$), it is seen while there are two more spokes emerging, the overall perimeter becomes smaller as intended. This is because the increase in the P_{xz} is cancelled by the decrease in P_{yz} and P_{xy} in combination, as $P = P_{xz} + P_{yz} + P_{xy} = 1402 = 596 + 186 + 620$ in Fig. 7.28(c) and $P = 1346 = 638 + 168 + 540$ in Fig. 7.28(d).
3. Fig. 7.29 gives topologies for different perimeter constraints on a finer mesh B. It displays the same tendency as in observation 1 on mesh A.
4. Comparing the corresponding topologies in Fig. 7.28 with Fig. 7.29 which has the same perimeter constraint, qualitative difference is observed. This may suggest that perimeter control for 3D problems may be insufficient to achieve a mesh independency.
5. From Tables 7.8 and 7.9, the mean compliance again varies arbitrarily, as observed and discussed in the previous examples.

**Table 7.8. Perimeter & Mean Compliance
(Example 7.4.2.2, coarse mesh A)**

	W	Perimeter (m)	Mean Compliance C (N.m)
$P^* = \infty$	29.93%	25.8561	16.0738
$P^* = 25\text{ m}$	29.93%	24.6761	15.7850
$P^* = 24\text{ m}$	30.00%	23.6883	15.7361
$P^* = 23\text{ m}$	29.86%	23.1455	15.6081

**Table 7.9. Perimeter & Mean Compliance
(Example 7.4.2.2, fine mesh b)**

	W	Perimeter (m)	Mean Compliance C (N.m)
P* = ∞	30.04%	26.287	16.084
P* = 26 m	30.04%	25.7961	15.854
P* = 25 m	30.04%	25.1050	15.723
P* = 24 m	29.84%	23.8853	15.984
P* = 23 m	30.00%	23.0334	15.879

7.4.3 Discussions

For both 2D and 3D problems, the perimeter control technique works effectively and reaches an optimum which satisfies both weight and perimeter constraints. This means that the proposed methodology is capable of addressing the problem stated as Eq. (7.4) and justifies the algorithms.

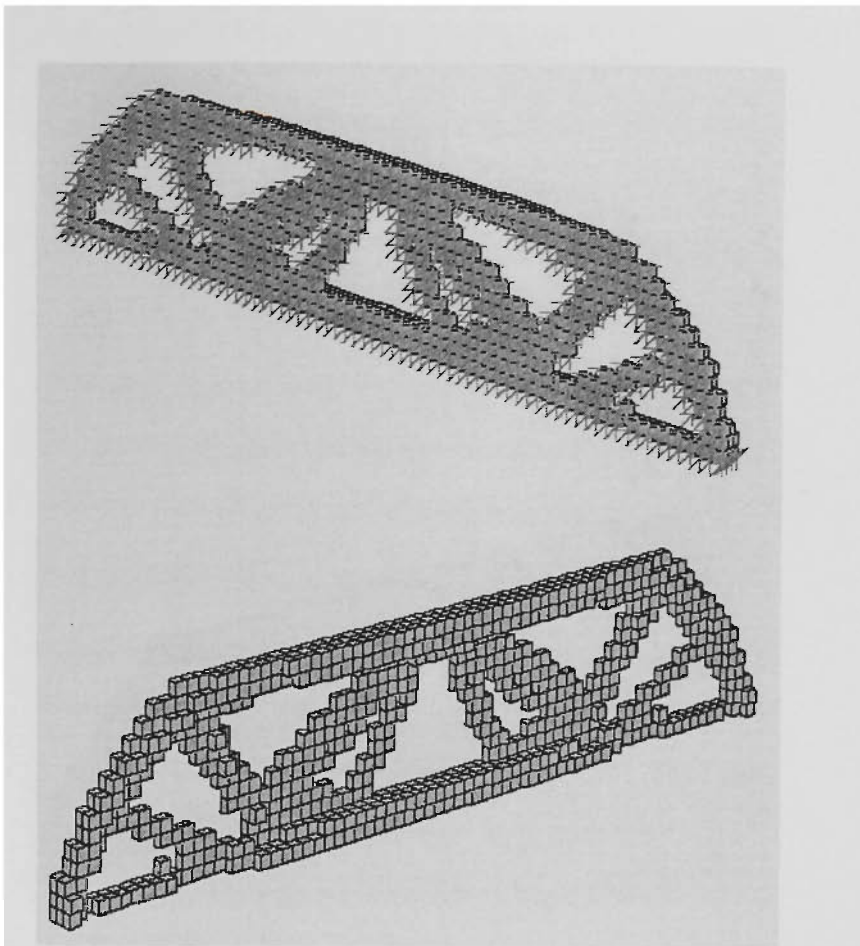
However, mesh dependency is still observed in 3D problems and it seems that a small measure of perimeter does not necessarily mean a ‘simpler’ topology (though it constitutes a solution to Eq. (7.4)). This then raises the question whether the perimeter is sufficient for describing the structural complexity for 3D structures. The answer can be problem dependent. For the 3D examples studied here, there are some common features: 1). Although modelled in 3D, the problem can be said quasi 2D, as the thickness is comparatively smaller than the height and length. This feature can be used when refining the finite element mesh, i.e. elements are refined more in the plane than in thickness (or not changed in thickness). 2). There is a plane whose topology dominates. In the forgoing comparison of topologies, we actually focus on the topology in this dominating plane. However, when trying to control the perimeter, it is the overall perimeter of all planes that has been considered. This can be a major reason that the

evolution possibly loses the control of the perimeter in the major plane though the overall perimeter is under control.

Apart from the above quasi 2D problems, it can be suggested that perimeter control be applied to 'true' 3D problems. It is found in the computer implementation that the level of mesh refinement for these problems is relatively limited. The refinement is normally required in three directions simultaneously and is at a similar level, rather than in preference of one or two directions. Suppose a 'coarse' mesh has a total number of $12 \times 12 \times 12 = 1728$ elements, doubling the elements in each direction will increase the total number by 2^3 times (13824 elements), which may go beyond the solver capacity used here. Alternatively, keep the number within the limit by, say, increasing by 1.5^3 times ($18 \times 18 \times 18 = 5832$ elements). Comparing this to a problem which has the same total but is not equal in three directions, say, $27 \times 18 \times 12 = 5832$, the former can be far more time consuming due to solving a larger band-width of equation. For this reason, a very fine mesh on 3D structures may not be practical at the present study.

Searching the literature reveals there is very few of 3D examples on mesh dependency. There is one example using perimeter control method on a 3D block structure (Fernandes *et al.* 1999), which is a similar to the problem of the four-leg stool as studied in Chapter 3. The main purpose for using the perimeter control, however, is to enforce a black-and-white pattern design rather than addressing the mesh independency problem. In BESO or ESO, firstly, solutions to all problems are free of grey area. Secondly, it can be said that the solution to this problem is mesh independent, as the load path is relatively clear, and the solution usually takes the form of simple 3D space truss configuration.

(a) $P^* = \infty$



(b) $P^* = 25.0m$

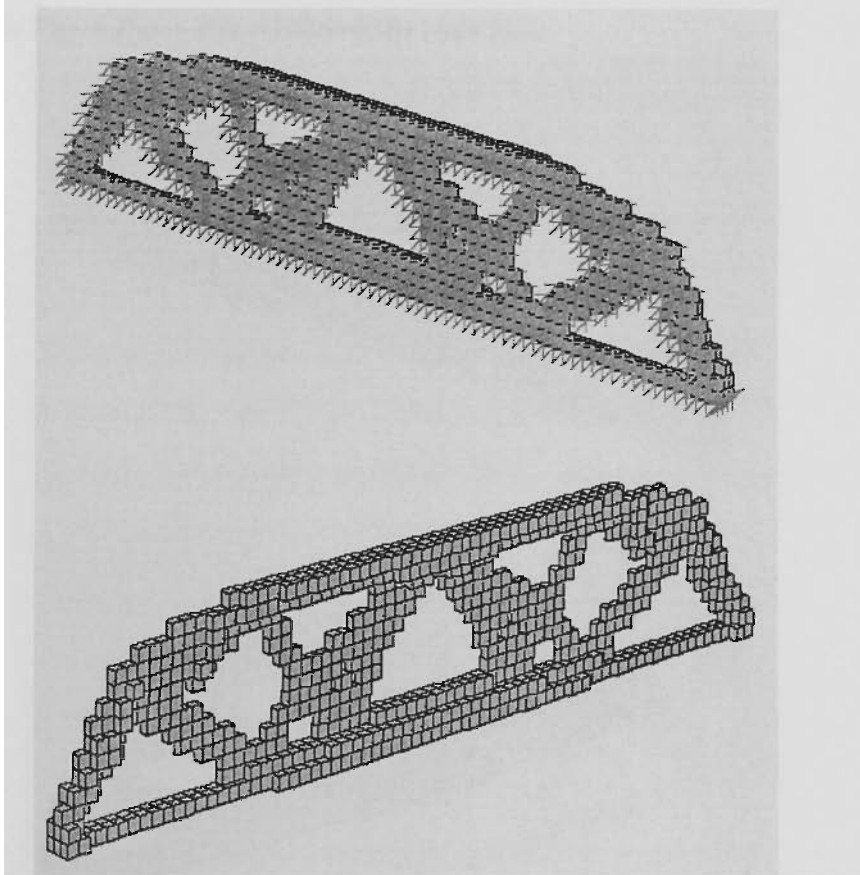
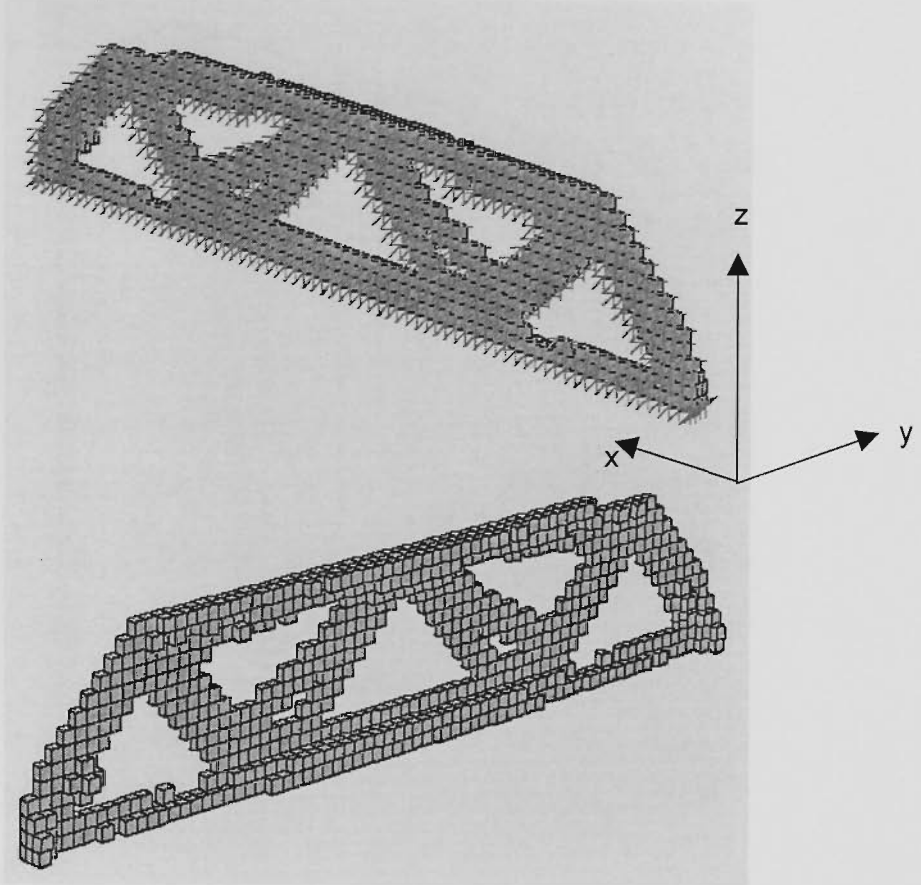


Fig. 7.28. Coarse Mesh A: Optimal topologies with different perimeter bound.

(c) $P^*=24.0\text{m}$, $P=P_{xz} + P_{yz} + P_{zx}=1402=596+186+620$.



(d) $P^*=23.0\text{m}$, $P=P_{xz} + P_{yz} + P_{zx}=1346=638+168+540$.

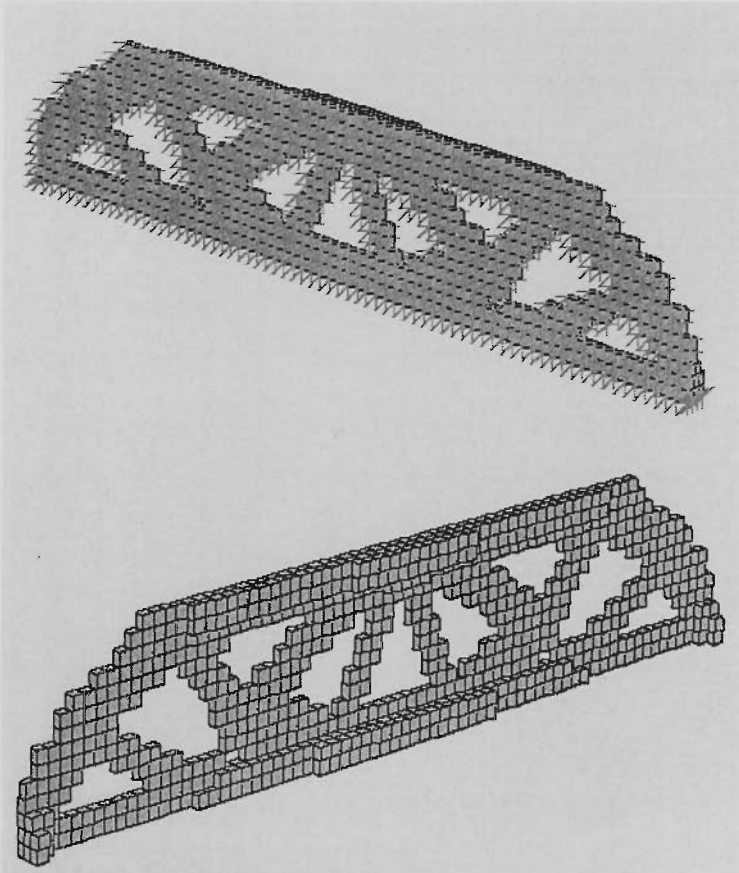
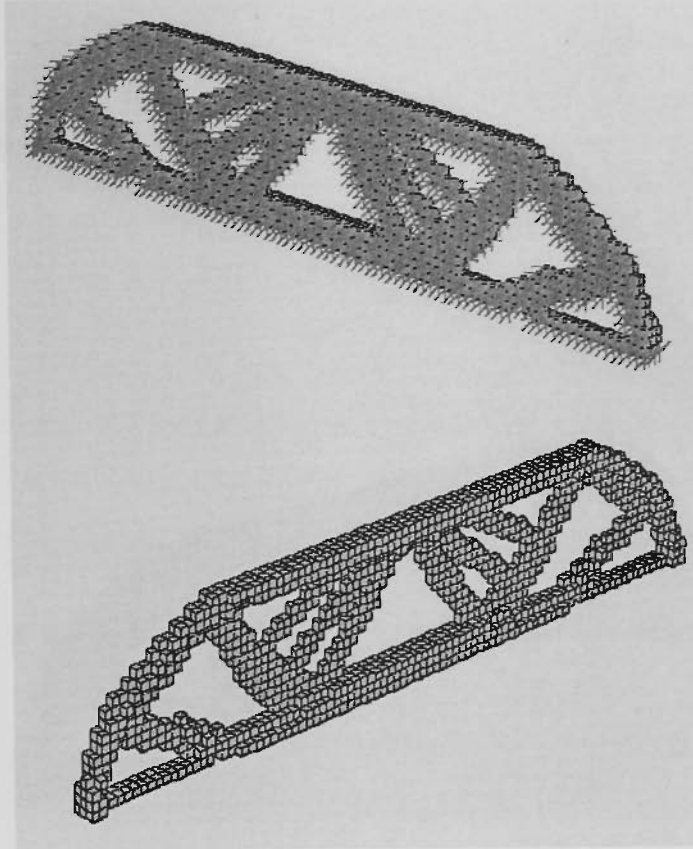


Fig. 7.28. (Cont.) Coarse Mesh A: Optimal topologies with different perimeter bound.

(a) $P^* = \infty$



(b) $P^* = 26 \text{ m}$

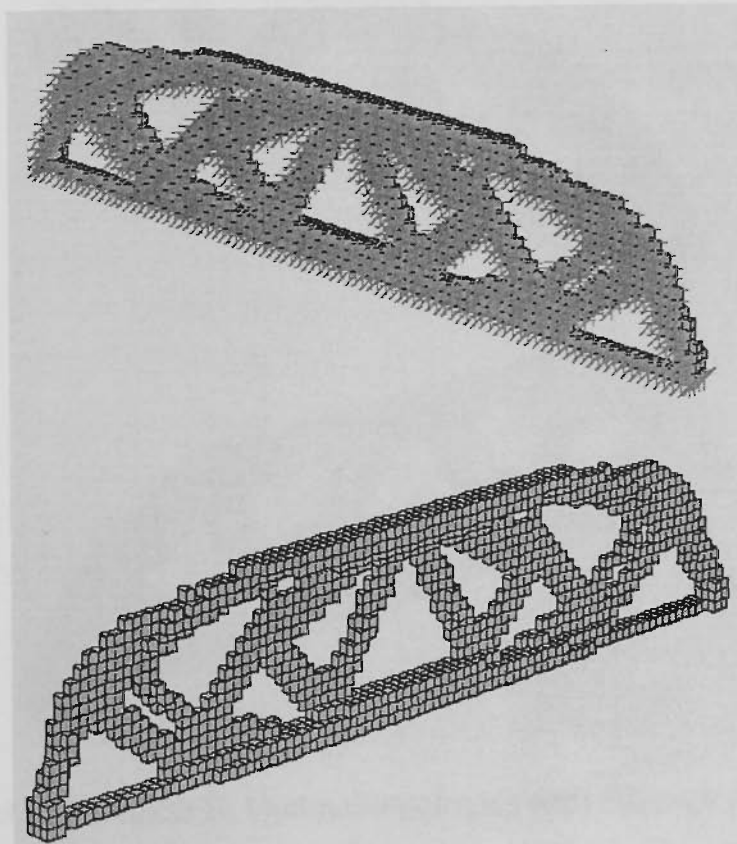
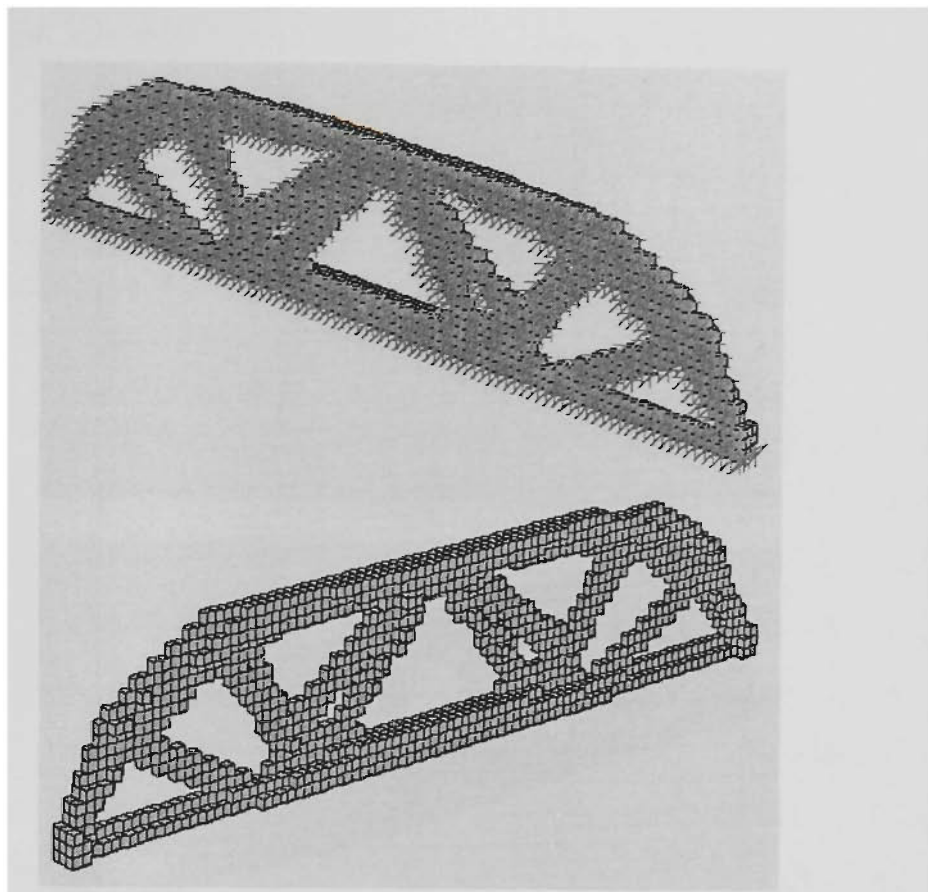


Fig. 7.29. Fine Mesh B: Optimal topologies with different perimeter bounds.

(c) $P^*=25$ m



(d) $P^*=24$ m

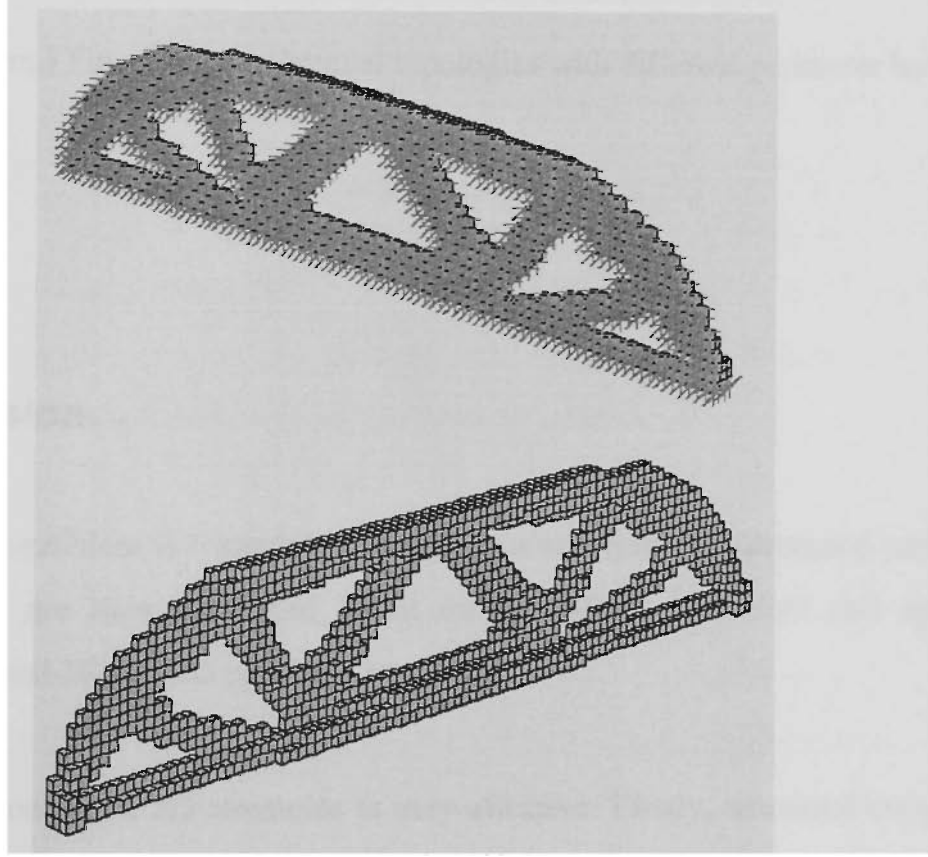


Fig. 7.29. (Cont.) Fine Mesh B: Optimal topologies with different perimeter bounds.

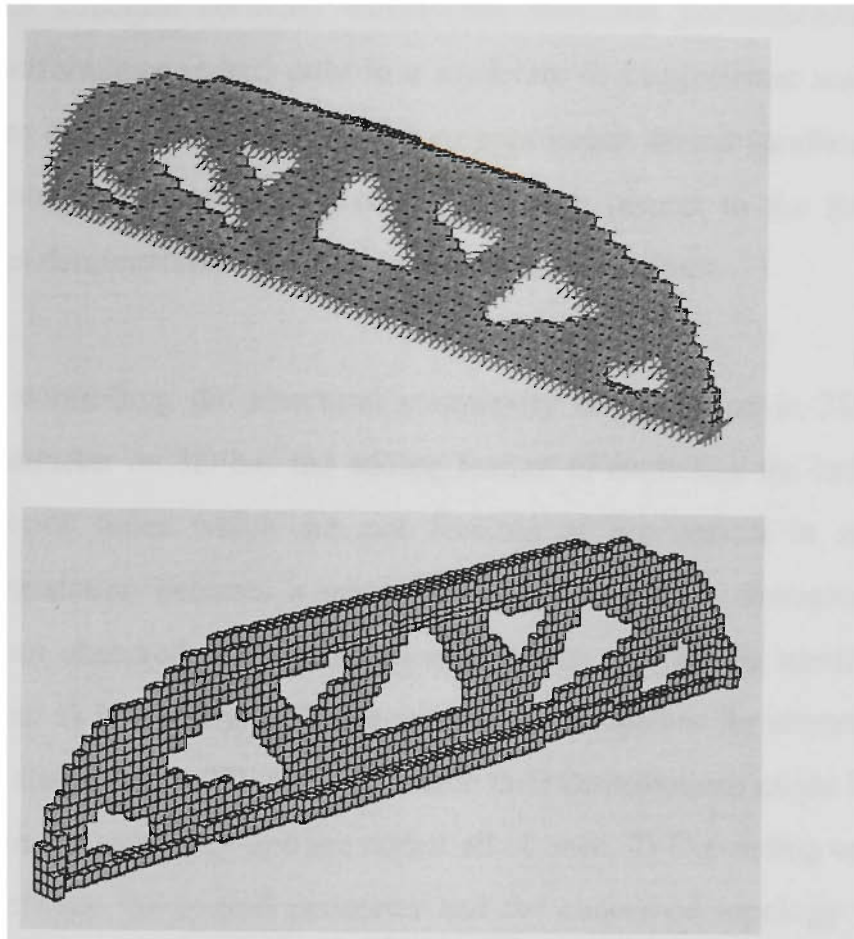
(e) $P^*=23$ m

Fig. 7.29. (Cont.) Fine Mesh B: Optimal topologies with different perimeter bounds.

7.5. Conclusion

An optimisation problem is formulated by adding a constraint on structural perimeter. The algorithms are then developed based on the BESO procedure and optimum solutions to several 2D and 3D problems are found.

The perimeter control on 2D structures is very effective. Firstly, structural complexity can be controlled by setting different perimeter bounds. In general, a more restrictive bound leads to a simpler topology, featured by less structural members or cavities of larger dimensions for the truss-like structure. Secondly, admitting an extra design

constraint on the structure normally affects the structural performance (i.e. mean compliance or performance index) only in a moderate or insignificant scale. Again, a good compromise can be reached by setting an appropriate bound (preferably, not too low). Thirdly, solution can be largely convergent with respect to the finite element discretization thus demonstrates its ability to reduce the size effect.

The strength of controlling the structural complexity is carried on in 3D structures. Bounding the perimeter on 3D has the adding feature of excluding the hollow region, hidden or half-open holes which are not feasible or economical in manufacture. However, the correlation between a restrictive constraint and a decreased structural performance is not observed, and the solution topology can also be mesh dependent. The reason can be: 1) Inherently, a 3D element has more options for element additions to the same core element than 2D (6 vs. 4). While their contributions might be different, they are treated in the same way and are added all at once. 2) Depending on problems, there is a gap between the overall perimeter and the concerned topology which only dominates at one or two plane. This is particularly true for some quasi 2D problems. In a conceptual design stage, it is suggested that these problems be modelled in 2D to control the topology on the dominating plane. On the other hand, for problems displaying typical 3D stress fields as studied in this thesis, the solution is not sensitive to the finite element size. The perimeter control technique, however, can be used mainly for fine tuning the structural surface, i.e. enabling a more regular member or excluding chattering design such as isolated elements or small holes.

Therefore, the proposed technique can deal with both 2D and 3D problems to enhance the numerical stability and/or improve manufacturability. We don not claim that BESO incorporated with perimeter control achieves mesh independency in a strict mathematical sense. However, it is observed that same or similar solutions are obtained on different meshes for most of problems. And also, its ability to control the structural complexity is very appealing and practical. It provides a means to reach a balance between the structural performance and manufacture viability, and thus can serve the engineering design, especially at the conceptual stage.

To specify the value of perimeter constraints needs a few trial experiments. The usual way is to first solve the unbound problem to get an idea on the upper bound, then conduct a series of case studies on perimeter control by successively tightening the constraint.

It is noted that although the chapter focuses on the stiffness optimisation, perimeter control can be equally applicable to other design objective and similar procedures can be followed.

Conclusions and Recommendations

Chapters 3~7 present the ESO/BESO methods for a range of static and dynamic problems, covering four major topics on stiffness optimisation, natural frequency optimisation, effect of algorithm parameters and technique to reduce the parameter effect. The principles of ESO/BESO, including the sensitivity analysis, removing/addition criteria and iterative evolution are described. These principles are applied to basic static and natural frequency optimisation, and also to its variations including optimisation of design-dependent load, frequency optimisation associated with a tracked mode shape and design with geometry constraints (perimeter constraint in this thesis). This chapter summarises the major conclusions from the previous chapters and makes recommendations for further studies.

8.1. Conclusions

For 2D and 3D continuum structures under investigation in this thesis, the ESO and BESO methods are effective in solving the stiffness optimisation and natural frequency optimisation, both their basic forms and variations. The variation in stiffness optimisation considered here is design-dependent loading, which can be due to gravity loading, transmissible loading and surface loading. The variation in natural optimisation under consideration is optimisation of a tracked mode shape. An iterative solution routine of *finite element analysis, sensitivity analysis, element removal/addition* is

followed in solving all the above problems. This routine, which is essential to the ESO/BESO algorithm, is easy to be implemented and generalised.

The comparison of ESO and BESO shows that:

Firstly, the two methods largely converge to solutions of close numerical results (mean compliance, natural frequency or performance index). This demonstrates the effectiveness of the evolution algorithms in finding the optimum solution, as the two methods start from the different searching points (ground structure vs. a simple initial structure).

For most problems, ESO can be effective in all cases, providing: 1). The ground structure is appropriate and adequate for the intended optimal design. 2). The step length is sufficiently small and the number of iteration is large. This implies that for a finite element problem of moderate scale, ESO can be used reliably and efficiently. The reliability of BESO compared to that of ESO can be two facets. Firstly, BESO can be more reliable as it has the capability of retrieving the prematurely removed elements (though this can be avoided by using a reasonably small step length in ESO). Secondly, despite the ability of BESO to admit or retrieve elements, the design domain for element addition is restricted to the current structural boundary elements, in comparison to ESO which uses the full design domain. This may affect the BESO solution. Apart from the reliability consideration, BESO demonstrates its advantage when the computation time becomes a major concern, such is the case for large scale problems and 3D structures. As the finite element analysis dominates the overall solution time, starting from a small finite element model can save considerable computing cost. Therefore, BESO has the flexibility of providing a balance between the solution accuracy and efficiency.

Thirdly, there are situations where ESO is more suitable than BESO, or Vice Versa. In optimisation considering gravity load, for example, BESO is not suitable due to complexity in the addition criteria. For another example, when investigating evolution algorithms incorporated with perimeter control, ESO is insufficient and BESO proves to be a necessity.

Therefore, ESO and BESO can be used on a comparative and complementary basis. The following summarises the two methods for different design objectives.

Optimisation on Different Design Objectives

Stiffness Optimisation

1. The problem is stated as minimising the mean compliance subjected to weight constraints. Element sensitivity number is calculated. The structure is modified by removing elements of the smallest sensitivity and adding elements around those of the largest sensitivity. For problems of fixed loading conditions, the sensitivity is equal to the ratio of element strain energy to weight.
2. On optimisation considering design-dependent loading:
 - 1) For optimal design with respect to transmissible loading, the transmissible condition is considered as an additional constraint stated as the nodal displacement being the same along the action line. In a finite element model, this uniform displacement condition is interpreted as fictitious bars of infinite stiffness in the action line. The element sensitivity number is in the same form as that of fixed loading conditions, i.e. element strain energy divided by element weight.
 - 2) For problems including the gravity load, the sensitivity analysis includes evaluating the contribution of load variation on the mean compliance. The element sensitivity number is thus in a form of element strain energy plus a term of load variation.
 - 3) For optimisation with respect to the surface loading, the calculation of sensitivity number depends on the loading condition of each element. For elements which are load-free in all edges/surfaces, the sensitivity is in the form of element strain energy. This sensitivity number is used as both removal and addition criteria. For loaded element, two sensitivity numbers are calculated.

One is based on the element strain energy and is used as the addition criterion. The other is the element strain energy plus contribution of load variation, and is used as removal criterion.

- 4) Compared to the optimal design of fixed loading, optimisation of design-dependent loading yields results of smaller mean compliance, as it allows for loading conditions to be optimised. For the same problem, understandably, by allowing for the largest extend of load condition relaxation, the optimal design with transmissible loading is the stiffest, followed by the design of surface load and then fixed loading.
- 5) For design considering gravity loading, stiffness optimisation and optimisation based on stress criterion are conducted. While the topology of the latter appears more realistic, the two approaches achieve their intended design objectives.

Natural Frequency Optimisation

1. Four design objectives are considered:
 - 1) Maximising a single frequency. The design objective is the intended eigenvalue.
 - 2) Satisfying a set of prescribed frequencies. The design objective is the weighed sum of average distances between the actual and target circular frequencies.
 - 3) Maximising multiple frequencies. The design objective takes the same form as 2), but the target circular frequencies are the maximum obtained by optimisation of each single frequency.
 - 4) Maximising the frequency associated with a prescribed mode shape. The design objective takes the form of 1) but a procedure to determine the correlation between the current mode and the prescribed mode is needed. This mode is tracked by using a modal assurance criterion (MAC) technique. The selected mode shape is then used for sensitivity analysis and structural modification.

2. For sensitivity analysis associated with close or repeated eigenvalues, a simple averaging technique is used, i.e. averaging the sensitivity number of all involved eigenvalues. The closed-ness can be judged by a relative difference of 5%.

Dealing with Sharp Change in Evolution Process

1. Two criteria to determine a sharp change are:
 - a. The relative difference in the objective function between the two consecutive iterations exceeds 5%.
 - b. The relative difference in the objective function between the predicted and actual values exceeds 2%.
2. Once the structure is checked against the above criteria and judged as a sharp change case, the operation of the current iteration is cancelled by recovering the removed elements and deleting the added elements. Those elements become temporarily unavailable for modification for say, 3 iterations.
3. Sharp change can occur frequently, especially when the structural members dimension becomes very small. If the total occurrence exceeds say, 15, the evolution is terminated.

Recommended Parameter Values

The parameters involved in ESO/BESO are modification ratio (*MR*), stage ratio (*SR*), initial structure and addition ratio (*AR*). *MR* has significant effects on the optimal solution of ESO and BESO. Additionally, for BESO, variations of *SR* and initial structure can cause significant difference in solutions. The effect of addition ratio is less significant.

The recommended ranges for the above parameters are given in Table 8.1. Within the range, the conservative value is normally used for relatively complicated cases, such as a final design which may exhibit truss features. As for initial structure, it is required to include supporting and boundary conditions, and preferably, to reflect an effective load path.

Table 8.1. Recommended parameter values

Items	Values
<i>MR</i>	1~4%
<i>SR</i>	50~60%
<i>AR</i>	0.25 or 0.33

Perimeter Control Technique

1. The perimeter is measured as the total length of the boundary for 2D continua, and the total surface area for 3D continua.
2. For 2D structure, imposing a perimeter constraint on the optimal design is effective as:
 - 1) For a relatively restrictive perimeter bound, similar topologies are obtained on finite element grid of different discretisation. This means that perimeter constraints can force the solution to converge with respect to the finite element grid.
 - 2) The structural performance (mean compliance or performance index) is affected by the perimeter bound. The mean compliance is the smallest if the perimeter is unbounded, and will increase while the bound is tightened. However, within a reasonable range of the perimeter bound variation, the increase is insignificant.
 - 3) The structural complexity can be controlled by setting different values of perimeter bound. A more restrictive bound generally yields a simpler design. Therefore, the final design can be a trade-off of structural performance and configuration simplicity.
3. For 3D structure,
 - 1) By imposing the same perimeter bound, the topologies can vary with different finite element grids. This implies bounding the perimeter may not sufficient to address the mesh dependency.

- 2) Nonetheless, the strength of reducing the topology complexity is retained in 3D, as it can suppress the manufacturing difficulties caused by hidden or half open holes and hollow regions.

8.2 Recommendations for Further Investigations

Extensive work has been conducted to develop ESO/BESO for size, shape and topology optimisation for various structural systems with a range of design objectives and constraints. Further work can be in extending ESO/BESO to including more objective/constraints such as multiple objectives consisting of stress, stiffness, natural frequency or frequency response. One problem is that of accommodating those objectives of different order of magnitude.

In implementing ESO/BESO, the computing time for 2D or truss structure is acceptable. 3D problem can be very time consuming, mostly due to the high computer cost of finite element analysis. This may limit its use for industrial and commercial purposes. Indeed, despite its wide acceptance in the academic community and frequent involvement in solving engineering problems, a systematic application package is yet to be developed.

The current research in the broad area of structural optimisation tends to solve problems of multi-physics and multi-disciplinaries . Further areas of research can be in:

1. Material design: topology optimisation can be applied to design material of desired elastic, thermal and electric properties. The previous work was concentrated on the optimal composite material which remains a promising field, as the increasing application of composite material in industries.
2. Mechanical converter design: the input displacement is to be converted to a desired displacement or force at the output. Geometric non-linearity should be considered. One of the many applications of the converter is sensors as used in smart structures/materials.

3. Optimisation with fracture requirements: it can be structural shape optimisation in order to minimise the stress intensity factor around a crack. Alternatively, the optimisation of repair patch to minimise the stress concentration. It has practical application especially in the aerospace industry in improving the aircraft damage tolerance and fatigue life.

References

- Allaire, G. and Kohn, R.V. (1993). Topology design and optimal shape design using homogenisation. In: Bendsøe, M.P; Mota Soares, C.A. (eds.), *Topology Design of Structures*. 239-248. Dordrecht, Kluwer.
- Ananthasuresh, G.K., Kota, S. and Kikuchi, N. (1994). Strategies for systematic synthesis of compliant MEMS. *Proceedings of the 1994 ASME Winter Annual Meeting*, Chicago, USA, 677-686.
- Avriel, M. and Williams, A. (1970). Complementary geometric programming. *SIAM J. Appl. Math.*, **19**, 125-141.
- Babuska, I. (1976 and 1977). Solution of interface problems by homogenisation I, II, III. *Journal of Mathematical Analysis*, 1976, **7**, 603-634 (I); 1976, **7**, 635-645 (II); 1977, **8**, 923-937 (III).
- Bartholomew, P. and Pitcher, N. (1984). Optimisation of structures with repeated normal-mode frequencies. *Eng. Optim.*, **7**, 195-208.
- Beckers, M. (1999). Topology optimization using a dual method with discrete variables. *Struct. Multidisc. Optim.* **17**, 14-24.
- Bendsøe, M.P. and Kikuchi, N. (1988). Generating optimal topologies in structural design using a homogenisation method. *Comput. Methods Appl. Mech. Eng.*, **71**, 197-224.
- Bendsøe, M.P. (1989). Optimal shape design as a material distribution problem. *Struct. Multidisc. Optim.*, **1**, 193-202.
- Bendsøe, M.P. (1995). *Methods for Optimization of Structural Topology, Shape and Material*. Springer-Verlag, Berlin.
- Bendsøe, M.P. and Sigmund, O. (1999). Material interpolations in topology optimisation. *Archive of Applied Mechanics*, **69**, 635-654.
- Bennett, J.A. and Botkin, M.E. (Eds.) (1986). *The Optimum Shape: Automated Structural Design*. Plenum, New York.
- Bulman, S. and Hinton, E. (1999). Constrained adaptive topology optimisation of engineering structures. *Design Optimisation* (submitted).
- Burns, A. S. (1987). Generalised geometric programming with many equality

- constraints. *Int. J. Numer. Methods Eng.*, **24**, 725-741.
- Chapman, C.D., Saitou, K. and Jakiela, M.J. (1994). Genetic algorithms as an approach to configuration and topology design. *Journal of Mechanical Design, ASME*, **116**, 1005-1012.
- Chen T.Y. (1993). Design sensitivity analysis for repeated eigenvalues in structural design. *AIAA J.*, **31**, 2347-2350.
- Chirehdast, M., Gea, H.C., Kikuchi, N. and Papalambros, P.Y. (1994). Structural configuration examples of an integrated optimal design process. *Journal of Mechanical Design*, **1**, 997-1004.
- Choi, K.K., Huang, E.J. and Seong, H. (1983). An iterative method for finite dimensional structural optimization problems with repeated eigenvalues. *Int. J. Numer. Methods in Eng.*, **19**, 93-112.
- Christie, W.C., Bettess, P. and Bull, J.W. (1998). Self design structures: a practical approach. *Engineering Computations*, **15**, 35-48.
- Chu, D.N. (1997). *Evolutionary Structural Optimisation Method for Systems with Stiffness and Displacement Constraints*. PhD thesis, Victoria University of Technology, Melbourne, Australia.
- Cook, R.D., Malkus, D.S. and Plesha, M.E. (1989). *Concepts and Application of Finite Element Analysis*. John Wiley & Sons Inc., Singapore.
- Díaz, A. and Bendsøe, M.P. (1992). Shape optimisation of structures for multiple loading conditions using a homogenisation method. *Struct. Multidisc. Optim.*, **4**, 17-22.
- Díaz, A. and Lipton, R. (1997). Optimal material layout for 3D elastic structures. *Struct. Multidisc. Optim.*, **13**, 60-64.
- Ding, Y. (1986). Shape optimisation of structures: a literature review. *Compt. Struct.*, **24**, 985-1004.
- Eldred, M., Venkayya, V.B. and Anerson, W. (1993). Model tracking issues in optimisation. *AIAA Paper 93-1216*.
- Fernandes, P., Guedes, J.M. and Rodrigues, H. (1999). Topology optimisation of three-dimensional linear elastic structures with a constraint on 'perimeter'. *Compt. Struct.*, **73**, 583-594.

- Fiacco, A.V. and McCormick, G.P. (1968). *Nonlinear Programming: Sequential Unconstrained Minimisation Techniques*, Wiley, New York.
- Fleury, C. (1979). Structural weight optimisation by dual methods for convex programming. *Int. J. Numer. Methods Eng.*, **14**, 1761-1783.
- Fleury, C. and Braibant, V. (1986). Structural optimisation - A new method using mixed variables. *Int. J. Numer. Methods Eng.*, **23**, 409-428.
- Fox, R.L. and Kapoor, M.D. (1968). Rates of change of eigenvalues and eigenvectors. *AIAA J.*, **6**, 2426-2429.
- Fuchs, M.B. and Moses, E. (2000). Optimal structural topologies with transmissible loads. *Struct. Multidisc. Optim.*, **19**, 263-273.
- Fuchs, M.B. and Moses, E. and Miller, Z. (2001). Engineering oriented topological design of structures. *Proceeding of the 2nd ASMO UK /ISSMO Conference on Engineering Design Optimisation*, Swansea, Wales, UK, July, 2000, 79-86.
- Fujii, D. and Kikuchi, N. (2000). Improvement of numerical stabilities in topology optimisation using the SLP method. *Struct. Multidisc. Optim.*, **19**, 113-121.
- Gellatly, R.A. and Berke, L. (1971). Optimal Structural Design. *USAF AFFDL-TR-70-165*.
- Goldberg, D.E. (1989). *Genetic Algorithms in Search, Optimisation and Machine Learning*. Addison-Wesley Publishing Co., Inc., Reading, Massachusetts.
- Grandhi, R. (1993). Structural optimisation with frequency constraints – a review. *AIAA J.*, **31**, 2296-2303.
- Haber, R.B., Jog, C.S. and Bendsøe, M.P. (1996). A new approach to variable-topology shape design using a constraint on perimeter. *Struct. Multidisc. Optim.*, **11**, 1-12.
- Haftka, R.T. and Grandhi, R.V. (1986). Structural optimisation - a survey. *Comput. Methods Appl. Mech. Eng.*, **57**, 91-106.
- Haftka, R.T. and Gürdal, Z. (1992). *Elements of Structural Optimisation*. 3rd revised edition, Kluwer Academic Publishers, Dordrecht.
- Hammer, V.B. and Olhoff, N. (2000). Topology optimisation of continuum structures subjected to pressure loading. *Struct. Multidisc. Optim.*, **19**, 85-92.
- Hassani, B. and Hinton, E. (1999). *Homogenisation and Structural Topology Optimisation*. Springer-Verlag, Berlin.

- Heyman, J. (1951). Plastic design of beams and frames for minimum material consumption. *Quarterly of Applied Mathematics*, **8**, 373-381.
- Hinton, E., Bulman, S., Sienz, J. and Ghasemi, M.R. (1998). Fully Integrated Design Optimisation. *Proceedings of the Australasian Conference on Structural Optimisation*, Sydney, Australia, 3-29.
- Holland, J.H. (1975). *Adaptation in Natural and Artificial Systems*. Univ. of Michigan Press, Ann Arbor, USA.
- Inou, N., Shimotai, N. and Uesugi, T. (1994). A cellular automaton generation topological structures. *Proceedings of the 2nd European Conference on Smart Structures and Materials*, Glasgow, UK, 47-50.
- Jog, C.S. (1993). *Variable-topology Shape Optimisation of Linear Elastic Structures*. Ph.D. Thesis, Department of Theoretical and Applied Mechanics, University of Illinois at Urbana-Champaign, USA.
- Kang, B.S., Choi, W.S. and Park, G.J. (2001). Structural optimisation under equivalent static loads transformed from dynamic loads based on displacement. *Compt. Struct.*, **79**, 145-154
- Kikuchi, N., Suzuchi, K. and Fukishima, I. (1991). Layout optimisation using the homogenisation method: generalised layout design of three-dimensional shells for car bodies. In: Rozvany GIN (ed.), *Optimisation of Large Structural Systems*. Lecture notes, NATO-ASI, Berchtesgaden, FRG, **3**, 110-126.
- Kim, H., Querin, O.M., Steven, G.P. and Xie, Y.M. (2000). A method for varying the number of cavities in an optimised topology using Evolutionary Structural Optimisation. *Struct. Multidisc. Optim.*, **19**, 140-147.
- Kim, T.S. and Kim, Y.Y. (2000). Mac-based mode-tracking in structural topology optimisation. *Compt. Struct.*, **74**, 375-383.
- Kosaka, I. and Swan, C. C. (1999). A symmetry reduction method for continuum structural topology optimisation. *Compt. Struct.*, **70**, 47-61.
- Krog, L.A. and Ohloff, N. (1999). Optimum topology and reinforcement design of disk and plate structures with multiple stiffness and eigenfrequency objectives. *Compt. Struct.*, **72**, 535-563.
- Le Riche, R. and Haftka, R.T. (1994). Optimisation of laminated stacking sequence for

- buckling load maximisation by genetic algorithm. *AIAA J.*, **31**, 951-956.
- Li, Q., Steven, G.P., Querin, O.M. and Xie, Y.M. (1997). Optimal shape design for steady heat conduction by the evolutionary procedure. *Proceedings of 1997 ASME National Heat Transfer Conference*, Baltimore, USA, 159-164.
- Li, Q., Steven G.P. and Xie, Y.M. (1999). On equivalence between stress criterion and stiffness criterion in evolutionary structural optimisation. *Struct. Multidisc. Optim.*, **18**, 67-73.
- Li, W., Steven, G.P. and Xie, Y.M. (1998). Shape design of elastic contact problems by evolutionary structural optimisation. *7th AIAA/USAF/NASA/ISSMO Symposium on Multidisciplinary Analysis and Optimisation*, St. Louis, USA, 1108-1114.
- Liang, Q.Q. (2001). *Performance-Based Optimisation Methods for Structural Topology and Shape Design*. PhD thesis, Victoria University of Technology, Melbourne, Australia.
- Liu, J-S., Parks, G.T. and Clarkson, P.J. (1999). Can a structure grow towards an optimum topology layout? – Metamorphic development: a new topology optimisation method. *Proceedings of the 3rd World Congress of Structural and Multidisciplinary Optimisation (WCSMO-3)*, Buffalo, USA, on CD-ROM.
- Liu, J-S., Parks, G.T. and Clarkson, P.J. (2000). Metamorphic Development: a new topology optimisation method for continuum structures. *Struct. Multidisc. Optim.*, in press.
- Liu, Z.S., Chen S.H. and Zhao, Y.Z. (1994). An accurate method for computing eigenvector derivatives for free-free structure. *Compt. Struct.*, **52**, 1135-1143.
- Lynch, R.W., Rogers, W.A. and Brayman, W.W. (1977). Aeroelastic tailoring of advanced composite structures for military aircraft, Volume II - wing preliminary design. *AFFDL-TR-72-130*.
- Ma, Z.D., Kikuchi, N. and Hagiwara, I. (1993). Structural topology and shape optimisation for a frequency response problem. *Computational Mechanics*, **13**, 151-174.
- Ma, Z.D., Kikuchi, N. and Cheng, H.C. (1995). Topology design for vibrating structures. *Comput. Methods Appl. Mech. Eng.*, **121**, 259-280.
- Manickarajah, D. (1998). *Optimal Design of Structures with Stability Constraints using*

- Evolutionary Optimisation Method*. PhD thesis, Victoria University of Technology, Melbourne, Australia.
- Manickarajah, D., Xie, Y.M. and Steven, G.P. (1998). An evolutionary method for optimisation of plate buckling resistance. *Finite Elements in Analysis and Design*, **29**, 205-230.
- Mattheck, C. (1997). *Design in Nature: Learning from Trees*. Springer-Verlag, Berlin.
- Maxwell, C. (1895). *Scientific Papers I*. Cambridge University Press.
- Michell, A.G.M. (1904). The limit of economy of material in frame-structures. *Phil. Mag.*, **8**, 589-597.
- Mijar, A. R., Swan, C. C., Arora, J. S. and Kosaka, I. (1998). Continuum topology optimisation for concept design of frame bracing systems. *Journal of Structural Engineering, ASCE*, **124**(5), 541-550.
- Mills-Curran, W.C. (1988). Calculation of eigenvector derivatives for structures with repeated eigenvalues. *AIAA J.*, **26**, 867-871.
- Min, S. and Kikuchi, N., Park, Y.C., Kim, S. and Chang, S. (1999). Optimal topology design under dynamic loads. *Struct. Multidisc. Optim.*, **17**, 208-218.
- Min, S. and Nishiwaki, S. and Kicuchi, N. (2000). Unified topology design of static and vibrating structures using multi-objective optimisation. *Compt. Struct.*, **75**, 93-116.
- Morris, A.J. (Ed.) (1982). *Foundation of Structural Optimisation: A Unified Approach*. John Wiley & Sons, New York.
- Nagendra, S., Haftka, R.T. and Gürdal, Z. (1993). Design of blade stiffened composite panels by a genetic algorithm approach. *Proceedings of the 34th AIAA/ASME/AHS SDM Conference*, La Jolla, USA, 2418-2436.
- Nelson, R.B. (1986). Simplified calculation of eigenvector derivatives. *AIAA J.*, **24**, 823-832.
- Ojalvo, I.U. (1998). Efficient computation of modal sensitivities for systems with repeated frequencies. *AIAA J.*, **26**, 361-366.
- Olhoff, N., Rønholt, E. and Scheel, J. (1998). Topology optimisation of three-dimensional structures using optimum microstructures. *Struct. Multidisc. Optim.*, **16**, 1-18.
- Petersson, J., Beckers, M. and Duysinx, P. (1999). Almost isotropic perimeters in

topology optimisation: theoretical and numerical aspects. *3rd ISSMO/UBCAD/UB/AIAA World Congress on Structural and Multidisciplinary Optimisation*, Amherst, USA, on CDROM.

Prager, W. and Shield, R.T. (1968). Optimal design of multi-purpose structures. *Int. J. Solids and Structures*, **4**, 469-475.

Prager, W. and Taylor, J.E. (1968). Problems of optimal structural design. *Journal of Applied Mechanics*, **35**, 102-106.

Prager, W. and Rozvany, G.I.N. (1977). Optimisation of structural geometry. In: Bednarek, A.R. and Cesari, L. (Eds.), *Dynamic Systems*. Academic Press, New York, 265-293.

Querin, O.M., Steven, G.P. and Xie Y.M. (1996). Topology optimisation of structures with material and geometric nonlinearities. *5th AIAA/USAF/NASA/ISSMO Symposium on Multidisciplinary Analysis and Optimisation*, Bellevue Washington, USA, 1812-1818.

Querin, O.M. (1997). *Evolutionary Structural Optimisation: Stress Based Formulation and Implementation*. Ph.D. Thesis, University of Sydney, Australia.

Querin, O.M., Steven, G.P. and Xie, Y.M. (1998). Evolutionary structural optimisation (ESO) using a bidirectional algorithm. *Engineering Computations*, **15**, 1031-1048.

Reynolds, D., McConnachie, J., Bettess, P., Christie, W.C. and Bull, J.W. (1999). Reverse adaptivity - a new evolutionary tool for structural optimisation. *Int. J. Numer. Mech. Eng.*, **45**, 529-552.

Reynolds, D., Christie, W.C., Bettess, P., McConnachie, J. and Bull, J.W. (2001). Evolutionary material translation: a tool for the automatic design of low weight, low stress structures. *Int. J. Numer. Mech. Eng.*, **50**, 147-167.

Rong, J.H., Xie, Y.M., Yang, X.Y. and Liang, Q.Q. (2001a). Topology optimisation of structures under dynamic response constraints. *Sound & Vibration*, **23**(4), 177-189.

Rong, J.H., Xie, Y.M. and Yang, X.Y. (2001b). An improved method of evolutionary structural optimisation against buckling. *Compt. Struct.*, **79**, 253-263.

Rosen, J.B. (1960). The gradient projection method for nonlinear programming. *Journal of the Society for Industrial and Applied Mathematics*, **8**, 181-217.

- Rozvany, G.I.N. and Prager, W. (1979). A new class of structural optimisation problems: optimal archgrids. *Comput. Methods Appl. Mech. Eng.*, **19**, 49-58.
- Rozvany, G.I.N. and Wang, C.M. (1983). On plane Prager-structures. *Int. J. Mech. Sci.*, **25**, 519-527.
- Rozvany, G.I.N. (1989). *Structural Design via Optimality Criteria*. Kluwer, Dordrecht.
- Sadek, E.A. (1995). Minimum weight design of structures under frequency and frequency response constraints. *Compt. Struct.*, **60**, 73-77.
- Saxena, A. and Ananthasuresh, G.K. (1998). Topological synthesis of compliant mechanism using the optimality criteria method. *7th AIAA/USAF/NASA/ISSMO Symposium on Multidisciplinary Analysis and Optimisation*, St. Louis, USA, 1900-1909.
- Schmit, L.A. (1960). Structural design by systematic synthesis. *Proceedings of the 2nd Conference on Electronic Computation, ASCE*, New York, 105-122.
- Seyranian, A.P., Lund E. and Olhoff, N. (1994). Multiple eigenvalues in structural optimisation problems. *Struct. Multidisc. Optim.*, **8**, 207-227.
- Sigmund, O. (1994). *Design of Material Structures Using Topology Optimisation*. Ph.D. Thesis, Technical University of Denmark, Denmark.
- Sigmund, O. and Petersson, J. (1998). Numerical instabilities in topology optimisation: a survey on procedures dealing with checkerboards, mesh-dependencies and local minima. *Struct. Multidisc. Optim.*, **16**, 68-75.
- Sigmund, O., Torquato, S. and Aksay, I.A. (1998). On the design of 1-3 piezo-composites using topology optimisation. *J. Mat. Res.* **13**(4), 197-224.
- Suzuchi, K. and Kickuchi, N. (1991). Shape and topology optimisation for generalised layout problems using the homogenisation method. *Comput. Methods Appl. Mech. Eng.*, **93**, 291-318.
- Svanberg, K. (1987). Method for moving asymptotes- A new method for structural optimisation. *Int. J. Numer. Methods Eng.*, **24**, 359-373.
- Tenek, L. H. and Hagiwara, I. (1993). Static and vibrational shape and topology optimisation using homogenisation and mathematical programming. *Comput. Methods Appl. Mech. Eng.*, **109**, 143-154.
- Ting, T., Chen, T. and Twomey, W. (1993). An automated mode-tracking strategy.

- AIAA* paper 93-1414.
- Topping, B.H.V. (1993). Topology design of discrete structures. In: Bendsøe, M.P. and Mota Soares, C.A. (eds.), *Topology Design of Structures*. Kluwer Academic Publishers, Netherlands.
- Vanderplaats, G.N. and Moses, F. (1972). Automated design of trusses for optimum geometry. *Journal of Structure Division, ASCE*, **98**, 671-690.
- Venkayya, V.B., Khot, N.S. and Reddy, V.S. (1968). Optimisation of structures based on the study of strain energy distribution. *AFFDL-TR-68-150*.
- Venkayya, V.B., Khot, N.S. and Berke, L. (1973). Application of optimisation criteria approaches to automated design of large practical structures. *Proceedings of 2nd Symposium on Structural Optimisation*, Milan, Italy.
- Wang, B.P. (1991). Improved approximate methods for computing eigenvector derivatives in structural dynamics. *AIAA J.*, **29**, 1018-1020.
- Wellen, H. and Bartholomew, P. (1990). Structural optimisation in aircraft construction. *Presented at the 1st Meeting of Garteur AG on Structural Optimisation*, Bremen, Germany.
- Xie, Y.M. and Steven, G.P. (1993). A simple evolutionary procedure for structural optimisation. *Compt. Struct.*, **49**, 885-896.
- Xie, Y.M. and Steven, G.P. (1994). A simple approach to structural frequency optimisation. *Compt. Struct.*, **53**, 1487-1491.
- Xie, Y.M. and Steven, G.P. (1996). Evolutionary structural optimisation for dynamic problems. *Compt. Struct.*, **58**, 1067-1073.
- Xie, Y.M. and Steven, G.P. (1997). *Evolutionary Structural Optimisation*. Springer-Verlag, Berlin.
- Yang, X.Y. (1999). *Bi-directional Evolutionary Method for Stiffness and Displacement Optimisation*. M.E. Thesis, Victoria University of Technology, Melbourne, Australia.
- Yang, X.Y., Xie, Y.M., Steven, G.P. and Querin, O.M. (1999a). Bi-directional evolutionary method for stiffness optimisation. *AIAA J.*, **37**, 1483-1488.
- Yang, X.Y., Xie, Y.M., Steven, G.P. and Querin, O.M. (1999b). Topology optimisation for frequencies using an evolutionary method. *Journal of Structural Engineering*,

ASCE, **125** (12), 1432-1438.

Young, V., Querin, O.M., Steven, G.P. and Xie, Y.M. (1998). 3D bi-directional evolutionary structural optimisation. *Proceedings of the Australasian Conference on Structural Optimisation, Sydney, Australia*, pp. 275-282.

Zhou, M. and Rozvany, G.I.N. (1991). The COC algorithm, Part II: Topological, geometry and generalised shape optimisation. *Comput. Methods Appl. Mech. Eng.*, **89**, 197-224.

Zhou, M. and Rozvany, G.I.N. (2001). On the validity of ESO type methods in topology optimisation. *Struct. Multidisc. Optim.*, **21**, 80-83.

Zoutendijk, G. (1960). *Methods for Feasible Direction*, Amsterdam, Elsevier.